UNIVERSITY OF CALIFORNIA,
IRVINE

Fluorescent Teixobactin Probes

DISSERTATION

submitted in partial satisfaction of the requirements
for the degree of

DOCTOR OF PHILOSOPHY

in Chemistry

by

Michael Anthony Morris

Dissertation Committee:
Professor James S. Nowick, Chair
Professor Jennifer A. Prescher
Professor David L. Van Vranken

2020

DEDICATION

To my family and friends for their unwavering support.

TABLE OF CONTENTS

LIST OF FIGURES

LIST OF TABLES

LIST OF SCHEMES

ACKNOWLEDGEMENTS

I would not have been able to complete graduate school without the help from so many generous people. First, I want to express my gratitude to my advisor and committee chair, Prof. James Nowick, for being a great mentor. James, I am grateful for all of your keen advice when it came to designing, analyzing, and troubleshooting experiments and data, as well as allowing me to participate in a variety of professional development and teaching opportunities.

I am also grateful for the support and guidance from my thesis committee: Prof. Jennifer Prescher and Prof. David Van Vranken. Prof. Prescher, you were incredibly helpful when it came to designing my orals proposal as well as suggesting helpful experiments for my research projects. I also thoroughly enjoyed your Chem 128 course and it remains as my favorite graduate course at UC Irvine. Prof. Van Vranken, you have always suggested helpful experiments for my thesis projects and I always admired your enthusiasm to learn more about my research.

I also need to acknowledge my team of undergraduate researchers who played instrumental roles in my research projects. Melody Malek and Mo Hashemian, thank you to you both for your dedicated support when it came to tackling multiple projects at the same time. I always appreciated you two asking questions and coming up with new project ideas. Betty Nguyen, I will always be impressed by your ability to make so many peptides in excellent purities. Your work was incredibly helpful during the last stretch of my graduate school career.

I would like to thank all of my teaching and pedagogical mentors, who have equipped me with the knowledge and tools to become a better teacher. First, I would like to thank Dr. Danny Mann for introducing me to pedagogy and evidence-based teaching; the Pedagogical Fellowship Program was a formative moment during my time in graduate school. I also want to thank Prof. Reneé Link for being my STAP mentor, providing me with the opportunity to teach Chem 51LB, and allowing me to do chemical education research with her. I am also grateful for Prof. Stephen Mang who provided me with the opportunity to teach Chem 101W and carrying out chemical education research. Lastly, I need to thank Dr. Kate McKnelly and Dr. Will Howitz for their incredible support and advice when I was teaching Chem 51LB and Chem 101W.

I also want to thank all of the members of the Nowick lab and my friends in graduate school for supporting me. Xing, thank you for helping me troubleshoot my experiments and being a good support system. Gretchen, I am so grateful for your help when it came to purifying challenging peptides, doing fluorescence measurements, and imaging on the Keyence. Maj, thanks for being a great desk mate and helping me out with various things in the lab. Thanks to Dr. Adam Kreutzer, Dr. Michał Wierzbicki, Tuan, Sheng, Chelsea P., James, Chelsea J., and Sarah for being great labmates. To my friends who have graduated – Dr. Kellen Kartub, Dr. Millie Fung, Dr. Adam Maley, Dr. Alana Ogata, and Dr. Brandon Matthews – thank you so much for your support and the fun adventures we had in graduate school.

Most importantly, I need to thank my family: Mom, Dad, Matt, Lisa, Skippy, Grandma Martinangelo, and Grandpa Morris. Without their unwavering support and love, I would not be the scientist that I am today. Even though I live >3,000 miles from my family, they always provided support when I needed it and I will always be thankful for that.

Michael A. Morris

Curriculum Vitae

EDUCATION

University of California, Irvine, Irvine, CA **2014 – Present**
Department of Chemistry
Research Advisor: Dr. James S. Nowick
Ph.D. Candidate in Chemistry, specialization in Chemical Biology

Union College, Schenectady, NY **2010 – 2014**
Department of Chemistry
Research Advisor: Dr. Laura A. MacManus-Spencer
B.S., Biochemistry, Magna Cum Laude, Phi Beta Kappa, 2014

RESEARCH EXPERIENCE

Graduate Research, *University of California, Irvine* **2014 – Present**

Fluorescent teixobactin analogues (PI: Dr. James S. Nowick)
Synthesized fluorescent teixobactin analogues to probe localization in bacteria. Techniques used include solid phase peptide synthesis, analytical and preparative high performance liquid chromatography (HPLC), electrospray ionization mass spectrometry, minimum inhibitory concentration (MIC) assays, fluorescence microscopy, time lapse microscopy, and spectral and FLIM-FRET microscopy.

Chemical Education Research, *University of California, Irvine* **2019 – Present**

New active learning tool and specifications grading (PIs: Dr. Renée D. Link and Dr. Stephen A. Mang)

- With Dr. Renée D. Link and Dr. Zachary Thammavongsy, evaluated a ^{1}H NMR spectroscopy board game as a new active learning tool in undergraduate organic chemistry lecture and laboratory courses.
- With Dr. Stephen A. Mang and Dr. Kate J. McNelly, redesigned an upper-division chemistry writing course that uses specifications grading. Evaluated impact of specifications grading on students' writing habits and attitudes.

Undergraduate Research

Probing the PFAA-HSA binding mechanism, *Union College* **2013 – 2014**
Investigated the binding mechanisms, quantitatively and qualitatively, between human serum albumin and perfluoroalkyl acids using LC-MS/MS and an improved approach to equilibrium dialysis (Advisor: Prof. MacManus-Spencer).

HSP60 binding interactions, *Consiglio Nazionale delle Ricerche* **2013**
Investigated the oligomeric equilibria of HSP60 and GroEL and their binding interactions with procaspase-3 using dynamic light scattering, static light scattering, and circular dichroism spectroscopy (Advisor: Dr. Silvia Vilasi).

LKB1 in Peutz-Jeghers Syndrome, *UMass Medical School* **2012 – 2013**
Utilized immunohistochemistry (IHC) to analyze transgenic mice tissues to elucidate the molecular role of LKB1 in Peutz–Jeghers syndrome (Advisor: Prof. Junhao Mao).

PUBLICATIONS

Morris, M. A., Nguyen, B. T., Hashemian, M. H., Malek, M., and Nowick, J. S. Fluorescent teixobactin analogues reveal amyloidogenic mode of action. *Manuscript in preparation*.

Zhang, S., Yoo, S., **Morris, M. A.**, Guaglianone, G. E., Jusuf, H., Huizar, G., Lin, J., Kreutzer, A. G., and Nowick, J. S. Expression of N-terminal cysteine Aβ42 and bioconjugation to generate fluorescent Aβ42. *Manuscript in preparation*, planned submission to *ACS Chem. Biol*.

Zhang, S., Krumberger, M.*, **Morris, M. A.***, Parrocha, C. M. T., and Nowick, J. S. Structure-based drug design of an inhibitor of the SARS-CoV-2 (COVID-19) main protease using free software: A tutorial for students and scientists. Preprint available on bioRxiv.

Kreutzer, A. G., Krumberger, M., Parrocha, C. M. T., **Morris, M. A.**, Guaglianone, G. and Nowick, J. S. Structure-based design of a cyclic peptide inhibitor of the SARS-CoV-2 main protease. Manuscript in preparation. Preprint available on bioRxiv.

McKnelly, K. J., **Morris, M. A.**, and Mang, S. A. Redesigning a "Writing for Chemists" course using specifications grading. Under revision at *J. Chem. Educ.* on October 5th, 2020.

Thammavongsy, Z.*, **Morris, M. A.***, and Link, R. D. ^{1}H NMR spectrum: A team-based tabletop game for molecular structure elucidation. Just accepted manuscript at *J. Chem. Educ.* on November 10th, 2020.

Morris, M. A., Malek, M., Hashemian, M. H., Nguyen, B. T., Manuse, S., Lewis, K., and Nowick, J. S. A fluorescent teixobactin analogue. *ACS Chem. Biol.* **2020**, *15,* 1222–1231.

*Authors contributed equally to manuscript.

TEACHING EXPERIENCE

All courses were taught for the Department of Chemistry, University of California, Irvine (UCI).

Instructor of Record, Writing for Chemists (Chem 101W) **Winter 2020**

Instructor of an upper division writing class for 13 chemistry undergraduate students. Performed all duties required of instructor of record at UCI including, but not limited to: developing course assignments, using an learning management system (Canvas), creating lectures, grading and critiquing students' assignments, and providing support to students. Evaluated students' attitudes towards specifications grading which culminated in a manuscript under revision at *J. Chem. Educ*. This course was designed to fulfil upper division writing (Ia) General Education Requirement at UCI. This course took place prior to the COVID-19 pandemic and was completed entirely in-person (face-to-face instruction). Final course evaluations are available upon request.

Instructor of Record, Organic Chemistry lab 1 (Chem 51LB) **Summer 2019**

Instructor of organic chemistry lab for 115 undergraduate students. Performed all duties required of instructor of record at UCI including, but not limited to: teaching a biweekly lab lecture, managing a team of six TAs, designing lab practical exams, and handling course logistics. Carried out a teaching as research (TAR) project to evaluate a new active learning tool which culminated in a first co-author publication in *J. Chem. Educ*. Final course evaluations are available upon request.

Teaching Assistant, Organic Chemistry 2 (Chem 51B) **Summer 2020**

Carried out discussion sections to teach undergraduate organic chemistry. Assisted in creating and grading assignments, quizzes, and exams. This course was carried out remotely.

Support Teaching Assistant, Organic Chemistry 1 (Chem 51A) **Summer 2020**

Assisted in creating and grading assignments, quizzes, and exams for organic chemistry lecture. This course was carried out remotely.

Teaching Assistant, Senior Thesis Writing (Chem 180W) **Spring 2020**

Assisted in creating and grading assignments for a senior thesis writing class for undergraduate chemistry majors. This course was carried out remotely.

Teaching Assistant, Writing for Chemists (Chem 101W) **Fall 2019 and Fall 2020**

Assisted in creating and grading assignments for an upper division writing class designed for chemistry majors. Assisted with a teaching as research (TAR) project to assess students' attitudes towards the specifications grading system used in the class. The course was taught in-person in Fall 2019, and was taught remotely in Fall 2020.

TA Professional Development Program (TAPDP) **Fall 2018 and 2019**

Designed and implemented 2018 and 2019 TA Professional Development Program (TAPDP) for the Chemistry and Pharmaceutical Sciences Departments. TAPDP is a two day course to train first year graduate students in: TA roles and responsibilities, educational technology, lesson planning, office hours, leading a class, active learning techniques, diversity and inclusion, teaching observation and feedback, and practice in giving a mini-lesson.

Teaching Assistant, **Organic Chemistry lab** **Winter and Spring 2015**

Taught laboratory experiments to highlight fundamentals of organic chemistry lab techniques. Prepared and carried out prelab lectures, supervised laboratory learning, and graded lab reports and lab practical exams.

Teaching Assistant, **General Chemistry lab** **Fall and Summer 2014 – 2015**

Taught laboratory experiments to highlight fundamentals of general chemistry lab techniques. Prepared and carried out prelab lectures, supervised laboratory learning, and graded lab reports and lab practical exams.

LEADERSHIP AND PROFESSIONAL SERVICE

Diversity & Inclusion Advisory Board member, *American Chemical Society* **2019 – Present**

Elected as the Division of Professional Relations liaison to develop actions and programming that promote diversity, inclusion, equity, and respect for the American Chemical Society (ACS).

Gay and Transgender Chemists and Allies Chair, *American Chemical Society* **2017 – 2019**

Elected as chair for the American Chemical Society subdivision. Organized and fundraised four LGBTQ+ symposia for American Chemical Society National Meetings between 2017 and 2019.

UCI Chemistry Outreach Program, *University of California, Irvine* **2015 – 2019**

Managed a chemistry outreach program for four years and taught chemistry to underserved Orange County K-12 students. Taught basic chemistry concepts through engaging chemical demonstrations and explained process of developing a career in STEM.

SYMPOSIA FOR ACADEMIC CONFERENCES

- I organized four symposia for American Chemical Society National Meetings and fundraised **over $54,000** to support these events.

Morris, M. A and Yoon, T. P. LGBTQ+ graduate student and postdoctoral scholar research symposium. Presented at the 257th American Chemical Society National Meeting, Orlando, FL, April 2019. **Fundraised $15,980.**

Morris, M. A. Importance of LGBTQ+ role models & mentors in the chemical sciences: A symposium in honor of Barbara Belmont. Presented at the 256th American Chemical Society National Meeting, Boston, MA, August 2018. **Fundraised $7,400.**

Morris, M. A. LGBTQ+ graduate student and postdoctoral scholar research symposium. Presented at the 255th American Chemical Society National Meeting, New Orleans, LA, March 2018. **Fundraised $13,700.**

Morris, M. A. and Nowick, J. S. LGBT graduate student and postdoctoral scholar research symposium. Presented at the 253rd American Chemical Society National Meeting, San Francisco, CA, April 2017. **Fundraised $17,100.**

INVITED PRESENTATIONS

Vertex Day **February 2020**
Invited oral presentation Irvine, CA

- Title: Fluorescent teixobactin analogues.
- Authors: **Morris, M. A.**, Malek, M., Hashemian, M. H., Nguyen, B. T., Manuse, S., Lewis, K., and Nowick, J. S.
- Hosted by Vertex Pharmaceuticals at University of California, Irvine, Department of Pharmaceutical Sciences.

University of Redlands, Department of Chemistry **October 2019**
Invited seminar speaker Redlands, CA

- Title: Fluorescent teixobactin analogues.
- Authors: **Morris, M. A.**, Malek, M., Hashemian, M. H., Nguyen, B. T., Manuse, S., Lewis, K., and Nowick, J. S.

Diversity in the Minerals, Metals, and Materials Professions 3 **July 2018**
Invited oral presentation Santa Barbara, CA

- Title: Illuminating the LGBTQ+ community in STEM – outlook and solutions.
- Authors: **Morris, M. A.**
- Presented at the LGBTQ+ Symposium.

CONTRIBUTED PRESENTATIONS

American Chemical Society (ACS) Fall 2019 National Meeting **August 2019**
Oral presentation San Diego, CA

- Title: Fluorescent teixobactin analogues (Abstract ID 3204791).
- Authors: **Morris, M. A.**, Malek, M., Hashemian, M. H., Nguyen, B. T., Manuse, S., Lewis, K., and Nowick, J. S.
- Presented at Division of Biological Chemistry, Graduate Student and Postdoctoral Scholar Symposium.

American Chemical Society (ACS) Spring 2019 National Meeting **April 2019**
Poster presentation Orlando, FL

- Title: Interaction of a fluorescent teixobactin analogue with bacteria (Abstract ID 3081969).
- Authors: **Morris, M. A.**, Malek, M., Hashemian, M. H., and Nowick, J. S.
- Presented at the LGBTQ+ Graduate Student and Postdoctoral Scholar Research Symposium.

American Chemical Society (ACS) Spring 2019 National Meeting **April 2019**
Panelist Orlando, FL

- Title: The LGBTQ+ community in chemistry – new frontiers for graduate students and postdoctoral scholars (Abstract ID 3068614).
- Panel discussion at the LGBTQ+ Graduate Student and Postdoctoral Scholar Research Symposium.

American Chemical Society (ACS) Fall 2018 National Meeting **August 2018**
Poster presentation Boston, MA

- Title: Interaction of a fluorescent teixobactin analogue with bacteria (Abstract ID 2982800).
- Authors: **Morris, M. A.**, Malek, M., Hashemian, M. H., and Nowick, J.
- Presented at the Division of Biological Chemistry, Graduate Student and Postdoctoral Scholar Poster Session.

American Chemical Society (ACS) Spring 2018 National Meeting **March 2018**
Panelist New Orleans, LA

- Title: The LGBTQ+ community in chemistry – opportunities, challenges, and perspectives for graduate students and postdoctoral scholars (Abstract ID 2853379).
- Panel discussion at the LGBTQ+ Graduate Student and Postdoctoral Scholar Research Symposium.

American Chemical Society (ACS) Spring 2017 National Meeting **April 2017**
Panelist San Francisco, CA

- Title: Celebrating LGBT identities in chemistry: opportunities, challenges, and perspectives (Abstract ID 2664708).
- Panel discussion at the LGBTQ+ Graduate Student and Postdoctoral Scholar Research Symposium.

Steinmetz Symposium **May 2014**
Oral presentation Schenectady, NY

- Title: Investigation of binding interactions of perfluoroalkyl acids with human serum albumin using an improved approach to equilibrium dialysis.
- Authors: **Morris, M. A.** and MacManus-Spencer, L. A.
- Hosted by Union College, Schenectady, NY.

Eastern NY ACS Undergraduate Research Symposium (Siena College) **April 2014**
Poster presentation Loudonville, NY

- Title: Investigation of binding interactions of perfluoroalkyl acids with human serum albumin using an improved approach to equilibrium dialysis.
- Authors: **Morris, M. A.** and MacManus-Spencer, L. A.
- Hosted by Siena College, Loudonville, NY.

American Chemical Society (ACS) Spring 2014 National Meeting **March 2014**
Poster presentation Dallas, TX

- Title: Investigation of binding interactions of perfluoroalkyl acids with human serum albumin using an improved approach to equilibrium dialysis (ENVR 325).
- Authors: **Morris, M. A.** and MacManus-Spencer, L. A.
- Presented at the Division of Environmental Chemistry Poster Session.

Union College Summer Research Seminar Series **August 2013**
Oral presentation Schenectady, NY

- Title: Protein binding of perfluoroalkyl acids.
- Authors: **Morris, M. A.** and MacManus-Spencer, L. A.
- Hosted by Union College, Schenectady, NY.

PROFESSIONAL DEVELOPMENT

Summer Teaching Apprenticeship Program, *University of California, Irvine* **2018 – 2019**
Attended lectures of Organic Chemistry Lab (Chem 51LB) to observe and receive pedagogical mentoring and training from Dr. Renee Link. Became an instructor of record of Organic Chemistry Lab during Summer 2019.

Pedagogical Fellow, *University of California, Irvine* **2017 – 2019**
Trained in advanced pedagogy, professional development, and instructional technology.

Certified CIRTL Associate, *University of California, Irvine* **2017**
Trained in implementing evidence-based teaching practices.

AWARDS AND FUNDING

ACS Division of Biological Chemistry Travel Award **2019**
257th American Chemical Society National Meeting, Orlando, FL, April 2019.

DTEI Pedagogical Fellowship, *University of California, Irvine* **2017**
For excellence in teaching and pedagogy.

Certificate in Teaching Excellence, *University of California, Irvine* **2018**
Recognition of training in course design using evidence-based pedagogy, teaching analysis and assessment, and learning assessment.

Union College Senior Chemistry Award, *Union College* **2014**
For achievements in chemistry.

Presidential Green Grant for Research, *Union College* **2013**

Union College Student Research Grant, *Union College* **2013**

Lee Davenport '37 Summer Research Fellowship, *Union College* **2013**

Union College Dean's List, *Union College* **2011 – 2014**

Union College Presidential Merit Scholarship, *Union College* **2010 – 2014**
Merit scholarship for academic excellence.

PROFESSIONAL AFFILIATIONS

Phi Beta Kappa Society **2014 – Present**
Member

American Chemical Society **2013 – Present**
Student Member

MENTORSHIP

TA Mentorship Program, *University of California, Irvine* **2018 – 2019**
Mentored five first-year graduate students in the Chemistry Department. Helped guide mentees through their first year in graduate school.

Undergraduate Research Mentorship, *University of California, Irvine* **2017 – Present**
Mentored three undergraduate students in the Nowick Lab for conducting research. Taught undergraduates research techniques, project and experimental design, and supervised their experiments. All three undergraduates successfully acquired research funding from the Undergraduate Research Opportunities Program. Undergraduates: **Melody Malek** (2017–2019), **Mo Hashemian** (2018–2019), and **Betty Nguyen** (2019–present). Melody and Mo are currently chemistry PhD students UC Davis.

SPECIFIC SKILLS

Chemistry: Proficient in solid phase peptide synthesis, LC-MS/MS, ^{1}H- and ^{13}C-NMR, analytical and preparative HPLC, ESI-MS, MALDI MS, UV-Vis spectroscopy, fluorescence spectroscopy, and small molecule synthesis and purification (small and large scale).

Biochemistry, microbiology, and tissue culture: Proficient in BSL2+ sterile technique, minimum inhibitory concentration (MIC) assay, culturing bacterial and mammalian cells, fluorescence microscopy of bacteria and mammalian cells, SDS-PAGE, equilibrium dialysis, immunohistochemistry, circular dichroism, PCR, and DNA gel electrophoresis.

Computer: Proficient in Microsoft Word, Excel, and PowerPoint; Adobe Illustrator and Photoshop; ChemDraw; PyMol; Maestro; AutoDock Vina; Chimera; Agilent MassHunter; Kaleidagraph.

ABSTRACT OF THE DISSERTATION

Fluorescent Teixobactin Probes

by

Michael Anthony Morris
Doctor of Philosophy in Chemistry
University of California, Irvine
2020
Professor James S. Nowick, Chair

Antibiotic resistant bacteria are an increasing threat to global human health. These drug resistant infections are challenging to treat and contain, and the antibiotic discovery pipeline does not match the pace of the growing number of antibiotic resistant bacteria. In Chapter 1, I summarize the outlook of antibiotic resistance and how the new antibiotic, teixobactin, serves as a promising template to combat drug resistant infections. Teixobactin is a peptide antibiotic that kills Gram-positive bacteria without detectable resistance and is able to kill pathogens that are considered as urgent and serious threats by the CDC. I provide a summary of the mechanism of action of teixobactin, structure-relationship studies of its pharmacophore, and various synthentic methods to make the antibiotic. In the last section of this chapter, I review how fluorescent antibiotics are versatile probes to understand the mode of action of antibiotics, elucidate off-target effects (toxicity studies), detect antibiotic resistance, and serve as diagnostics for detecting infections *in-vivo* or *ex-vivo*.

Chapter 2 describes the first synthesis and application of a fluorescent teixobactin analogue that exhibits antibiotic activity and binds to the cell walls of Gram-positive bacteria. The teixobactin analogue, Lys(Rhod)$_9$,Arg$_{10}$-teixobactin, has a fluorescent tag at position 9 and an arginine in place of the natural *allo*-enduracididine residue at position 10. The fluorescent teixobactin analogue retains partial antibiotic activity, with minimum inhibitory concentrations of 4–8 μg/mL across a panel of Gram-positive bacteria, as compared to 1–4 μg/mL for the unlabeled Arg$_{10}$-teixobactin analogue. Lys(Rhod)$_9$,Arg$_{10}$-teixobactin is prepared by a regioselective labeling strategy that labels Lys$_9$ with an amine-reactive rhodamine fluorophore during solid-phase peptide synthesis, with the resulting conjugate tolerating subsequent solid-phase peptide synthesis reactions. Treatment of Gram-positive bacteria with Lys(Rhod)$_9$,Arg$_{10}$-teixobactin results in septal and lateral staining, which is consistent with an antibiotic targeting cell wall precursors. Concurrent treatment of Lys(Rhod)$_9$,Arg$_{10}$-teixobactin and BODIPY FL vancomycin results in septal co-localization, providing further evidence that Lys(Rhod)$_9$,Arg$_{10}$-teixobactin binds to cell wall precursors. Controls with either Gram-negative bacteria, or an inactive fluorescent homologue with Gram-positive bacteria, showed little or no staining in fluorescence micrographic studies. Lys(Rhod)$_9$,Arg$_{10}$-teixobactin can thus serve as a functional probe to study Gram-positive bacteria and their interactions with teixobactin.

Chapter 3 describes a new approach to selectively label Lys$_9$,Arg$_{10}$-teixobactin and Lys$_{10}$-teixobactin with a variety of *N*-Hydroxysuccinimide (NHS) ester fluorophores. The reaction affords regioselective labeling of the lysine sidechain amines of either Lys$_{10}$- or Lys$_9$,Arg$_{10}$-teixobactin. Using this labeling method, we were able to generate four fluorescent teixobactin analogues, bearing different fluorophores, that retain antibiotic activity and stain the cell walls of Gram-positive bacteria. This approach also enabled us to determine that position 10 tolerates

fluorophores better than position 9, using MIC assays and fluorescence microscopy as readouts. Structured illumination microscopy of the fluorescent teixobactin analogues in live *B. subtilis* cells enabled further study of the aggregation of teixobactin in bacterial membranes, with observation of both clusters and aggregates of the antibiotic in bacterial membranes. To further understand the aggregation of teixobactin in live bacteria, we used fluorescence lifetime imaging Förster resonance energy transfer (FLIM-FRET) microscopy, which demonstrated that fluorescent teixobactin analogues are in intimately interacting with each other in live cells. Lastly, we treated NRK-52E rat kidney cells with our fluorescent teixobactin analogues to determine if teixobactin had any nephrotoxic effects due to its unfavorable aggregation propensity. Taken together, we demonstrate useful applications of fluorescent teixobactin analogues that enabled elucidation of its on-target and off-target effects in bacterial and kidney cells, respectively.

Chapter 4 reports the biological activities of a toxic, fluorescent peptide derived from A$\beta_{15\text{-}36}$ (peptide 1*) using the LDH release assay as well as confocal laser scanning microscopy (CLSM). The fluorescent L-(7-hydroxycoumarin-4-yl) ethyl glycine (7-HC) amino acid was synthesized and incorporated into coumarin-$QK_{15\text{-}36}$ (peptide 1*), thereby making it suitable for localization studies. Peptide 1* was shown to be toxic to human neuroblastoma SH-SY5Y cells over a range of concentrations using the LDH release assay. Furthermore, peptide 1* was uniformly internalized in the cytosol of SH-SY5Y cells, suggesting that it mediates toxicity by disrupting intracellular homeostasis. This is the first time the Nowick lab has characterized the cellular localization of a toxic peptide and the results from this study may further our understanding of Aβ neurotoxicity.

Chapter 5 summarizes my teaching and chemical education research experiences at UC Irvine. I provide reflections of my experiences in two pedagogical training programs offered at UC

Irvine and summarize my experiences as an instructor of record for Chemistry 51LB and Chemistry 101W. This chapter concludes with a summary of my involvement in two chemical education research studies, where I learned about research survey design and data analysis.

Chapter 1

Antibiotic Resistance, Teixobactin, and Fluorescent Antibiotics

Introduction

Antibiotics have been a transformative component of modern medicine since the first successful clinical use of penicillin in 1942 to treat streptococcal meningitis.[1,2] Since then, hundreds of antibiotics were approved by the FDA, which have been used to treat severe bacterial infections and consequently reduced global morbidity and mortality by a significant margin.[1] However, the widespread use and misuse of antibiotics causes the unintended consequence of antibiotic resistance, resulting in many antibiotics becoming unviable treatments. Antibiotic resistant bacteria are challenging to contain because they may not be sensitive to alternative treatments, they tend to have heterogenous resistance mechanisms, and they pose high infectivity potential in clinical and public settings.[1,3–5] As more cases of antibiotic resistant bacteria are increasing worldwide, many public health and infectious disease experts are concerned that antibiotic resistant bacteria could cause the next pandemic, if left unchecked.[6,7]

Antibiotic resistant bacteria are mounting threat to human health. Antibiotic resistance occurs when bacteria become insensitive to drugs that were designed to kill them, and thus creates challenges for medical treatment and containment.[1,2] Bacteria can acquire antibiotic resistance through evolutionary pressure or exchange of genetic information, where favorable genomic modifications allow the organism to survive in the presence of one or more antibiotics, thus enabling the resistant bacteria to proliferate.[1,5,8,9] These genomic modifications confer antibiotic resistance via four different molecular mechanisms by: (1) reducing cellular uptake of the drug; (2) modifying a drug target; (3) inactivating the drug via a chemical modification; and/or (4) pumping out a drug via efflux.[1,5,8,10] These resistance mechanisms allow pathogenic bacteria to

quickly propagate in the clinic, making it challenging to treat and contain these infections since they may have one or more resistance mechanisms against one or more drugs.[1,10]

Not only is antibiotic resistance a devastating threat to global public health, but it also poses a substantial economic threat. Antibiotic resistant bacteria cause at least 2.8 million infections and more than 35,000 deaths each year in the United States.[1] The loss in productivity from these illnesses produces a significant economic burden, with losses of $20 billion in direct costs and $35 billion in indirect costs in the United States.[1] Antibiotic resistance also complicates critical medical procedures, such as surgery and organ transplants, which are highly suspectable to bacterial infections and where drug resistant infections can be life threatening.[1] As such, antibiotic resistance poses mounting medical and economic burdens that will only worsen if newer antibiotics are not developed.

Antibiotic resistant Gram-positive bacteria are of particular concern since they comprise more than 54% and 85% of illnesses and deaths caused by resistant bacteria.[1] These Gram-positive pathogens consist of erythromycin-resistant *Streptococcus*, clindamycin-resistant *Streptococcus*, vancomycin-resistant *Enterococcus* (VRE), methicillin-resistant *Staphylococcus aureus* (MRSA), drug-resistant *Mycobacterium tuberculosis*, and *Clostridioides difficile*. The last two pathogens are especially prevalent and dire: *Mycobacterium tuberculosis* is one of the top ten causes of death globally[11] and *Clostridioides difficile* causes more than 223,900 illnesses and 12,800 deaths annually in the United States.[1] The alarming rate of illnesses caused by resistant Gram-positive pathogens necessitates the development and deployment of new and effective therapies in order to save lives.

Unfortunately, the antibiotic discovery pipeline does not match the speed of the growing number of antibiotic resistant bacteria. Since 1990, 78% of drug makers have reduced efforts in

antibiotic development,[1,3] leaving health professionals with fewer options to treat drug resistant infections. The decline in antibiotic discovery is linked to the lack of funding and financial incentives from the government and private investors.[3] In addition, antibiotics have low profitability – they are usually prescribed for short-term treatments, making them unprofitable compared to blockbuster drugs that treat chronic conditions.[3] Despite the current antibiotic discovery void, there have been some advances in antibiotic development – 42 novel antibiotics are in development as of 2019.[1] Unfortunately, these advances may not be expansive enough to fight against newer incidences of antibiotic resistant bacteria. For example, resistance has emerged against recently approved antibiotics, including tigecycline (2005), doripenem (2007), ceftaroline (2010), and ceftazidime-avibactam (2015).[1,3] Thus, there is a desperate need to expand the antibiotic pipeline in order to combat antibiotic resistance and save lives.

Teixobactin: a new antibiotic that evades resistance

In 2015, a new peptide antibiotic, teixobactin (Figure 1.1), was reported by Lewis et al.[12] The report of teixobactin was met with much excitement because it kills Gram-positive pathogens without developing resistance and has excellent antibacterial activity against resistant pathogens, including ones that are considered to be urgent and serious threats by the CDC.[1,12] Teixobactin has narrow-spectrum activity against many Gram-positive pathogens, including *Staphylococcus aureus*, MRSA, VRE, *Streptococcus pneumoniae*, *Mycobacterium tuberculosis*, *Clostridioides difficile*, and *Bacillus anthracis*, and teixobactin is able to kill these bacteria with excellent potency (MIC values range from 0.005–0.5 μg/mL).[12] Another remarkable property of teixobactin is its *in-vivo* activity, where it protects mice against death from MRSA at 0.2 mg/kg, making it more than an order of magnitude more effective than vancomycin, which requires 3 mg/kg to obtain comparable protection.[12] Thus, teixobactin, with its impressive antibacterial properties and ability

to evade resistance, has the transformative potential to compensate the increasing threat of antibiotic resistance.

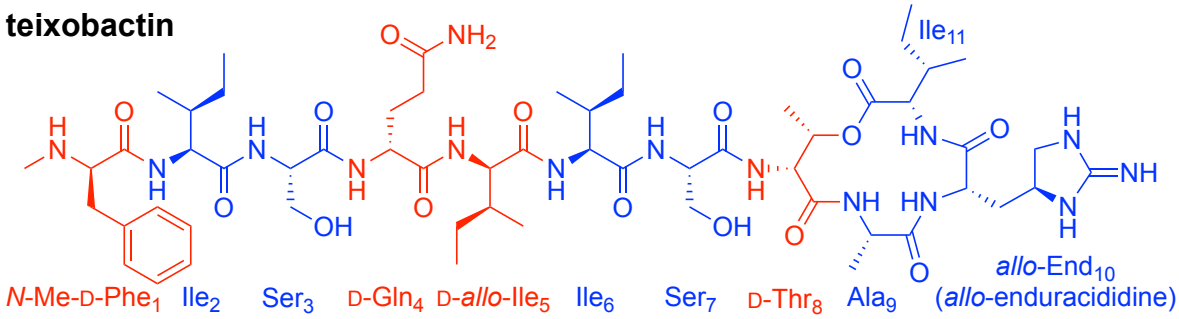

Figure 1.1. The structure of teixobactin, where D-amino acids are red, while L-amino acids are blue.

Teixobactin is a nonribosomal secondary metabolite that was first isolated from "unculturable" *Eleftheria terrae* using the isolation chip (iChip) technology. Soil bacteria, such as *E. terrae*, are difficult to culture using standard inoculation procedures, so the iChip was developed to culture soil bacteria *in vitro* in a high-throughput fashion. Each well in the iChip was inoculated with a diluted soil sample such that each well contains one bacterium, and was then sealed with a semipermeable membrane. The iChip was then inserted into the soil of origin, where soil nutrients diffuse through the semipermeable membrane to each bacterium, allowing the cells to grow in a self-sustaining colony.[12] The iChip technology is important because it allows difficult-to-culture bacteria to grow in a controlled setting, and has the potential to produce new natural products with promising medicinal properties, like teixobactin.

Teixobactin has a complex peptide architecture with non-proteinogenic features (Figure 1.1). The antibiotic is comprised of eleven amino acids with a linear, hydrophobic tail (residues 1-7) and a 13-membered macrolactone ring (residues 8–11). Out of the eleven amino acids, five of them are non-proteinogenic: *N*-Me-D-Phe$_1$, D-Gln$_4$, D-*allo*-Ile$_5$, D-Thr$_8$, and L-*allo*-enduracididine$_{10}$ (L-*allo*-End$_{10}$). The macrolactone of teixobactin is composed of

D-Thr$_8$−Ala$_9$−*allo*-End$_{10}$−Ile$_{11}$ where the *C*-terminus of Ile$_{11}$ and the hydroxy group of D-Thr$_8$ form an ester that closes the ring. The macrolactone also contains the non-proteinogenic amino acid L-*allo*-End$_{10}$, a cyclic arginine analogue. Teixobactin has an important stereochemical sequence in its tail residues consisting of a D−L−L−D−D−L−L pattern with a hydrophobic−hydrophobic−hydrophilic−hydrophilic−hydrophobic−hydrophobic−hydrophilic pattern of side chains, which is important for its antibiotic activity.[13–15]

Teixobactin has a mechanism of action that is unique compared to antibiotics that are currently used in the clinic. Teixobactin inhibits cell wall biosynthesis and precursor recycling in Gram-positive bacteria by binding to cell wall precursor molecules, which consequently causes cellular lysis.[12,16] Teixobactin specifically binds to lipid II, a peptidoglycan building block, and lipid III, a wall teichoic acid (WTA) building block. Both peptidoglycan and WTA are essential components of the bacterial cell wall, making them vulnerable targets for disrupting cell wall biosynthesis. A dimer of teixobactin binds to the highly conserved prenyl-phosphate-saccharide regions of lipids II and related cell wall precursors, and specifically binds to the anionic phosphates of these molecules (Figure 1.2).[12,14,16] These targets are extracellular and immutable, making it difficult or impossible for bacteria to become resistant to this mode of action. A recent solid state NMR structure of a teixobactin analogue bound to lipid II confirmed this binding mode, where the amide protons of the macrolactone and *N*-terminal amine of teixobactin coordinate to the pyrophosphate anions of lipid II.[14]

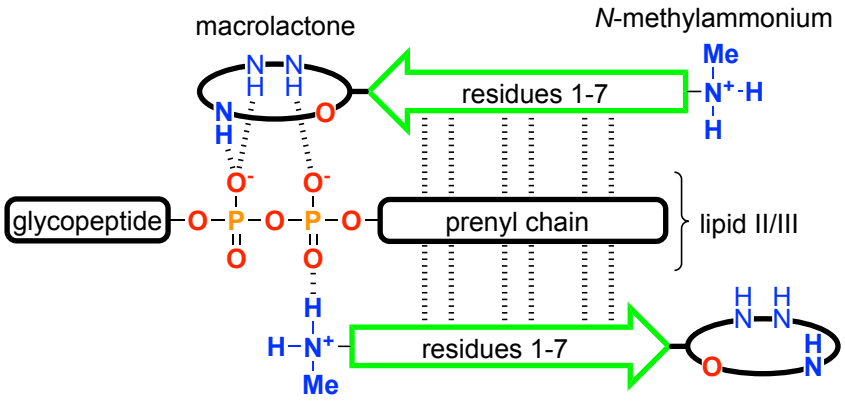

Figure 1.2. A simplified binding model of teixobactin complexed with lipid II and related cell wall precursors. This graphic was made by James H. Griffin and was used with permission.

There are various reported methods to synthesize teixobactin and its analogues, which have enabled insightful structure—activity relationship (SAR) studies of the teixobactin pharmacophore. Currently, four total syntheses of teixobactin have been reported, where three of them involve solid phase peptide synthesis (SPPS),[17–19] while one involves solution phase synthesis.[20] These syntheses have facilitated SAR studies of more than 120 teixobactin analogues, where residues in the teixobactin pharmacophore were modified to determine which residues are critical for antibiotic activity.[13,15,21-45] Figure 1.3 summarizes the tolerance of amino acids towards substitution in the teixobactin pharmacophore. Taken together, these SAR analyses have determined which residues can tolerate modification and have lead to the development of analogues that have comparable *in vitro* and *in vivo* activity to teixobactin against MRSA and VRE.

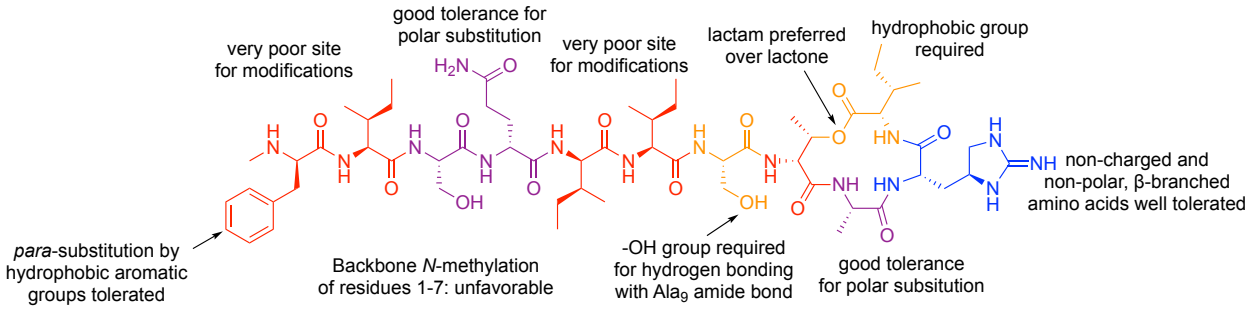

Figure 1.3. Summary of modifiable residues of the teixobactin pharmacophore, where red indicates poorest tolerance and purple indicates best tolerance for modifications. This Figure was adapted from Reddy et al.[15]

Even though these SAR studies elucidated the roles of individual residues, there is much to be learned from teixobactin mechanistically. A thorough understanding of the teixobactin pharmacophore could provide a framework for second-generation teixobactin analogues with improved antibiotic activity or better pharmacological properties. Teixobactin also offers promise as a potential tool for understanding the biosynthesis of peptidoglycan and teichoic acids, as well as undecaprenyl phosphate metabolism and recycling due to its unique mechanism of action. Thus, teixobactin provides a unique and informative blueprint for designing improved antibiotics, probing cell wall biosynthesis, and understanding antibiotic resistance.

Fluorescent antibiotics: mechanistic probes and useful diagnostics

Although antibiotics are usually considered as drugs, they also serve as a template for probes to facilitate our understanding of antibiotic mechanisms and of biological processes in bacteria. Antibiotic probes have the potential to offer spatiotemporal information about their mode of action, since these drugs bind to one or more biological targets. Antibiotics also can elucidate important physiological processes in bacteria since antibiotics bind to vital components in bacteria. One common strategy to use antibiotics as probes is using fluorescence as a sensitive spectroscopic readout. This is achieved either from using intrinsic fluorescence from the antibiotic itself or from

the conjugation of a fluorescent dye to the antibiotic. As such, fluorescent antibiotics can be applied in various types of experiments, with important applications in fluorescence-based assays, microscopy, and biomedical imaging.[46,47]

Fluorescent antibiotics are versatile tools. They can provide unique insights into the modes of action of antibiotics and antibiotic resistance and have enabled the development of new antibiotics.[46,47] Fluorescent antibiotics allow tracking of the drug and its interactions in bacterial cells,[38,46–48] mammalian cells,[49,50] human tissue,[51] and live[52–54] and postmortem animals.[55] Fluorescent antibiotics have valuable applications, such as understanding the mode of action of antibiotics, elucidating off-target effects (toxicity studies), detecting antibiotic resistance, and serving as diagnostics for detecting infections *in-vivo* or *ex-vivo* (Figure 1.4). More importantly, antibiotic probes have been used to study complicated biological mechanisms that orchestrate cell wall biosynthesis in bacteria, thus serving as tools to teach us fundamental biology.[48,56] For example, fluorescein-labeled vancomycin has enabled the study of peptidoglycan biosynthesis in *B. subtilis* by fluorescence microscopy and has revealed a possible helical pattern of cylindrical wall synthesis.[56] Studies with fluorescent antibiotic analogues are likely to become more important against the growing threat of antibiotic-resistant pathogens because they can illuminate modes of antibiotic action, elucidate cell wall biosynthetic mechanisms, and serve as rapid diagnostics that can detect bacterial infections.

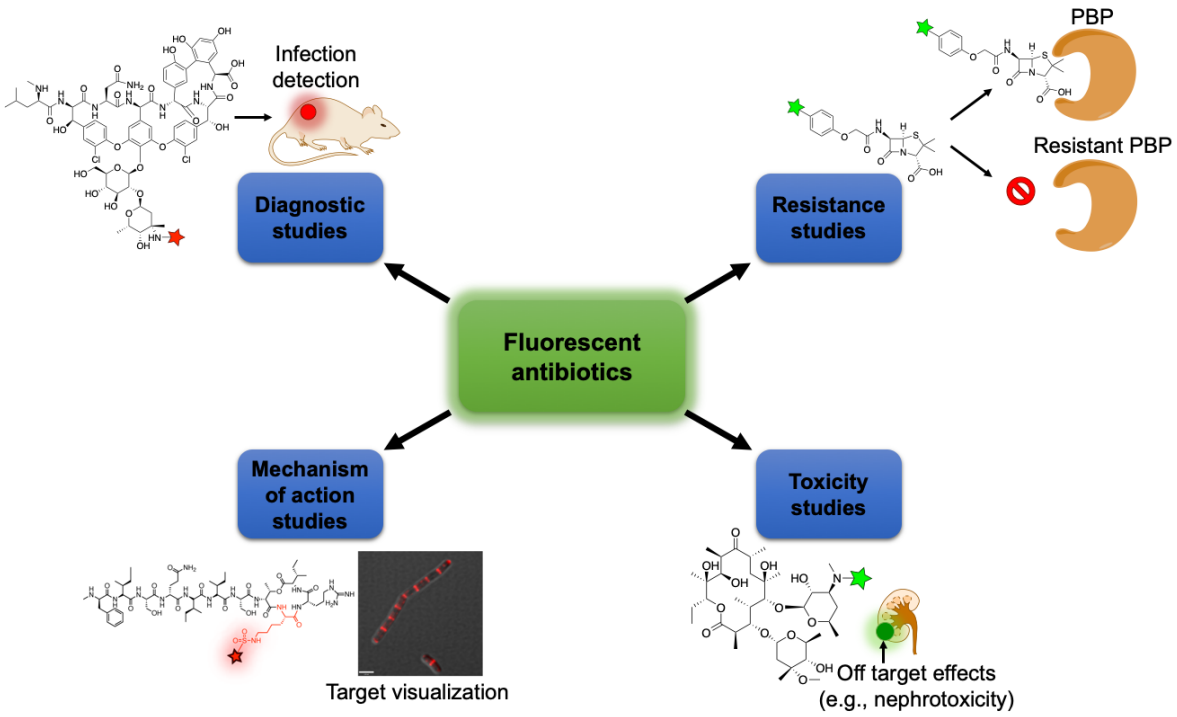

Figure 1.4. Applications of fluorescent antibiotics: mechanism of action studies, toxicity studies, resistance studies, and diagnostic studies. This Figure was adapted from Blaskovich et al.[47]

In my dissertation, I utilized the teixobactin pharmacophore as a template for designing new fluorescent probes. In Chapter 2, I describe the first application of a fluorescent teixobactin analogue to study the mechanism of action of teixobactin.[38] In Chapter 3, I discuss the development of a small library of fluorescent teixobactin analogues, describe the optimal location for conjugation in the teixobactin pharmacophore, and summarize efforts in bacterial and kidney cell microscopy. In Chapter 4, I summarize current efforts in elucidating *in-vivo* interactions of fluorescent teixobactin analogues in live *B. subtilis* cells using FRET microscopy.

References

(1) Services, U. . D. of H. and H. Antibiotic Resistance Threats in the United States. *Centers Dis. Control Prev.* **2019**, 1–113.

(2) Fleming, A. Streptococcal Meningitis Treated With Penicillin. *Lancet* **1943**, *242* (6267), 434–438. https://doi.org/10.1016/s0140-6736(00)87452-8.

(3) Ventola CL. The Antibiotic Resistance Crisis: Causes and Threats. *P T J.* **2015**, *40* (4), 277–283.

(4) Zaman, S. Bin; Hussain, M. A.; Nye, R.; Mehta, V.; Mamun, K. T.; Hossain, N. A Review on Antibiotic Resistance: Alarm Bells Are Ringing. *Cureus* **2017**, *9* (6). https://doi.org/10.7759/cureus.1403.

(5) Wang, W.; Arshad, M. I.; Khurshid, M.; Rasool, M. H.; Nisar, M. A.; Aslam, M. A.; Qamar, M. U. Antibiotic Resistance : A Rundown of a Global Crisis. *Infect. Drug Resist.* **2018**, 1645–1658.

(6) Strathdee, S. A.; Davies, S. C.; Marcelin, J. R. Confronting Antimicrobial Resistance beyond the COVID-19 Pandemic and the 2020 US Election. *Lancet* **2020**, *396* (10257), 1050–1053. https://doi.org/10.1016/S0140-6736(20)32063-8.

(7) Anderson, R. M. The Pandemic of Antibiotic Resistance. *Nat. Med.* **1999**, *5* (2), 147–149. https://doi.org/10.1038/5507.

(8) Laws, M.; Shaaban, A.; Rahman, K. M. Antibiotic Resistance Breakers: Current Approaches and Future Directions. *FEMS Microbiol. Rev.* **2019**, *43* (5), 490–516. https://doi.org/10.1093/femsre/fuz014.

(9) Davies, J. Origins and Evolution of Antibiotic Resistance. *Microbiol. Mol. Biol. Rev.* **1996**, *12* (1), 9–16. https://doi.org/10.1128/mmbr.00016-10.

(10) C Reygaert, W. An Overview of the Antimicrobial Resistance Mechanisms of Bacteria. *AIMS Microbiol.* **2018**, *4* (3), 482–501. https://doi.org/10.3934/microbiol.2018.3.482.

(11) *Global Tuberculosis Report 2020*; World Health Organization: Geneva, 2020.

(12) Ling, L. L.; Schneider, T.; Peoples, A. J.; Spoering, A. L.; Engels, I.; Conlon, B. P.; Mueller, A.; Schäberle, T. F.; Hughes, D. E.; Epstein, S.; Jones, M.; Lazarides, L.; Steadman, V. A.; Cohen, D. R.; Felix, C. R.; Fetterman, K. A.; Millett, W. P.; Nitti, A. G.; Zullo, A. M.; Chen, C.; Lewis, K. A New Antibiotic Kills Pathogens without Detectable Resistance. *Nature* **2015**, *517* (7535), 455–459. https://doi.org/10.1038/nature14098.

(13) Yang, H.; Wierzbicki, M.; Du Bois, D. R.; Nowick, J. S. X-Ray Crystallographic Structure of a Teixobactin Derivative Reveals Amyloid-like Assembly. *J. Am. Chem. Soc.* **2018**, 8–12. https://doi.org/10.1021/jacs.8b07709.

(14) Shukla, R.; Medeiros-Silva, J.; Parmar, A.; Vermeulen, B. J. A.; Das, S.; Paioni, A. L.; Jekhmane, S.; Lorent, J.; Bonvin, A. M. J. J.; Baldus, M.; Lelli, M.; Veldhuizen, E. J. A.; Breukink, E.; Singh, I.; Weingarth, M. Mode of Action of Teixobactins in Cellular Membranes. *Nat. Commun.* **2020**, *11* (1), 1–10. https://doi.org/10.1038/s41467-020-16600-2.

(15) Gunjal, V. B.; Thakare, R. P.; Chopra, S.; Reddy, D. S. Teixobactin: A Paving Stone towards A New Class of Antibiotics? *J. Med. Chem.* **2020**. https://doi.org/10.1021/acs.jmedchem.0c00173.

(16) Homma, T.; Nuxoll, A.; Gandt, A. B.; Ebner, P.; Engels, I.; Schneider, T.; Götz, F.; Lewis, K.; Conlon, B. P. Dual Targeting of Cell Wall Precursors by Teixobactin Leads to Cell Lysis. *Antimicrob. Agents Chemother.* **2016**, *60* (11), 6510–6517. https://doi.org/10.1128/AAC.01050-16.

(17) Giltrap, A. M.; Dowman, L. J.; Nagalingam, G.; Ochoa, J. L.; Linington, R. G.; Britton, W. J.; Payne, R. J. Total Synthesis of Teixobactin. *Org. Lett.* **2016**, *18* (11), 2788–2791. https://doi.org/10.1021/acs.orglett.6b01324.

(18) Jin, K.; Sam, I. H.; Po, K. H. L.; Lin, D.; Ghazvini Zadeh, E. H.; Chen, S.; Yuan, Y.; Li, X. Total Synthesis of Teixobactin. *Nat. Commun.* **2016**, *7*. https://doi.org/10.1038/ncomms12394.

(19) Liu, L.; Wu, S.; Wang, Q.; Zhang, M.; Wang, B.; He, G.; Chen, G. Total Synthesis of Teixobactin and Its Stereoisomers. *Org. Chem. Front.* **2018**, *5* (9), 1431–1435. https://doi.org/10.1039/c8qo00145f.

(20) Gao, B.; Chen, S.; Hou, Y. N.; Zhao, Y. J.; Ye, T.; Xu, Z. Solution-Phase Total Synthesis of Teixobactin. *Org. Biomol. Chem.* **2019**, *17* (5), 1141–1153. https://doi.org/10.1039/c8ob02803f.

(21) Jin, K.; Po, K. H. L.; Wang, S.; Reuven, J. A.; Wai, C. N.; Lau, H. T.; Chan, T. H.; Chen, S.; Li, X. Synthesis and Structure-Activity Relationship of Teixobactin Analogues via Convergent Ser Ligation. *Bioorganic Med. Chem.* **2017**, *25* (18), 4990–4995. https://doi.org/10.1016/j.bmc.2017.04.039.

(22) Chen, K. H.; Le, S. P.; Han, X.; Frias, J. M.; Nowick, J. S. Alanine Scan Reveals Modifiable Residues in Teixobactin. *Chem. Commun.* **2017**, *53* (82), 11357–11359. https://doi.org/10.1039/c7cc03415f.

(23) Monaim, S. A. H. A.; Noki, S.; Ramchuran, E. J.; El-Faham, A.; Albericio, F.; Torre, B. G. d. la. Investigation of the N-Terminus Amino Function of Arg10-Teixobactin. *Molecules* **2017**, *22* (10), 1–9. https://doi.org/10.3390/molecules22101632.

(24) Schumacher, C. E.; Harris, P. W. R.; Ding, X. B.; Krause, B.; Wright, T. H.; Cook, G. M.;

Furkert, D. P.; Brimble, M. A. Synthesis and Biological Evaluation of Novel Teixobactin Analogues. *Org. Biomol. Chem.* **2017**, *15* (41), 8755–8760. https://doi.org/10.1039/c7ob02169k.

(25) Parmar, A.; Iyer, A.; Prior, S. H.; Lloyd, D. G.; Leng Goh, E. T.; Vincent, C. S.; Palmai-Pallag, T.; Bachrati, C. Z.; Breukink, E.; Madder, A.; Lakshminarayanan, R.; Taylor, E. J.; Singh, I. Teixobactin Analogues Reveal Enduracididine to Be Non-Essential for Highly Potent Antibacterial Activity and Lipid II Binding. *Chem. Sci.* **2017**, *8* (12), 8183–8192. https://doi.org/10.1039/c7sc03241b.

(26) Jin, K.; Po, K. H. L.; Kong, W. Y.; Lo, C. H.; Lo, C. W.; Lam, H. Y.; Sirinimal, A.; Reuven, J. A.; Chen, S.; Li, X. Synthesis and Antibacterial Studies of Teixobactin Analogues with Non-Isostere Substitution of Enduracididine. *Bioorganic Med. Chem.* **2018**, *26* (5), 1062–1068. https://doi.org/10.1016/j.bmc.2018.01.016.

(27) Parmar, A.; Lakshminarayanan, R.; Iyer, A.; Mayandi, V.; Leng Goh, E. T.; Lloyd, D. G.; Chalasani, M. L. S.; Verma, N. K.; Prior, S. H.; Beuerman, R. W.; Madder, A.; Taylor, E. J.; Singh, I. Design and Syntheses of Highly Potent Teixobactin Analogues against Staphylococcus Aureus, Methicillin-Resistant Staphylococcus Aureus (MRSA), and Vancomycin-Resistant Enterococci (VRE) in Vitro and in Vivo. *J. Med. Chem.* **2018**, *61* (5), 2009–2017. https://doi.org/10.1021/acs.jmedchem.7b01634.

(28) Girt, G. C.; Mahindra, A.; Al Jabri, Z. J. H.; De Ste Croix, M.; Oggioni, M. R.; Jamieson, A. G. Lipopeptidomimetics Derived from Teixobactin Have Potent Antibacterial Activity against: Staphylococcus Aureus. *Chem. Commun.* **2018**, *54* (22), 2767–2770. https://doi.org/10.1039/c7cc06093a.

(29) Guo, C.; Mandalapu, D.; Ji, X.; Gao, J.; Zhang, Q. Chemistry and Biology of Teixobactin.

Chem. - A Eur. J. **2018**, *24* (21), 5406–5422. https://doi.org/10.1002/chem.201704167.

(30) Zong, Y.; Sun, X.; Gao, H.; Meyer, K. J.; Lewis, K.; Rao, Y. Developing Equipotent Teixobactin Analogues against Drug-Resistant Bacteria and Discovering a Hydrophobic Interaction between Lipid II and Teixobactin. *J. Med. Chem.* **2018**, *61* (8), 3409–3421. https://doi.org/10.1021/acs.jmedchem.7b01241.

(31) Jad, Y. E.; Acosta, G. A.; Naicker, T.; Ramtahal, M.; El-Faham, A.; Govender, T.; Kruger, H. G.; De La Torre, B. G.; Albericio, F. Synthesis and Biological Evaluation of a Teixobactin Analogue. *Org. Lett.* **2015**, *17* (24), 6182–6185. https://doi.org/10.1021/acs.orglett.5b03176.

(32) Ng, V.; Kuehne, S. A.; Chan, W. C. Rational Design and Synthesis of Modified Teixobactin Analogues: In Vitro Antibacterial Activity against Staphylococcus Aureus, Propionibacterium Acnes and Pseudomonas Aeruginosa. *Chem. - A Eur. J.* **2018**, *24* (36), 9136–9147. https://doi.org/10.1002/chem.201801423.

(33) Mandalapu, D.; Ji, X.; Chen, J.; Guo, C.; Liu, W. Q.; Ding, W.; Zhou, J.; Zhang, Q. Thioesterase-Mediated Synthesis of Teixobactin Analogues: Mechanism and Substrate Specificity. *J. Org. Chem.* **2018**, *83* (13), 7271–7275. https://doi.org/10.1021/acs.joc.7b02462.

(34) Ramchuran, E. J.; Somboro, A. M.; Monaim, S. A. H. A.; Amoako, D. G.; Parboosing, R.; Kumalo, H. M.; Agrawal, N.; Albericio, F.; de La Torre, B. G.; Bester, L. A. In Vitro Antibacterial Activity of Teixobactin Derivatives on Clinically Relevant Bacterial Isolates. *Front. Microbiol.* **2018**, *9* (JUL), 1–10. https://doi.org/10.3389/fmicb.2018.01535.

(35) Malkawi, R.; Iyer, A.; Parmar, A.; Lloyd, D. G.; Leng Goh, E. T.; Taylor, E. J.; Sarmad,

S.; Madder, A.; Lakshminarayanan, R.; Singh, I. Cysteines and Disulfide-Bridged Macrocyclic Mimics of Teixobactin Analogues and Their Antibacterial Activity Evaluation against Methicillin-Resistant Staphylococcus Aureus (MRSA). *Pharmaceutics* **2018**, *10* (4), 1–8. https://doi.org/10.3390/pharmaceutics10040183.

(36) Gunjal, V. B.; Reddy, D. S. Total Synthesis of Met10-Teixobactin. *Tetrahedron Lett.* **2019**, *60* (29), 1909–1912. https://doi.org/10.1016/j.tetlet.2019.06.027.

(37) Zong, Y.; Fang, F.; Meyer, K. J.; Wang, L.; Ni, Z.; Gao, H.; Lewis, K.; Zhang, J.; Rao, Y. Gram-Scale Total Synthesis of Teixobactin Promoting Binding Mode Study and Discovery of More Potent Antibiotics. *Nat. Commun.* **2019**, *10* (1). https://doi.org/10.1038/s41467-019-11211-y.

(38) Morris, M. A.; Malek, M.; Hashemian, M. H.; Nguyen, B. T.; Manuse, S.; Lewis, K.; Nowick, J. S. A Fluorescent Teixobactin Analogue. *ACS Chem. Biol.* **2020**, *15* (5), 1222–1231. https://doi.org/10.1021/acschembio.9b00908.

(39) Parmar, A.; Iyer, A.; Vincent, C. S.; Van Lysebetten, D.; Prior, S. H.; Madder, A.; Taylor, E. J.; Singh, I. Efficient Total Syntheses and Biological Activities of Two Teixobactin Analogues. *Chem. Commun.* **2016**, *52* (36), 6060–6063. https://doi.org/10.1039/c5cc10249a.

(40) Yang, H.; Chen, K. H.; Nowick, J. S. Elucidation of the Teixobactin Pharmacophore. *ACS Chem. Biol.* **2016**, *11* (7), 1823–1826. https://doi.org/10.1021/acschembio.6b00295.

(41) Abdel Monaim, S. A. H.; Jad, Y. E.; Acosta, G. A.; Naicker, T.; Ramchuran, E. J.; El-Faham, A.; Govender, T.; Kruger, H. G.; De La Torre, B. G.; Albericio, F. Re-Evaluation of the N-Terminal Substitution and the D-Residues of Teixobactin. *RSC Adv.* **2016**, *6* (77), 73827–73829. https://doi.org/10.1039/c6ra17720d.

(42) Abdel Monaim, S. A. H.; Jad, Y. E.; Ramchuran, E. J.; El-Faham, A.; Govender, T.; Kruger, H. G.; de la Torre, B. G.; Albericio, F. Lysine Scanning of Arg 10 –Teixobactin: Deciphering the Role of Hydrophobic and Hydrophilic Residues . *ACS Omega* **2016**, *1* (6), 1262–1265. https://doi.org/10.1021/acsomega.6b00354.

(43) Wu, C.; Pan, Z.; Yao, G.; Wang, W.; Fang, L.; Su, W. Synthesis and Structure-Activity Relationship Studies of Teixobactin Analogues. *RSC Adv.* **2017**, *7* (4), 1923–1926. https://doi.org/10.1039/c6ra26567g.

(44) Parmar, A.; Prior, S. H.; Iyer, A.; Vincent, C. S.; Van Lysebetten, D.; Breukink, E.; Madder, A.; Taylor, E. J.; Singh, I. Defining the Molecular Structure of Teixobactin Analogues and Understanding Their Role in Antibacterial Activities. *Chem. Commun.* **2017**, *53* (12), 2016–2019. https://doi.org/10.1039/c6cc09490b.

(45) Yang, H.; Du Bois, D. R.; Ziller, J. W.; Nowick, J. S. X-Ray Crystallographic Structure of a Teixobactin Analogue Reveals Key Interactions of the Teixobactin Pharmacophore. *Chem. Commun.* **2017**, *53* (18), 2772–2775. https://doi.org/10.1039/c7cc00783c.

(46) Kocaoglu, O.; Carlson, E. E. Progress and Prospects for Small-Molecule Probes of Bacterial Imaging. *Nat. Chem. Biol.* **2016**, *12* (7), 472–478. https://doi.org/10.1038/nchembio.2109.

(47) Stone, M. R. L.; Butler, M. S.; Phetsang, W.; Cooper, M. A.; Blaskovich, M. A. T. Fluorescent Antibiotics: New Research Tools to Fight Antibiotic Resistance. *Trends Biotechnol.* **2018**, *36* (5), 523–536. https://doi.org/10.1016/j.tibtech.2018.01.004.

(48) Tiyanont, K.; Doan, T.; Lazarus, M. B.; Fang, X.; Rudner, D. Z.; Walker, S. Imaging Peptidoglycan Biosynthesis in Bacillus Subtilis with Fluorescent Antibiotics. *Proc. Natl. Acad. Sci. U. S. A.* **2006**, *103* (29), 11033–11038.

https://doi.org/10.1073/pnas.0600829103.

(49) Calloway, N. T.; Choob, M.; Sanz, A.; Sheetz, M. P.; Miller, L. W.; Cornish, V. W. Optimized Fluorescent Trimethoprim Derivatives for in Vivo Protein Labeling. *ChemBioChem* **2007**, *8* (7), 767–774. https://doi.org/10.1002/cbic.200600414.

(50) Wang, T. Y.; Friedman, L. J.; Gelles, J.; Min, W.; Hoskins, A. A.; Cornish, V. W. The Covalent Trimethoprim Chemical Tag Facilitates Single Molecule Imaging with Organic Fluorophores. *Biophys. J.* **2014**, *106* (1), 272–278. https://doi.org/10.1016/j.bpj.2013.11.4488.

(51) Akram, A. R.; Avlonitis, N.; Lilienkampf, A.; Perez-Lopez, A. M.; Mcdonald, N.; Chankeshwara, S. V.; Scholefield, E.; Haslett, C.; Bradley, M.; Dhaliwal, K. A Labelled-Ubiquicidin Antimicrobial Peptide for Immediate in Situ Optical Detection of Live Bacteria in Human Alveolar Lung Tissue. *Chem. Sci.* **2015**, *6* (12), 6971–6979. https://doi.org/10.1039/c5sc00960j.

(52) Leevy, W. M.; Gammon, S. T.; Jiang, H.; Johnson, J. R.; Maxwell, D. J.; Jackson, E. N.; Marquez, M.; Piwnica-Worms, D.; Smith, B. D. Optical Imaging of Bacterial Infection in Living Mice Using a Fluorescent Near-Infrared Molecular Probe. *J. Am. Chem. Soc.* **2006**, *128* (51), 16476–16477. https://doi.org/10.1021/ja0665592.

(53) Leevy, W. M.; Gammon, S. T.; Johnson, J. R.; Lampkins, A. J.; Jiang, H.; Marquez, M.; Piwnica-Worms, D.; Suckow, M. A.; Smith, B. D. Noninvasive Optical Imaging of Staphylococcus Aureus Bacterial Infection in Living Mice Using a Bis-Dipicolylamine-Zinc(II) Affinity Group Conjugated to a near-Infrared Fluorophore. *Bioconjug. Chem.* **2008**, *19* (3), 686–692. https://doi.org/10.1021/bc700376v.

(54) Van Oosten, M.; Schäfer, T.; Gazendam, J. A. C.; Ohlsen, K.; Tsompanidou, E.; De

Goffau, M. C.; Harmsen, H. J. M.; Crane, L. M. A.; Lim, E.; Francis, K. P.; Cheung, L.; Olive, M.; Ntziachristos, V.; Van Dijl, J. M.; Van Dam, G. M. Real-Time in Vivo Imaging of Invasive- and Biomaterial-Associated Bacterial Infections Using Fluorescently Labelled Vancomycin. *Nat. Commun.* **2013**, *4*. https://doi.org/10.1038/ncomms3584.

(55) Chen, H.; Liu, C.; Chen, D.; Madrid, K.; Peng, S.; Dong, X.; Zhang, M.; Gu, Y. Bacteria-Targeting Conjugates Based on Antimicrobial Peptide for Bacteria Diagnosis and Therapy. *Mol. Pharm.* **2015**, *12* (7), 2505–2516. https://doi.org/10.1021/acs.molpharmaceut.5b00053.

(56) Daniel, R. A.; Errington, J. Control of Cell Morphogenesis in Bacteria: Two Distinct Ways to Make a Rod-Shaped Cell. *Cell* **2003**, *113* (6), 767–776. https://doi.org/10.1016/S0092-8674(03)00421-5.

Chapter 2[a]

A Fluorescent Teixobactin Analogue

Introduction

Fluorescent analogues of antibiotics can provide valuable insights into the modes of action of antibiotics and antibiotic resistance and have facilitated the development of new antibiotics.[1,2] Fluorescent antibiotic analogues enable tracking the drug and its interactions not only within bacterial cells but also within mammalian cells,[3,4] human tissue,[5] and live[6-8] and postmortem[9] animals. Penicillin V tagged with BODIPY FL (BOCILLIN-FL) has been used to characterize mechanisms of antibiotic resistance in bacteria by targeting penicillin-binding proteins (PBPs) using profiling assays and flow cytometry.[10-12] Fluorescein-labeled vancomycin has enabled the study of peptidoglycan biosynthesis in *B. subtilis* by fluorescence microscopy and has revealed a possible helical pattern of cylindrical wall synthesis.[13] Vancomycin and ramoplanin functionalized with fluorescent dyes have been used to study the complicated machinery involved in the biosynthesis of peptidoglycan and have revealed information about fundamental growth processes in Gram-positive bacteria.[14] Fluorescent analogues of cephalosporin C have been shown to label a specific subset of PBPs and were used to investigate the localization of PBPs in Gram-positive bacteria.[15] Studies with fluorescent antibiotic analogues are likely to become more important against the growing threat of antibiotic-resistant pathogens because they can illuminate modes of antibiotic action and serve as rapid diagnostics that can detect bacterial infections.

[a]This chapter is adapted from Morris, M. A., Malek, M., Hashemian, M. H., Nguyen, B. T., Manuse, S., Lewis, K., and Nowick, J. S. *ACS Chem. Biol.* **2020**, *15,* 1222–1231.

In 2015, the antibiotic teixobactin was reported.[16] Teixobactin is a nonribosomal peptide composed of eleven amino acids and containing a depsipeptide macrocycle. Teixobactin inhibits the biosynthesis of peptidoglycan and teichoic acid, interfering with cell wall formation and resulting in cell lysis.[16,17] Teixobactin binds to the pyrophosphates of lipids II and III and related cell wall precursors, which are thought to be immutable targets, making it difficult or impossible for bacteria to become resistant. To our knowledge, the cellular localization of teixobactin has not been characterized by fluorescence microscopy.[18]

As part of a program of research aimed at understanding the mechanism of action of teixobactin and developing analogues with improved biological properties, we now introduce a fluorescent analogue of teixobactin and demonstrate that it stains the septa and sidewalls of Gram-positive bacteria. The analogue, Lys(Rhod)$_9$,Arg$_{10}$-teixobactin, contains the fluorophore sulforhodamine B (Lissamine^{TM} rhodamine B) attached to the ε-amino group of lysine, in place of the native alanine residue at position 9, and arginine in place of the native *allo*-enduracididine residue at position 10 (Figure 2.1). We incorporated a fluorescent tag at position 9, because structure activity relationship (SAR) studies of the teixobactin pharmacophore established that position 9 tolerates mutations without substantial loss of antibiotic activity.[19,20] We chose sulforhodamine B, because it is suitable for fluorescence microscopy, compatible with solid-phase peptide synthesis (SPPS), easy to incorporate, relatively inexpensive, and commercially available as a single isomer. In aqueous solutions, the sulforhodamine B fluorophore has reported absorption and emission maxima of 564 nm and 583 nm, respectively, with a molar absorptivity coefficient of 71,500 M^{-1} cm^{-1} and a quantum yield of 0.33.[21] Sulforhodamine B is commercially available as the reactive sulfonyl chloride for about $300/g, making it suitable for use as a building block in SPPS. Many other popular fluorescent dyes, including the Alexa Fluor® and BODIPY families,

are prohibitively expensive for the reaction scales used in SPPS. Efforts to use fluorescein isothiocyanate (FITC) — another popular and economical fluorophore — were unsuccessful in the synthetic route that we developed, as the label proved incompatible with the cyclization reaction.

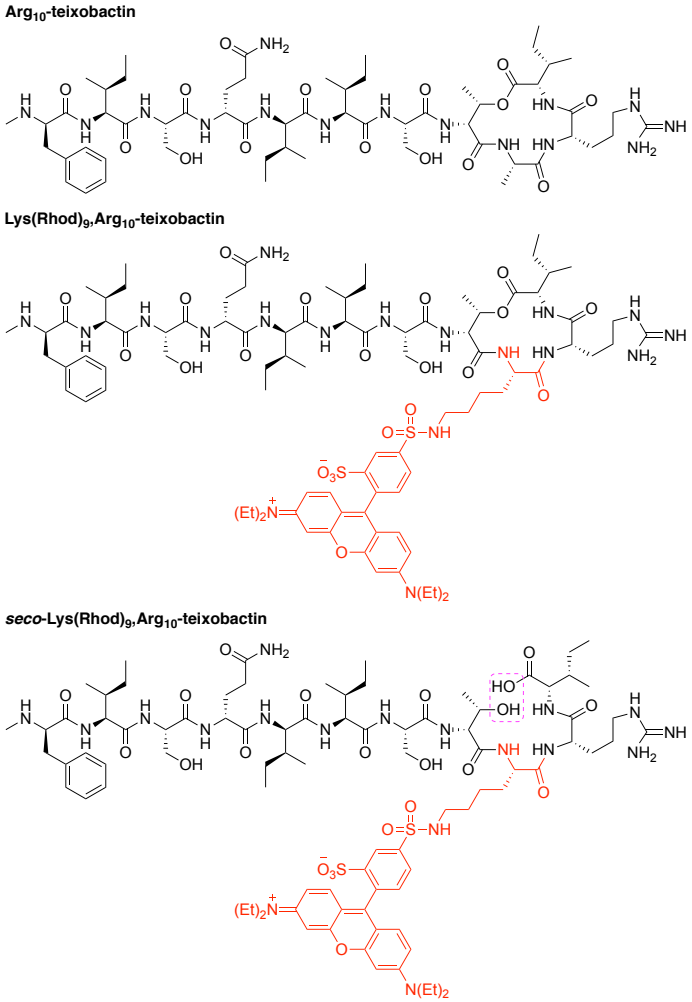

Figure 2.1. Structures of Arg_{10}-teixobactin, Lys(Rhod)$_9$,Arg_{10}-teixobactin, and *seco*-Lys(Rhod)$_9$,Arg_{10}-teixobactin.

Results and Discussion

We adapted our research group's synthesis of teixobactin analogues[22] to allow incorporation of sulforhodamine B at position 9. I synthesized Lys(Rhod)$_9$,Arg_{10}-teixobactin by Fmoc-based SPPS to give the protected linear peptide, where the side-chain amino group of Lys_9 is protected with the allyloxycarbonyl (Alloc) group (Scheme 2.1). The Alloc protecting group

was removed using $Pd(PPh_3)_4$ and $PhSiH_3$, and the side-chain of Lys_9 was labeled using sulforhodamine B sulfonyl chloride.[23] The on-resin synthesis allows regioselective labeling, efficient reaction, and removal of excess fluorophore. The rhodamine fluorophore tolerated subsequent SPPS reactions — Ile_{11} esterification with DIC and DMAP, cleavage with HFIP, cyclization with HBTU and HOBt, and global deprotection with $TFA/H_2O/TIPS$. Synthesis on a 0.16 mmol scale typically yielded 3–11 mg of $Lys(Rhod)_9,Arg_{10}$-teixobactin as the trifluoroacetate (TFA) salt after purification by RP-HPLC.[24] I also synthesized the acyclic analogue *seco*-$Lys(Rhod)_9,Arg_{10}$-teixobactin as a negative control containing the fluorophore but lacking antibiotic activity (Figure 2.1).

Scheme 2.1. Synthesis of $Lys(Rhod)_9,Arg_{10}$-teixobactin.

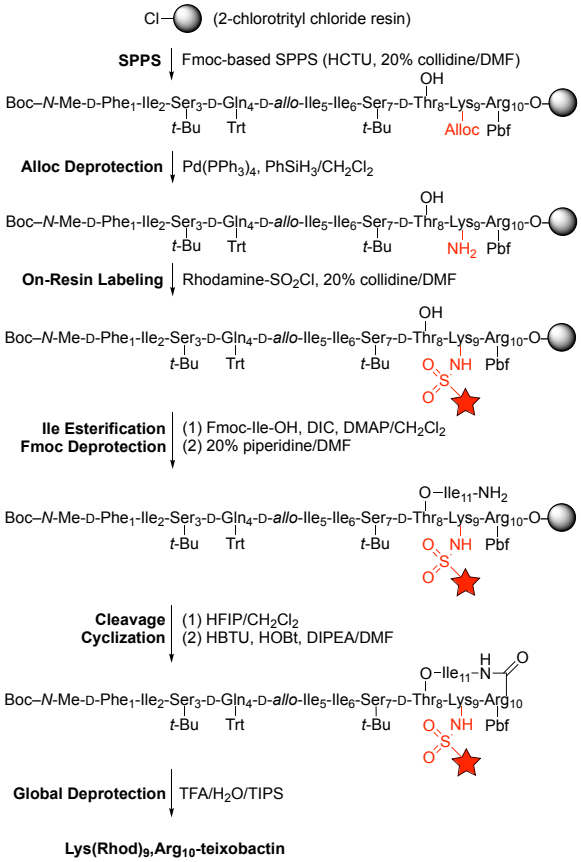

I evaluated the antimicrobial activity of Lys(Rhod)$_9$,Arg$_{10}$-teixobactin using minimum inhibitory concentration (MIC) assays with five Gram-positive bacteria. I used Arg$_{10}$-teixobactin as a positive control and *E. coli* and the acyclic analogue *seco*-Lys(Rhod)$_9$,Arg$_{10}$-teixobactin as negative controls. Lys(Rhod)$_9$,Arg$_{10}$-teixobactin partially retained antibiotic activity, with minimum inhibitory concentrations of 4–8 μg/mL against the five Gram-positive bacteria, making it ca. four-fold less active than the parent Arg$_{10}$-teixobactin (Table 2.1). Comparable diminution of antibiotic activity has been observed in a number of fluorescent analogues of other antibiotics.[2] Like teixobactin and other teixobactin analogues, Lys(Rhod)$_9$,Arg$_{10}$-teixobactin proved inactive against the Gram-negative bacterium *E. coli*. *seco*-Lys(Rhod)$_9$,Arg$_{10}$-teixobactin was inactive toward all bacteria tested, reflecting the need for an intact macrolactone ring[22] and establishing that the sulforhodamine B moiety does not impart antibiotic activity.[24]

Table 2.1. MIC values of teixobactin analogues in μg/mL.

	Bacillus subtilis ATCC 6051	*Enterococcus durans* ATCC 6056	*Streptococcus salivarius* ATCC 13419	*Staphylococcus aureus* ATCC 29213	*Staphylococcus epidermidis* ATCC 14990	*Escherichia coli* ATCC 10798
Lys(Rhod)$_9$,Arg$_{10}$-teixobactin	4	8	4	8	8	>32
Arg$_{10}$-teixobactin	1	4	1	2	2	>32
seco-Lys(Rhod)$_9$,Arg$_{10}$-teixobactin	>32	>32	>32	>32	>32	>32

I initially attempted to image *B. subtilis* with a 4 μg/mL Lys(Rhod)$_9$,Arg$_{10}$-teixobactin solution, which we prepared by diluting a 1 mg/mL DMSO stock solution with sodium phosphate buffer. When we treated *B. subtilis* with this solution, I observed aggregates of the fluorescent teixobactin analogue surrounding the bacteria (Figure 2.2). These aggregates are visible as a red haze and bright red spots in fluorescence micrographs. The aggregates appear to be a manifestation of the propensity of teixobactin and active teixobactin analogues to form gels and amyloid-like

fibrils in water, buffer, and culture media.[20,25] The adhesion of these aggregates to the bacteria may reflect binding of the aggregated teixobactin to the wall teichoic acid (WTA), which in conjunction with peptidoglycan comprises the bacterial cell wall of Gram-positive bacteria. Our laboratory has previously observed that fibril-like assemblies formed by a teixobactin analogue bind sulfate anions, and we envision that aggregates of teixobactin or Lys(Rhod)$_9$,Arg$_{10}$-teixobactin could bind to the phosphate groups of WTA in a similar fashion.[25]

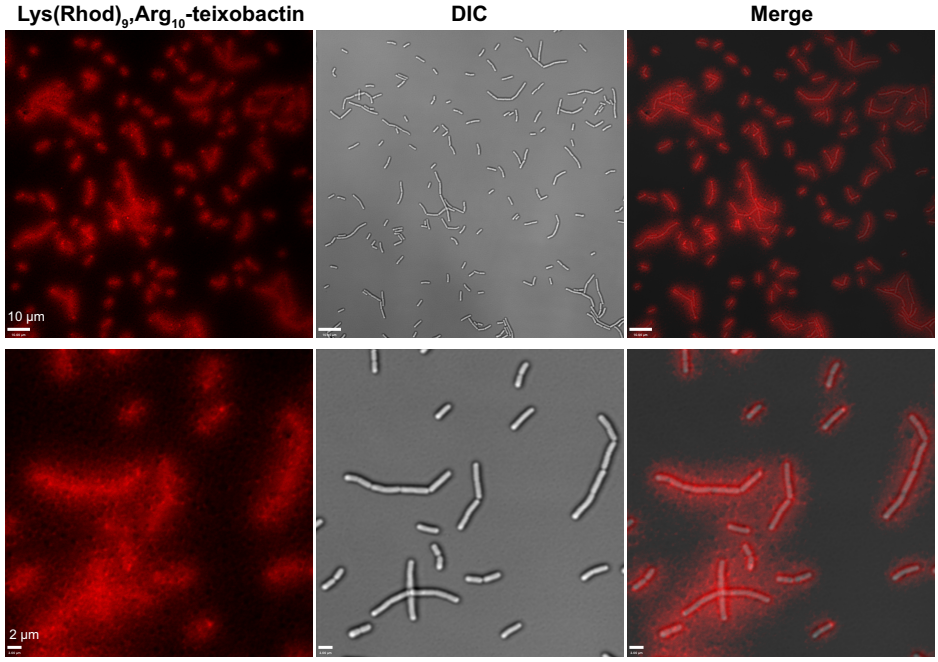

Figure 2.2. Fluorescence and differential interference contrast (DIC) micrographs of *B. subtilis* treated with 4 µg/mL of Lys(Rhod)$_9$,Arg$_{10}$-teixobactin in sodium phosphate buffer containing no polysorbate 80. Fluorescence micrographs were recorded with excitation at 561 nm. Scale bars of the top row images are 10 µm, while the scale bars of the bottom row images are 2 µm.

To eliminate these fluorescent aggregates, I drew upon the original report of teixobactin, in which 0.002% polysorbate 80, a mild nonionic detergent, was added to the test media for MIC assays.[16] When I included 0.002% polysorbate 80 in the diluted solutions of Lys(Rhod)$_9$,Arg$_{10}$-teixobactin, the formation of fluorescent aggregates was reduced. Inclusion of 0.05% polysorbate 80 in the diluted solutions of Lys(Rhod)$_9$,Arg$_{10}$-teixobactin further reduced the formation of

aggregates and led to cleaner staining of the bacteria. When I performed MIC assays with either 0.002% or 0.05% polysorbate 80, the antibiotic activity of Lys(Rhod)$_9$,Arg$_{10}$-teixobactin improved for *B. subtilis* and *S. salivarius*, worsened for *S. aureus* and *E. durans*, and remained the same for *S. epidermidis* (Table 2.2).

Table 2.2. MIC values of teixobactin analogues in μg/mL with 0.002% and 0.05% polysorbate 80.

	Bacillus subtilis ATCC 6051	*Enterococcus durans* ATCC 6056	*Streptococcus salivarius* ATCC 13419	*Staphylococcus aureus* ATCC 29213	*Staphylococcus epidermidis* ATCC 14990	*Escherichia coli* ATCC 10798
Lys(Rhod)$_9$,Arg$_{10}$-teixobactin	2[a]	16[a]	1[a]	16–32[a]	8[a]	>32[a]
	2[b]	16[b]	0.25[b]	32–64[b]	8[b]	>32[b]
Arg$_{10}$-teixobactin	<0.03[a]	2[a]	<0.03[a]	1[a]	0.5[a]	>32[a]
	<0.03[b]	2[b]	<0.03[b]	1[b]	0.5[b]	>32[b]
seco-Lys(Rhod)$_9$,Arg$_{10}$-teixobactin	>32[a]	>32[a]	>32[a]	>32[a]	>32[a]	>32[a]
	>32[b]	>32[b]	>32[b]	>32[b]	>32[b]	>32[b]

[a]Culture media containing 0.002% polysorbate 80
[b]Culture media containing 0.05% polysorbate 80

When I treated *B. subtilis* with 4 μg/mL Lys(Rhod)$_9$,Arg$_{10}$-teixobactin in the presence of 0.05% polysorbate 80, I observed staining of the bacteria with minimal formation of fluorescent aggregates (Figure 2.3A).[26] Staining was pronounced at the septa and weaker at the sidewalls. The staining resulted in a banded pattern in chains of *B. subtilis*, with particularly intense bands at the new division sites and weaker bands at the older division sites, which gave rise to an alternating pattern of weaker and stronger bands. The more intense staining of new division sites is consistent with the antibiotic targeting cell wall biosynthesis and cell division,[13,14] thus supporting the model of teixobactin binding to lipid II, lipid III, and related cell wall precursors. To corroborate the staining of Gram-positive bacteria by Lys(Rhod)$_9$,Arg$_{10}$-teixbactin, I treated and imaged *E. durans*, *S. salivarius*, and *S. aureus* (Figure 2.3B–2.3D). Treatment of *E. durans*, *S. salivarius*, and *S. aureus* with 4 μg/mL of Lys(Rhod)$_9$,Arg$_{10}$-teixobactin resulted in strong septal staining, with notable lateral staining in *E. durans* and *S. salivarius*.

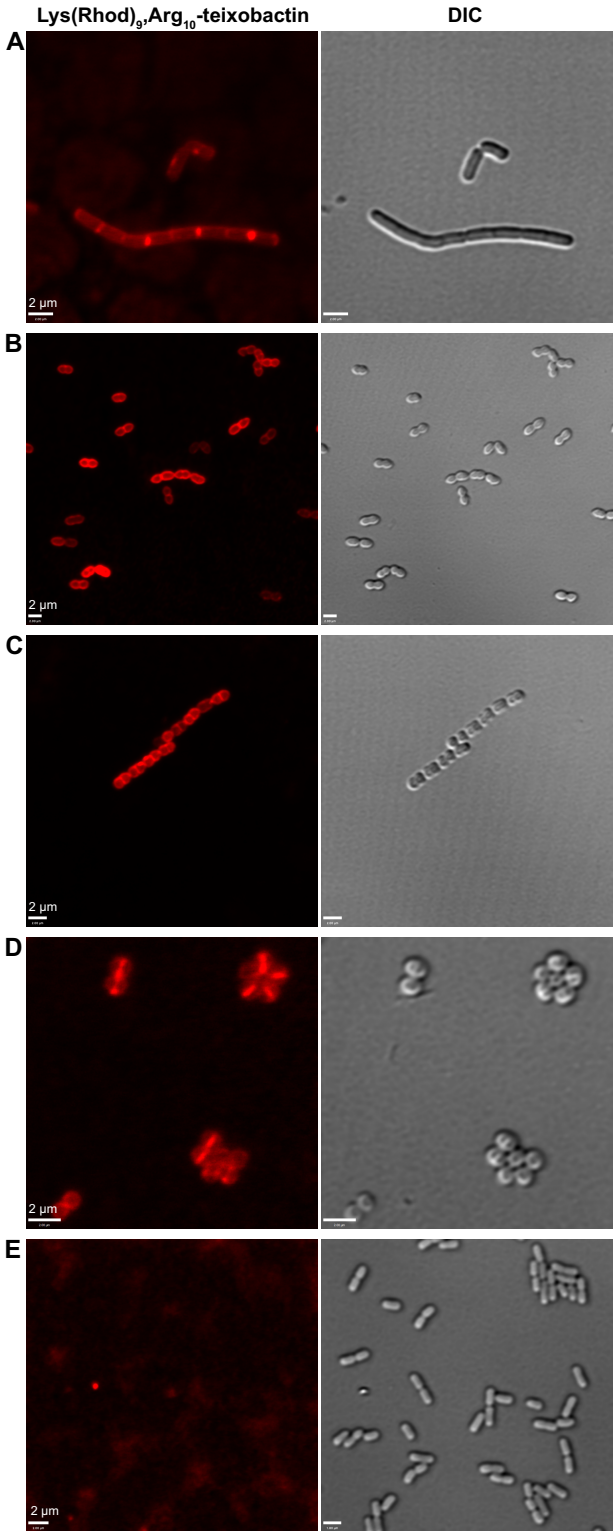

Figure 2.3. Fluorescence and differential interference contrast (DIC) micrographs of (A) *B. subtilis*, (B) *E. durans*, (C) *S. salivarius*, (D) *S. aureus*, and (E) *E. coli* treated with 4 µg/mL of Lys(Rhod)$_9$,Arg$_{10}$-teixobactin in sodium phosphate buffer containing 0.05% polysorbate 80. Fluorescence micrographs were recorded with excitation at 561 nm. Scale bars are 2 µm.

Walker et al. previously demonstrated that equimolar mixtures of unlabeled vancomycin and BODIPY FL vancomycin resulted in enhanced intensity of septal and sidewall staining in *B. subtilis*.[14] They observed similar effects with equimolar mixtures of labeled and unlabeled ramoplanin. When I treated *B. subtilis* concurrently with 1 μg/mL of Lys(Rhod)$_9$,Arg$_{10}$-teixobactin and 1 μg/mL of Arg$_{10}$-teixobactin, I observed intense staining of both old and new division sites and moderate staining of the sidewalls (Figure 2.4). The Walker group hypothesized that the improved staining by 1:1 mixtures of the labeled and unlabeled antibiotics reflects improved fluorescence properties of dimeric vancomycin or ramoplanin bearing only a single fluorescent label. I believe a similar effect occurs with the mixture of labeled and unlabeled teixobactin analogues.

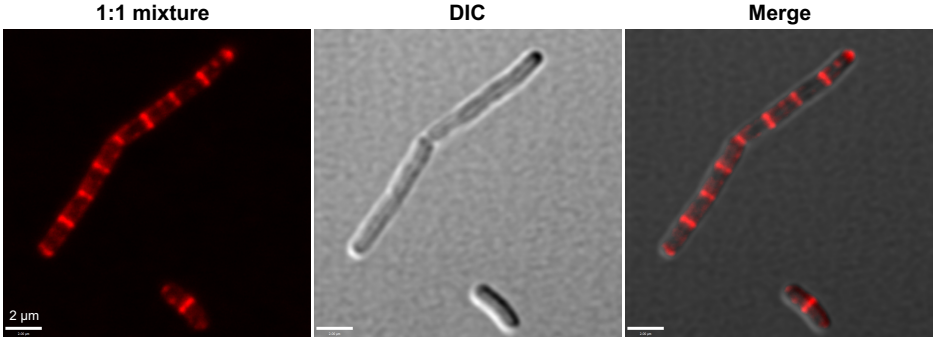

Figure 2.4. Fluorescence and differential interference contrast (DIC) micrographs of *B. subtilis* concurrently treated with 1 μg/mL of Lys(Rhod)$_9$,Arg$_{10}$-teixobactin and 1 μg/mL of Arg$_{10}$-teixobactin in sodium phosphate buffer containing 0.05% polysorbate 80. Fluorescence micrographs were recorded with excitation at 561 nm. Scale bars are 2 μm.

To gain further insight into the staining patterns of Lys(Rhod)$_9$,Arg$_{10}$-teixobactin, I co-stained with BODIPY FL vancomycin, which has previously been used to study peptidoglycan biosynthesis in *B. subtilis*.[14] Although both the teixobactin and vancomycin antibiotics target cell wall precursors, teixobactin targets the undecaprenyl-pyrophosphate-sugar moieties of peptidoglycan and WTA precursors, while vancomycin targets the D-Ala-D-Ala transpeptidase substrate in peptidoglycan cross-linking.[27] Concurrent treatment of *B. subtilis*, *E. durans*, *S.*

salivarius, and *S. aureus* with 4 µg/mL of Lys(Rhod)$_9$,Arg$_{10}$-teixobactin and 4 µg/mL of BODIPY FL vancomycin resulted staining by both fluorescent antibiotics, with prominent staining of the septa and weaker staining of the side walls, and with Lys(Rhod)$_9$,Arg$_{10}$-teixobactin favoring new division sites (Figure 2.5). The septal co-localization of Lys(Rhod)$_9$,Arg$_{10}$-teixobactin and BODIPY FL vancomycin provides further evidence that Lys(Rhod)$_9$,Arg$_{10}$-teixobactin binds to cell wall precursors. Some differences were observed between the staining by the two antibiotics, which may reflect the differing molecular targets of teixobactin and vancomycin.

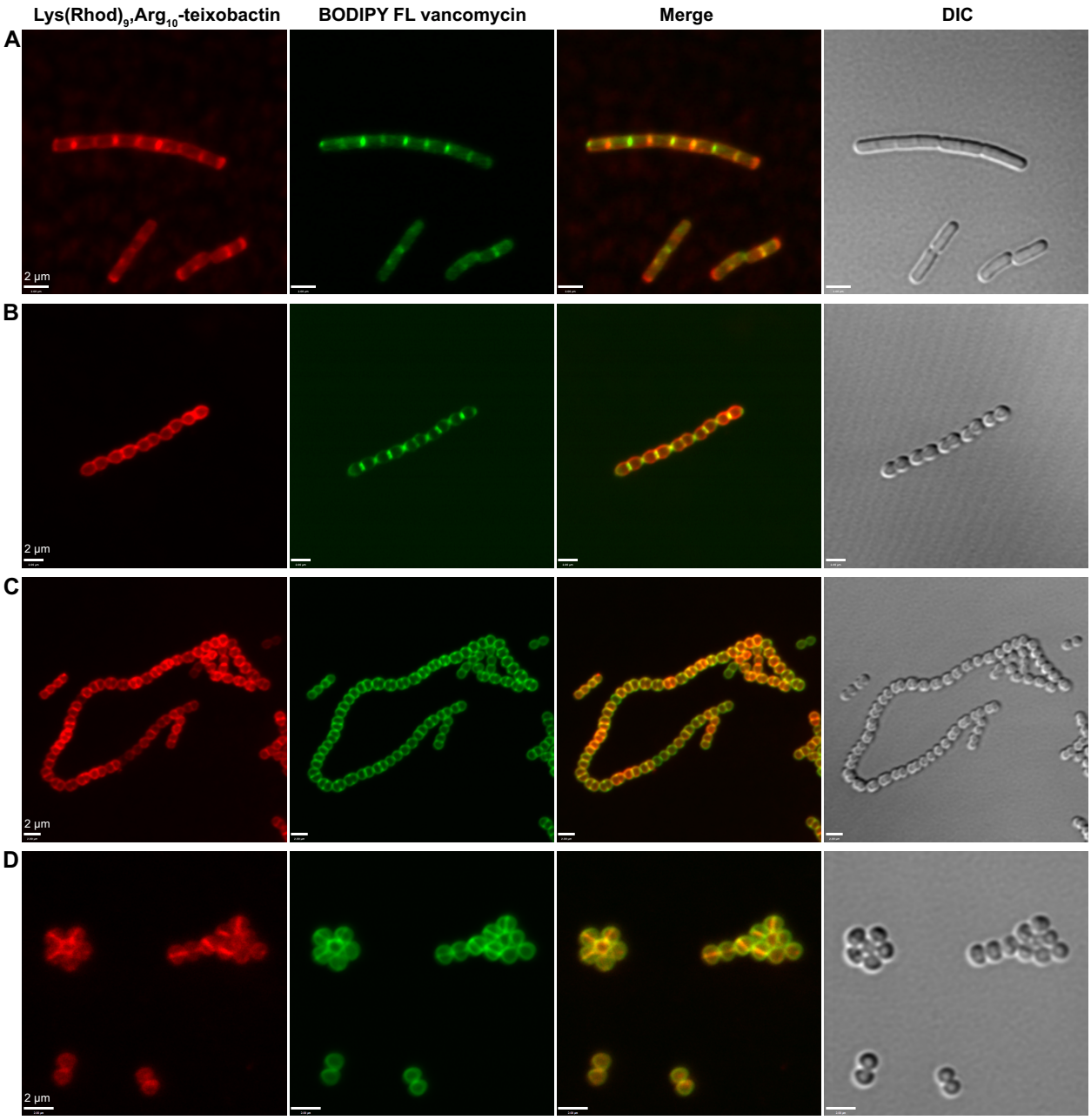

Figure 2.5. Fluorescence and differential interference contrast (DIC) micrographs of (A) *B. subtilis*, (B) *E. durans*, (C) *S. salivarius*, (D) *S. aureus* concurrently treated with 4 µg/mL of Lys(Rhod)$_9$,Arg$_{10}$-teixobactin and 4 µg/mL of BODIPY FL vancomycin in sodium phosphate buffer containing 0.05% polysorbate 80. Fluorescence micrographs were recorded with excitation at 561 nm (left column panel) and 488 nm (right column panel). Scale bars are 2 µm.

I performed three negative controls to establish the specificity of Lys(Rhod)$_9$,Arg$_{10}$-teixobactin toward Gram-positive bacteria: (1) treating *E. coli* (Gram-negative) with

Lys(Rhod)$_9$,Arg$_{10}$-teixobactin, (2) treating *B. subtilis, E. durans*, *S. salivarius*, and *S. aureus* (Gram-positive) with the inactive *seco*-Lys(Rhod)$_9$,Arg$_{10}$-teixobactin analogue, and (3) treating *B. subtilis* with sulforhodamine B *N*-butylsulfonamide. Treatment of *E. coli* with 4 μg/mL of Lys(Rhod)$_9$,Arg$_{10}$-teixobactin resulted in little to no staining (Figure 2.3E). A few (<2%) of the *E. coli* cells showed brighter staining, at levels comparable to the Gram-positive bacteria. The lack of significant staining in *E. coli* indicates that Lys(Rhod)$_9$,Arg$_{10}$-teixobactin, like teixobactin itself, is specific toward Gram-positive bacteria. Treatment of *B. subtilis*, *E. durans*, and *S. salivarius* and *S. aureus* with 4 μg/mL of *seco*-Lys(Rhod)$_9$,Arg$_{10}$-teixobactin resulted in only very weak staining of cells, at levels only slightly above background (Figure 2.6). The lack of significant staining from the *seco*-Lys(Rhod)$_9$,Arg$_{10}$-teixobactin analogue suggests that the intact teixobactin pharmacophore is necessary for staining Gram-positive bacteria. Treatment of *B. subtilis* with 4 μg/mL of sulforhodamine B *N*-butylsulfonamide resulted in no staining (Figure 2.7), further demonstrating that the staining patterns observed in Figures 2.2–2.5 result from specific interactions between Lys(Rhod)$_9$,Arg$_{10}$-teixobactin and bacteria, and not from sulforhodamine B itself.

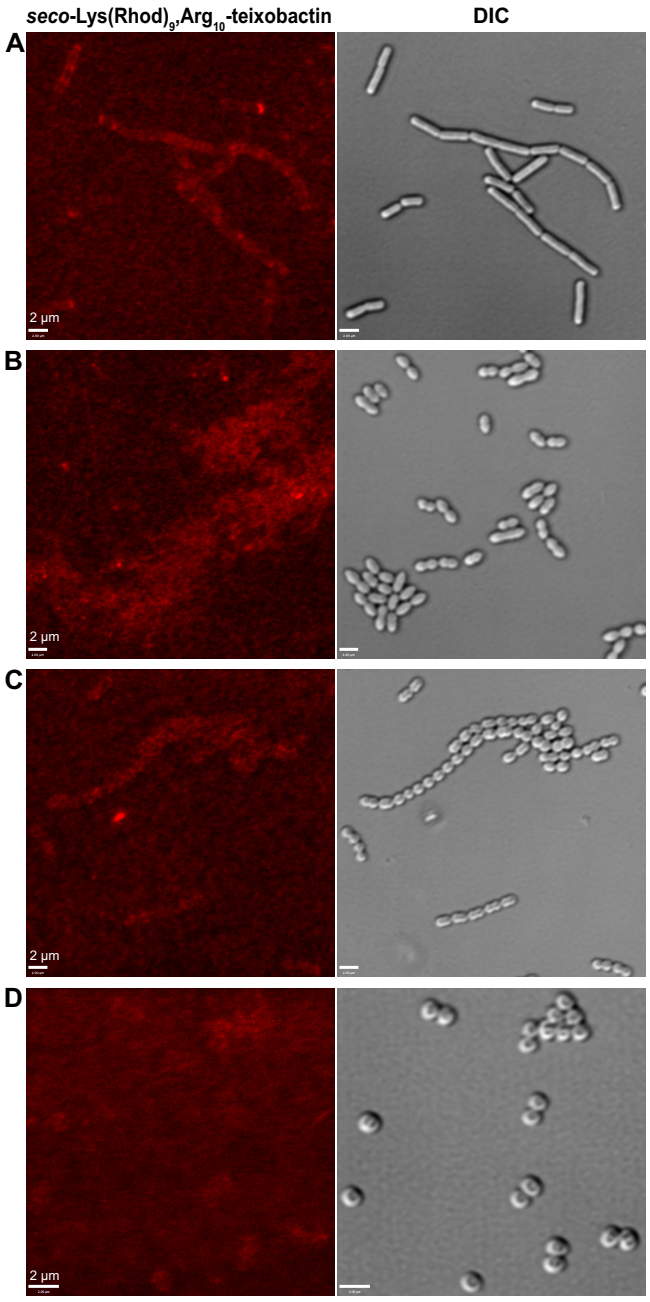

Figure 2.6. Fluorescence and differential interference contrast (DIC) micrographs of (A) *B. subtilis*, (B) *E. durans*, (C) *S. salivarius*, and (D) *S. aureus* treated with 4 µg/mL of *seco*-Lys(Rhod)$_9$,Arg$_{10}$-teixobactin in sodium phosphate buffer containing 0.05% polysorbate 80. Fluorescence micrographs were recorded with excitation at 561 nm. Scale bars are 2 µm.

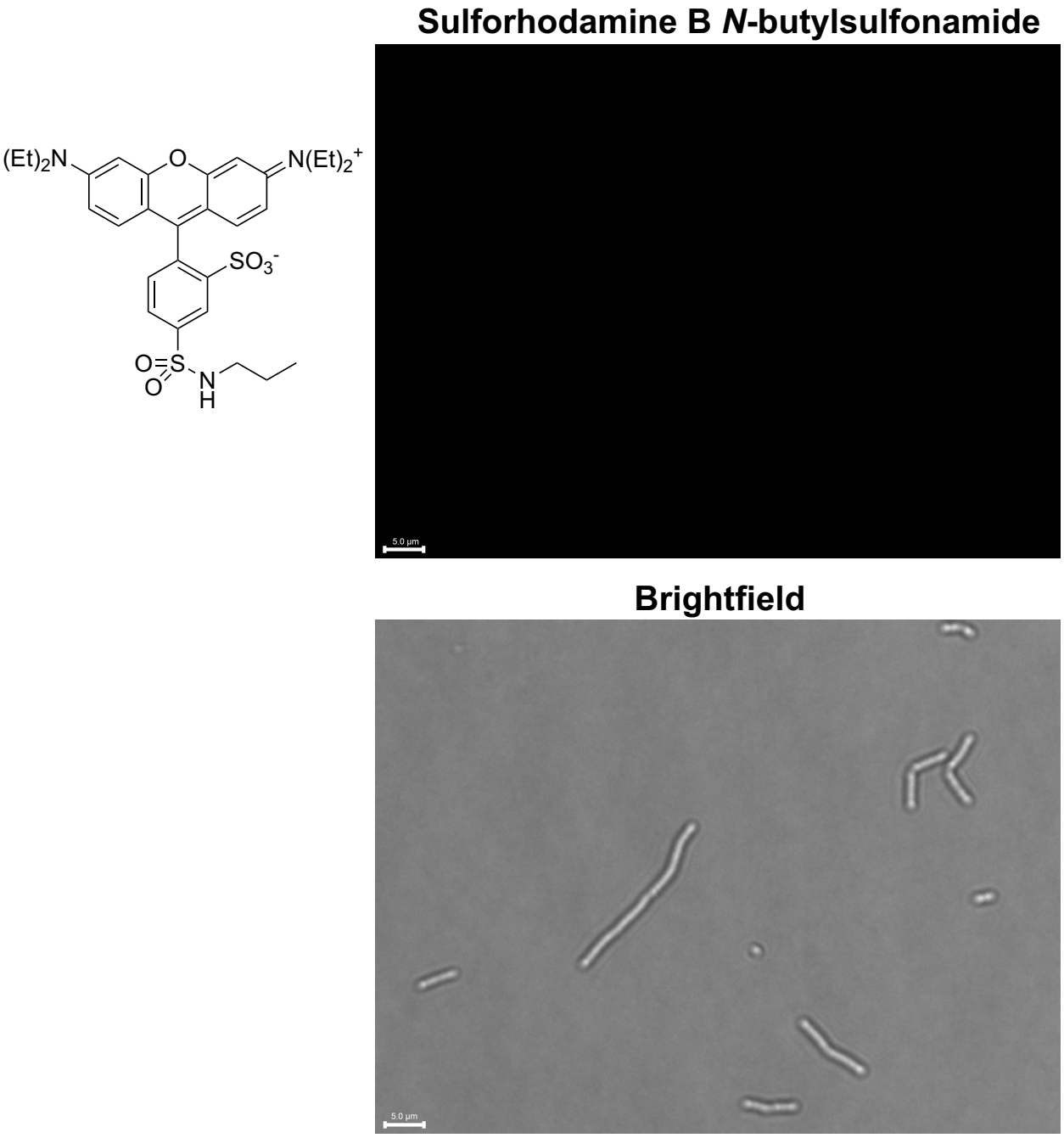

Figure 2.7. Fluorescence and brightfield micrographs of *B. subtilis* treated with 4 µg/mL of sulforhodamine B *N*-butylsulfonamide. Scale bars are 5 µm. Cells were imaged on a Keyence BZ-X810 fluorescence microscope using the TexasRed filter cube (excitation wavelength = 560/40 nm and emission wavelength = 630/75 nm). The exposure was set to 1/10 s. Images were collected with a 60x oil immersion objective lens with optical zoom using the high resolution camera sensitivity and oblique illumination settings.

I also carried out a competition experiment in which we first stained *B. subtilis* with Lys(Rhod)$_9$,Arg$_{10}$-teixobactin and then treated with Arg$_{10}$-teixobactin, to determine if Arg$_{10}$-teixobactin could displace Lys(Rhod)$_9$,Arg$_{10}$-teixobactin. We also carried out a second experiment in which we first treated *B. subtilis* with Arg$_{10}$-teixobactin and then stained with Lys(Rhod)$_9$,Arg$_{10}$-teixobactin, to see if Arg$_{10}$-teixobactin could block staining by Lys(Rhod)$_9$,Arg$_{10}$-teixobactin (Figure 2.8). As controls, I carried out two complementary experiments in which we first stained *B. subtilis* with BODIPY FL vancomycin and then treated with vancomycin, or first blocked with vancomycin and then stained with BODIPY FL vancomycin (Figure 2.9). In *all* of the experiments staining was observed. The bacteria that were treated with Lys(Rhod)$_9$,Arg$_{10}$-teixobactin and then with Arg$_{10}$-teixobactin exhibited fluorescent staining; the bacteria that were treated with Arg$_{10}$-teixobactin and then with Lys(Rhod)$_9$,Arg$_{10}$-teixobactin also exhibited fluorescent staining. The bacteria that were treated with BODIPY FL vancomycin and then with vancomycin exhibited fluorescent staining; the bacteria that were treated with vancomycin and then with BODIPY FL vancomycin also exhibited fluorescent staining. These experiments, coupled with the observation that co-treatment with mixtures of fluorescent and non-fluorescent antibiotics result in more pronounced staining, suggest that complete displacement or blocking do not occur and demonstrate that staining with fluorescent vancomycin or teixobactin analogues can survive competition experiments.

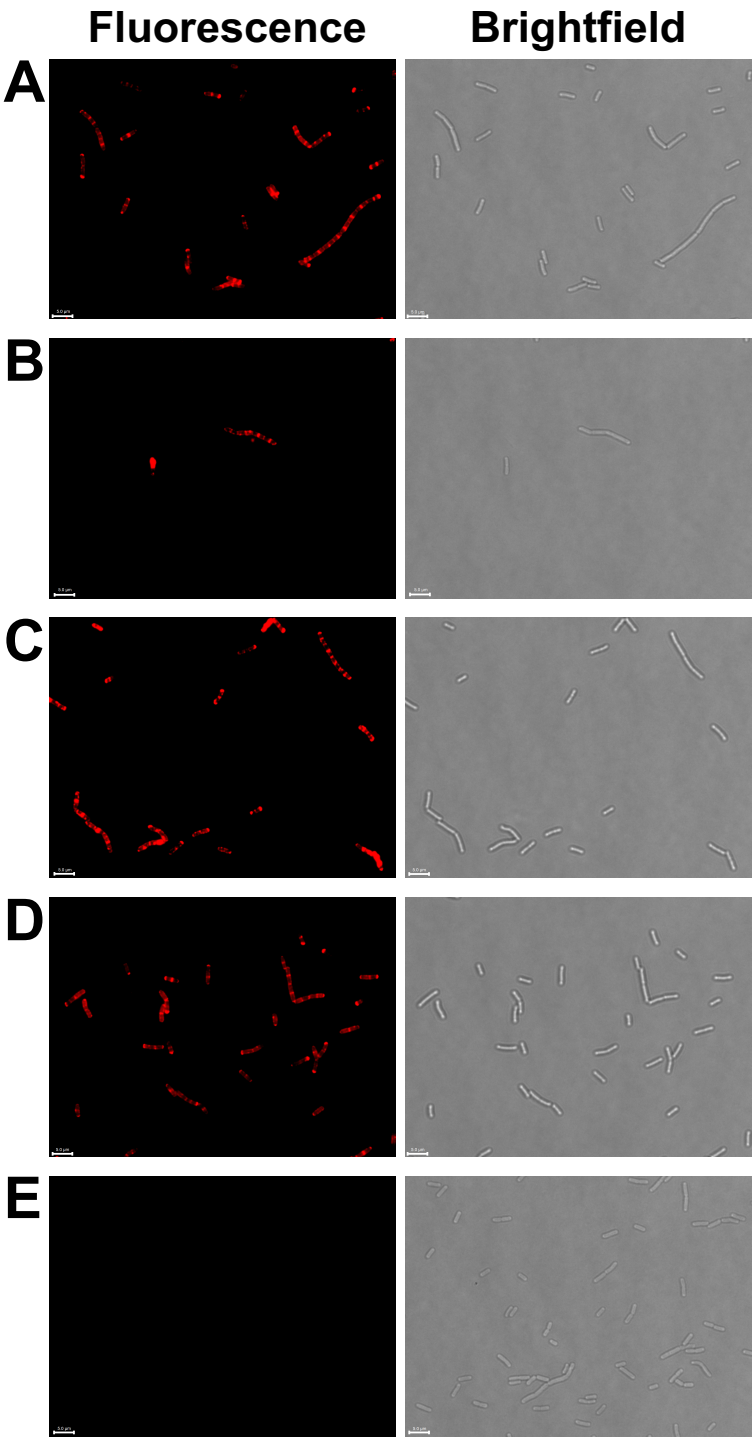

Figure 2.8. Competition experiments using Lys(Rhod)$_9$,Arg$_{10}$-teixobactin and Arg$_{10}$-teixobactin. (A) *B. subtilis* first stained with 4 µg/mL Lys(Rhod)$_9$,Arg$_{10}$-teixobactin, then treated with 4 µg/mL Arg$_{10}$-teixobactin. (B) *B. subtilis* first treated with 4 µg/mL Arg$_{10}$-teixobactin, then stained with 4 µg/mL Lys(Rhod)$_9$,Arg$_{10}$-teixobactin. (C) *B. subtilis* first stained with 4 µg/mL Lys(Rhod)$_9$,Arg$_{10}$-teixobactin, then treated with 4 µg/mL Arg$_{10}$-teixobactin three times consecutively. (D) *B. subtilis* stained with 4 µg/mL Lys(Rhod)$_9$,Arg$_{10}$-teixobactin only. (E) *B. subtilis* treated with 4 µg/mL Arg$_{10}$-teixobactin only. Scale bars are 5 µm.

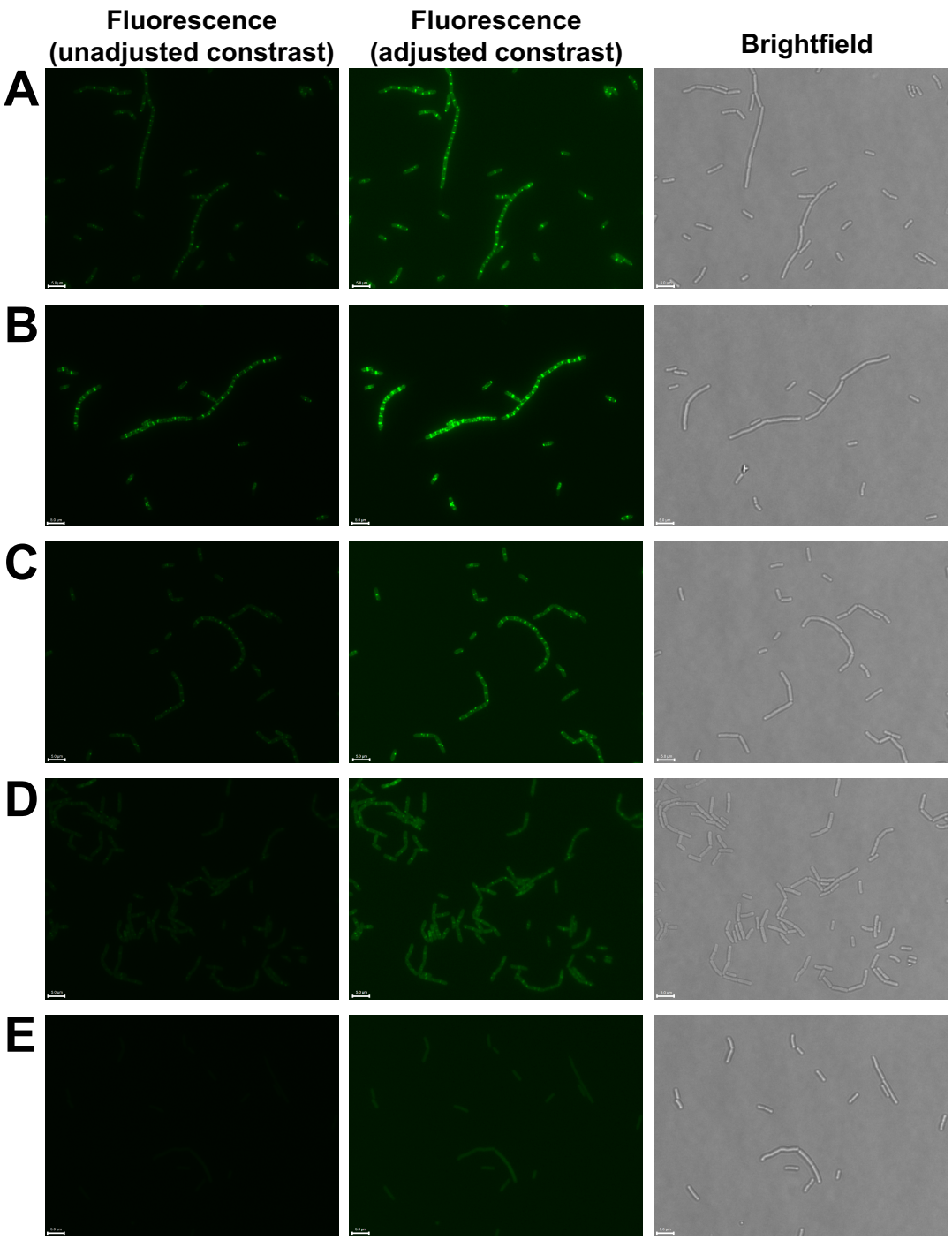

Figure 2.9. Competition experiments using BODIPY FL vancomycin and unlabeled vancomycin. (A) *B. subtilis* first stained with 2.5 µg/mL BODIPY FL vancomycin, then treated with 2.5 µg/mL vancomycin. (B) *B. subtilis* first treated with 2.5 µg/mL vancomycin, then stained with 2.5 µg/mL BODIPY FL vancomycin. (C) *B. subtilis* first stained with 2.5 µg/mL BODIPY FL vancomycin, then treated with 2.5 µg/mL vancomycin three times consecutively. (D) *B. subtilis* stained with 2.5 µg/mL BODIPY FL vancomycin only. (E) *B. subtilis* treated with 2.5 µg/mL vancomycin only. We report both the unadjusted fluorescence (raw) images and the contrast adjusted fluorescence images since the BODIPY FL fluorescence was weak. For all adjusted images, an equal amount of contrast adjustment was applied. Scale bars are 5 µm.

Conclusion

Lys(Rhod)$_9$,Arg$_{10}$-teixobactin exhibits antibiotic activity and stains Gram-positive bacteria, allowing its visualization by fluorescence microscopy. The sulforhodamine B fluorophore tolerates reaction conditions used in peptide synthesis, such as coupling agents, piperidine, and trifluoroacetic acid, and is suitable for confocal fluorescence microscopy. MIC studies show that Lys(Rhod)$_9$,Arg$_{10}$-teixobactin exhibits moderate antibiotic activity, with MIC values of 4–8 μg/mL. This fluorescent teixobactin analogue labels the septa and sidewalls of Gram-positive bacteria, supporting a model in which teixobactin binds to lipids II and III and related cell wall precursors. We anticipate that Lys(Rhod)$_9$,Arg$_{10}$-teixobactin will be useful in studying the mechanism of action of teixobactin, the biosynthesis of peptidoglycan and teichoic acids, and undecaprenyl phosphate metabolism and recycling.[28]

References and Notes

(1) Kocaglu, O. and Carlson, E. E. Progress And Prospects for Small-Molecule Probes of Bacterial Imaging. *Nat. Chem. Biol.* **2016**, *12*, 472–478.

(2) Stone, M. R. L., Butler, M. S., Phetsang, W., Cooper, M. A., and Blaskovich, M. A. T. Fluorescent Antibiotics: New Research Tools to Fight Antibiotic Resistance. *Trends Biotechnol.* **2018**, *36*, 523−536.

(3) Calloway, N. T., Choob, M., Sanz, A., Sheetz, M. P., Miller, L. W., and Cornish, V. W. Optimized Fluorescent Trimethoprim Derivatives for In Vivo Protein Labeling. *ChemBioChem* **2007**, *8*, 767–774.

(4) Wang T. Y., Friedman, L. J., Gelles, J., Min, W., Hoskins, A. A., and Cornish V. W. The Covalent Trimethoprim Chemical Tag Facilitates Single Molecule Imaging with Organic Fluorophores. *Biophys. J.* **2014**, *106*, 272–278.

(5) Akram, A. R., Avlonitis, N., Lilienkampf, A., Perez-Lopez, A. M., McDonald, N., Chankeshwara, S. V., Scholefield, E., Haslett, C., Bradley, M., Dhaliwal, K. A Labelled-Ubiquicidin Antimicrobial Peptide for Immediate In Situ Optical Detection of Live Bacteria in Human Alveolar Lung Tissue. *Chem. Sci.* **2015**, *6*, 6971–6979.

(6) Leevy, W. M., Gammon, S. T., Jiang, H., Johnson, J. R., Maxwell, D. J., Jackson, E. N., Marquez, M., Piwnica-Worms, D., and Smith, B. D. Optical Imaging of Bacterial Infection in Living Mice Using a Fluorescent Near-Infrared Molecular Probe. *J. Am. Chem. Soc.* **2006**, *128*, 16476–16477.

(7) Leevy, W. M., Leevy W. M., Gammon, S. T., Johnson, J. R., Jiang, H., Marquez, M., Piwnica-Worms, D., Suckow, M. A., and Smith, B. D. Noninvasive Optical Imaging of Staphylococcus

aureus Bacterial Infection in Living Mice Using a Bis-Dipicolylamine-Zinc(II) Affinity Group Conjugated to a Near-Infrared Fluorophore. *Bioconjug. Chem.* **2008**, *19*, 686–692.

(8) van Oosten M., Schäfer, T., Gazendam, J. A., Ohlsen, K., Tsompanidou, E., de Goffau, M. C., Harmsen, H. J., Crane, L. M., Lim, E., Francis, K. P., Cheung, L., Olive, M., Ntziachristos, V., van Dijl, J. M., and van Dam, G. M. Real-Time In Vivo Imaging of Invasive- and Biomaterial-Associated Bacterial Infections Using Fluorescently Labelled Vancomycin. *Nat. Commun.* **2013**, *4*, 2584.

(9) Chen, H., Liu, C., Chen, D., Madrid, K., Peng, S., Dong, X., Zhang, M., and Gu, Y. Bacteria-Targeting Conjugates Based on Antimicrobial Peptide for Bacteria Diagnosis and Therapy. *Mol. Pharm.* **2015**, *12*, 2505–2516.

(10) Moyá, B., Beceiro, A., Cabot, G., Juan, C., Zamorano, L., Alberti, S., and Oliver, A. Pan-Beta-Lactam Resistance Development in Pseudomonas aeruginosa Clinical Strains: Molecular Mechanisms, Penicillin-Binding Protein Profiles, and Binding Affinities. *Antimicrob. Agents Chemother.* **2012**, *56*, 4771–4778.

(11) Jarzembowski, T., Wiśniewska, K., Józwik, A., Bryl, E., and Witkowski, J. Flow Cytometry as a Rapid Test for Detection of Penicillin Resistance Directly in Bacterial Cells in Enterococcus faecalis and Staphylococcus aureus. *Curr. Microbiol.* **2008**, *57*, 167–169.

(12) Izdebski, R., Rutschmann, J., Fiett, J., Sadowy, E., Gniadkowski, M., Hryniewicz, W., and Hakenbeck, R. Highly Variable Penicillin Resistance Determinants PBP 2x, PBP 2b, and PBP 1a in Isolates of Two Streptococcus pneumoniae Clonal Groups Poland(23F)-16 and Poland(6B)-20. *Antimicrob. Agents Chemother.* **2008**, *52*, 1021–1027.

(13) Daniel, R. A. and Errington, J. Control of Cell Morphogenesis in Bacteria: Two Distinct Ways to Make a Rod-Shaped Cell. *Cell* **2003**, *113*, 767-776.

(14) Tiyanont, K., Doan, T., Lazarus, M. B., Fang, X., Rudner, D. Z., and Walker, S. Imaging Peptidoglycan Biosynthesis in Bacillus subtilis with Fluorescent Antibiotics. *Proc. Natl. Acad. Sci. USA* **2006**, *103*, 11033−11038.

(15) Kocaoglu, O., Calvo, R. A., Sham, L. T., Cozy, L. M., Lanning, B. R., Francis, S., Winkler, M. E., Kearns, D. B., Carlson, E. E. Selective Penicillin-Binding Protein Imaging Probes Reveal Substructure in Bacterial Cell Division. *ACS Chem. Biol.* **2012**, *7*, 1746−1753.

(16) Ling, L. L., Schneider, T., Peoples, A. J., Spoering, A. L., Engels, I., Conlon, B. P., Mueller, A., Schaberle, T. F., Hughes, D. E., Epstein, S., Jones, M., Lazarides, L., Steadman, V. A., Cohen, D. R., Felix, C. R., Fetterman, K. A., Millett, W. P., Nitti, A. G., Zullo, A. M., Chen, C., and Lewis, K. A New Antibiotic Kills Pathogens without Detectable Resistance. *Nature* **2015**, *517*, 455−459.

(17) Homma, T., Nuxoll, A., Gandt, A. B., Ebner, P., Engels, I., Schneider, T., Götz, F., Lewis, K., and Conlon, B. P. Dual Targeting of Cell Wall Precursors by Teixobactin Leads to Cell Lysis. *Antimicrob. Agents Chemother*. **2016**, *60*, 6510−6517.

(18) Liu, L., Wu, S., Wang, Q., Zhang, M., Wang, B., He, G., Chen, G. Total Synthesis of Teixobactin and its Stereoisomers. *Org. Chem. Front.* **2018**, *5*, 1431−1435.

(19) Abdel Monaim, S. A. H., Jad, Y. E., Ramchuran, E. J., El-Faham, A., Govender, T., Kruger, H. G., de la Torre, B. G., and Albericio A. Lysine Scanning of Arg_{10}–Teixobactin: Deciphering the Role of Hydrophobic and Hydrophilic Residues. *ACS Omega* **2016**, *1*, 1262−1265.

(20) Chen, K. H., Le, S. P., Han, X., Frais, J. M., and Nowick J. S. Alanine Scan Reveals Modifiable Residues in Teixobactin. *Chem. Commun*. **2017**, *53*, 11357−11359.

(21) Smith, S. N. and Steer, R. P. The Photophysics of Lissamine Rhodamine-B Sulphonyl Chloride in Aqueous Solution: Implications for Fluorescent Protein−Dye Conjugates. *J. Photochem. Photobiol., A* **2001**, *139*, 151−156.

(22) Yang, H., Chen, K. H., and Nowick, J. S. Elucidation of the Teixobactin Pharmacophore. *ACS Chem. Biol.* **2016**, *11*, 1823−1826.

(23) The on-resin synthesis of the Lys(Rhod)$_9$ residue from Lys(Alloc) and sulforhodamine B sulfonyl chloride allows use of off-the-shelf building blocks. It should also be possible to directly incorporate Fmoc-Lys(Rhod)-OH as a building block in the solid phase peptide synthesis. Doing so requires the synthesis of Fmoc-Lys(Rhod)-OH, which is not commercially available.

(25) To test the effect of Lys(Rhod)$_9$,Arg$_{10}$-teixobactin staining on the viability of *B. subtilis*, we carried out the following time-lapse microscopy experiment. We treated *B. subtilis* with either sodium phosphate buffer containing 0.05% polysorbate 80 (Figure S2.7), 4 μg/mL Lys(Rhod)$_9$,Arg$_{10}$-teixobactin (1 x MIC, Figure S2.8), or 8 μg/mL Lys(Rhod)$_9$,Arg$_{10}$-teixobactin (2 x MIC, Figure S2.9) and performed time-lapse imaging at 37 °C. After 90 minutes, the bacteria treated with 8 μg/mL Lys(Rhod)$_9$,Arg$_{10}$-teixobactin, showed no evidence of growth, while the bacteria treated with either the vehicle control or 4 μg/mL Lys(Rhod)$_9$,Arg$_{10}$-teixobactin grew.

(26) Yang, H., Wierzbicki, M., Du Bois, D. R., and Nowick J. S. X-Ray Crystallographic Structure of a Teixobactin Derivative Reveals Amyloid-Like Assembly. *J. Am. Chem. Soc*. **2018**, *140*, 14028−14032.

(27) When we used concentrations of Lys(Rhod)$_9$,Arg$_{10}$-teixobactin lower than 4 μg/mL, we observed weaker septal staining and moderate sidewall staining.

(28) Rajagopal, M. and Walker, S. Envelope Structures of Gram-Positive Bacteria. *Curr. Top. Microbiol. Immunol*. **2017**, *404*, 1−44.

Chapter 2 Supporting Information

Table of Contents

Supplementary data

Magnified fluorescence micrographic images, Figures 2.3–2.6

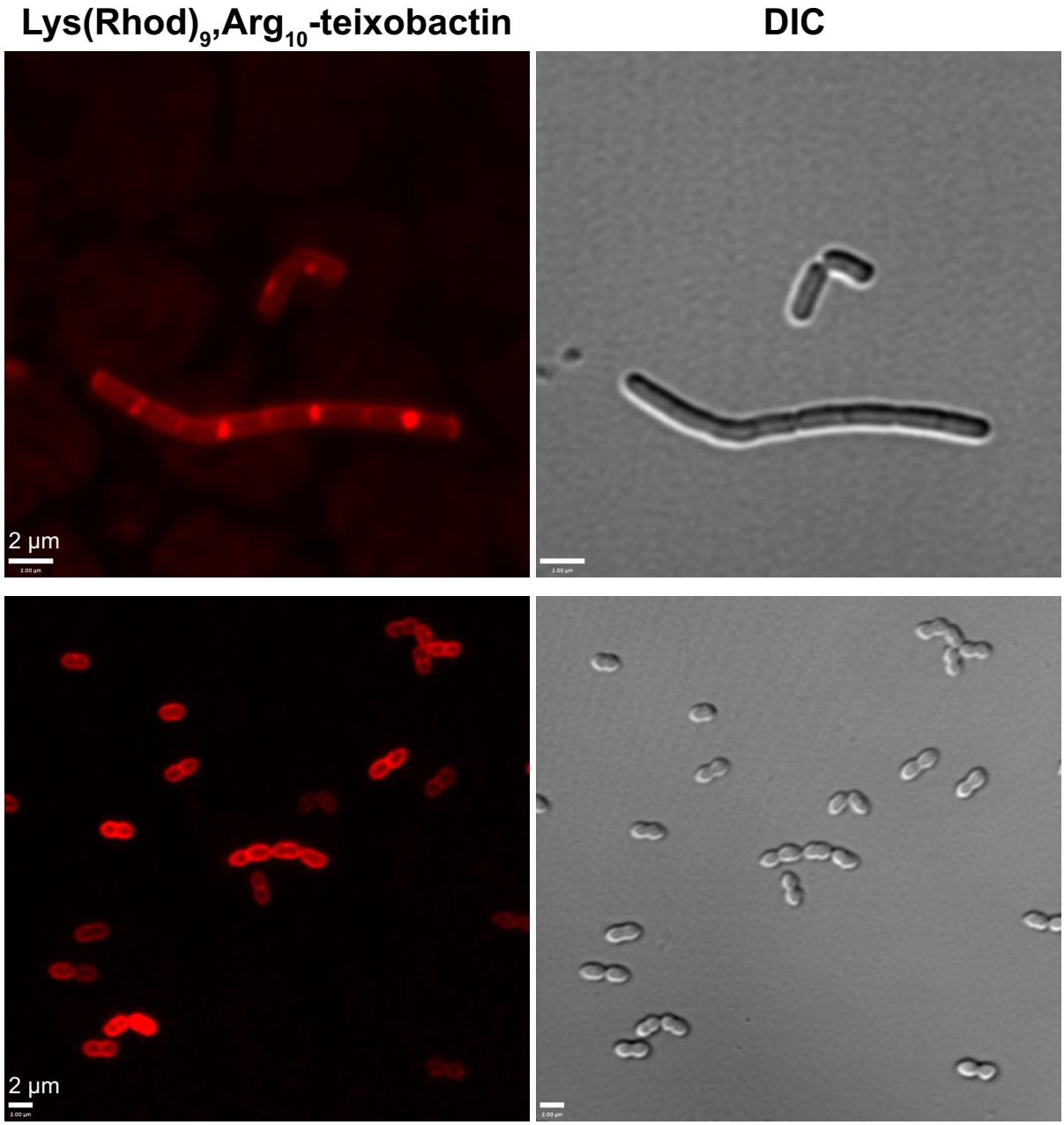

Magnified image from Figure 2.3. Fluorescence and differential interference contrast (DIC) micrographs of *B. subtilis* (top) and *E. durans* (bottom) treated with 4 µg/mL of Lys(Rhod)$_9$,Arg$_{10}$-teixobactin in sodium phosphate buffer containing 0.05% polysorbate 80. Fluorescence micrographs were recorded with excitation at 561 nm. Scale bars are 2 µm.

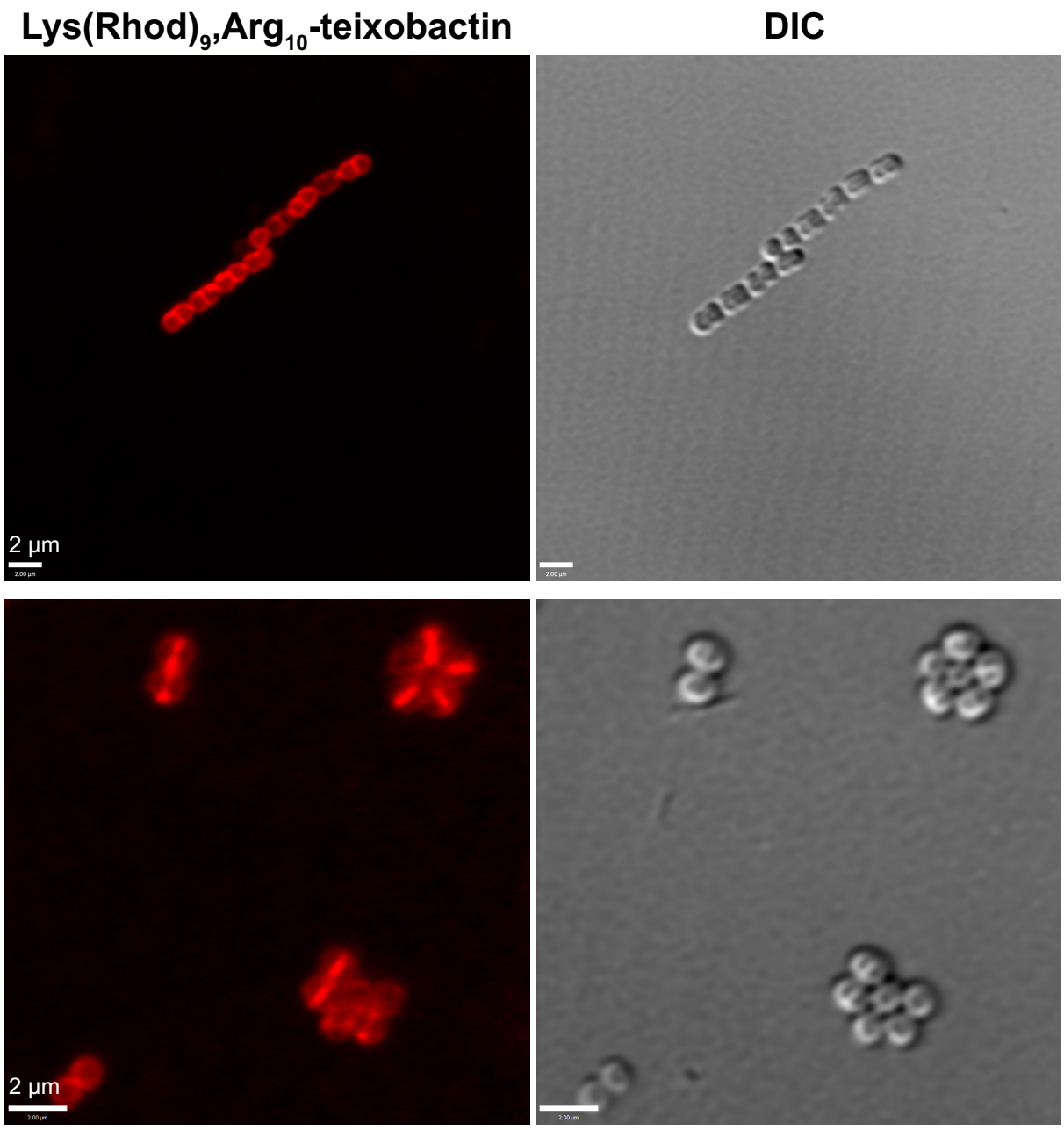

Magnified image from Figure 2.3. Fluorescence and differential interference contrast (DIC) micrographs of *S. salivarius* (top) and *S. aureus* (bottom) treated with 4 µg/mL of Lys(Rhod)$_9$,Arg$_{10}$-teixobactin in sodium phos-phate buffer containing 0.05% polysorbate 80. Fluorescence micrographs were recorded with excitation at 561 nm. Scale bars are 2 µm.

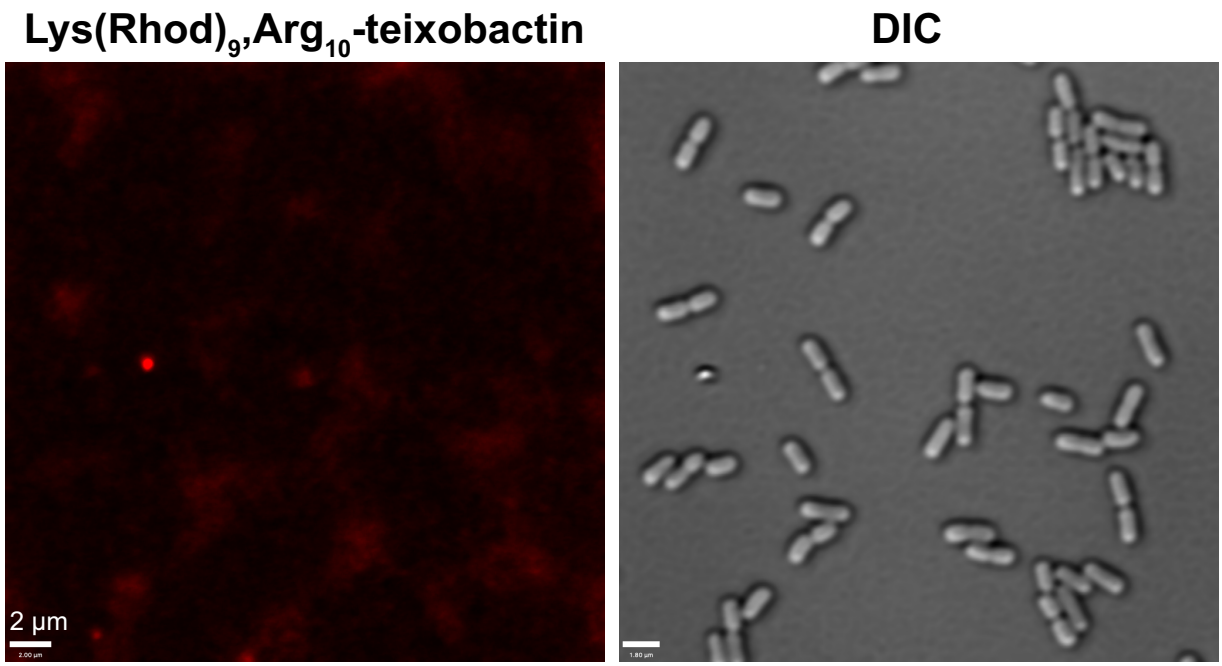

Magnified image from Figure 2.3. Fluorescence and differential interference contrast (DIC) micrographs of *E. coli* treated with 4 µg/mL of Lys(Rhod)$_9$,Arg$_{10}$-teixobactin in sodium phosphate buffer containing 0.05% poly-sorbate 80. Fluorescence micrographs were recorded with excitation at 561 nm. Scale bars are 2 µm.

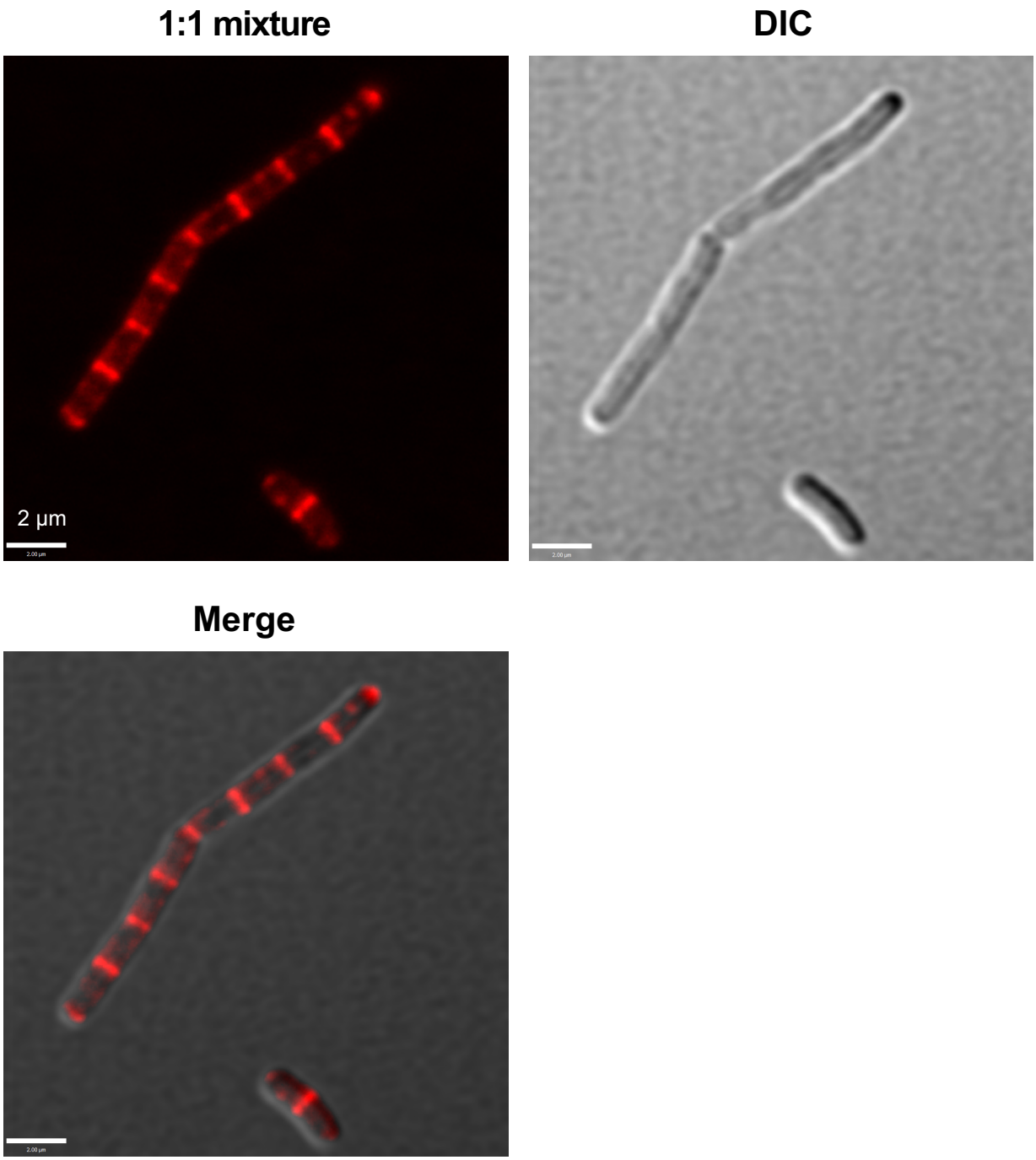

Magnified image from Figure 2.4. Fluorescence and differential interference contrast (DIC) micrographs of *B. subtilis* treated with 1 µg/mL of Lys(Rhod)$_9$,Arg$_{10}$-teixobactin and 1 µg/mL of Arg$_{10}$-teixobactin in sodium phosphate buffer containing 0.05% polysorbate 80. Fluorescence micrographs were recorded with excitation at 561 nm. Scale bars are 2 µm.

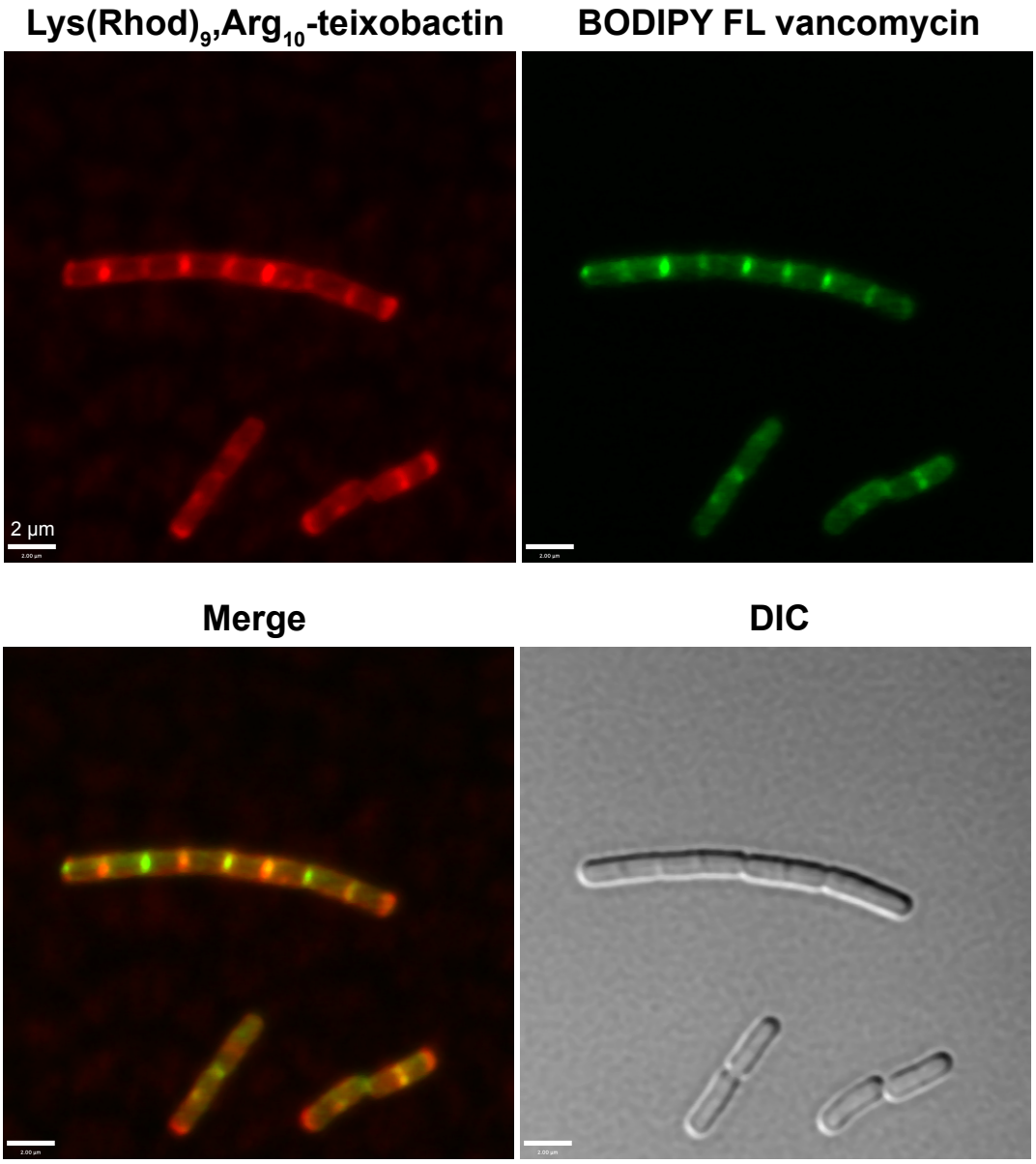

Magnified image from Figure 2.5. Fluorescence and differential interference contrast (DIC) micrographs of *B. subtilis* concurrently treated with 4 µg/mL of $Lys(Rhod)_9,Arg_{10}$-teixobactin and 4 µg/mL of BODIPY FL vanco-mycin in sodium phosphate buffer containing 0.05% polysorbate 80. Fluorescence micrographs were recorded with excitation at 561 nm (left column panel) and 488 nm (right column panel). Scale bars are 2 µm.

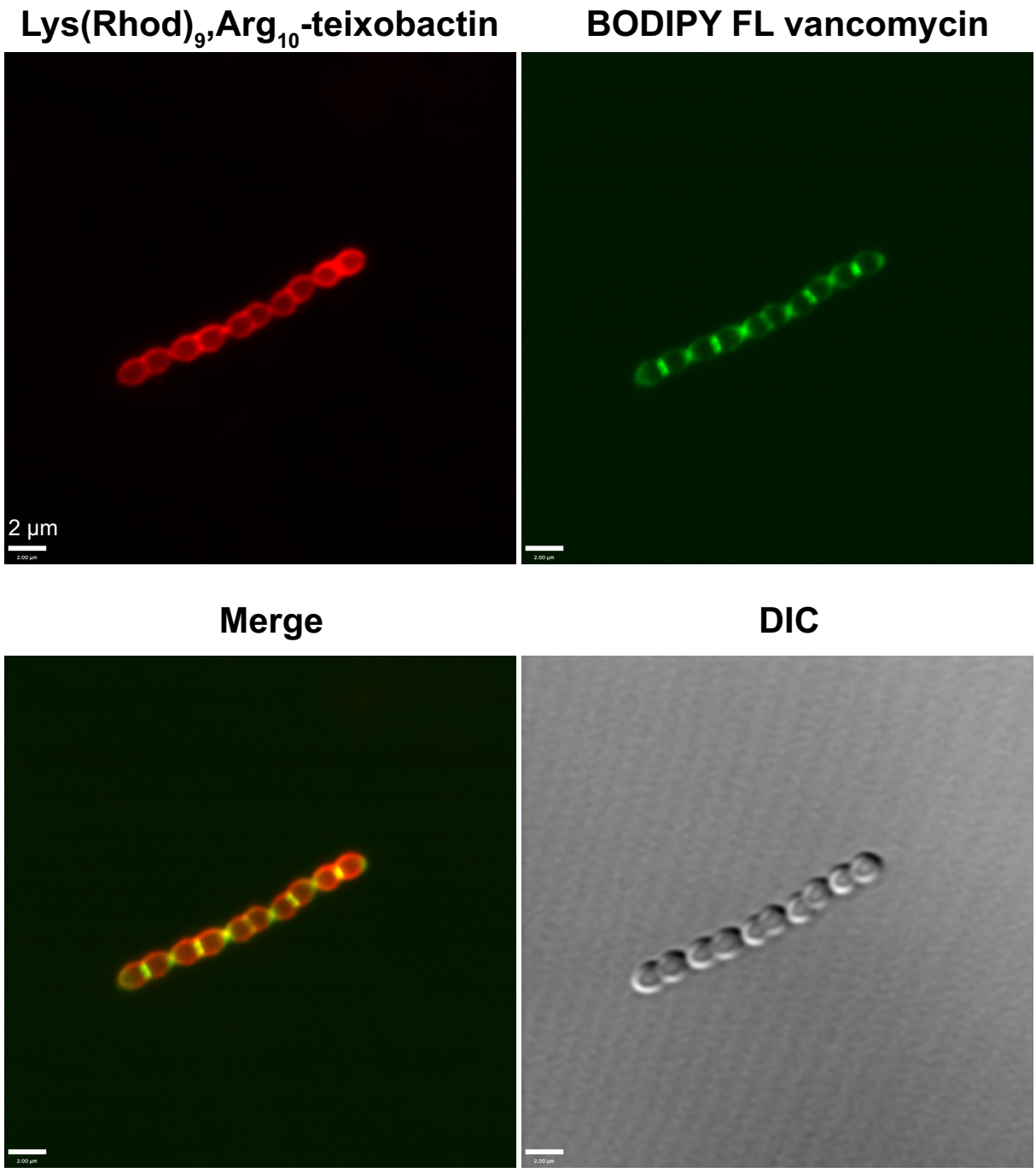

Magnified image from Figure 2.5. Fluorescence and differential interference contrast (DIC) micrographs of *E. durans* concurrently treated with 4 µg/mL of Lys(Rhod)$_9$,Arg$_{10}$-teixobactin and 4 µg/mL of BODIPY FL vanco-mycin in sodium phosphate buffer containing 0.05% polysorbate 80. Fluorescence micrographs were recorded with excitation at 561 nm (top left) and 488 nm (top right). Scale bars are 2 µm.

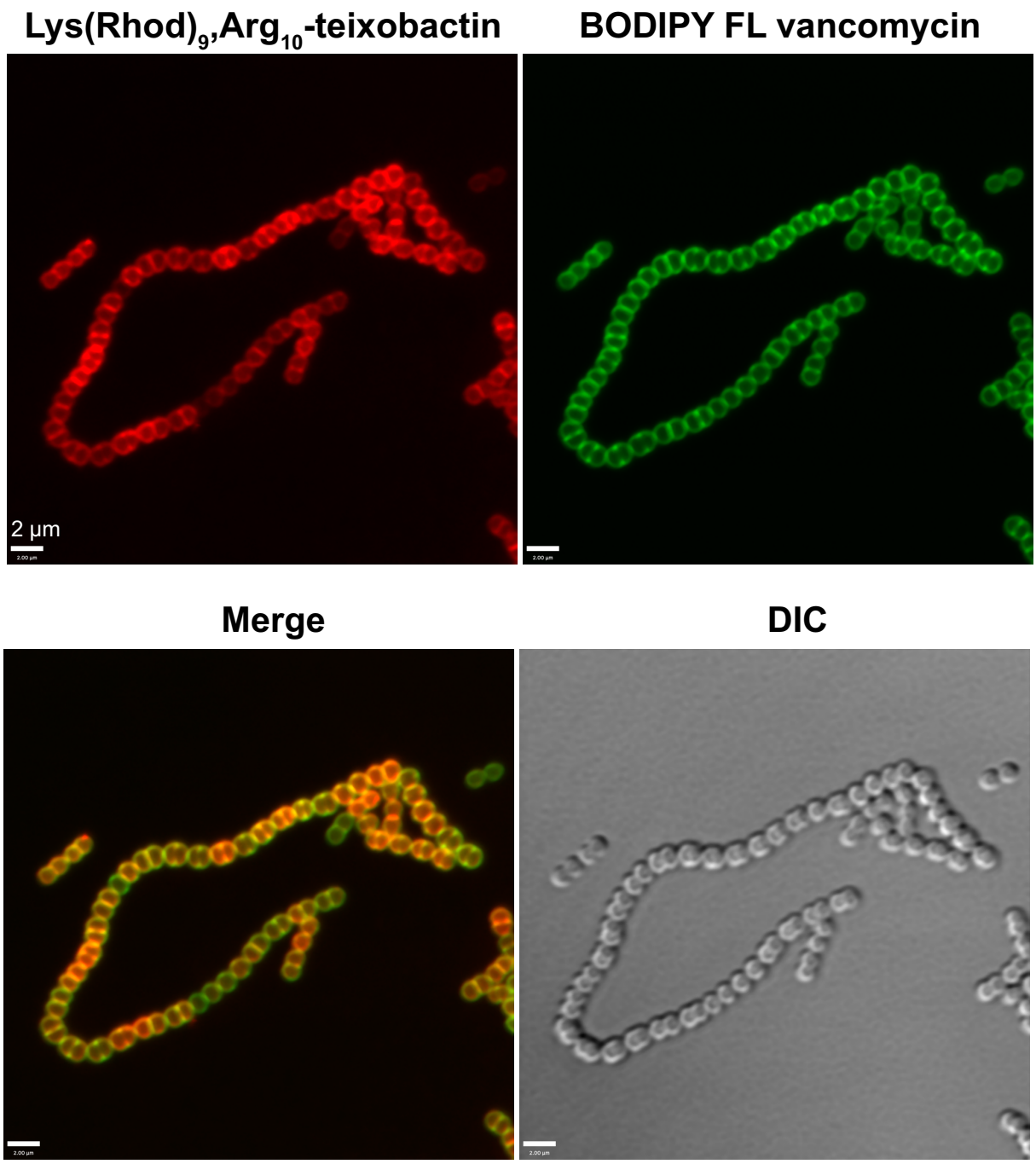

Magnified image from Figure 2.5. Fluorescence and differential interference contrast (DIC) micrographs of *S. salivarius* concurrently treated with 4 µg/mL of $Lys(Rhod)_9,Arg_{10}$-teixobactin and 4 µg/mL of BODIPY FL vancomycin in sodium phosphate buffer containing 0.05% polysorbate 80. Fluorescence micrographs were recorded with excitation at 561 nm (left column panel) and 488 nm (right column panel). Scale bars are 2 µm.

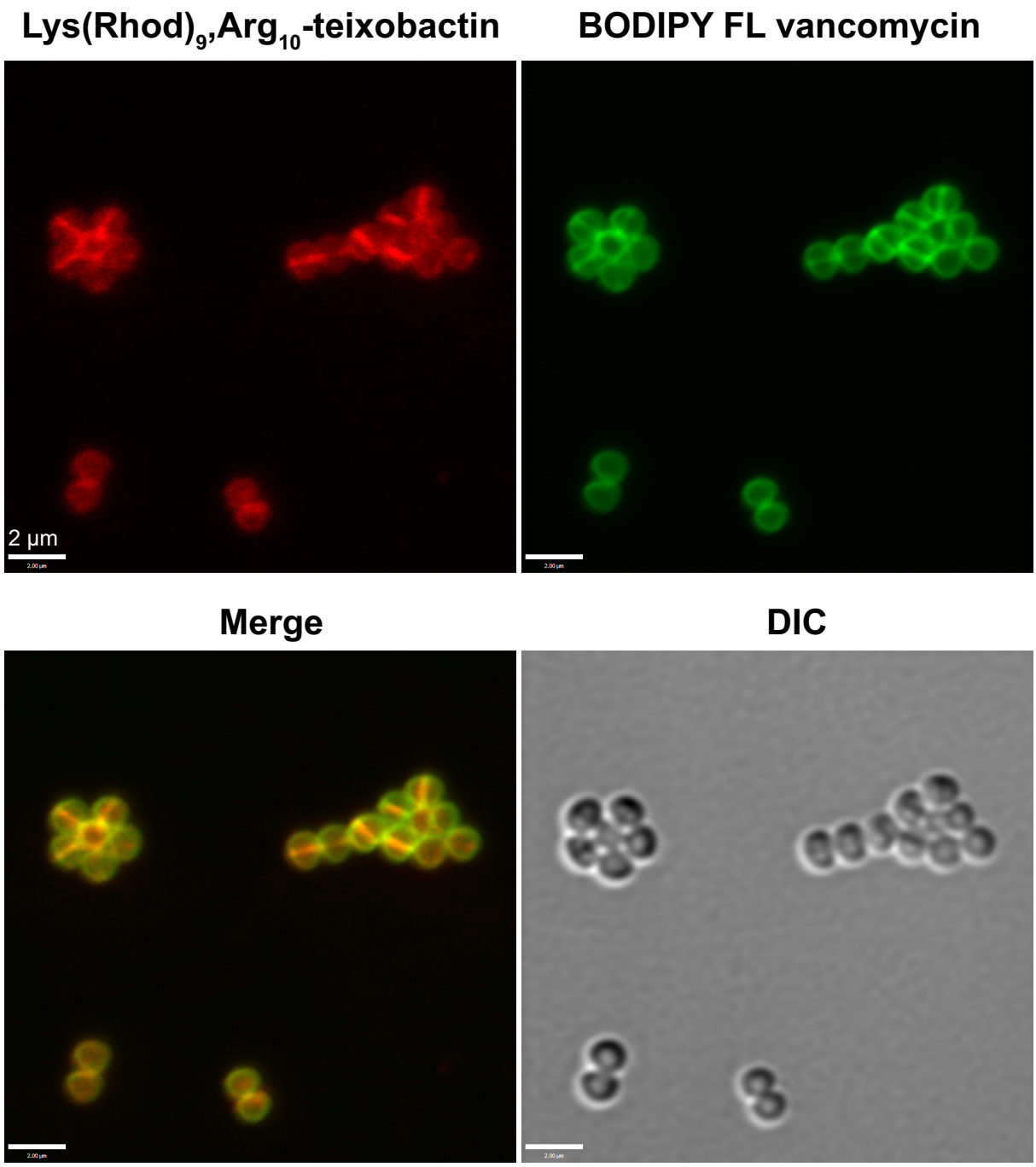

Magnified image from Figure 2.5. Fluorescence and differential interference contrast (DIC) micrographs of *S. aureus* concurrently treated with 4 µg/mL of Lys(Rhod)$_9$,Arg$_{10}$-teixobactin and 4 µg/mL of BODIPY FL vanco-mycin in sodium phosphate buffer containing 0.05% polysorbate 80. Fluorescence micrographs were recorded with excitation at 561 nm (left column panel) and 488 nm (right column panel). Scale bars are 2 µm.

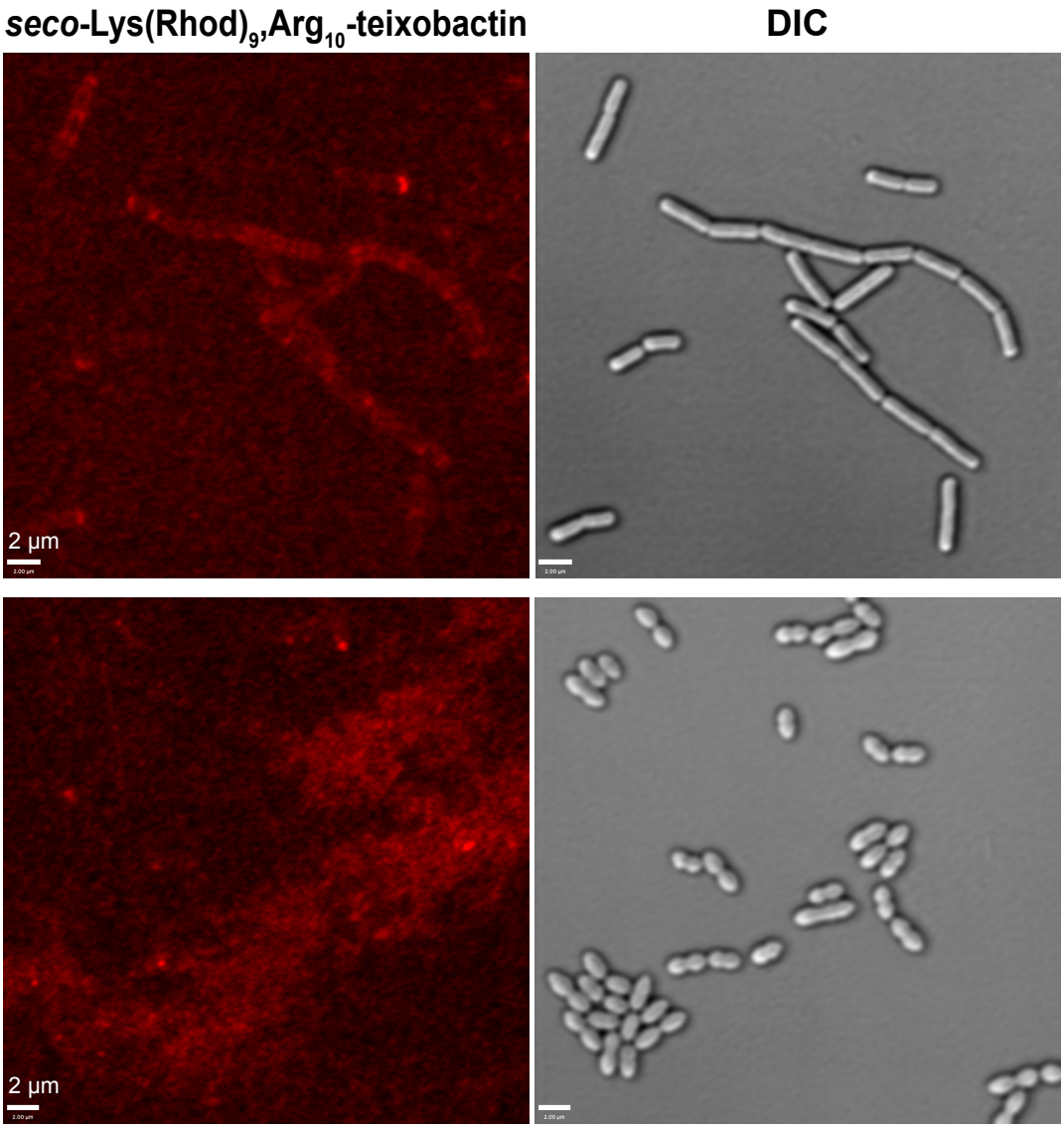

Magnified image from Figure 2.6. Fluorescence and differential interference contrast (DIC) micrographs of *B. subtilis* (top) and *E. durans* (bottom) treated with 4 µg/mL of *seco*-Lys(Rhod)$_9$,Arg$_{10}$-teixobactin in sodium phosphate buffer containing 0.05% polysorbate 80. Fluorescence micrographs were recorded with excitation at 561 nm. Scale bars are 2 µm.

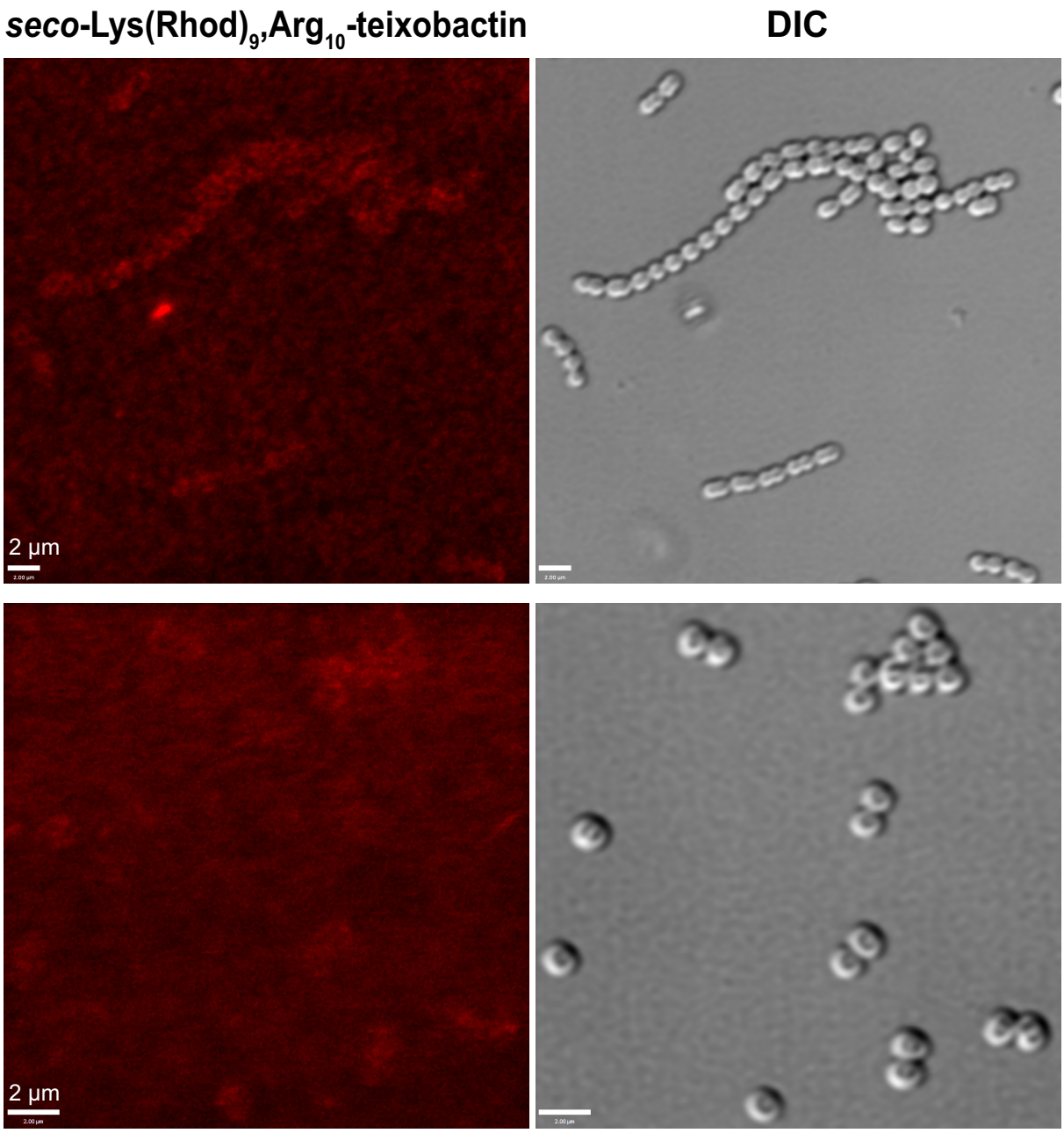

Magnified image from Figure 2.6. Fluorescence and differential interference contrast (DIC) micrographs of *S. salivarius* (top) and *S. aureus* (bottom) treated with 4 µg/mL of *seco*-Lys(Rhod)$_9$,Arg$_{10}$-teixobactin in sodium phosphate buffer containing 0.05% polysorbate 80. Fluorescence micrographs were recorded with excitation at 561 nm. Scale bars are 2 µm.

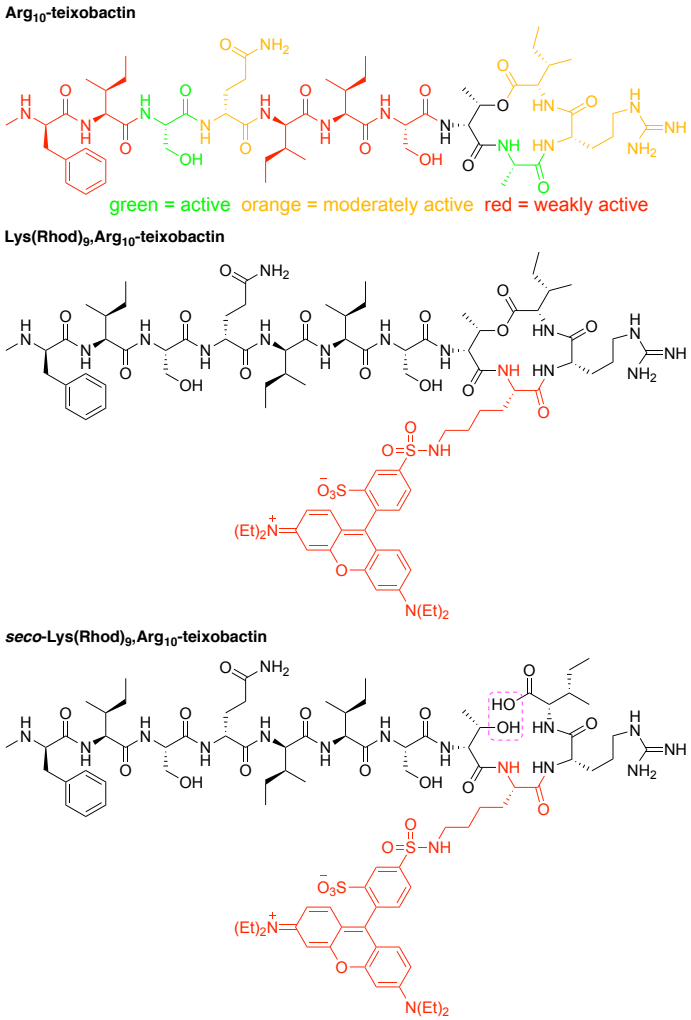

Figure S2.1. Structure of Arg_{10}-teixobactin, illustrating tolerance of amino acids toward substitution. Image is from *Chem. Commun.* **2017**, *53*, 11357-11359. Positions 3 and 9 are especially tolerant of substitution. $Lys(Rhod)_9,Arg_{10}$-teixobactin, and *seco*-$Lys(Rhod)_9,Arg_{10}$-teixobactin are shown for comparison.

Figures S2.2–S2.6, Additional fluorescence micrographic images:

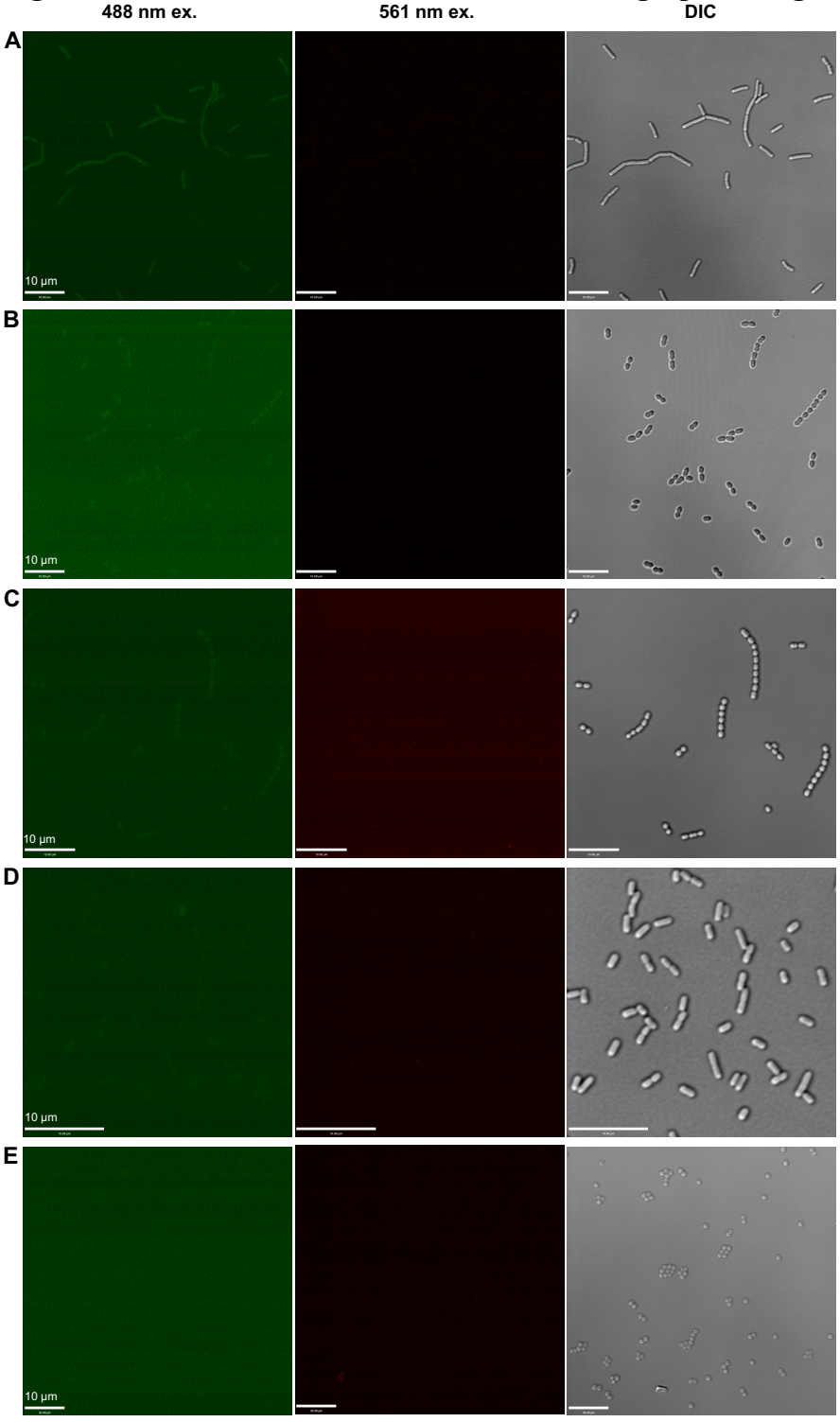

Figure S2.2. Fluorescence and differential interference contrast (DIC) micrographs of (A) *B. subtilis*, (B) *E. durans*, (C) *S. salivarius*, (D) *E. coli*, and (E), *S. aureus* treated with sodium phosphate buffer containing 0.05% polysorbate 80 (vehicle). Fluorescence micrographs were recorded with excitation at 561 and 488 nm. Scale bars are 10 µm.

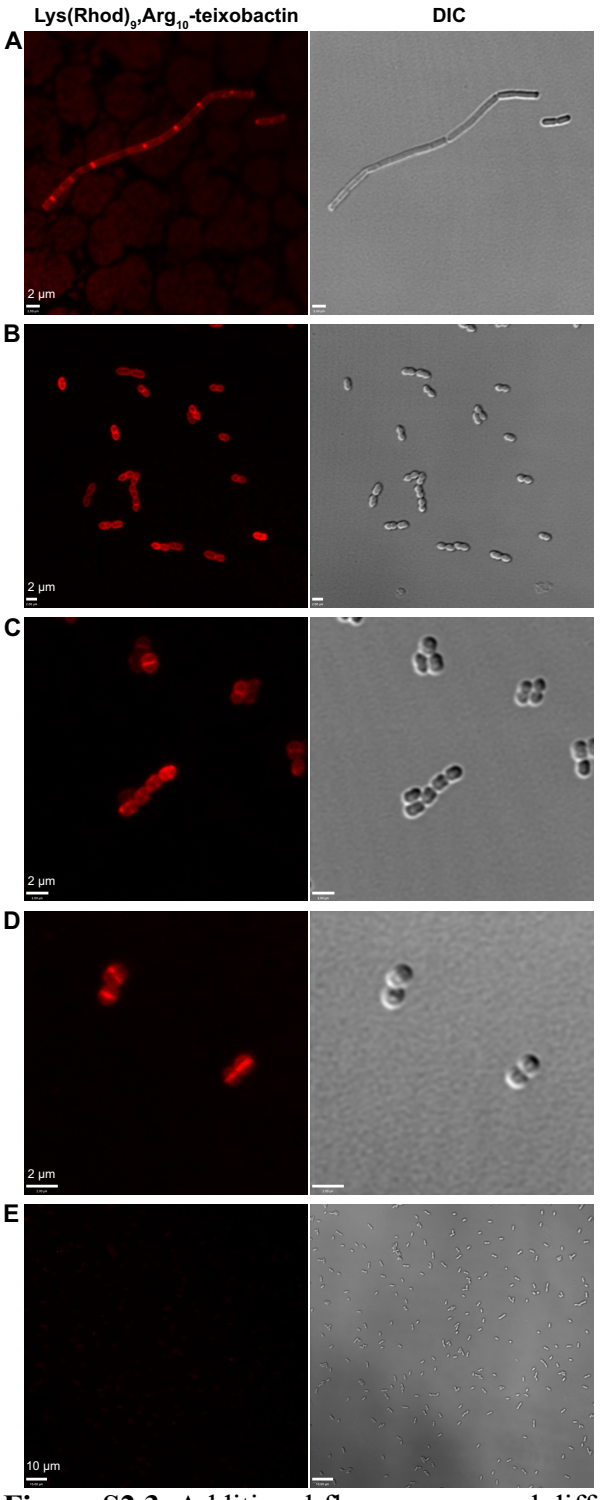

Figure S2.3. Additional fluorescence and differential interference contrast (DIC) micrographs of (A) *B. subtilis*, (B) *E. durans*, (C) *S. salivarius*, (D) *S. aureus*, and (E) *E. coli* treated with 4 µg/mL of Lys(Rhod)$_9$,Arg$_{10}$-teixobactin in sodium phosphate buffer containing 0.05% polysorbate 80. Fluorescence micrographs were recorded with excitation at 561 nm. Scale bars of *B. subtilis*, *E. durans*, *S. salivarius*, and *S. aureus* images are 2 µm, while the scale bars of the *E. coli* images are 10 µm.

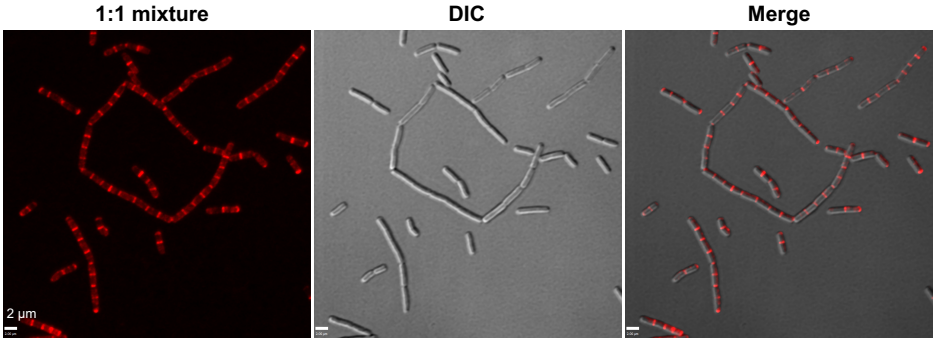

Figure S2.4. Additional fluorescence and differential interference contrast (DIC) micrographs of *B. subtilis* treated with a mixture of 1 µg/mL of Lys(Rhod)$_9$,Arg$_{10}$-teixobactin and 1 µg/mL of Arg$_{10}$-teixobactin in sodium phosphate buffer containing 0.05% polysorbate 80. Fluorescence micrographs were recorded with excitation at 561 nm. Scale bars are 2 µm.

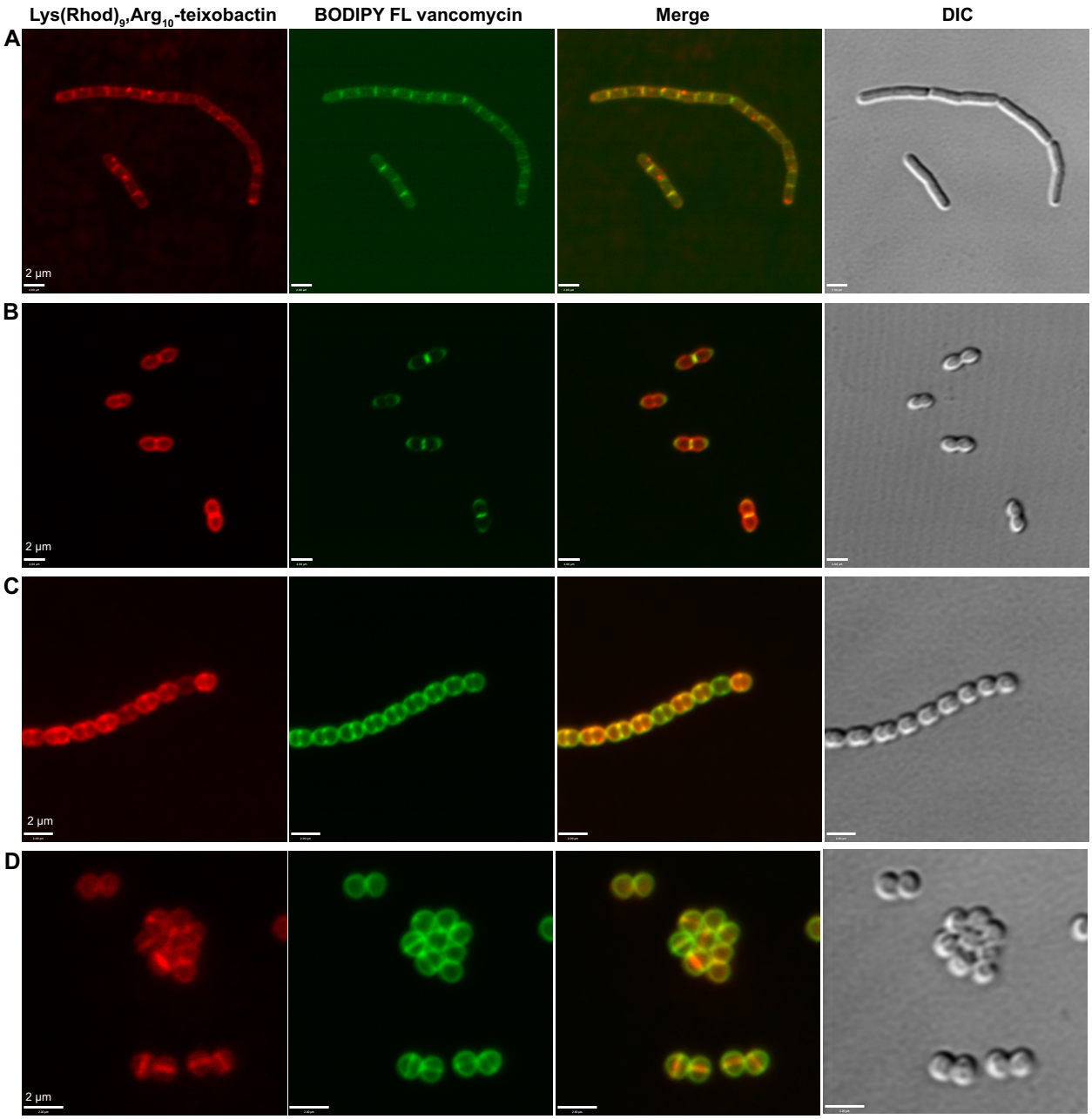

Figure S2.5. Additional fluorescence and differential interference contrast (DIC) micrographs of (A) *B. subtilis*, (B) *E. durans*, (C) *S. salivarius*, and (D) *S. aureus* simultaneously treated with 4 µg/mL of Lys(Rhod)$_9$,Arg$_{10}$-teixobactin and 4 µg/mL of BODIPY FL vancomycin in sodium phosphate buffer containing 0.05% polysorbate 80. Fluorescence micrographs were recorded with excitation at 561 and 488 nm. Scale bars are 2 µm.

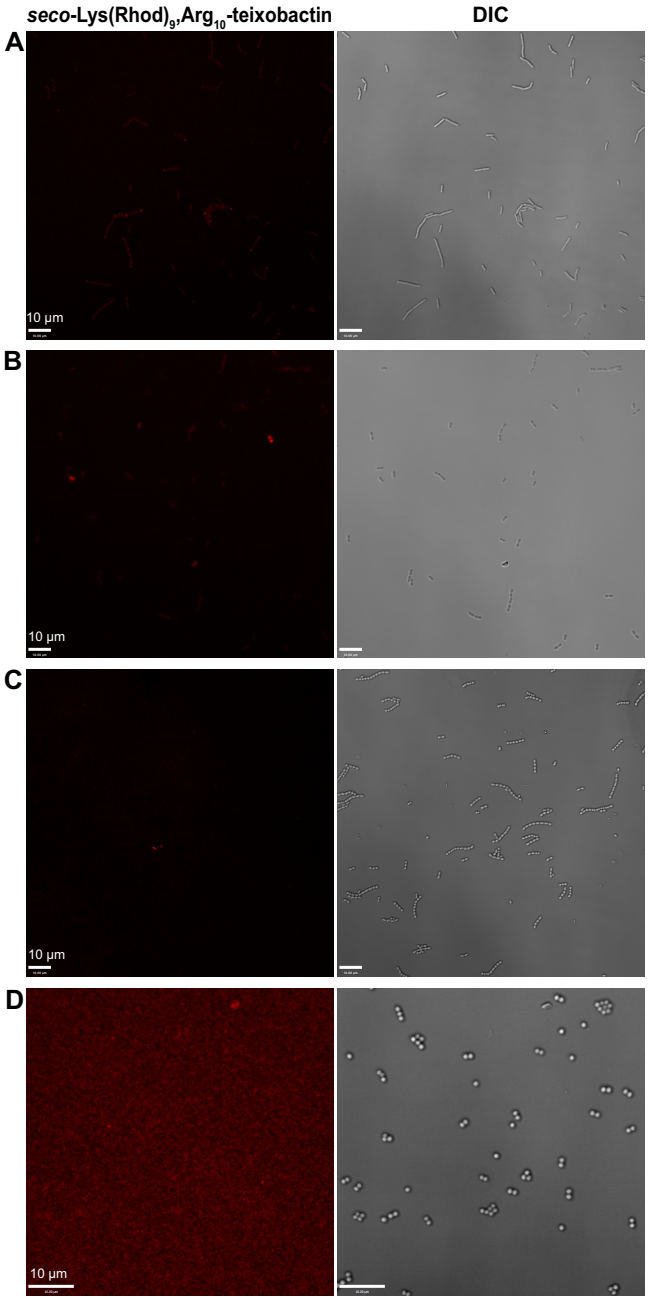

Figure S2.6. Additional fluorescence and differential interference contrast (DIC) micrographs of (A) *B. subtilis*, (B) *E. durans*, (C) *S. salivarius*, and (D) *S. aureus* treated with 4 µg/mL of *seco*-Lys(Rhod)$_9$,Arg$_{10}$-teixobactin in sodium phosphate buffer containing 0.05% polysorbate 80. Fluorescence micrographs were recorded with excitation at 561 nm. Scale bars are 10 µm.

Sulforhodamine B *N*-butylsulfonamide: ^{1}H NMR spectrum in DMSO-d_6 (400 MHz)

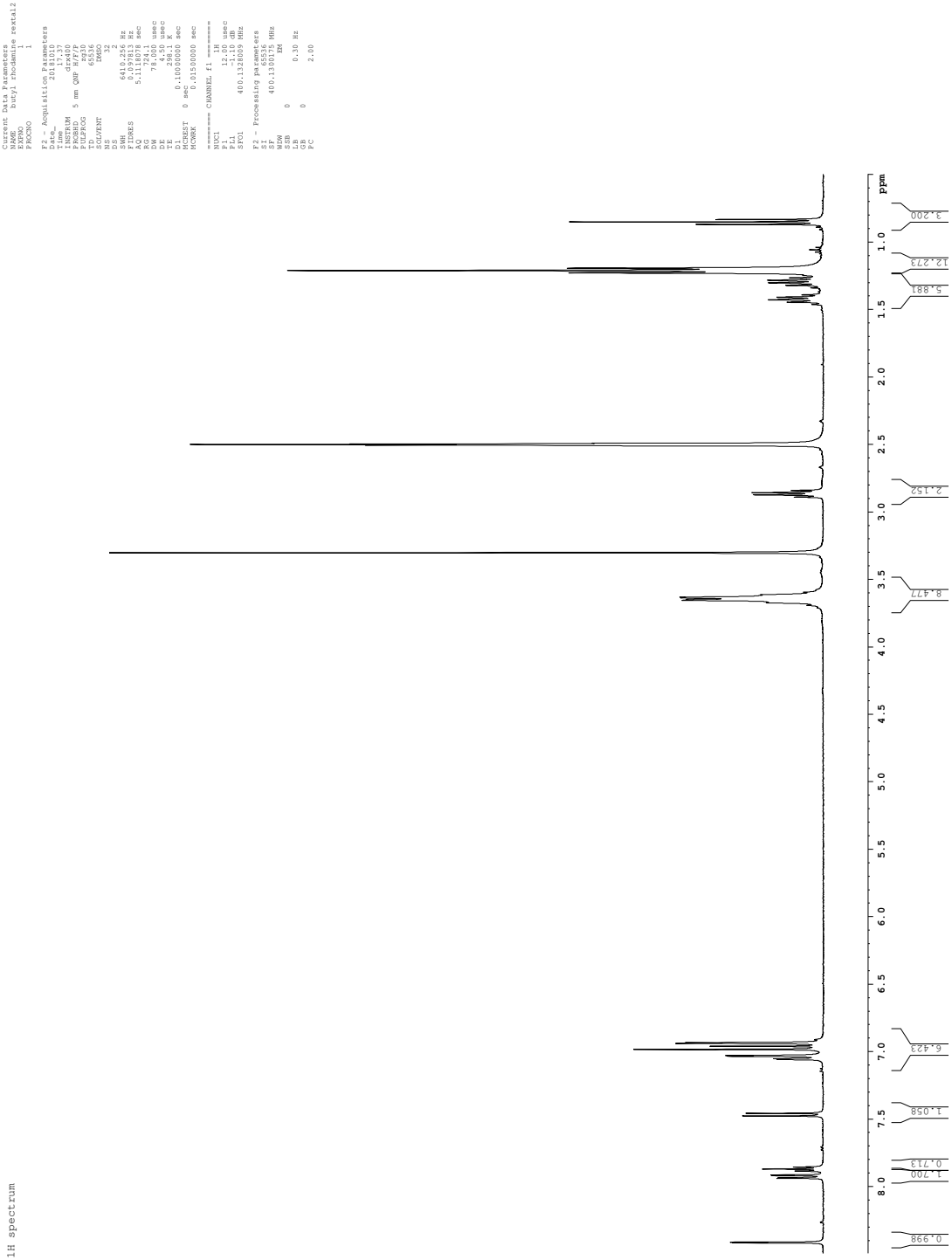

Effect of Lys(Rhod)$_9$,Arg$_{10}$-teixobactin treatment on the viability of *B. subtilis*. To test the effect of Lys(Rhod)$_9$,Arg$_{10}$-teixobactin staining upon the viability of *B. subtilis*, we carried out the following time-lapse microscopy experiment. We treated *B. subtilis* with either sodium phosphate buffer containing 0.05% polysorbate 80 (Figure S10), 4 µg/mL Lys(Rhod)$_9$,Arg$_{10}$-teixobactin (1 x MIC, Figure S11), or 8 µg/mL Lys(Rhod)$_9$,Arg$_{10}$-teixobactin (2 x MIC, Figure S12) and then applied the bacteria to coverslip-bottom dishes, covered with a sheet of LB agar, and performed time-lapse imaging at 37 °C. After 90 minutes, the bacteria treated with 8 µg/mL Lys(Rhod)$_9$,Arg$_{10}$-teixobactin, showed no evidence of growth, while the bacteria treated with either the vehicle control or 4 µg/mL Lys(Rhod)$_9$,Arg$_{10}$-teixobactin grew. Cells were imaged on a Keyence BZ-X810 fluorescence microscope using phase contrast brightfield imaging. Images were collected with a 60x oil immersion objective lens using the high resolution camera sensitivity and oblique illumination settings.

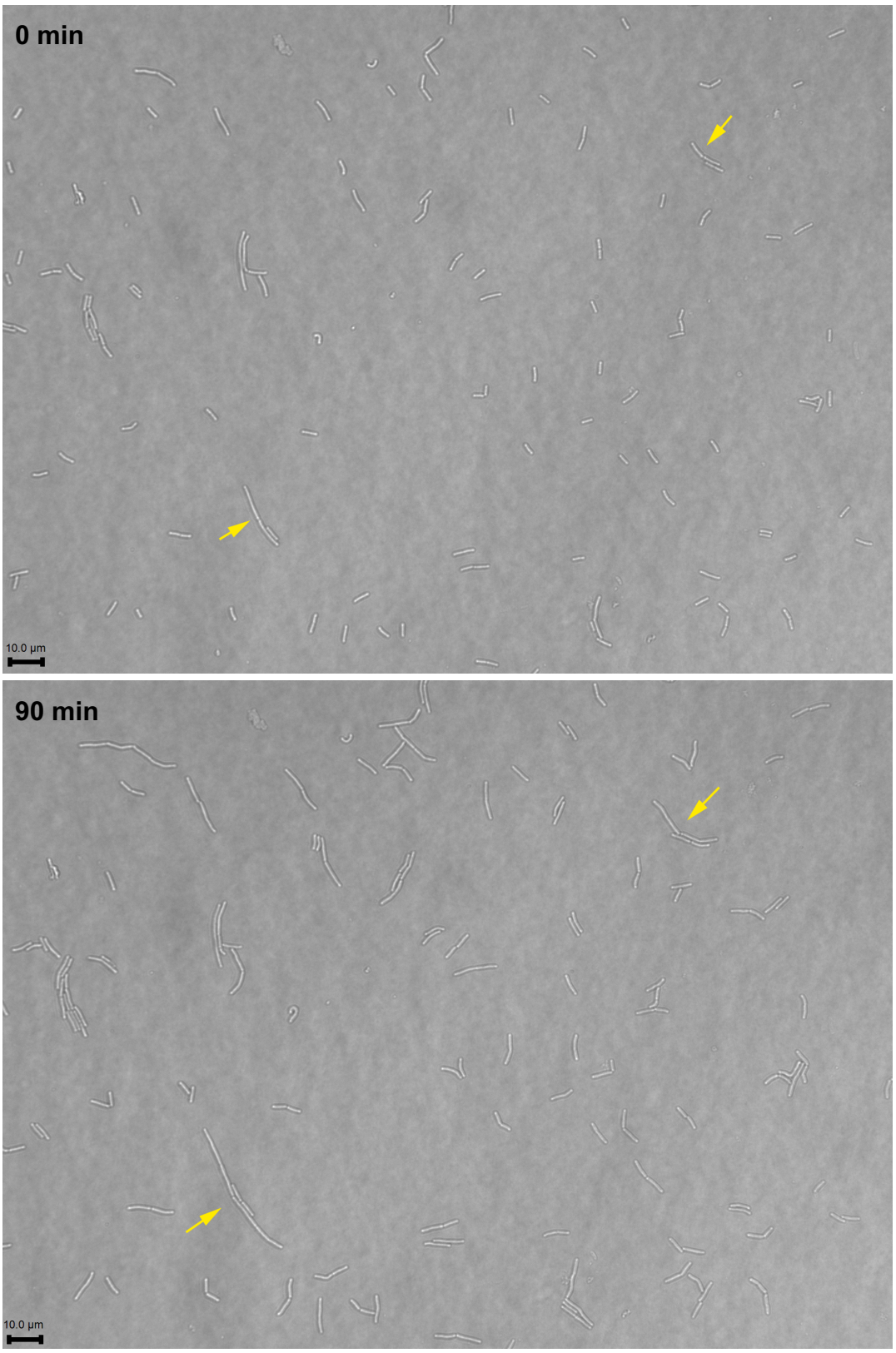

Figure S2.7. Time lapse microscopy of *B. subtilis* treated with sodium phosphate buffer containing 0.05% polysorbate 80. Cells were incubated at 37 °C under a sheet of LB agar. Most or all of the cells grew; yellow arrows illustrate representative growing cells.

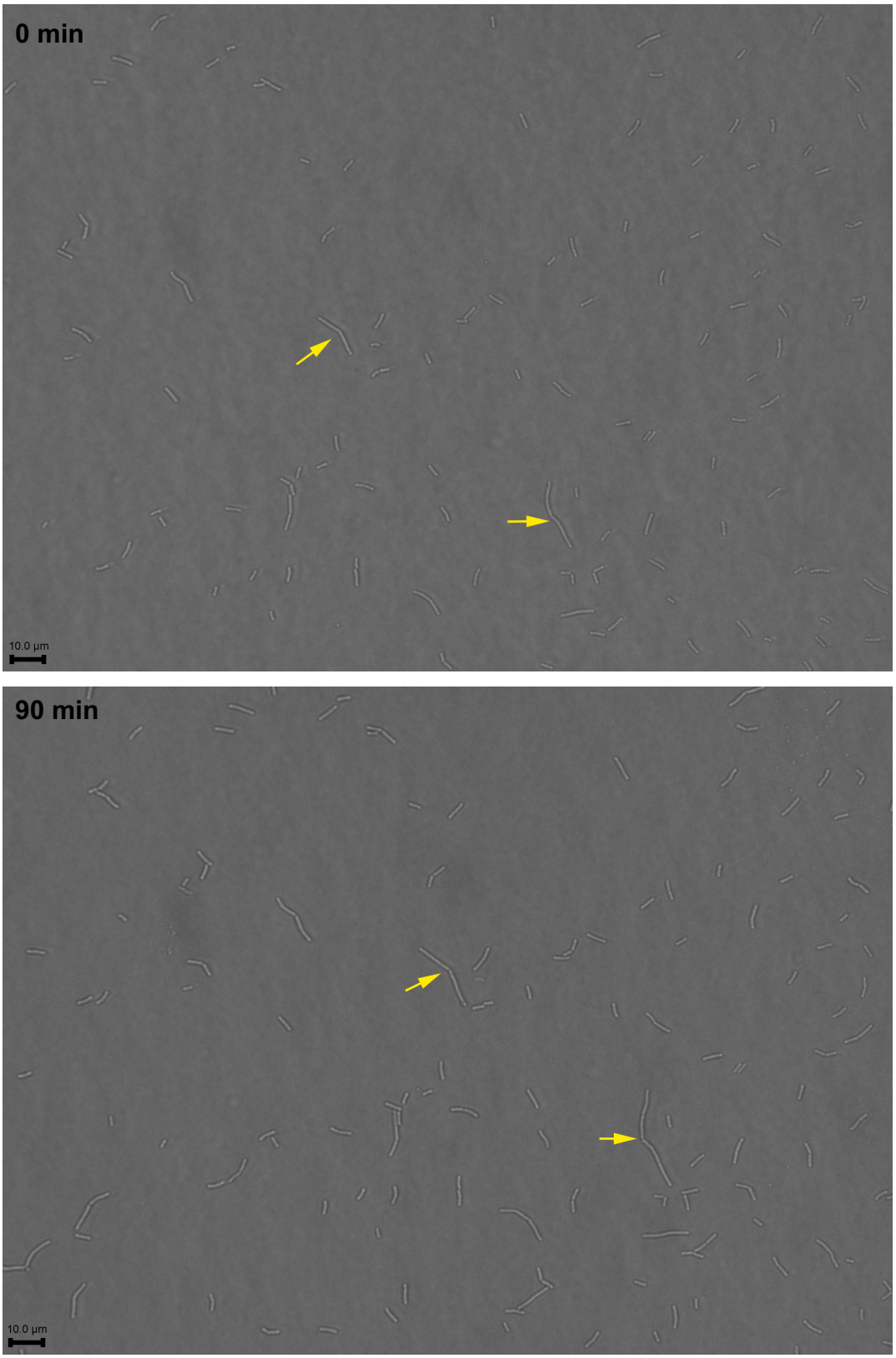

Figure S2.8. Time lapse microscopy of *B. subtilis* treated with 4 µg/mL Lys(Rhod)$_9$,Arg$_{10}$-teixobactin. Cells were incubated at 37 °C under a sheet of LB agar. Many of the cells grew; yellow arrows illustrate representative growing cells.

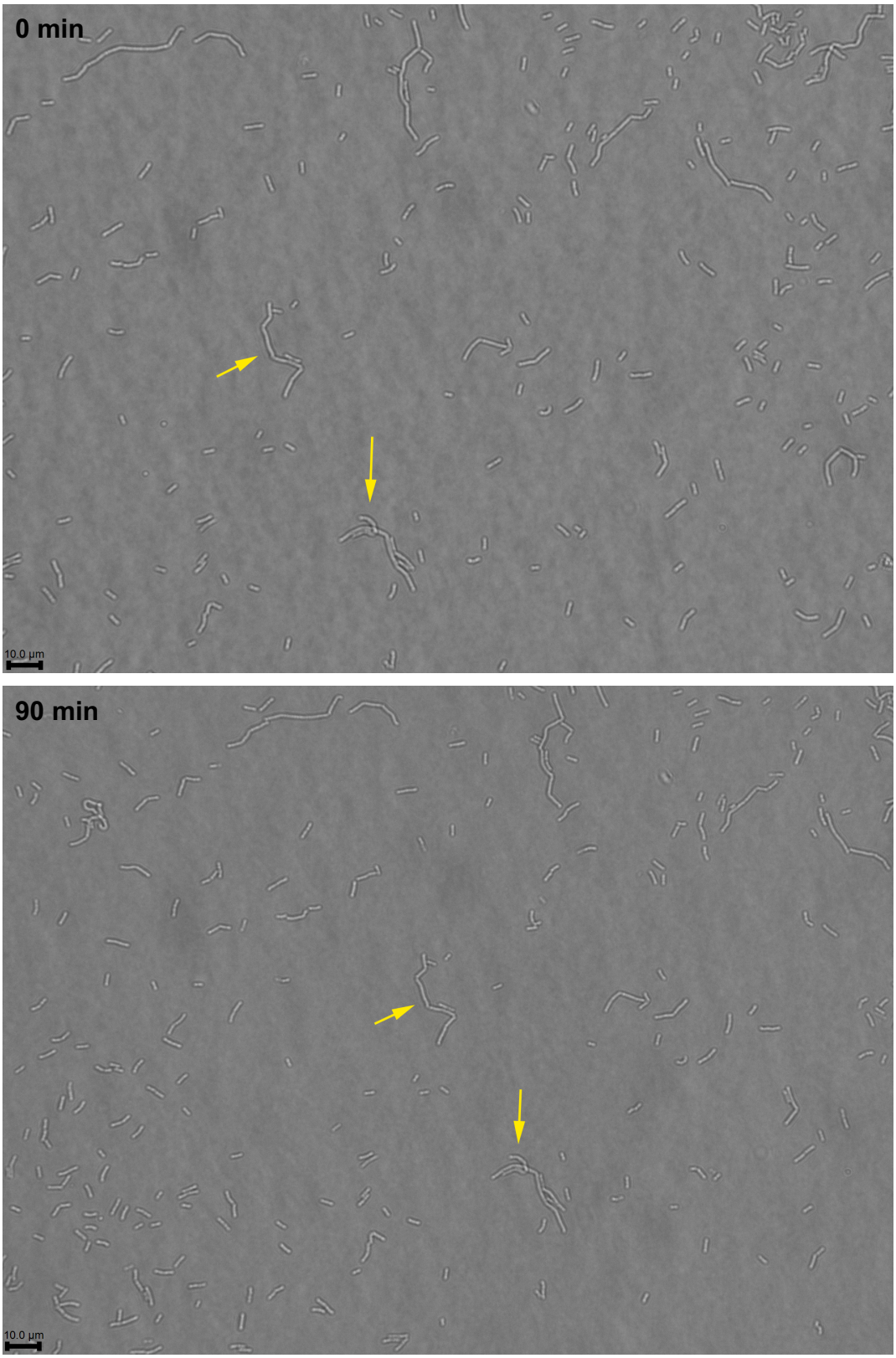

Figure S2.9. Time lapse microscopy of *B. subtilis* treated with 8 µg/mL Lys(Rhod)$_9$,Arg$_{10}$-teixobactin. Cells were incubated at 37 °C under a sheet of LB agar. Few or none of the cells grew; yellow arrows illustrate representative arrested cells.

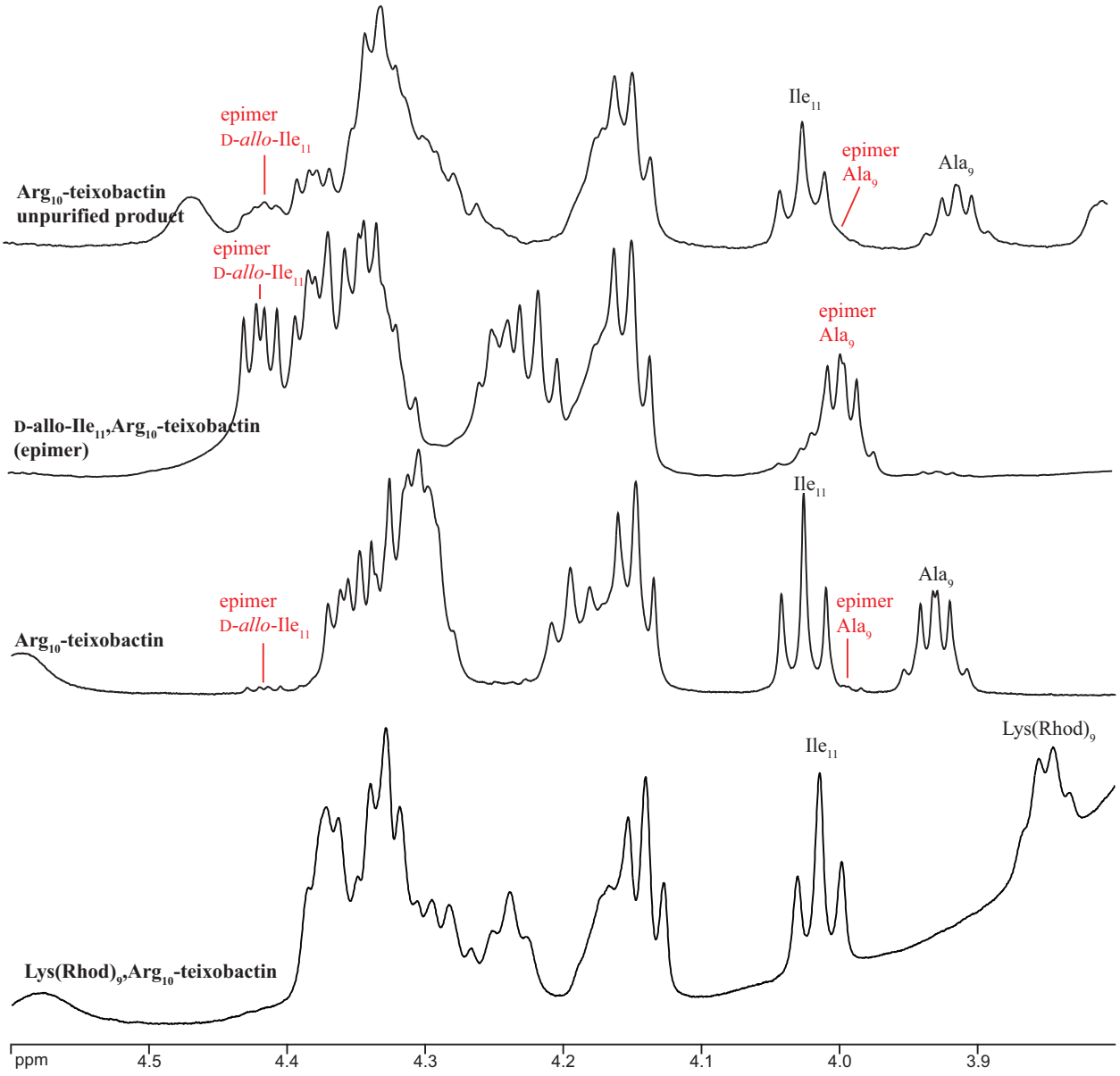

Figure S2.10. Lys(Rhod)$_9$,Arg$_{10}$-teixobactin is a single pure epimer. 600 MHz NMR spectrum of 2 mM Lys(Rhod)$_9$,Arg$_{10}$-teixobactin in DMSO-d_6, in comparison to Arg$_{10}$-teixobactin and the epimeric D-allo-Ile$_{11}$,Arg$_{10}$-teixobactin impurity. The spectra of Arg$_{10}$-teixobactin and the epimeric D-allo-Ile$_{11}$,Arg$_{10}$-teixobactin impurity are from *ACS Chem. Biol.* **2016**, *11*, 1823–1826 Supporting Information Figure S1.

Materials and Methods

General Methods. Amino acids, coupling agents, 2-chlorotrityl chloride resin, DIC, palladium-tetrakis(triphenylphosphine), and triisopropylsilane were purchased from Chem-Impex. Phenylsilane was purchased from TCI. DMF (amine-free), DIPEA, 2,4,6-collidine, piperidine, and paraformaldehyde were purchased from Alfa-Aesar. Sulforhodamine B sulfonyl chloride, DMAP, and polysorbate 80 were purchased from Acros Organics. HPLC-grade acetonitrile, dichloromethane, and LB agar were purchased from Fisher Scientific. TFA and hexafluoroisopropanol were purchased from Oakwood Chemical. Difco Mueller Hinton broth was obtained from Becton, Dickinson and Company. Brain Heart Infusion broth was obtained from Teknova. Molecular biology grade agarose and BODIPY FL vancomycin were obtained from Thermo Scientific. Sterile DMSO was obtained from Tocris.

Reagent-grade solvents, chemicals, amino acids, and resin were used as received, with the exception of dichloromethane, which was dried through an alumina column under argon, and dimethylformamide, which was dried through an alumina column and an amine scavenger resin column under argon. Solid-phase peptide synthesis was carried out manually in a solid phase reaction vessel. Analytical reverse-phase HPLC was performed on an Agilent 1200 instrument equipped with an Aeris PEPTIDE 2.6u XB-C18 column (Phenomonex). Preparative reverse-phase HPLC was performed on a Rainin Dynamax instrument equipped with a ZORBAX SB-C18 column (Agilent). UV detection (214 nm) was used for analytical and preparative HPLC. HPLC grade acetonitrile and 18 MΩ deionized water, each containing 0.1% trifluoroacetic acid, were used for analytical and preparative reverse-phase HPLC. Matrix-assisted laser desorption ionization time-of-flight (MALDI-TOF) mass spectrometry was performed on an AB SCIEX TOF/TOF 5800 system and 2,5-dihydroxybenzoic acid was used as the sample matrix. All peptides

were prepared and used as the trifluoroacetate salts and were assumed to have one trifluoroacetate ion per ammonium group present in each peptide. Excitation and emission spectra of Lys(Rhod)$_9$,Arg$_{10}$-teixobactin and *seco*-Lys(Rhod)$_9$,Arg$_{10}$-teixobactin were recorded on a Cary Eclipse fluorescence spectrometer. ^{1}H NMR spectra of Lys(Rhod)$_9$,Arg$_{10}$-teixobactin were collected on a Bruker Avance 600 MHz NMR equipped with a BBFO cryoprobe.

Synthesis of Lys(Rhod)$_9$,Arg$_{10}$-teixobactin.[1] *Resin loading*. 2-Chlorotrityl chloride resin (300 mg, 1.46 mmol/g) was added to a 10-mL Bio-Rad Poly-Prep chromatography column. The resin was suspended in dry CH_2Cl_2 (10 mL) and allowed to swell for 30 min. The resin was loaded with a solution of Fmoc-Arg(Pbf)-OH (180 mg, 0.28 mmol, 0.78 equiv) and 2,4,6-collidine (300 μL) in dry CH_2Cl_2 (8 mL). The suspension was agitated for 4−12 h until a resin loading of at least 50% was achieved. The solution was drained, and the resin was washed with dry CH_2Cl_2 (3x). A mixture of CH_2Cl_2/MeOH/DIPEA (17:2:1, 5 mL) was added to the resin and agitated for 1 h to cap any unreacted 2-chlorotrityl chloride sites. The solution was drained, and the resin was washed with dry CH_2Cl_2 (3x). The resin was then dried with a flow of nitrogen.

Quantifying resin loading. A small portion of loaded resin was removed from the column and dried under vacuum. 1.0 mg of the dried resin was weighed out and transferred to a scintillation vial containing 3 mL of 20% piperidine/DMF and a small magnetic stirring bar. The reaction mixture was allowed to stir for 10 min and the absorbance at 290 nm was measured. The resin loading was determined to be 0.16 mmol (0.54 mmol/g, 57% loading) using the following formula:

$$\%\ \text{loading} = \frac{A_{290\ \text{nm}} \times V \times 10^3}{6089 \times m_{\text{resin}} \times l} \times 100\%$$

where:

A_{290} nm = Absorbance measured at 290 nm

ε = Molar absorptivity of piperidine adduct (6,089 L mol^{-1} cm^{-1})

m_{resin} = Mass of resin in mg (1.0 mg)

V = Volume of piperidine in DMF in mL (3.0 mL)

l = Cell pathlength in cm (1.0 cm)

Linear peptide synthesis. The loaded resin was suspended in dry DMF and transferred to a solid-phase peptide synthesis reaction vessel for manual peptide synthesis using Fmoc-Lys(Alloc)-OH, Fmoc-D-Thr-OH (free alcohol OH), Fmoc-Ser(*t*-Bu)-OH, Fmoc-Ile-OH, Fmoc-D-*allo*-Ile-OH, Fmoc-D-Gln(Trt)-OH, Fmoc-Ser(*t*-Bu)-OH, Fmoc-Ile-OH, and Boc-*N*-methyl-D-Phe-OH. The linear peptide was synthesized through the following cycles: *i*. Fmoc deprotection with 20% (*v/v*) piperidine in dry DMF (5 mL) for 10 min (2x), *ii*. resin washing with dry DMF (3x), *iii*. coupling of amino acid (0.64 mmol, 4 equiv) with HCTU (267 mg, 0.64 mmol, 4 equiv) in 20% (*v/v*) 2,4,6-collidine in dry DMF (5 mL) for 20 min, and *iv*. resin washing with dry DMF (3x). After the linear synthesis was completed, the resin was then washed with dry CH_2Cl_2 in the solid-phase peptide synthesis reaction vessel (3x).

On-resin Alloc deprotection.[2] $PhSiH_3$ (478 μL, 3.87 mmol, 24 equiv) and $Pd(PPh_3)_4$ (19 mg, 0.02 mmol, 0.1 equiv) were dissolved in 4 mL dry CH_2Cl_2. The solution was added to the resin in the solid-phase peptide synthesis reaction vessel with agitation by bubbling of nitrogen gas. After 10 min, the solution was drained, and the resin was washed with dry CH_2Cl_2 (8x). The deprotection reaction was repeated once more using the same procedure, and the solution was drained.

On-resin labeling with sulforhodamine B sulfonyl chloride. The resin was washed with dry DMF (3x) in the solid-phase peptide synthesis reaction vessel. Sulforhodamine B sulfonyl chloride (188 mg, 0.32 mmol, 2 equiv) was dissolved in 20% 2,4,6-collidine in dry DMF (5 mL). The solution was transferred to the reaction vessel and allowed to react with the resin for 1 h while bubbling under nitrogen gas. The solution was drained and the resin was washed with dry DMF (20x) until residual dye was removed.

NOTE: These procedures were performed in an unlit fume hood and the reaction vessel was protected from excess exposure to light by draping with black felt when not manipulating the resin. During subsequent steps, similar efforts were made to protect the labeled peptide from light.

Esterification.[3] The resin was transferred to a 10-mL Bio-Rad Poly-Prep chromatography column and washed with dry CH_2Cl_2 (3x). In a test tube, Fmoc-Ile-OH (570 mg, 1.6 mmol, 10 equiv) and diisopropylcarbodiimide (250 μL, 1.6 mmol, 10 equiv) were dissolved in dry CH_2Cl_2 (5 mL). The resulting solution was filtered through 0.20-μm nylon filter, and then 4-dimethylaminopyridine (19.7 mg, 0.16 mmol, 1 equiv) was added to the filtrate. The resulting solution was transferred to the resin and was gently agitated for 1 h. The solution was drained and the resin was washed with dry CH_2Cl_2 (3x) and DMF (3x).

Fmoc deprotection and peptide cleavage. The Fmoc protecting group on Ile_{11} was removed by treatment with 20% piperidine in dry DMF (5 mL) for 10 min (2x). The solution was drained and the resin was washed with dry DMF (3x) and then with dry CH_2Cl_2 (3x). To cleave the peptide, the resin was treated with 20% hexafluoroisopropanol (HFIP) in dry CH_2Cl_2 (6 mL) with agitation for 1 h. The filtrate was collected in a round-bottom flask. The HFIP treatment was repeated, and the filtrate was added to the round-bottom flask. The resin was washed with an additional aliquot of 20% HFIP (6 mL) and then washed with dry CH_2Cl_2 (3x). The combined filtrates and methylene

chloride washes were concentrated under reduced pressure to afford a red oil. The oil was placed under vacuum (≤ 0.1 mmHg) to remove any residual solvents.

Cyclization. The oil was dissolved in 125 mL of dry DMF. HBTU (367 mg, 0.97 mmol, 6 equiv) and HOBt (131 mg, 0.97 mmol, 6 equiv) were added to the solution. The reaction mixture was stirred under nitrogen for 30 min. DIPEA (170 μL, 0.97 mmol, 6 equiv) was added over ca. 10 s to the solution, and the reaction mixture was stirred for 12 h. The mixture was concentrated under reduced pressure to afford the cyclized peptide as a pink solid. The solid was placed under vacuum (≤ 0.1 mmHg) to remove any residual solvents.

Global deprotection, ether precipitation, and purification. The crude protected peptide was dissolved in a mixture of trifluoroacetic acid (TFA)/triisopropylsilane/H_2O (90:5:5, 10 mL), and the solution was stirred under nitrogen for 1 h. The deprotection mixture was then evenly aliquoted between two 40-mL portions of ice-cold diethyl ether in 50-mL conical tubes. The 50-mL conical tubes were centrifuged (400 x G) for 15 min to precipitate the crude peptide. The diethyl ether supernatant was discarded and the precipitated pellets were dried under nitrogen. The pellets were dissolved in 40% (*v/v*) CH_3CN in water (8 mL) and centrifuged at 3300 rpm (1380 x G) for 5 min, and the solution was filtered through 0.20-μm nylon filter. The peptide was purified by reverse-phase HPLC with H_2O/CH_3CN (gradient elution of 20–60% CH_3CN with 0.1% TFA over 120 min), with the C18 column being heated to 50 °C in a Sterlite plastic bin water bath equipped with a Kitchen Gizmo Sous Vide immersion circulator.[4] Fractions analyzed by analytical HPLC and MALDI mass spectrometry. The pure fractions were combined and lyophilized to give 5 mg (1.7% yield based on resin loading) of $Lys(Rhod)_9$,Arg_{10}-teixobactin trifluoroacetate (TFA) salt as red powder.

Synthesis of *seco*-Lys(Rhod)$_9$,Arg$_{10}$-teixobactin.[1] The *seco*-Lys(Rhod)$_9$,Arg$_{10}$-teixobactin analogue was prepared using similar procedures to those described above. The analogue was prepared as a linear peptide by conventional Fmoc-based solid-phase peptide synthesis, starting with Fmoc-Ile-OH on 2-chlorotrityl resin. Purification afforded 8.9 mg (3.0% yield based on resin loading) of *seco*-Lys(Rhod)$_9$,Arg$_{10}$-teixobactin trifluoroacetate (TFA) salt as red powder.

Preparation of DMSO Stock Solutions. A 1 mg/mL DMSO stock solution of Lys(Rhod)$_9$,Arg$_{10}$-teixobactin was prepared gravimetrically by dissolving 1.0 mg of the lyophilized peptide in 1 mL of sterile DMSO in an autoclaved Eppendorf tube. BODIPY FL vancomycin (100 μg, ThermoFisher) was dissolved in 100 μL of sterile DMSO to create a 1 mg/mL stock solution. The 1 mg/mL DMSO stock solutions were wrapped in black felt and stored in a −20 °C freezer for subsequent experiments.

NOTE: Solutions of Lys(Rhod)$_9$,Arg$_{10}$-teixobactin were protected from excessive exposure to light in MIC assays and other experiments by use of an unlit biosafety cabinet, black felt, and minimizing exposure to room lights.

MIC Assays.[1] *Bacillus subtilis* (ATCC 6051), *Staphylococcus epidermidis* (ATCC 14990), *Staphylococcus aureus* (ATCC 29213), and *Escherichia coli* (ATCC 10798) were cultured from glycerol stocks in Mueller-Hinton broth overnight in a shaking incubator at 37 °C. *Enterococcus durans* (ATCC 6056) and *Streptococcus salivarius* (ATCC 13419) were cultured from glycerol stocks in brain heart infusion broth overnight in a shaking incubator at 37 °C. An aliquot of the 1 mg/mL antibiotic stock solution was diluted with culture media to make a 64 μg/mL solution. A 200-μL aliquot of the 64 μg/mL solution was transferred to a 96-well plate. Two-fold serial dilutions were made with media across a 96-well plate to achieve a final volume of 100 μL in each

well. These solutions had the following concentrations: 64, 32, 16, 8, 4, 2, 1, 0.5, 0.25, 0.125, and 0.0625 μg/mL. The overnight cultures of each bacterium were diluted with either Mueller-Hinton broth (*Bacillus subtilis*, *Staphylococcus epidermidis*, *Staphylococcus aureus*, and *Escherichia coli*) or brain heart infusion broth (*Enterococcus durans* and *Streptococcus salivarius*) to an OD_{600} of 0.075 as measured for 200 μL in a 96-well plate. The diluted mixture was further diluted to 1 x 10^6 CFU/mL with the appropriate media (dilution of 50x for *B. subtilis*, 60x for *E. durans*, 50x for *S. salivarius*, 10x for *S. aureus*, 10x for *S. epidermidis*, and 50x for *E. coli*).[22] A 100-μL aliquot of the 1 x 10^6 CFU/mL bacterial solution was added to each well in 96-well plates, resulting in final bacteria concentrations of 5 x 10^5 CFU/mL in each well. As 100 μL of bacteria were added to each well, the teixobactin analogues were also diluted to the following concentrations: 32, 16, 8, 4, 2, 1, 0.5, 0.25, 0.125, 0.0625, and 0.03125 μg/mL. The plate was covered with a lid and incubated at 37 °C for 16 h. The optical density measurements were recorded at 700 nm instead of 600 nm due to sulforhodamine absorbance and were measured using a 96-well UV/Vis plate reader (MultiSkan GO, Thermo Scientific). The MIC values were taken as the lowest concentration that had no bacteria growth. Each MIC assay was run in triplicate in three independent runs to ensure reproducibility. MIC assays were performed in test media containing with and without polysorbate 80 (0.002% or 0.05%).

Fluorescence Microscopy Studies. *Preparation of sodium phosphate buffers*. A 10x sodium phosphate buffer was prepared by dissolving 14.4 g of Na_2HPO_4 (0.100 moles) and 2.4 g of KH_2PO_4 (0.018 moles) in 1 L of 18 MΩ deionized water. The solution was stirred and gently heated on a hot plate until the buffer salts were completely dissolved. The pH of the 10x sodium phosphate buffer was adjusted to 7.4 using either 6 M HCl or 6 M NaOH and was subsequently sterile filtered. To create a 1x sodium phosphate buffer (12 mM), the 10x sodium phosphate buffer

was diluted 10-fold using 18 MΩ deionized water and, if necessary, the pH was adjusted using either 6 M HCl or 6 M NaOH. If needed, the desired amount of polysorbate 80 was added to the 12 mM sodium phosphate buffer, with gentle heating and stirring on a hot plate until the polysorbate 80 dissolved. All buffers were sterile filtered.

Culturing bacteria for imaging. Bacteria were allowed to grow overnight (ca. 16 h) in the appropriate broth (Mueller-Hinton broth or brain heart infusion broth) in a shaking incubator at 37 °C. The following morning, the cultures were diluted 1:100 in the appropriate broth and were allowed to grow exponentially in a shaking incubator at 37 °C. Once an OD_{600} of ca. 0.3 was achieved, 500 µL of bacteria was transferred to a sterile Eppendorf tube and the bacteria were centrifuged at 4000 rpm (1300 x G) for 5 min.

Preparation of 2% agarose beds for imaging bacteria. A 2% stock solution of agarose was prepared by adding 1 g of agarose into 50 mL of sodium phosphate buffer, autoclaving, and allowing the solution to cool until it completely solidified. While the bacteria were growing in the shaking incubator, fresh 2% agarose beds were prepared to immobilize bacteria for fluorescence microscopy studies as follow: On a laboratory bench equipped with an alcohol burner [to help maintain sterility], microscope slides were gently warmed on a hot plate. While the slides were gently warming, the solidified 2% agarose solution was heated in a microwave oven until it became a homogenous liquid. Once the microscope slides were warm to the touch, a 75-µL aliquot of the molten 2% agarose solution was applied to each microscope slide, and a No. 1.5 coverslip was immediately applied gently to the drop of agarose. The assembly was allowed to set for at least 45 minutes before use.

Preparation of Lys(Rhod)$_9$,Arg$_{10}$-teixobactin and BODIPY FL vancomycin solutions for fluorescence microscopy studies. While the bacteria were being centrifuged, a 4 µg/mL solution

of Lys(Rhod)$_9$,Arg$_{10}$-teixobactin was freshly prepared and then used immediately to stain the bacteria. The 4 μg/mL solution was prepared by diluting 2.4 μL of the 1 mg/mL DMSO stock solution with 597.6 μL of sterile sodium phosphate buffer containing 0.05% polysorbate 80. A solution containing 1 μg/mL of Lys(Rhod)$_9$,Arg$_{10}$-teixobactin and 1 μg/mL of Arg$_{10}$-teixobactin was prepared by combining 2 μL of each 1 mg/mL DMSO stock solution and then diluting with 1.996 mL of sterile sodium phosphate buffer containing 0.05% polysorbate 80. A solution containing 4 μg/mL of Lys(Rhod)$_9$,Arg$_{10}$-teixobactin and 4 μg/mL of BODIPY FL vancomycin was prepared by combining 2.4 μL of each 1 mg/mL DMSO stock solution, followed by dilution with 595.2 μL of sterile sodium phosphate buffer containing 0.05% polysorbate 80. The fluorescent antibiotic solutions were subsequently vortexed for 30 seconds and then used immediately to stain the bacteria, in order to avoid aggregation of the Lys(Rhod)$_9$,Arg$_{10}$-teixobactin probe. [The stained bacteria should also be imaged immediately, as formation of Lys(Rhod)$_9$,Arg$_{10}$-teixobactin aggregates on the bacteria was observed when the stained bacteria were incubated on the microscope slides.]

Staining bacteria for fluorescence microscopy studies. After centrifuging the bacteria (see above), the supernatant was removed, the pellet was resuspended in 500 μL of 4 μg/mL of the probe solution, and the bacteria were incubated in a shaking incubator at 37 °C for 10 min. The bacteria were centrifuged at 4000 rpm (1300 x G) for 5 min, and the supernatant was removed. The pellet was resuspended in 500 μL of sterile sodium phosphate buffer containing 0.05% polysorbate 80, the suspension was centrifuged at 4000 rpm (1300 x G) for 5 min, and the supernatant was removed. This washing process was repeated two additional times. After the last wash, the cells were resuspended in 200−500 μL of sterile sodium phosphate buffer containing 0.05% polysorbate 80. [The volume of phosphate buffer was selected based on the size of the pellet

remaining after the washing steps.] On a sterile bench, the coverslip of each agarose bed was removed, and a 5-µL aliquot of the stained bacteria was applied to the coverslip. The coverslip was then sandwiched on top of the agarose bed.

S. aureus staining and fixation. Methicillin sensitive *S. aureus* (ATCC 29213) was fixed with formalin prior to imaging, because it is a BSL-2 pathogen. *S. aureus* was cultured, diluted, stained, and washed using the same protocols as described above. After the final wash, the stained *S. aureus* cells were centrifuged and the supernatant was removed. The pellet was resuspended in 50 µL of sodium phosphate buffer containing 0.05% polysorbate 80. 500 µL of 4% formalin in sodium phosphate buffer[5] was added, and the suspension was gently mixed by pipetting. The Eppendorf tube containing the cells was wrapped in black felt and was agitated for 20 min at room temperature on an orbital shaker. The cells isolated by centrifugation at 4000 rpm (1300 x G) for 5 min and then resuspended in 500 µL sodium phosphate buffer containing 0.05% polysorbate 80. The stained, fixed *S. aureus* cells were then immobilized onto agarose pads using the same procedure described above.

Imaging the bacteria. The stained bacteria were immediately imaged on a Zeiss LSM 780 confocal fluorescence microscope. Images were collected with a 63x oil immersion objective lens, with additional optical zoom used as needed to provide detailed images. Fluorescence micrographs of bacteria treated with Lys(Rhod)$_9$,Arg$_{10}$-teixobactin or *seco*-Lys(Rhod)$_9$,Arg$_{10}$-teixobactin were recorded with excitation at 561 nm and emission between 568–639 nm. Fluorescence micrographs of bacteria treated with BODIPY FL vancomycin were recorded with excitation at 488 nm and emission between 490–544 nm. For both the Lys(Rhod)$_9$,Arg$_{10}$-teixobactin and BODIPY FL vancomycin channels, the pinhole size was set to 53–64 µm and the gain was set to 650–700 AU. The image brightness of the Lys(Rhod)$_9$,Arg$_{10}$-teixobactin and BODIPY FL vancomycin channels

were adjusted linearly using Volocity 6.3 (Quorum Technologies), and a medium filter in the Volocity software was used to reduce noise in all channels.

*Treatment of B. subtilis with sulforhodamine B N-butylsulfonamide***.** To test whether sulforhodamine B is responsible for the staining patterns observed in Figures 3–5, we treated *B. subtilis* with sulforhodamine B *N*-butylsulfonamide. Sulforhodamine B *N*-butylsulfonamide was synthesized as follows: Sulforhodamine B sulfonyl chloride (289 mg, 0.5 mmol) was dissolved in 5 mL of anhydrous ether at 0 °C. To this solution, butylamine (0.49 mL, 5.0 mmol) was added over ca. 30 s, and the reaction mixture was allowed to stir at 0 °C for 2 h. The reaction mixture was concentrated *in-vacuo*, the residue was recrystallized from 5 mL of boiling hot EtOH, and solids were isolated by vacuum filtration and rinsed with ice-cold EtOH. After drying under vacuum (≤ 0.1 mmHg), pure sulforhodamine B *N*-butylsulfonamide was obtained as a red solid (252 mg, 84%). ^{1}H NMR (400 MHz, DMSO-d_6): δ 8.41 (d, J = 1.8 Hz, 1 H), 7.93 (dd, J = 8.0, 1.9 Hz, 2 H), 7.87 (t, J = 5.6 Hz, 1 H), 7.46 (d, J = 7.8 Hz, 1 H), 7.04 (dd, J = 9.5, 2.6 Hz, 2 H), 6.97 (d, J = 9.5 Hz, 2 H), 6.94 (d, J = 2.4 Hz, 2 H), 3.59–3.69 (m, 8 H), 2.86 (q, J = 6.6 Hz, 2 H), 1.43 (quint, J = 7.3 Hz, 2 H), 1.29 (sextet, J = 7.4 Hz, 2 H), 1.21 (t, J = 7.0 Hz, 12 H), 0.85 (t, J = 7.3 Hz, 3 H) ppm.

Competition experiments using Lys(Rhod)$_9$,Arg$_{10}$-teixobactin and Arg$_{10}$-teixobactin. B. subtilis was treated with 4 µg/mL Lys(Rhod)$_9$,Arg$_{10}$-teixobactin for 10 min at 37 °C, then treated with 4 µg/mL Arg$_{10}$-teixobactin for 10 min at 37 °C, and finally washed with phosphate buffer containing 0.05% polysorbate 80 twice to determine if Arg$_{10}$-teixobactin could displace Lys(Rhod)$_9$,Arg$_{10}$-teixobactin (Figure 2.8A). We also carried out a second experiment in which we first treated *B. subtilis* with 4 µg/mL Arg$_{10}$-teixobactin for 10 min at 37 °C, then stained with 4 µg/mL Lys(Rhod)$_9$,Arg$_{10}$-teixobactin for 10 min at 37 °C, and finally washed with phosphate

buffer containing 0.05% polysorbate 80 twice to see if Arg_{10}-teixobactin could block staining by Lys(Rhod)$_9$,Arg_{10}-teixobactin (Figure 2.8B). We carried out a third experiment where *B. subtilis* was stained with 4 μg/mL of Lys(Rhod)$_9$,Arg_{10}-teixobactin for 10 min at 37 °C, then treated with 4 μg/mL of Arg_{10}-teixobactin for 10 min at 37 °C three times consecutively to determine if three successive treatments of Arg_{10}-teixobactin could displace Lys(Rhod)$_9$,Arg_{10}-teixobactin (Figure 2.8C). As controls, we also stained *B. subtilis* with either 4 μg/mL Lys(Rhod)$_9$,Arg_{10}-teixobactin for 10 min at 37 °C followed by three washes (Figure S8D), or 4 μg/mL Arg_{10}-teixobactin for 10 min at 37 °C followed by three washes (Figure S8E). As expected, the bacteria treated with 4 μg/mL Lys(Rhod)$_9$,Arg_{10}-teixobactin exhibited staining (Figure S8D), whereas the bacteria treated with 4 μg/mL Arg_{10}-teixobactin exhibited no staining (Figure 2.8E). Cells were imaged on a Keyence BZ-X810 fluorescence microscope using the TexasRed filter cube (excitation wavelength = 560/40 nm and emission wavelength = 630/75 nm). The exposure was set to 1/10 s. Images were collected with a 60x oil immersion objective lens with optical zoom using the high-resolution camera sensitivity and oblique illumination settings.

Competition experiments using BODIPY FL vancomycin and unlabeled vancomycin. B. subtilis was treated with 2.5 μg/mL BODIPY FL vancomycin for 10 min at 37 °C, then treated with 2.5 μg/mL vancomycin for 10 min at 37 °C, and finally washed with phosphate buffer containing 0.05% polysorbate 80 twice to determine if unlabeled vancomycin could displace BODIPY FL vancomycin (Figure 2.9A). We also carried out a second experiment in which we first treated *B. subtilis* with 2.5 μg/mL vancomycin for 10 min at 37 °C, then stained with 2.5 μg/mL BODIPY FL vancomycin for 10 min at 37 °C, and finally washed with phosphate buffer containing 0.05% polysorbate 80 twice to see if unlabeled vancomycin could block staining by BODIPY FL vancomycin (Figure 2.9B). We carried out a third experiment where *B. subtilis* was

stained with 2.5 µg/mL of BODIPY FL vancomycin for 10 min at 37 °C, then treated with 2.5 µg/mL of vancomycin for 10 min at 37 °C three times consecutively to determine if three successive treatments of vancomycin could displace BODIPY FL vancomycin (Figure 2.9C). As controls, we also stained *B. subtilis* with either 2.5 µg/mL BODIPY FL vancomycin for 10 min at 37 °C followed by three washes (Figure 2.9D), or 2.5 µg/mL vancomycin for 10 min at 37 °C followed by three washes (Figure 2.9E). As expected, the bacteria treated with 2.5 µg/mL BODIPY FL vancomycin exhibited staining (Figure 2.9D), whereas the bacteria treated with 2.5 µg/mL vancomycin exhibited no staining (Figure 2.9E). Cells were imaged on a Keyence BZ-X810 fluorescence microscope using the eGFP filter cube (excitation wavelength = 470/40 nm and emission wavelength = 525/50 nm). The exposure was set to 1/2 s. Images were collected with a 60x oil immersion objective lens with optical zoom using the high-resolution camera sensitivity and oblique illumination settings.

Characterization data

Lys(Rhod)$_9$,Arg$_{10}$-teixobactin

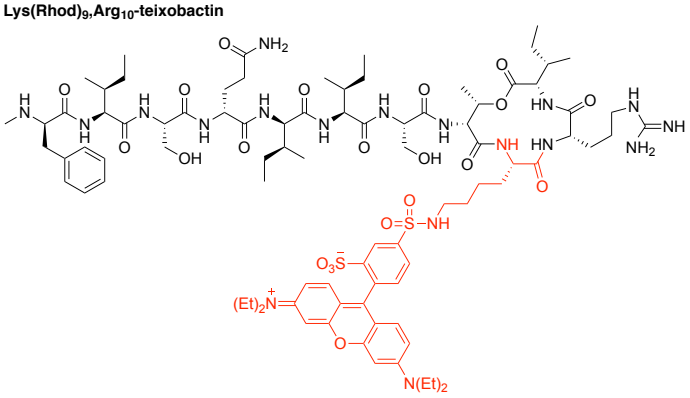

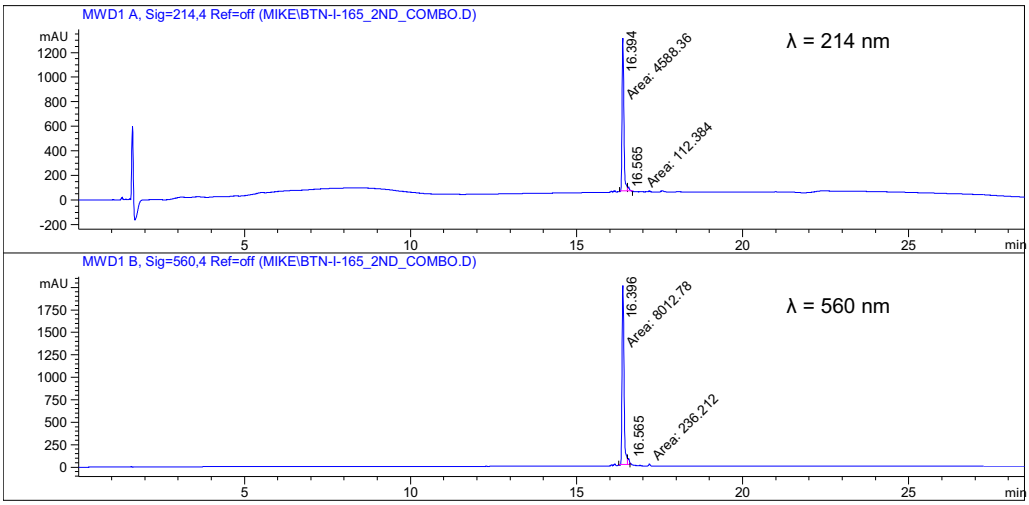


```
=====================================================================
                        Area Percent Report
=====================================================================

Sorted By             :      Signal
Multiplier            :      1.0000
Dilution              :      1.0000
Sample Amount:                :     20.00000  [ng/ul]    (not used in calc.)
Do not use Multiplier & Dilution Factor with ISTDs


Signal 1: MWD1 A, Sig=214,4 Ref=off

Peak RetTime Type  Width     Area      Height     Area
  #   [min]        [min]   [mAU*s]     [mAU]       %
----|-------|----|-------|----------|----------|--------|
   1  16.394 MF    0.0614 4588.35986 1245.82031  97.6092
   2  16.565 FM    0.0632  112.38380   29.63955   2.3908
```

Analytical HPLC with gradient elution of 5–100% acetonitrile over 20 min on an Aeris PEPTIDE 2.6u XB-C18 column (Phenomonex).

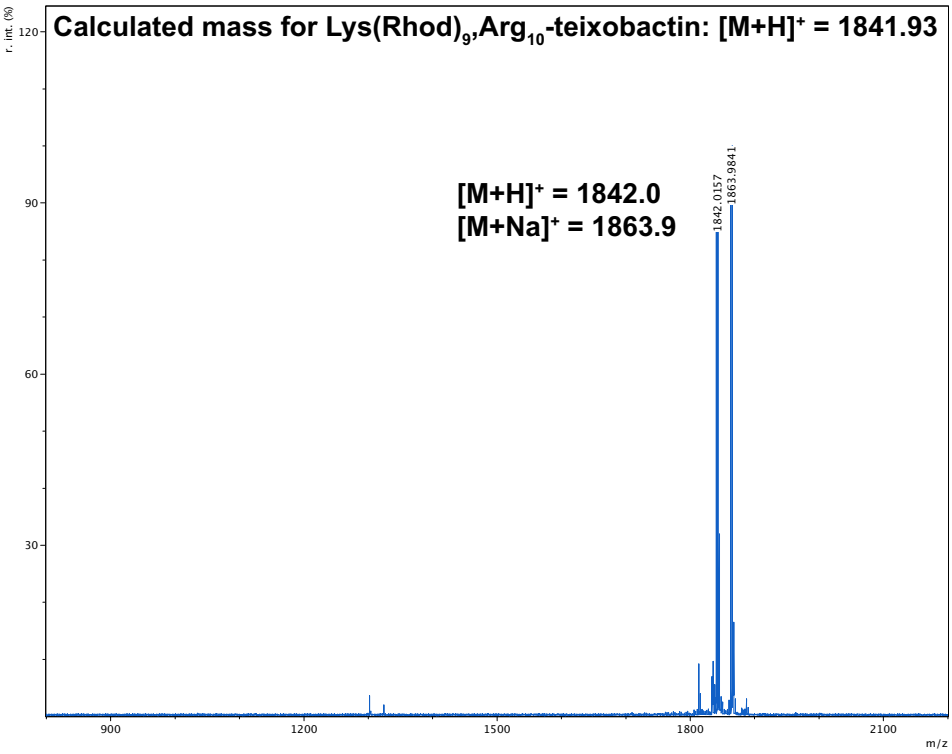
Calculated mass for Lys(Rhod)9,Arg10-teixobactin: [M+H]+ = 1841.93
[M+H]+ = 1842.0
[M+Na]+ = 1863.9
1842.0157
1863.9841
r. int. (%)
m/z

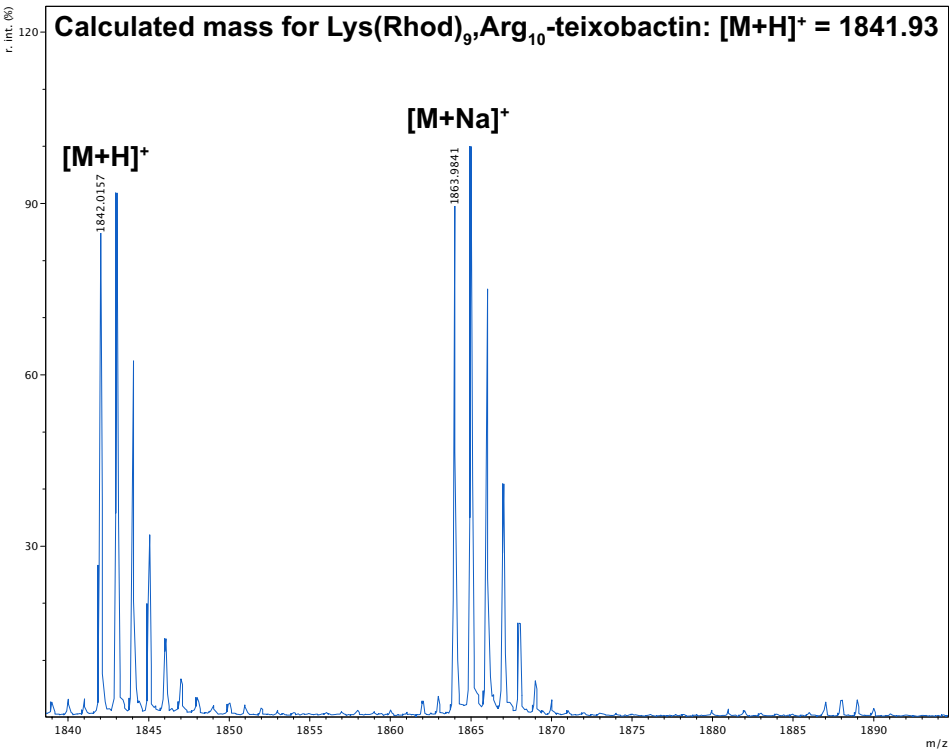
Calculated mass for Lys(Rhod)9,Arg10-teixobactin: [M+H]+ = 1841.93
[M+H]+
[M+Na]+
1842.0157
1863.9841
r. int. (%)
m/z

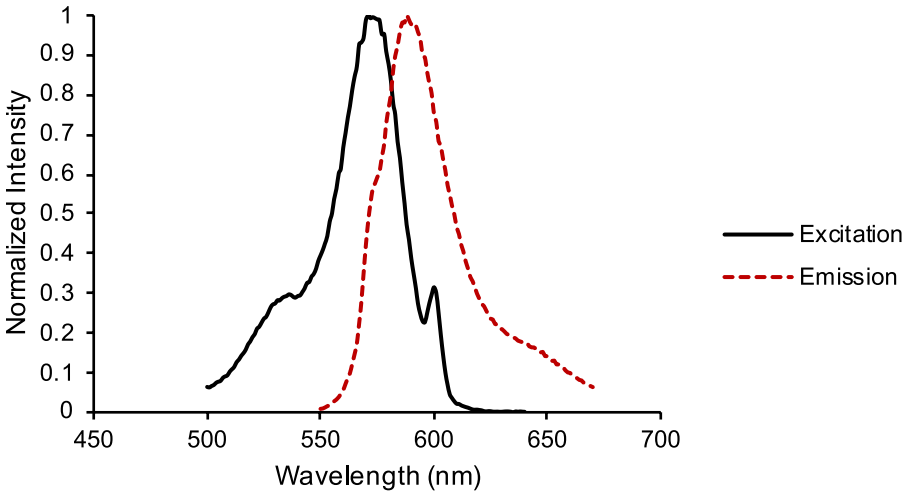

Figure S2.11. Excitation and emission spectra of 4 μg/mL of Lys(Rhod)$_9$,Arg$_{10}$-teixobactin in sodium phosphate buffer with 0.05% polysorbate 80 (pH 7.4). The emission spectrum was collected with excitation at 572 nm. The absorption and emission maxima are 571 nm and 588 nm, respectively.

2 mM Lys(Rhod)$_9$,Arg$_{10}$-teixobactin: ^{1}H NMR spectrum in DMSO-d_6 (600 MHz)

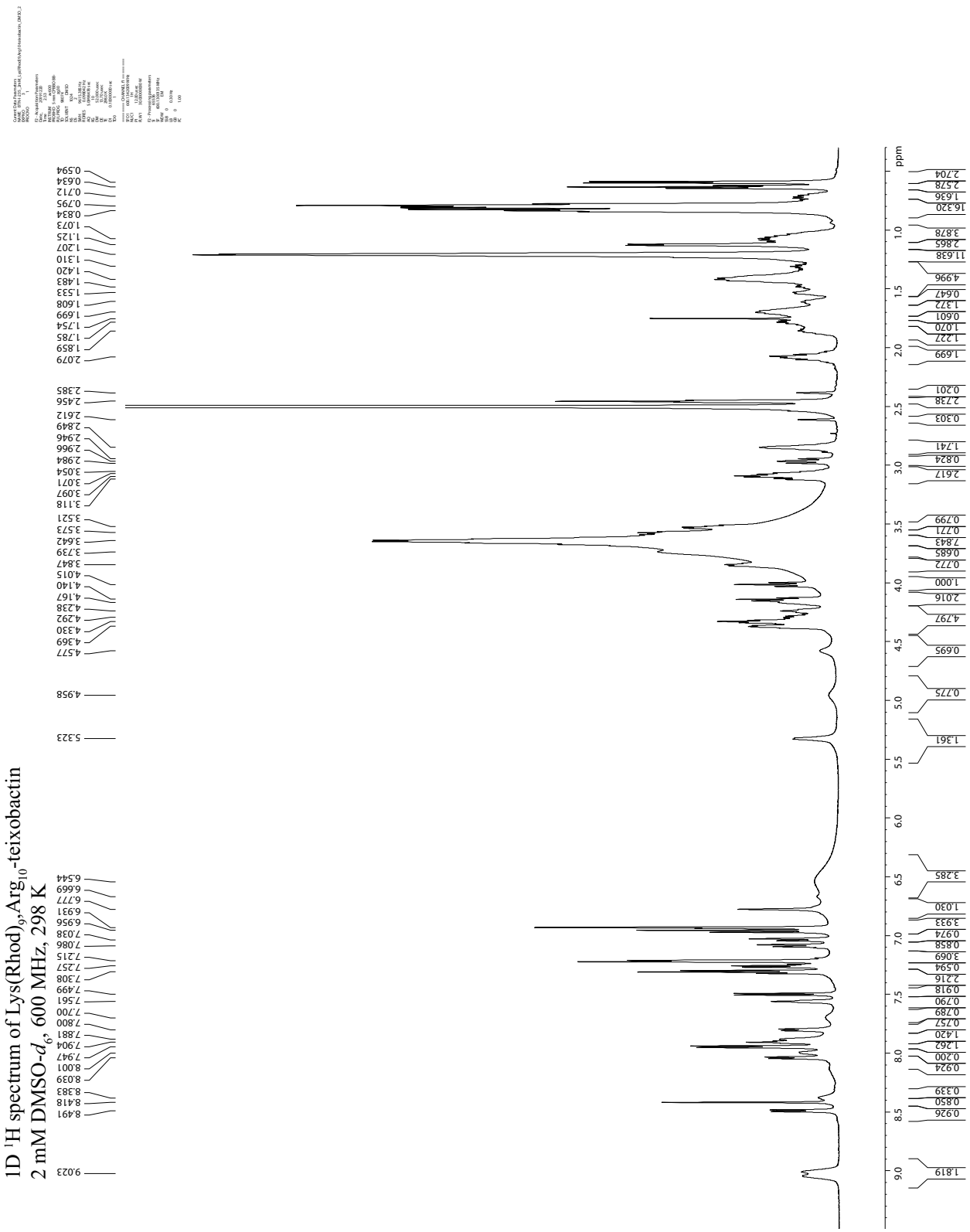

2 mM Lys(Rhod)$_9$,Arg$_{10}$-teixobactin: ^{1}H NMR spectrum in DMSO-d_6 (600 MHz)

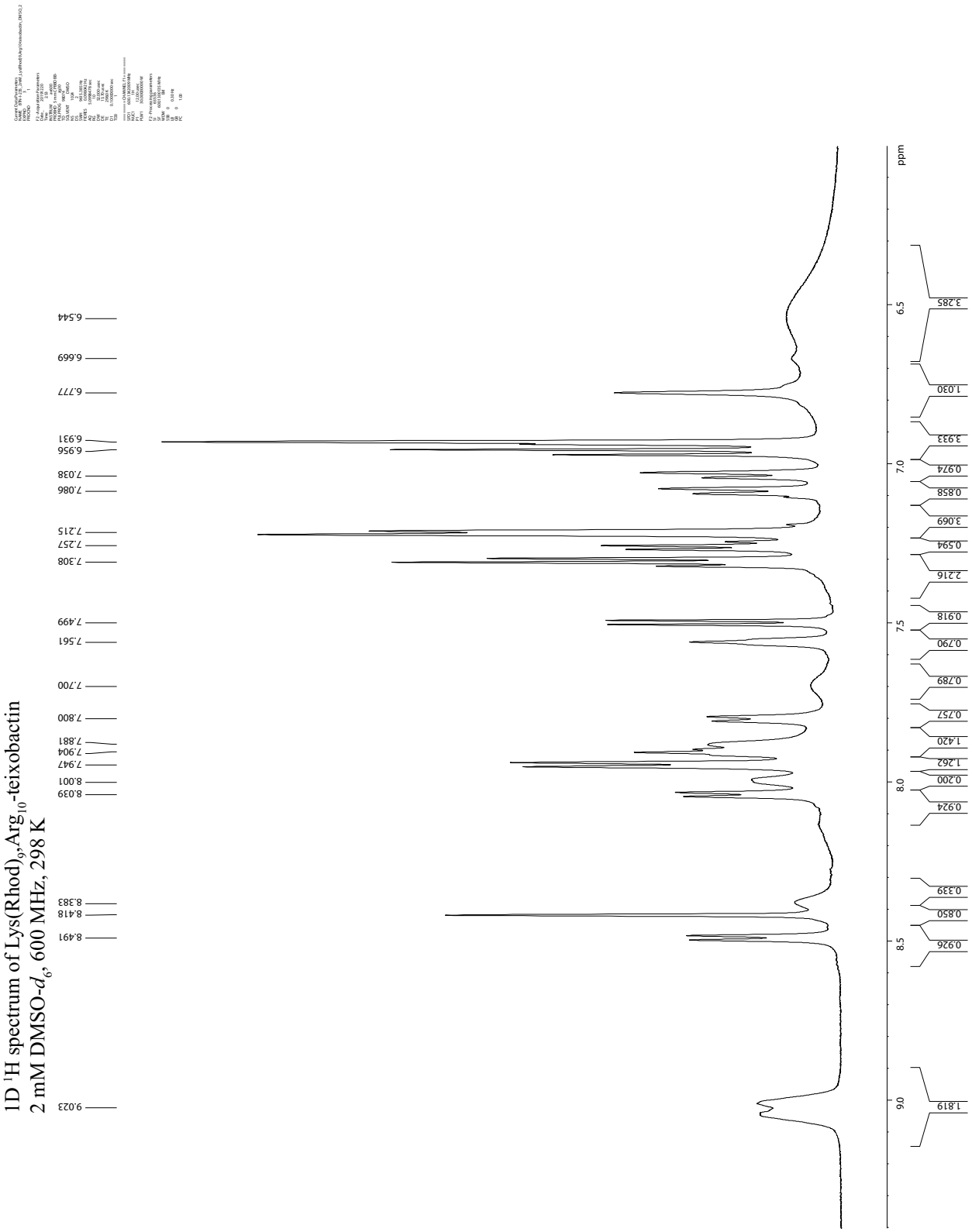

2 mM Lys(Rhod)$_9$,Arg$_{10}$-teixobactin: ^{1}H NMR spectrum in DMSO-d_6 (600 MHz)

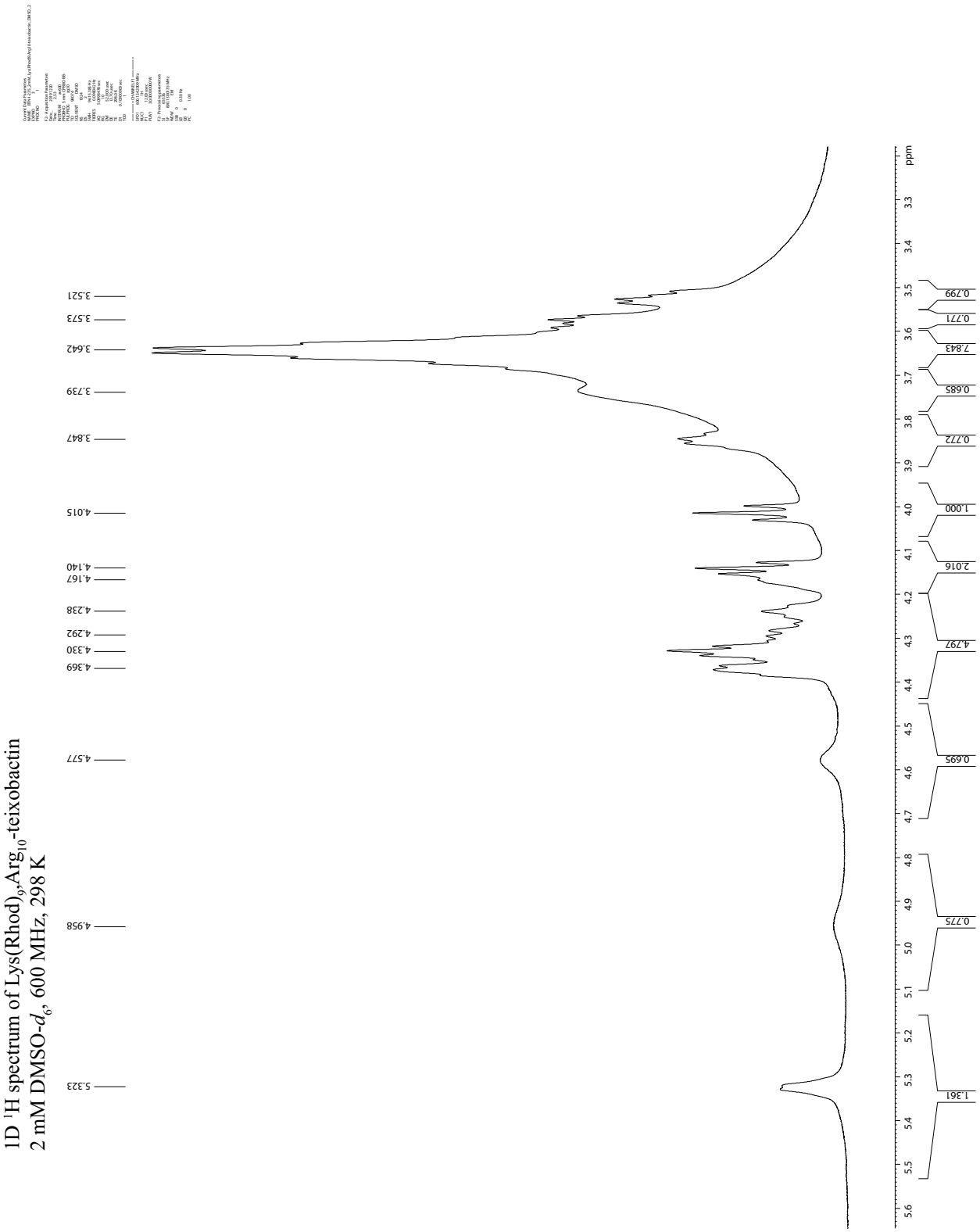

2 mM Lys(Rhod)$_9$,Arg$_{10}$-teixobactin: ^{1}H NMR spectrum in DMSO-d_6 (600 MHz)

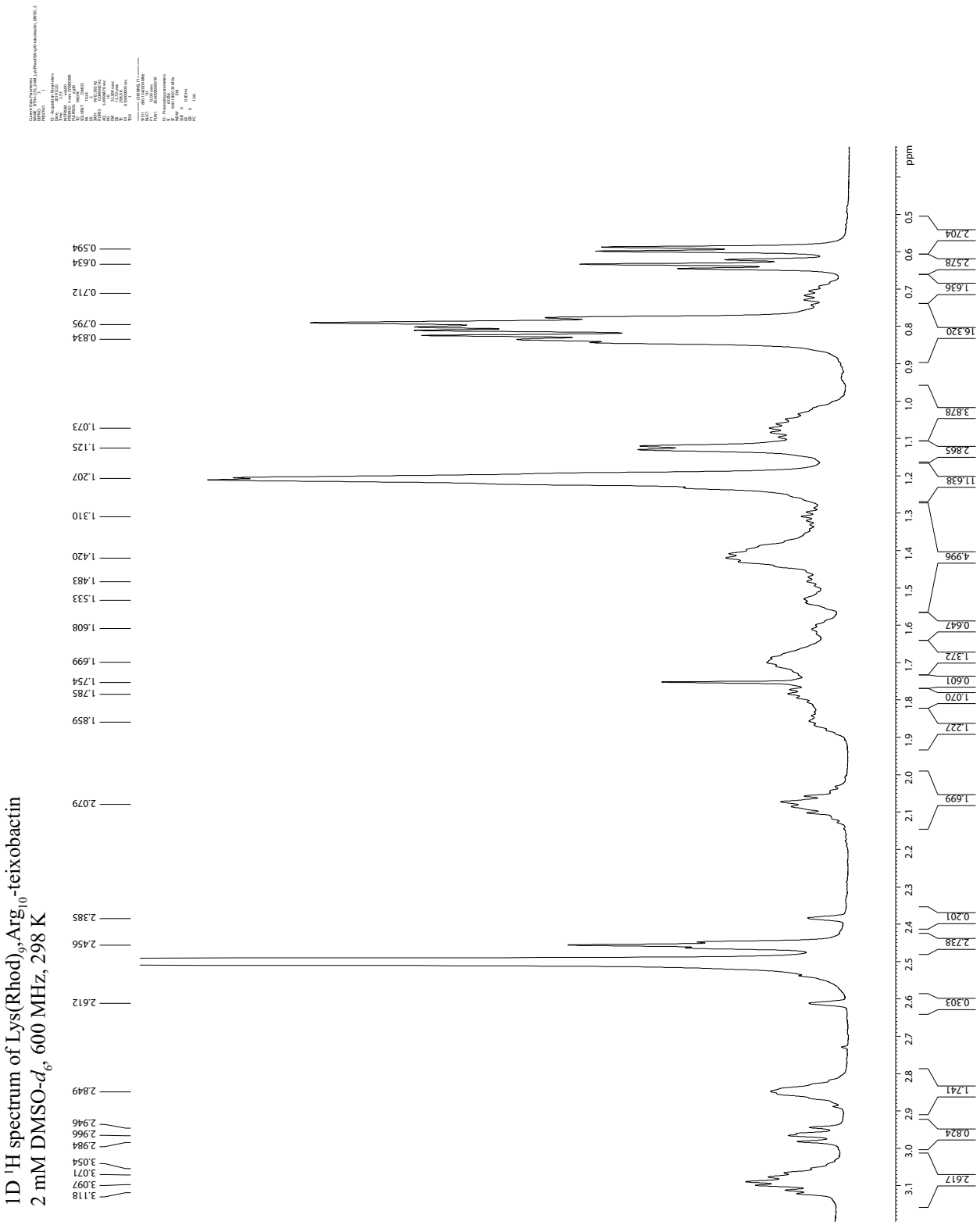

***seco*-Lys(Rhod)$_9$,Arg$_{10}$-teixobactin**

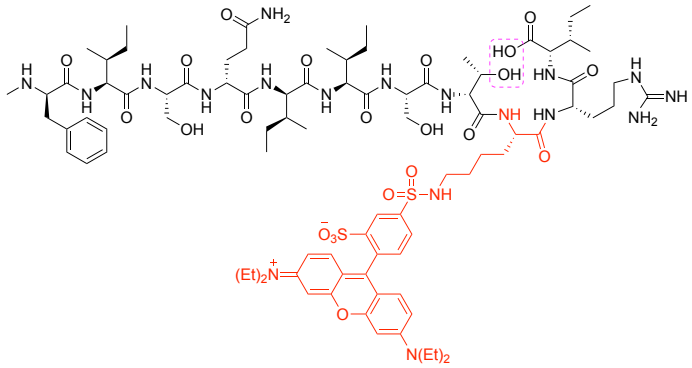

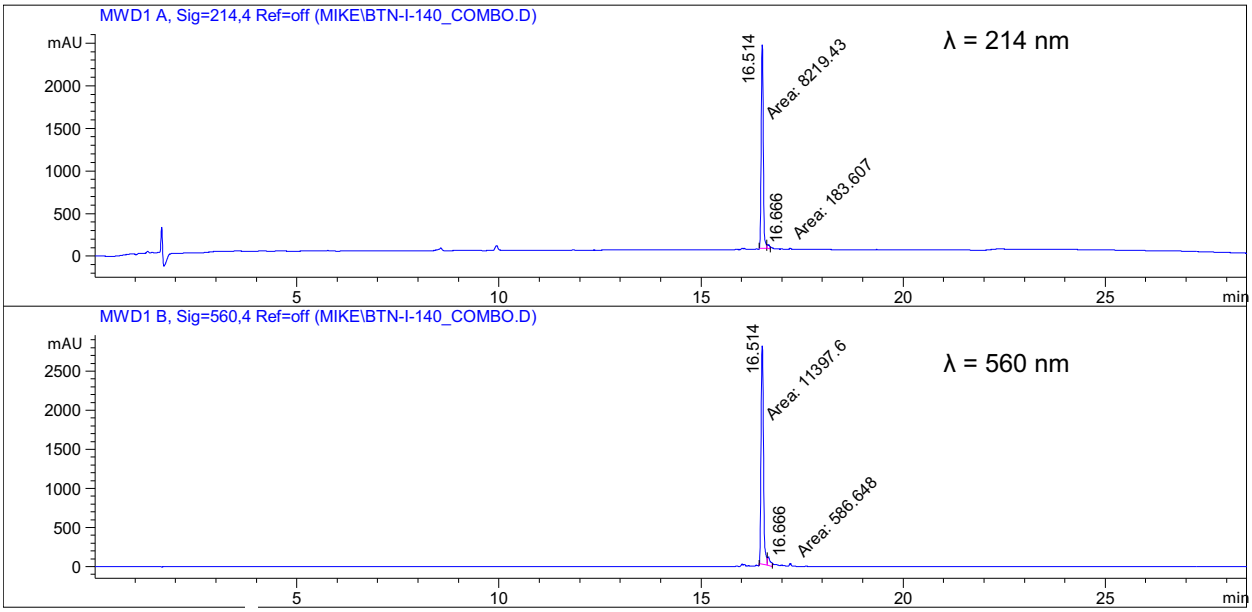


```
=====================================================================
                        Area Percent Report
=====================================================================

Sorted By             :      Signal
Multiplier            :      1.0000
Dilution              :      1.0000
Do not use Multiplier & Dilution Factor with ISTDs


Signal 1: MWD1 A, Sig=214,4 Ref=off

Peak RetTime Type  Width     Area      Height     Area
  #   [min]        [min]   [mAU*s]     [mAU]       %
----|-------|----|-------|----------|----------|--------|
   1  16.514 MF    0.0570 8219.43359 2401.49878  97.8150
   2  16.666 FM    0.0665  183.60716   46.04204   2.1850
```

Analytical HPLC with gradient elution of 5–100% acetonitrile over 20 min on an Aeris PEPTIDE 2.6u XB-C18 column (Phenomonex).

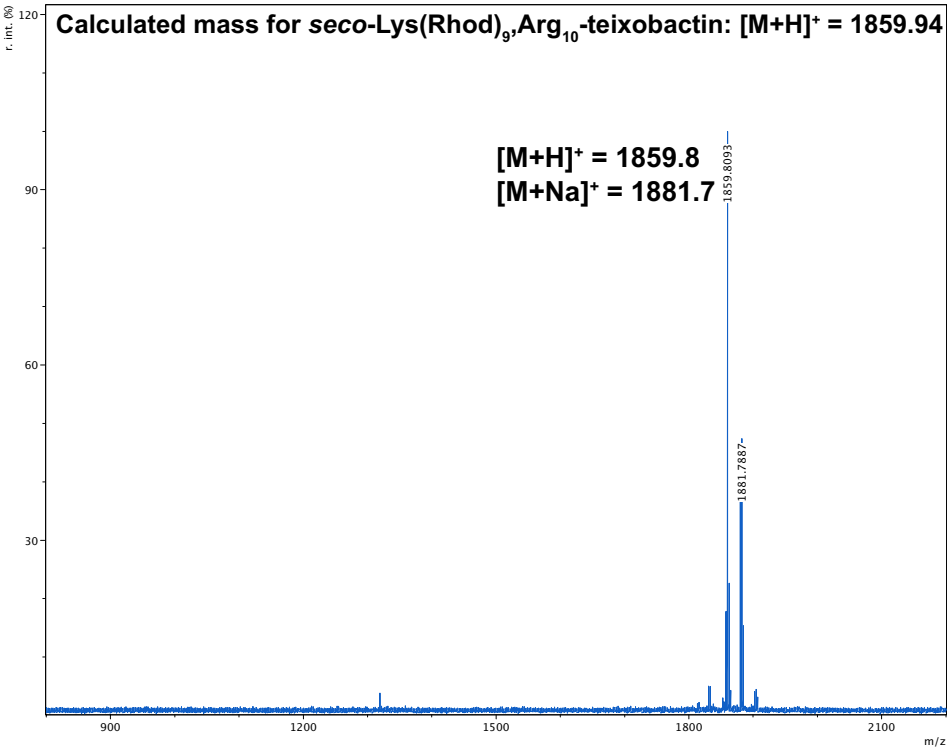
Calculated mass for seco-Lys(Rhod)9,Arg10-teixobactin: [M+H]+ = 1859.94
[M+H]+ = 1859.8
[M+Na]+ = 1881.7
1859.8093
1881.7887
r. int. (%)
m/z

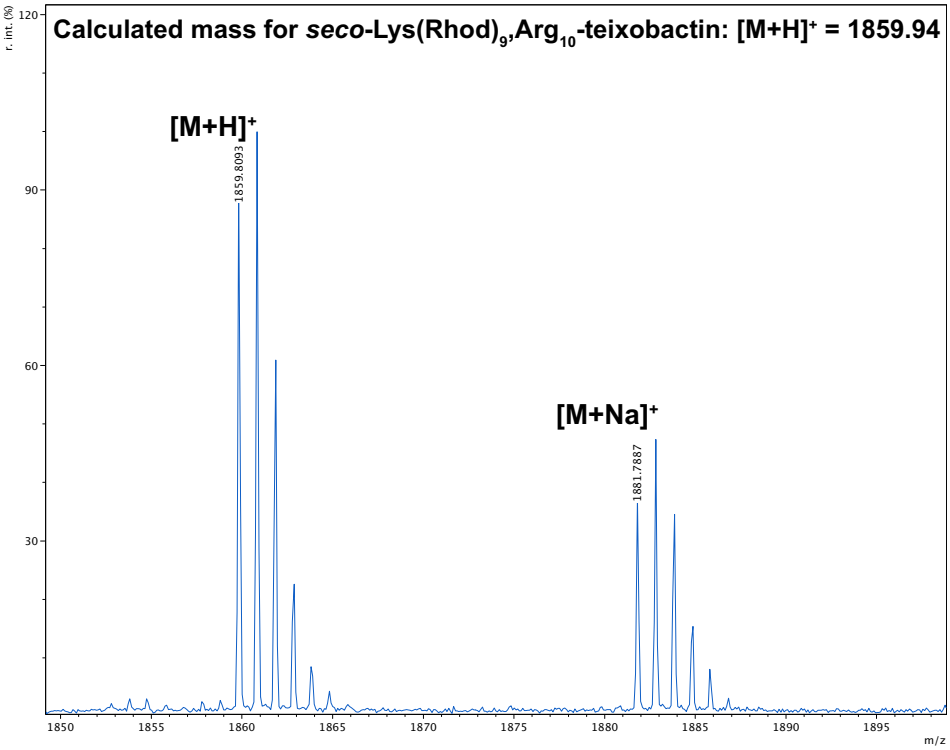
Calculated mass for seco-Lys(Rhod)9,Arg10-teixobactin: [M+H]+ = 1859.94
[M+H]+
[M+Na]+
1859.8093
1881.7887
r. int. (%)
m/z

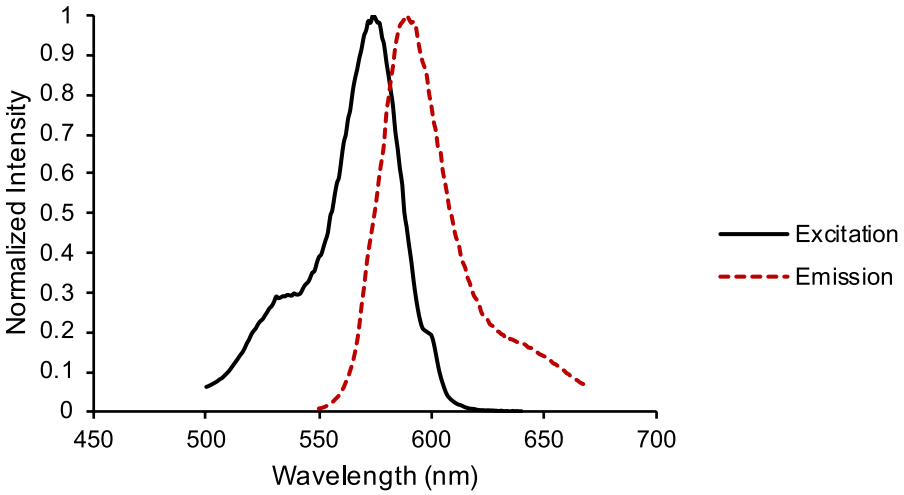

Figure S2.12. Excitation and emission spectra of 4 µg/mL of *seco*-Lys(Rhod)$_9$,Arg$_{10}$-teixobactin in sodium phosphate buffer with 0.05% polysorbate 80 (pH 7.4). The emission spectrum was collected with excitation at 572 nm. The absorption and emission maxima are 574 nm and 589 nm, respectively.

Arg_{10}-teixobactin

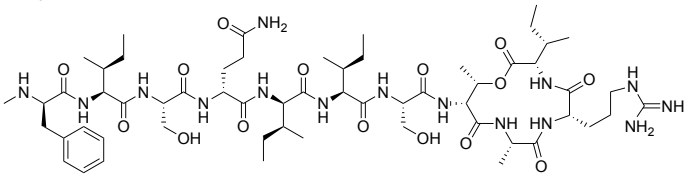

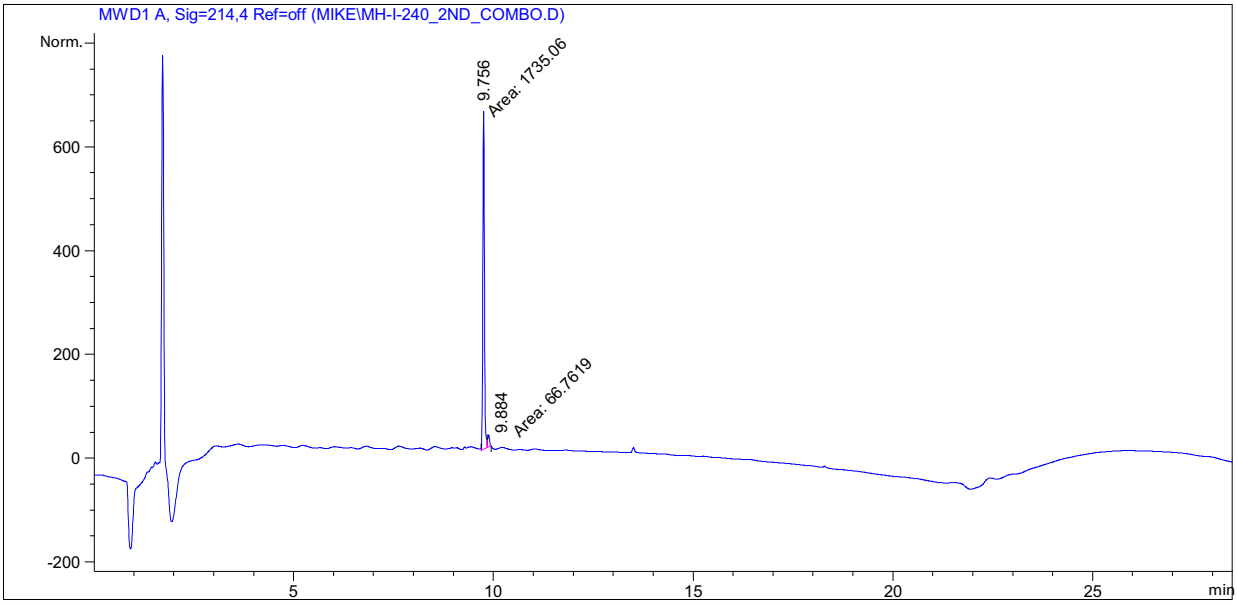


```
=====================================================================
                        Area Percent Report
=====================================================================

Sorted By             :      Signal
Multiplier            :      1.0000
Dilution              :      1.0000
Do not use Multiplier & Dilution Factor with ISTDs


Signal 1: MWD1 A, Sig=214,4 Ref=off

Peak RetTime Type  Width     Area      Height     Area
  #   [min]        [min]   [mAU*s]     [mAU]       %
----|-------|----|-------|----------|----------|--------|
   1   9.756 MF    0.0484 1735.06360  597.96252  96.2948
   2   9.884 FM    0.0528   66.76187   21.05681   3.7052

Totals :                  1801.82547  619.01934
```

Analytical HPLC with gradient elution of 5–100% acetonitrile over 20 min on an Aeris PEPTIDE 2.6u XB-C18 column (Phenomonex).

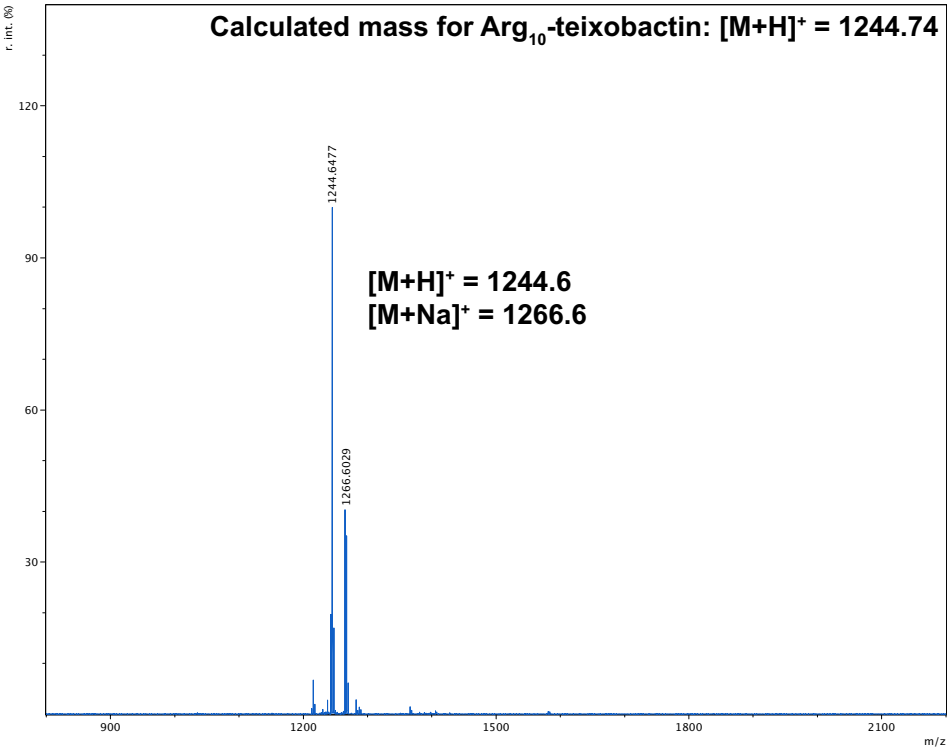
Calculated mass for Arg10-teixobactin: [M+H]+ = 1244.74
r. int. (%)
120
90
60
30
1244.6477
1266.6029
[M+H]+ = 1244.6
[M+Na]+ = 1266.6
900
1200
1500
1800
2100
m/z

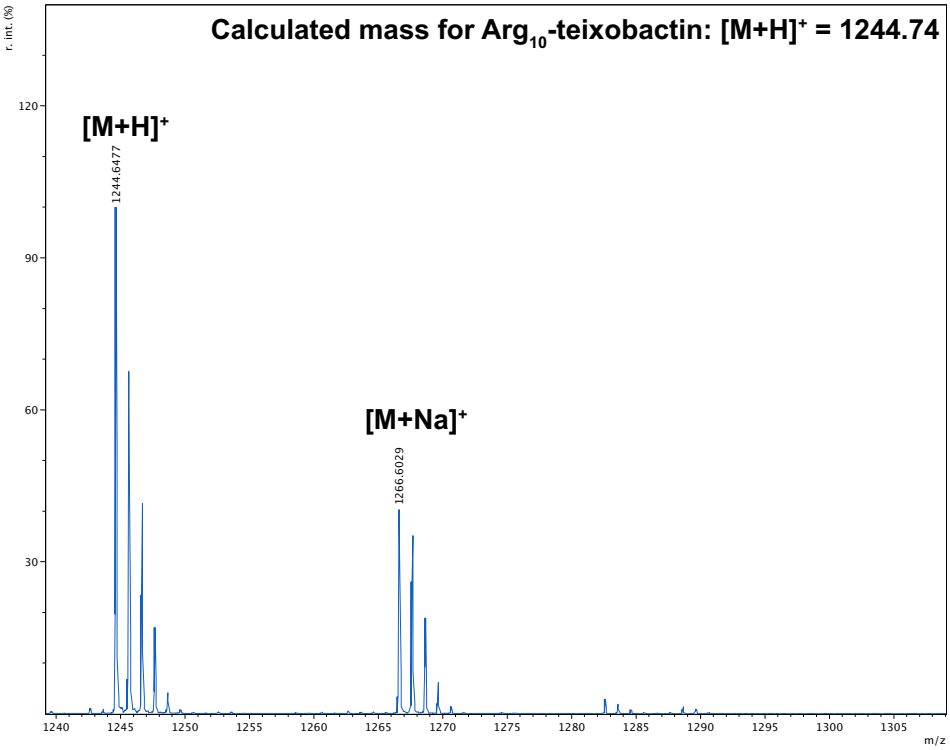
Calculated mass for Arg10-teixobactin: [M+H]+ = 1244.74
r. int. (%)
120
90
60
30
[M+H]+
1244.6477
[M+Na]+
1266.6029
1240
1245
1250
1255
1260
1265
1270
1275
1280
1285
1290
1295
1300
1305
m/z

References and notes for Chapter 2 Supporting Information

(1) Yang, H., Chen, K. H., and Nowick, J. S. Elucidation of the Teixobactin Pharmacophore. *ACS Chem. Biol.* **2016**, *11*, 1823−1826.

(2) Thieriet, N., Alsina, J., Giralt, E., Guibé, F., Albericio, F. Use of Alloc-Amino Acids in Solid-Phase Peptide Synthesis. Tandem Deprotection-Coupling Reactions using Neutral Conditions. *Tetrahedron Lett.* **1997**, *38*, 7275−7278.

(3) Our laboratory has previously observed that the Ile esterification using DIC and DMAP gives a ca. 2:1 epimeric mixture of Ile and D-*allo*-Ile at position 11.[1] HPLC purification of the final peptide product allows removal of the Lys(Rhod)$_9$,Arg$_{10}$,D-*allo*-Ile$_{11}$-teixobactin epimer and affords pure Lys(Rhod)$_9$,Arg$_{10}$-teixobactin (Figure S2.10).

(4) The 50 °C water bath for the HPLC purification is necessary to maintain solubility of the peptide during purification and prevent clogging of the HPLC column. A long (120 min) gradient during HPLC purification facilitates the separation of Lys(Rhod)$_9$,Arg$_{10}$-teixobactin from the Lys(Rhod)$_9$,Arg$_{10}$,D-*allo*-Ile$_{11}$-teixobactin epimer, which is generated from the DMAP-catalyzed esterification reaction.

(5) Cold Spring Harbor Protocols. http://cshprotocols.cshlp.org/content/2006/1/pdb.rec9959.short (accessed December 6, 2019).

Chapter 3[a]

Synthesis of Diverse Fluorescent Teixobactin Analogues and Application in FLIM-FRET Studies

Introduction

Teixobactin is an antimicrobial peptide that kills Gram-positive pathogens without developing resistance and has excellent antibacterial activity against drug resistant pathogens, including ones that are considered to be urgent and serious threats by the CDC.[1,2] For example, teixobactin is able to kill methicillin resistant *Staphylococcus aureus* (MRSA), vancomycin resistant *Enterococcus* (VRE), *Streptococcus pneumoniae*, *Mycobacterium tuberculosis*, *Clostridioides difficile*, and *Bacillus anthracis*, with excellent potency (minimum inhibitory concentration values range from 0.005–0.5 μg/mL).[1] In this era where antibiotic resistance is an increasing threat to global health, teixobactin provides a promising template to combat these drug resistant infections.

The putative mode of action of teixobactin involves disrupting cell wall biosynthesis by binding to lipid II, a peptidoglycan building block, and lipid III, a wall teichoic acid building block, resulting in cellular lysis.[1,3] Our reported X-ray crystallographic studies of teixobactin analogues have suggested a working model for the antibiotic activity of teixobactin in which teixobactin forms dimers, higher-order assemblies, or fibrils through antiparallel β-sheet interactions.[4,5] This model of antiparallel β-sheet assemblies was corroborated by the recent report of a solid state NMR structure of a teixobactin analogue complexed with lipid II membranes, where the teixobactin analogue assembles in antiparallel fiber-like β-sheets with its macrolactone ring

[a]This chapter represents a preliminary manuscript in preparation.

coordinating to the pyrophosphates of lipid II.[6] The same study also revealed that teixobactin has an additional mechanism of action that explains its excellent antibiotic activity.[6] The authors demonstrated that the Arg_4,Leu_{10}-teixobactin analogue forms micron-sized clusters in fluorescent lipid II GUVs, suggesting that teixobactin also disrupts cell wall biosynthesis by sequestering lipid II in clusters.

Recently, we developed a fluorescent teixobactin analogue, $Lys(Rhod)_9$,Arg_{10}-teixobactin, that retains antibiotic activity and stains the cell walls of various Gram-positive bacteria.[7] When we treated *B. subtilis* with 4 μg/mL $Lys(Rhod)_9$,Arg_{10}-teixobactin, we observed two different staining patterns depending on whether the buffer contained the nonionic detergent polysorbate 80. In the absence of polysorbate 80, the teixobactin analogue formed hazy fluorescent aggregates that adhered to the exterior of the bacteria (Figure S3.1A). However, in the presence of polysorbate 80, the teixobactin analogue stained the septa and sidewalls of the bacteria (Figure S3.1B). The fluorescent aggregates surrounding the bacteria observed in Figure S3.1A may suggest that the aggregated teixobactin either binds to or sequesters wall teichoic acid (WTA), whereas the septal and lateral staining is consistent with binding to peptidoglycan precursors, such as lipid II and III. The first binding mode we observed, where aggregates of the fluorescent teixobactin are anchored to the bacteria, may reflect sequestration of cell wall precursors in clusters, as observed by Weingarth et al.[6] The sequestration of lipid II in clusters has been observed before in lantibiotics, such as nisin, and represents an important bactericidal mechanism for these antibiotics.[8,9] However, the first binding mode, where the fluorescent teixobactin analogue formed aggregates surrounding the exterior of bacteria, to our knowledge, is unique to teixobactin due to the large size of the aggregates. Further studies on these teixobactin aggregates will improve our

understanding of the mode of action of teixobactin and could inspire the development of new antibiotics.

To enable the study of teixobactin and its interactions with bacteria, we developed a convenient synthesis of fluorescent teixobactin analogues that only requires stoichiometric amounts of Lys_{10}-teixobactin or Lys_9,Arg_{10}-teixobactin, an NHS ester, and a non-nucleophilic base. The reaction affords regioselective labeling of the lysine sidechain amines of either Lys_{10}- or Lys_9,Arg_{10}-teixobactin. Using this labeling method, I was able to generate four fluorescent teixobactin analogues, bearing different fluorophores, that retain antibiotic activity and stain the cell walls of Gram-positive bacteria. The incorporation of different fluorophores in teixobactin analogues enabled the use of FLIM-FRET studies to determine if teixobactin forms assemblies in live bacteria. Taken together, our fluorescent teixobactin analogues permitted further study of the mode of action of teixobactin in live cells.

Results and Discussion

I adapted our research group's synthesis of teixobactin analogues[11] to allow selective incorporation of fluorophores at either position 9 or 10 of the teixobactin pharmacophore. Structure activity relationship (SAR) studies of the teixobactin pharmacophore revealed that substitutions of alanine$_9$ or *allo*-enduracididine$_{10}$ are well tolerated and do not cause substantial loss of antibiotic activity.[11–13] I also recently determined that the incorporation of the sulforhodamine B fluorophore at position 9 of Lys_9,Arg_{10}-teixobactin only reduced antibiotic activity 2–4 fold compared to the unlabeled parent antibiotic.[7] As such, I anticipated that Lys_9,Arg_{10}-teixobactin and Lys_{10}-teixobactin could tolerate the incorporation of various types of fluorophores at their lysine sidechains, which serve as a handle for amine-reactive dyes (Figure 1).

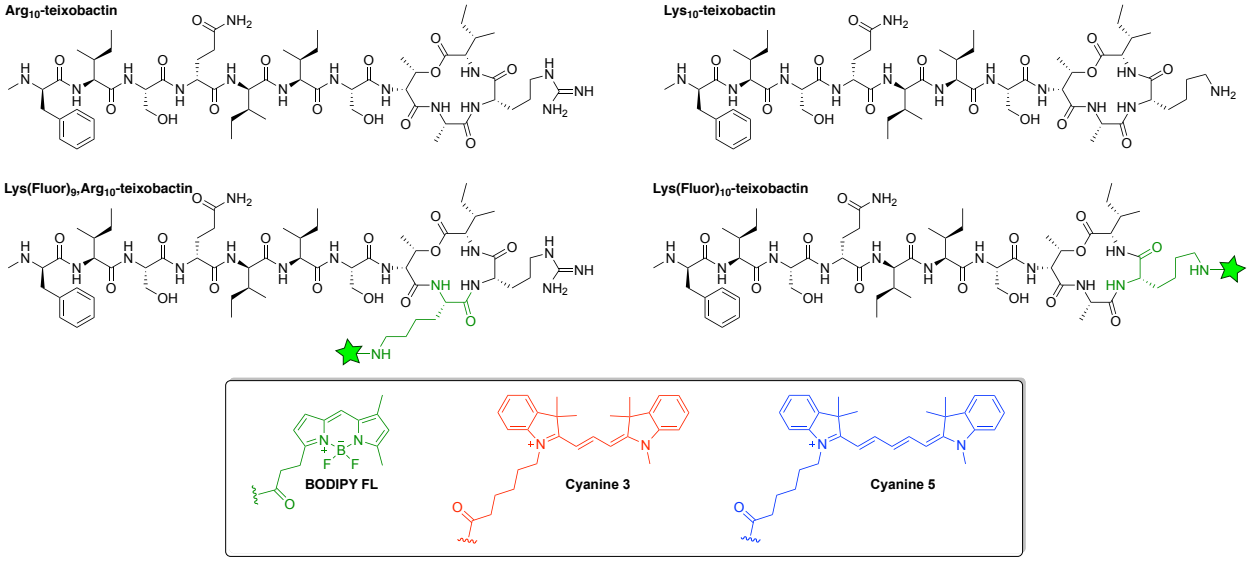

Figure 3.1. Structures of Arg_{10}-teixobactin, $Lys(Fluor)_9,Arg_{10}$-teixobactin, Lys_{10}-teixobactin, and $Lys(Fluor)_{10}$-teixobactin, where the green star represents an amide conjugate of a fluorophore.

We synthesized Lys_9,Arg_{10}-teixobactin and Lys_{10}-teixobactin using our previously developed Fmoc-based SPPS route[11] and labeled the purified peptides with *N*-hydroxysuccinimide (NHS) esters fluorophores (Scheme 3.1). This post-functionalization approach is the first example of NHS ester labeling of teixobactin and affords regioselective, quantitative, and efficient labeling (10–60 min), and enables simple removal of excess fluorophore by RP-HPLC purification. The labeling reaction proceeds efficiently in a small reaction volume (100 µL total) using 1.0 eq of peptide, 1.2 eq of NHS ester fluorophore, and 5.0 eq of a non-nucleophilic bulky base (e.g., DIPEA). DMF was used as the reaction solvent in order to solubilize teixobactin and its labeled conjugate and to prevent peptide aggregation. Synthesis on a 5 mg (3.4 µmol) peptide scale typically yielded 1.2–3.3 mg (22–53% yield) of labeled teixobactin as the trifluoroacetate (TFA) salt after purification by RP-HPLC. We chose to label the teixobactin analogues with NHS esters because these electrophiles tend to react efficiently and selectively with primary amines in proteins and peptides.[14–16] There are also hundreds of NHS esters commercially available that contain

different tags, which makes this method versatile and convenient. Although Lys_9,Arg_{10}-teixobactin and Lys_{10}-teixobactin contain other nucleophilic groups that might react with NHS esters, such as the *N*-terminal amine and the guanidium sidechain of arginine, mono-labeling of the lysine amine was exclusively observed in both Lys_9,Arg_{10}-teixobactin and Lys_{10}-teixobactin using this labeling reaction (Scheme 3.1).

Scheme 3.1. Representative synthesis of fluorescent teixobactin analogues using NHS esters.

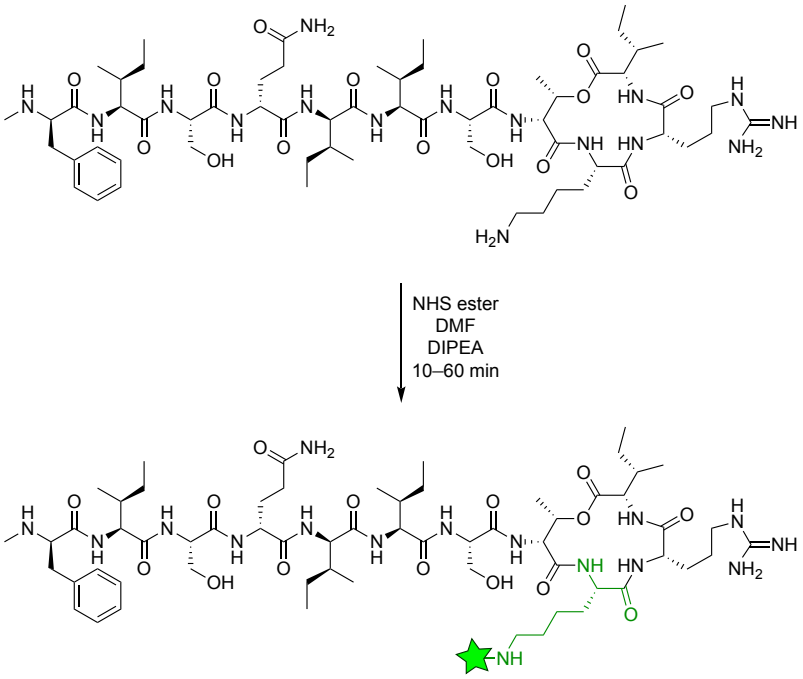

I initially evaluated Lys_9,Arg_{10}-teixobactin as a scaffold for incorporating fluorophores using minimum inhibitory concentration (MIC) assay as a readout for antibiotic activity. Using the reaction conditions presented in Scheme 3.1, we were able to label Lys_9,Arg_{10}-teixobactin with BODIPY FL NHS ester to afford Lys(BDY FL)$_9$,Arg_{10}-teixobactin. We chose BODIPY FL because of its high quantum yield (0.97), high extinction coefficient (92,000 L mol^{-1} cm^{-1}), and its small, compact size that might be less perturbing to the teixobactin pharmacophore compared to larger dyes. We evaluated the antibiotic activity of Lys(BDY FL)$_9$,Arg_{10}-teixobactin against two Gram-positive bacteria, *B. subtilis* and *S. epidermidis*, in our MIC assays. We used Arg_{10}-

teixobactin and Lys_{10}-teixobactin as positive controls and the Gram-negative bacterium *E. coli* as a negative control. Lys(BDY FL)$_9$,Arg_{10}-teixobactin partially retained antibiotic activity, with minimum inhibitory concentrations of 8 μg/mL against *B. subtilis* and *S. epidermidis*, making it ca. four-fold and eight-fold, respectively, less active than the parent, unlabeled Arg_{10}-teixobactin (Table 1). We also investigated the effects of polysorbate 80 in our MIC assays. Polysorbate 80 is a gentle nonionic surfactant and is a common additive in MIC assays to prevent soluble drug adsorbing to the plastic assay plate.[17] We and others found that the inclusion of 0.002% polysorbate 80 in MIC test media improves the antibiotic activity of teixobactin and teixobactin analogues,[1,5] including our previously reported fluorescent teixobactin analogue.[7] When we performed MIC assays with 0.002% polysorbate 80, the antibiotic activity of Lys(BDY FL)$_9$,Arg_{10}-teixobactin improved four-fold for both *B. subtilis* and *S. salivarius* (Table 1).

Table 3.1. MIC values of teixobactin analogues in μg/mL with 0% and 0.002% polysorbate 80.

	Bacillus subtilis ATCC 6051	*Staphylococcus epidermidis* ATCC 14990	*Escherichia coli* ATCC 10798
Lys(BDY FL)$_9$,Arg_{10}-teixobactin	8[a]	8[a]	>32[a]
	2[b]	2[b]	>32[b]
Lys(BDY FL)$_{10}$-teixobactin	2[a]	4[a]	>32[a]
	0.125[b]	1[b]	>32[b]
Lys(Cy3)$_{10}$-teixobactin	4[a]	4[a]	>32[a]
	1[b]	2[b]	>32[b]
Lys(Cy5)$_{10}$-teixobactin	8[a]	16[a]	>32[a]
	2[b]	16–32[b]	>32[b]
Arg_{10}-teixobactin	1[a]	2[a]	>32[a]
	<0.03[b]	0.5[b]	>32[b]
Lys_{10}-teixobactin	1[a]	1–2[a]	>32[a]
	<0.03[b]	0.5[b]	>32[b]

[a]Culture media containing 0% polysorbate 80
[b]Culture media containing 0.002% polysorbate 80

SAR studies of the teixobactin pharmacophore determined that position 10 tolerates substitution,[11,13] so we synthesized Lys(BDY FL)$_{10}$-teixobactin using the same conditions in Scheme 3.1 to determine if position 10 can tolerate fluorophores. Lys(BDY FL)$_{10}$-teixobactin had

improved antibiotic activity compared to Lys(BDY FL)$_9$,Arg$_{10}$-teixobactin, with MIC values of 2–4 μg/mL against *B. subtilis* and *S. epidermidis*, making it ca. four-fold and eight-fold, respectively, less active than the parent Arg$_{10}$-teixobactin (Table 1). When 0.002% polysorbate 80 was included in the MIC test media, the antibiotic activity of Lys(BDY FL)$_{10}$-teixobactin improved 16-fold for *B. subtilis* and four-fold for *S. epidermidis* (Table 1), making it the most potent fluorescent teixobactin reported. From this observation, we decided to exclusively use position 10 for the incorporation of other fluorophores since it tolerates BODIPY FL well. We synthesized Lys(Cy3)$_{10}$-teixobactin and Lys(Cy5)$_{10}$-teixobactin, and both exhibited moderate antibiotic activity against *B. subtilis* in the presence of 0.002% polysorbate 80 (Table 1).

We first evaluated the staining of Lys(BDY FL)$_{10}$-teixobactin in live *B. subtilis* bacteria using fluorescence microscopy without using polysorbate 80. We treated *B. subtilis* with 1 μg/mL of Lys(BDY FL)$_{10}$-teixobactin since it resulted in bright staining and this concentration is below the MIC value of this peptide against *B. subtilis*. High concentrations of antibiotic (≥MIC) may perturb normal pattern of peptidoglycan biosynthesis, so lower concentrations of the antibiotic may provide a more accurate reflection of how teixobactin perturbs peptidoglycan biosynthesis.[18] Z-stacks of *B. subtilis* stained with Lys(BDY FL)$_{10}$-teixobactin revealed a continuum of staining patterns: (1) septal staining was observed when focused in the interior of the bacteria (Figure 3.2A); and (2) aggregates adhered to the bacterial membranes were observed when focused on the exterior of the bacteria (Figure 3.2B). These staining patterns are consistent with what we observed with our previous fluorescent teixobactin analogue Lys(Rhod)$_9$,Arg$_{10}$-teixobactin, except that the rhodamine analogue was only able to stain the septa of *B. subtilis* in the presence of 0.05% polysorbate 80. Interestingly, we observed a few splotchy aggregates of Lys(BDY FL)$_{10}$-teixobactin along the interior of *B. subtilis* cells (see white arrows in Figure 3.2A). These splotchy

aggregates could represent Lys(BDY FL)$_{10}$-teixobactin clustering peptidoglycan precursors, which was observed when fluorescent lipid II GUVs where treated by a teixobactin analogue.[6] The sequestration of lipid II into clusters was also observed with a fluorescent nisin analogue, which resulted in splotchy dots along the sidewalls of *B. subtilis*.[8,9] Taken together, we believe Lys(BDY FL)$_{10}$-teixobactin represents an improved fluorescent teixobactin analogue since it has reasonable antibiotic activity against *B. subtilis* and results in septal, clustered, and aggregated staining without using polysorbate 80.

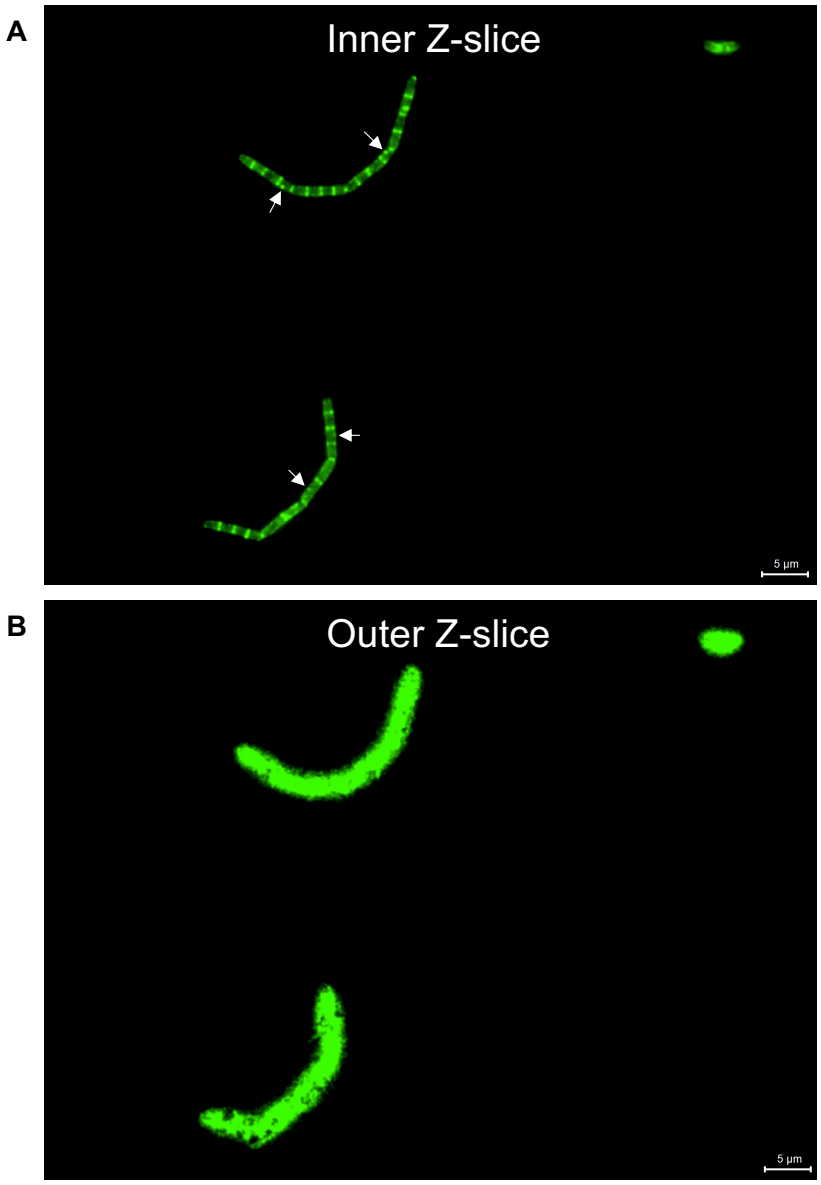

Figure 3.2. Representative fluorescence micrographs from a Z-stack of *B. subtilis* stained with 1 µg/mL Lys(BDY FL)$_{10}$-teixobactin in sodium phosphate buffer without polysorbate 80. Scale bars are 5 µm. (A) Inner Z-slice of *B. subtilis* showing septal staining of Lys(BDY FL)$_{10}$-teixobactin. White arrows indicate possible clusters of peptidoglycan precursors. (B) Outer Z-slice of *B. subtilis* showing aggregates of Lys(BDY FL)$_{10}$-teixobactin adhering to the surfaces of bacteria.

To investigate the clustering of Lys(BDY FL)$_{10}$-teixobactin that was present in Figure 3.2A, we utilized structured illumination microscopy (SIM) to provide more detail of these fluorescent structures in *B. subtilis*. SIM is a super resolution microscopy technique that provides resolution up to 20 nm and does not require special fluorophores or sample preparation.[19] In these

imaging studies, 0.05% polysorbate 80 was included in the sodium phosphate buffer to prevent excessive aggregation of the fluorescent teixobactin analogues. We individually treated *B. subtilis* with 1 μg/mL of either Lys(BDY FL)$_{10}$-teixobactin (Figure 3.3A), Lys(BDY FL)$_9$,Arg$_{10}$-teixobactin (Figure 3.3B), Lys(Cy3)$_{10}$-teixobactin (Figure 3.3C), or Lys(Cy5)$_{10}$-teixobactin (Figure 3.3D). Lys(BDY FL)$_{10}$-teixobactin resulted in clear septal and sidewall staining, with a few splotchy aggregates of the antibiotic present along the sidewalls of *B. subtilis* (see white arrows in Figure 3.3A). In contrast, the septal and sidewall staining from Lys(BDY FL)$_9$,Arg$_{10}$-teixobactin in *B. subtilis* was not as bright, but had more clusters present compared to Lys(BDY FL)$_{10}$-teixobactin. Both Lys(Cy3)$_{10}$-teixobactin (Figure 3.3C) and Lys(Cy5)$_{10}$-teixobactin (Figure 3.3D) behaved similar to Lys(BDY FL)$_{10}$-teixobactin, where the septa and sidewalls of *B. subtilis* were clearly stained, and a few clusters of peptidoglycan precursors were also present. Taken together, these imaging studies suggest that analogues with fluorophores at position 10 are better probes since they resulted in brighter staining compared to Lys(BDY FL)$_9$,Arg$_{10}$-teixobactin.

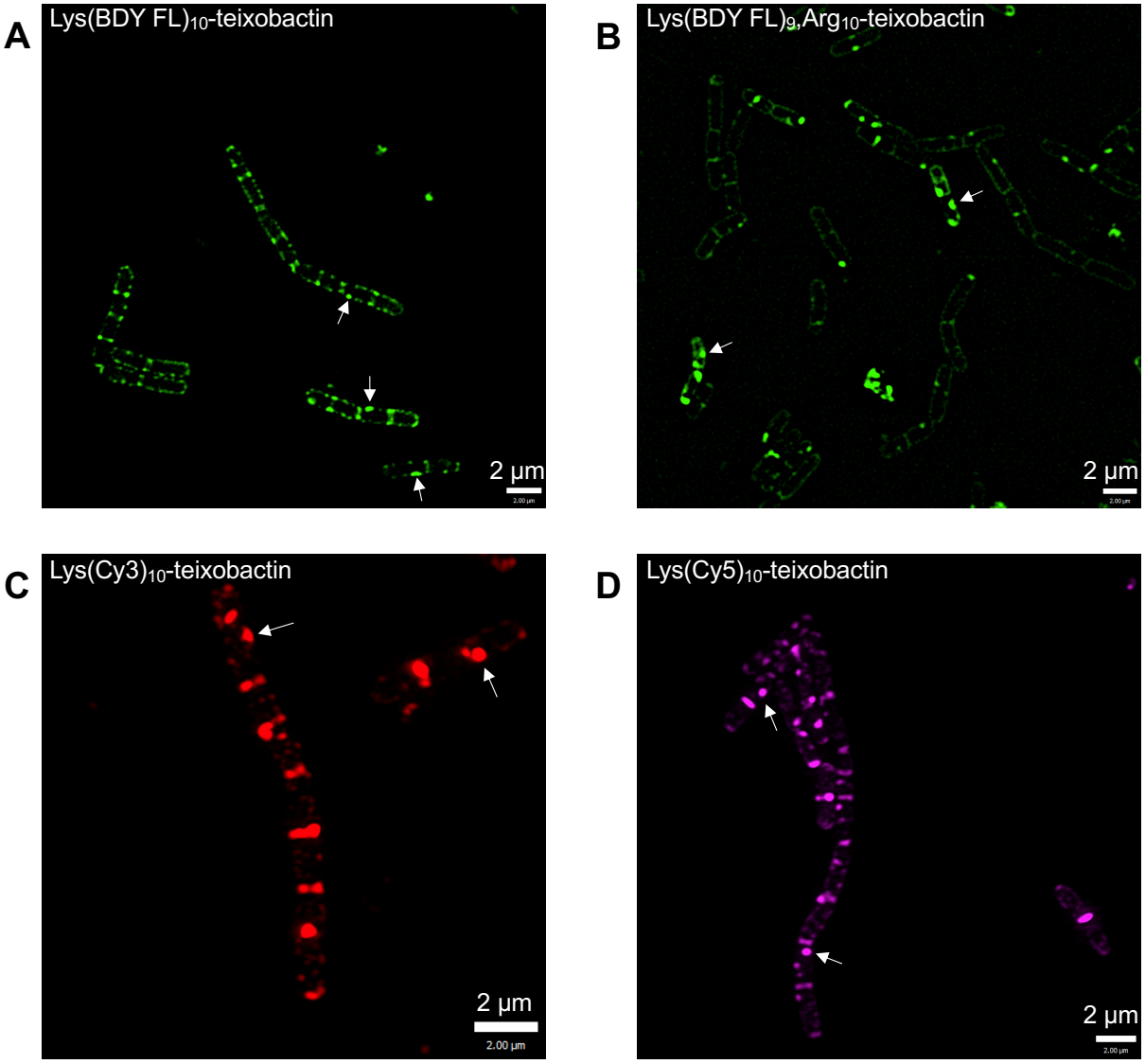

Figure 3.3. SIM micrographs of *B. subtilis* stained with different fluorescent teixobactin analogues. White arrows indicate presence of possible clusters of peptidoglycan precursors. Scale bars are 2 µm. (A) *B. subtilis* treated with 1 µg/mL Lys(BDY FL)$_{10}$-teixobactin in sodium phosphate buffer with 0.05% polysorbate 80. (B) *B. subtilis* treated with 1 µg/mL Lys(BDY FL)$_9$,Arg$_{10}$-teixobactin in sodium phosphate buffer with 0.05% polysorbate 80. (C) *B. subtilis* treated with 1 µg/mL Lys(Cy3)$_{10}$-teixobactin in sodium phosphate buffer with 0.05% polysorbate 80. (D) *B. subtilis* treated with 1 µg/mL Lys(Cy5)$_{10}$-teixobactin in sodium phosphate buffer with 0.05% polysorbate 80.

To further explore the self-assembly of teixobactin in live bacteria, we performed FLIM-FRET microscopy using Lys(Cy3)$_{10}$-teixobactin and Lys(Cy5)$_{10}$-teixobactin in live *B. subtilis* cells. In our crystallographically observed teixobactin dimers,[4,5] the macrolactone rings are 2–3

nm apart, thus falling well within the Förster radius of typical FRET donor and acceptor partners, which is generally 4–6 nm.[20] We chose Cy3 and Cy5 as a FRET pair since these labels are commonly used in single molecule FRET studies.[20] Using FLIM as a readout for FRET is advantageous over spectral ratiometric techniques since FLIM only requires measurement of the donor fluorophore and reduces false positive measurements from spectral crosstalk.[21] We also used phasor analysis for FLIM-FRET measurements since it is a model-free approach and simplifies data analysis.[22]

To carry out the FLIM-FRET experiment, we treated *B. subtilis* with 1 μg/mL of Lys(Cy3)$_{10}$-teixobactin and 1 μg/mL of Lys(Cy5)$_{10}$-teixobactin, in which we anticipated the two labeled antibiotics to intimately colocalize in live cells. In addition to our FLIM-FRET sample, we also prepared the following samples in parallel as controls: *B. subtilis* treated with 1 μg/mL of Lys(Cy3)$_{10}$-teixobactin, *B. subtilis* treated with 1 μg/mL of Lys(Cy5)$_{10}$-teixobactin, and *B. subtilis* treated with buffer. All FLIM-FRET samples were prepared in sodium phosphate buffer with 0.05% polysorbate 80 in order to prevent probe aggregation.

When *B. subtilis* was treated with 1 μg/mL of Lys(Cy3)$_{10}$-teixobactin, we observed a decrease in Cy3 fluorescence lifetime in some of the cells (shown as orange/yellow signal in Figure 3.4), meaning that Lys(Cy3)$_{10}$-teixobactin was forming oligomers in *B. subtilis*. This data is consistent with the finding that dimers of teixobactin is required for optimal lipid II binding.[1,6] However, not all *B. subtilis* cells exhibited decreased fluorescence lifetime, which suggests that some of the Lys(Cy3)$_{10}$-teixobactins were not intimately colocalizing (shown as green signal in Figure 3.4). The heterogeneity of monomeric and oligomeric Lys(Cy3)$_{10}$-teixobactin suggests that there might be an equilibrium of assembling species in bacteria. Another interesting observation is that extracellular aggregates of Lys(Cy3)$_{10}$-teixobactin (shown as red signal in Figure 3.4)

exhibited strong self-quenching and very short fluorescence lifetimes, indicating that the Lys(Cy3)$_{10}$-teixobactins exhibit tighter assemblies compared to the assemblies found in the cells.

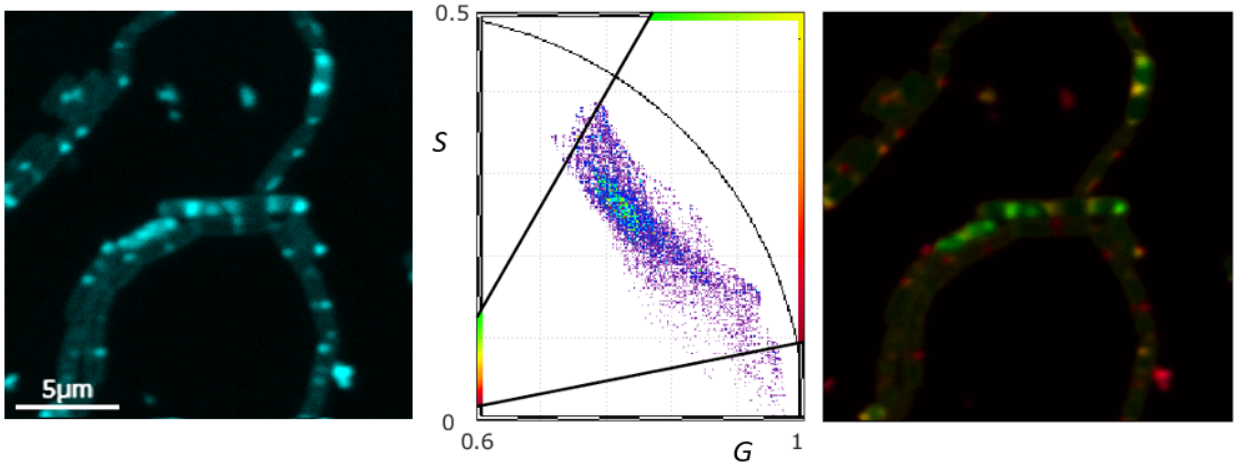

Figure 3.4. Fluorescence lifetime micrograph (left), FLIM-FRET phasor plot (middle), and associated FLIM-FRET micrograph (right) of *B. subtilis* treated with 1 µg/mL Lys(Cy3)$_{10}$-teixobactin. In the FLIM-FRET micrograph, green signal indicates normal Cy3 fluorescence lifetimes, orange/yellow signal indicates Cy3 self-quenching, and red signal indicates strong Cy3 self-quenching.

When *B. subtilis* was treated with 1 µg/mL of Lys(Cy5)$_{10}$-teixobactin, we observed a normal Cy5 fluorescence lifetime in most of the cells (Figure 3.5A). This may indicate that the larger Cy5 label might prevent Lys$_{10}$-teixobactin from assembling, when compared to Lys(Cy3)$_{10}$-teixobactin, which has the smaller Cy3 label. *B. subtilis* treated with sodium phosphate buffer only exhibited background fluorescence lifetimes (Figure 3.5B), so the fluorescence lifetimes we observe from Cy3 and Cy5 are from the fluorophores themselves, and not from background noise.

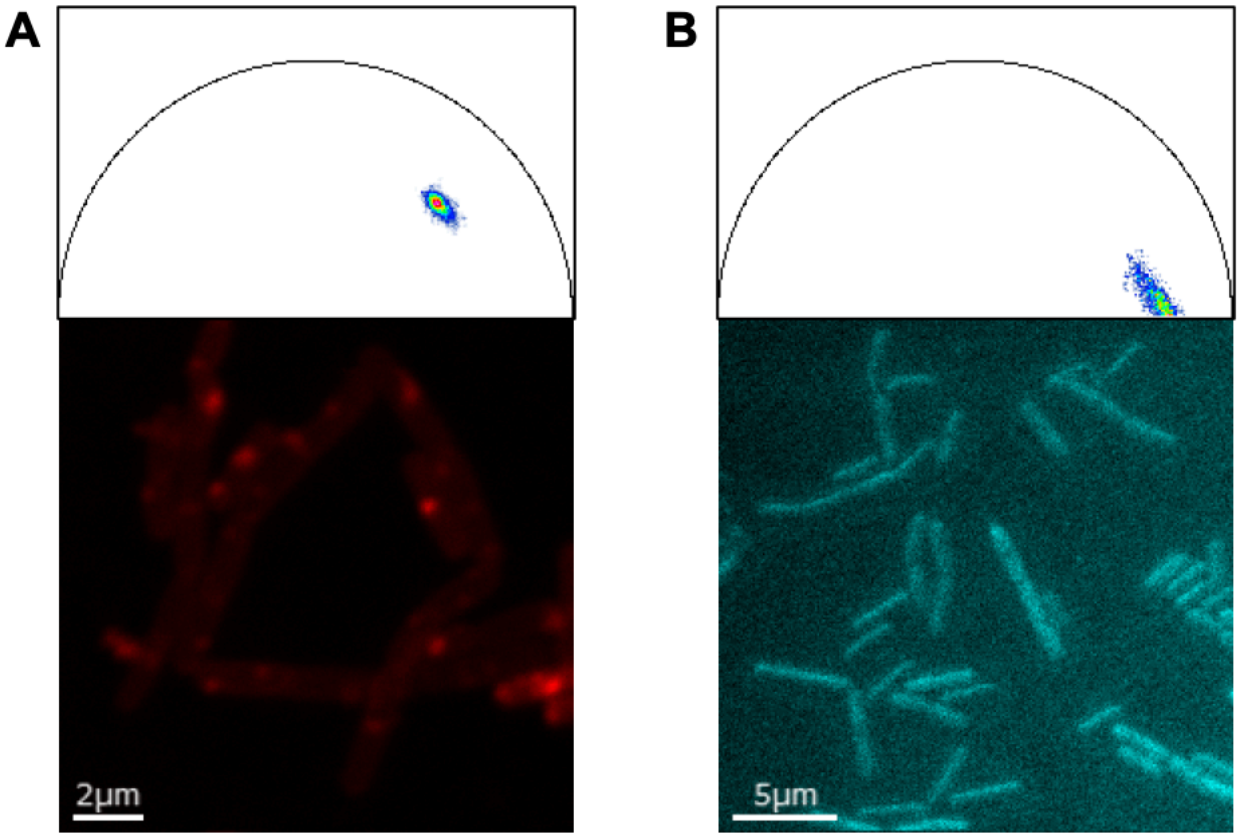

Figure 3.5. FLIM-FRET phasor plots (top) and associated micrographs (bottom) of *B. subtilis* treated with either Lys(Cy5)$_{10}$-teixobactin or buffer only. (A) FLIM-FRET micrograph and associated phasor plot of *B. subtilis* treated with 1 μg/mL of Lys(Cy5)$_{10}$-teixobactin. (B) FLIM-FRET micrograph and associated phasor plot of *B. subtilis* treated with sodium phosphate buffer.

When *B. subtilis* was treated with 1 μg/mL of Lys(Cy3)$_{10}$-teixobactin and 1 μg/mL of Lys(Cy5)$_{10}$-teixobactin, we observed Cy5 diminishing the fluorescence lifetime of Cy3 in most cells (shown as orange/yellow signal in Figure 3.6), indicating that Lys(Cy3)$_{10}$-teixobactin and Lys(Cy5)$_{10}$-teixobactin are exhibiting FRET and are in close contact with each other in *B. subtilis* cells. The detection of close assemblies of these two probes support the model of teixobactin forming tight dimers in the presence of lipid II in Gram-positive bacteria.[1,6] However, some of the cells did not exhibit quenching of Cy3 fluorescence lifetime (shown as green signal in Figure 3.6), indicating that Lys(Cy3)$_{10}$-teixobactin and Lys(Cy5)$_{10}$-teixobactin are not always in close proximity with each other in *B. subtilis*. Taken together, the FLIM-FRET studies demonstrated

that teixobactin forms heterogenous interactions in *B. subtilis*, where the antibiotic can exist in either monomeric or dimeric forms in bacteria.

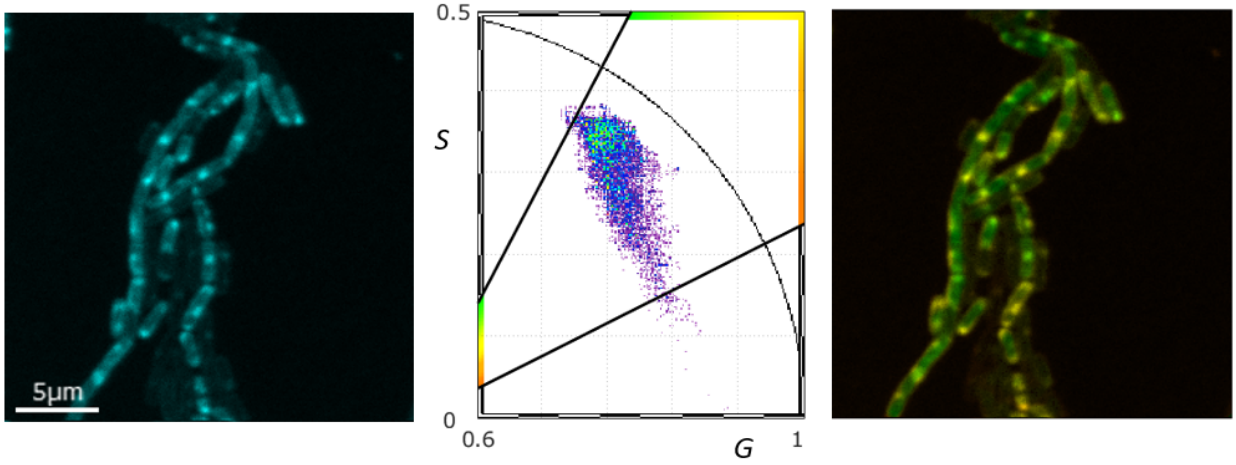

Figure 3.6. Fluorescence lifetime micrograph (left), FLIM-FRET phasor plot (middle), and associated FLIM-FRET micrograph (right) of *B. subtilis* treated with 1 µg/mL Lys(Cy3)$_{10}$-teixobactin and 1 µg/mL Lys(Cy5)$_{10}$-teixobactin. In the FLIM-FRET micrograph, green signal indicates normal Cy5 fluorescence lifetimes, while orange/yellow signal indicates FRET between Cy3 and Cy5.

Even though teixobactin is a promising antibiotic candidate, its unfavorable solubility[13] and aggregation propensity[4,6] are concerning pharmacological properties and could result in off-target effects *in vivo*. To our knowledge, the localization of teixobactin in mammalian cells has not been characterized, and doing so could provide clues into understanding the off-target effects of teixobactin in mammalian cells. In an effort to understand how teixobactin interacts with mammalian cells, we treated NKR-52E rat kidney cells with either 5 µg/mL of Lys(BDY FL)$_{10}$-teixobactin or 5 µg/mL of Lys(Cy3)$_{10}$-teixobactin and used fluorescence microscopy to study the localization of these probes in NRK-52E cells. Both Lys(BDY FL)$_{10}$-teixobactin and Lys(Cy3)$_{10}$-teixobactin were internalized in NRK-52E cells, and both probes appear to be staining the exterior of the nucleus. Thus, the fluorescent teixobactin analogues appear to interact with NRK-52E cells; however, additional experiments need to be performed to further understand this interaction.

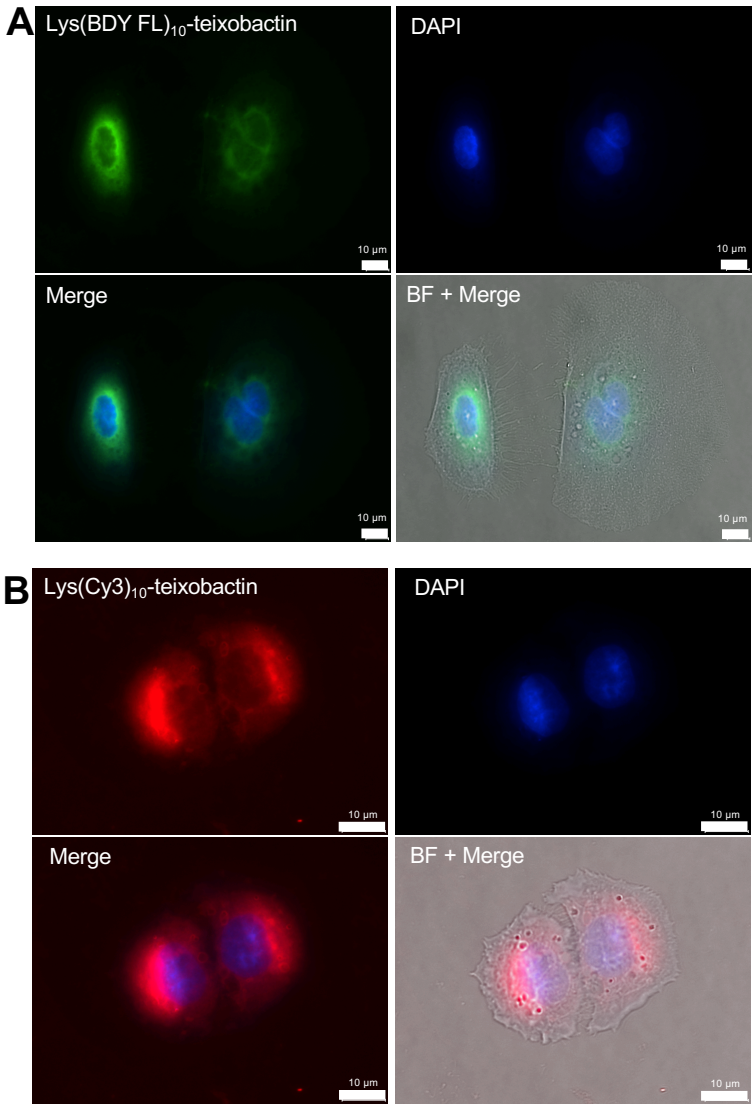

Figure 3.7. Localization of Lys(BDY FL)$_{10}$-teixobactin and Lys(Cy3)$_{10}$-teixobactin in NRK-52E cells. (A) NRK-52E cells treated with 5 µg/mL of Lys(BDY FL)$_{10}$-teixobactin and counterstained with 1 µg/mL of DAPI. (B) NRK-52E cells treated with 5 µg/mL of Lys(Cy3)$_{10}$-teixobactin and counterstained with 1 µg/mL of DAPI.

Conclusion

We present a versatile and selective approach to construct fluorescent teixobactin analogues. This labeling reaction allowed us to determine that the incorporation of fluorophores at position 10 in the teixobactin pharmacophore resulted in probes with better MIC values and brighter staining compared to fluorophores at position 9. The Lys(BDY FL)$_{10}$-teixobactin analogue

resulted in septal, sidewall, and aggregated staining patterns in *B. subtilis*, illustrating various ways teixobactin binds to peptidoglycan precursors. We also demonstrated for the first time the presence of monomeric and oligomeric teixobactin in live *B. subtilis* using FLIM-FRET microscopy, which may highlight the importance of teixobactin self-assembly in its mode of action. We anticipate that our labeling reaction will generate a variety of teixobactin probes that will further elucidate the mechanism of action of teixobactin and its possible off-target effects in mammalian and human cells.

References

(1) Ling, L. L.; Schneider, T.; Peoples, A. J.; Spoering, A. L.; Engels, I.; Conlon, B. P.; Mueller, A.; Schäberle, T. F.; Hughes, D. E.; Epstein, S.; Jones, M.; Lazarides, L.; Steadman, V. A.; Cohen, D. R.; Felix, C. R.; Fetterman, K. A.; Millett, W. P.; Nitti, A. G.; Zullo, A. M.; Chen, C.; Lewis, K. A New Antibiotic Kills Pathogens without Detectable Resistance. *Nature* **2015**, *517* (7535), 455–459. https://doi.org/10.1038/nature14098.

(2) Services, U. . D. of H. and H. Antibiotic Resistance Threats in the United States. *Centers Dis. Control Prev.* **2019**, 1–113.

(3) Homma, T.; Nuxoll, A.; Gandt, A. B.; Ebner, P.; Engels, I.; Schneider, T.; Götz, F.; Lewis, K.; Conlon, B. P. Dual Targeting of Cell Wall Precursors by Teixobactin Leads to Cell Lysis. *Antimicrob. Agents Chemother.* **2016**, *60* (11), 6510–6517. https://doi.org/10.1128/AAC.01050-16.

(4) Yang, H.; Wierzbicki, M.; Du Bois, D. R.; Nowick, J. S. X-Ray Crystallographic Structure of a Teixobactin Derivative Reveals Amyloid-like Assembly. *J. Am. Chem. Soc.* **2018**, 8–12. https://doi.org/10.1021/jacs.8b07709.

(5) Yang, H.; Pishenko, A. V.; Li, X.; Nowick, J. S. Design, Synthesis, and Study of Lactam and Ring-Expanded Analogues of Teixobactin. *J. Org. Chem.* **2020**, *85* (3), 1331–1339. https://doi.org/10.1021/acs.joc.9b02631.

(6) Shukla, R.; Medeiros-Silva, J.; Parmar, A.; Vermeulen, B. J. A.; Das, S.; Paioni, A. L.; Jekhmane, S.; Lorent, J.; Bonvin, A. M. J. J.; Baldus, M.; Lelli, M.; Veldhuizen, E. J. A.; Breukink, E.; Singh, I.; Weingarth, M. Mode of Action of Teixobactins in Cellular Membranes. *Nat. Commun.* **2020**, *11* (1), 1–10. https://doi.org/10.1038/s41467-020-16600-2.

(7) Morris, M. A.; Malek, M.; Hashemian, M. H.; Nguyen, B. T.; Manuse, S.; Lewis, K.; Nowick, J. S. A Fluorescent Teixobactin Analogue. *ACS Chem. Biol.* **2020**, *15* (5), 1222–1231. https://doi.org/10.1021/acschembio.9b00908.

(8) Hasper, H. E.; Kramer, N. E.; Smith, J. L.; Hillman, J. D.; Zachariah, C.; Kuipers, O. P.; de Kruijff, B.; Breukink, E. An Alternative Bactericidal Mechanism of Action for Lantibiotic Peptides That Target Lipid II. *Science (80-.).* **2006**, *313* (5793), 1636–1637. https://doi.org/10.1126/science.1129818.

(9) Lages, M. C. A.; Beilharz, K.; Morales Angeles, D.; Veening, J. W.; Scheffers, D. J. The Localization of Key Bacillus Subtilis Penicillin Binding Proteins during Cell Growth Is Determined by Substrate Availability. *Environ. Microbiol.* **2013**, *15* (12), 3272–3281. https://doi.org/10.1111/1462-2920.12206.

(10) Liu, L.; Wu, S.; Wang, Q.; Zhang, M.; Wang, B.; He, G.; Chen, G. Total Synthesis of Teixobactin and Its Stereoisomers. *Org. Chem. Front.* **2018**, *5* (9), 1431–1435. https://doi.org/10.1039/c8qo00145f.

(11) Yang, H.; Chen, K. H.; Nowick, J. S. Elucidation of the Teixobactin Pharmacophore. *ACS Chem. Biol.* **2016**, *11* (7), 1823–1826. https://doi.org/10.1021/acschembio.6b00295.

(12) Abdel Monaim, S. A. H.; Jad, Y. E.; Ramchuran, E. J.; El-Faham, A.; Govender, T.; Kruger, H. G.; de la Torre, B. G.; Albericio, F. Lysine Scanning of Arg 10 –Teixobactin: Deciphering the Role of Hydrophobic and Hydrophilic Residues . *ACS Omega* **2016**, *1* (6), 1262–1265. https://doi.org/10.1021/acsomega.6b00354.

(13) Chen, K. H.; Le, S. P.; Han, X.; Frias, J. M.; Nowick, J. S. Alanine Scan Reveals Modifiable Residues in Teixobactin. *Chem. Commun.* **2017**, *53* (82), 11357–11359. https://doi.org/10.1039/c7cc03415f.

(14) Hermanson, G. T. *Bioconjugate Techniques: Third Edition*; Elsevier, 2013. https://doi.org/10.1016/C2009-0-64240-9.

(15) Boutureira, O.; Bernardes, G. J. L. Advances in Chemical Protein Modification. *Chem. Rev.* **2015**, *115* (5), 2174–2195. https://doi.org/10.1021/cr500399p.

(16) Koniev, O.; Wagner, A. Developments and Recent Advancements in the Field of Endogenous Amino Acid Selective Bond Forming Reactions for Bioconjugation. *Chem. Soc. Rev.* **2015**, *44* (15), 5495–5551. https://doi.org/10.1039/c5cs00048c.

(17) Kavanagh, A.; Ramu, S.; Gong, Y.; Cooper, M. A.; Blaskovich, M. A. T. Effects of Microplate Type and Broth Additives on Microdilution MIC Susceptibility Assays. *Antimicrob. Agents Chemother.* **2019**, *63* (1). https://doi.org/10.1128/AAC.01760-18.

(18) Tiyanont, K.; Doan, T.; Lazarus, M. B.; Fang, X.; Rudner, D. Z.; Walker, S. Imaging Peptidoglycan Biosynthesis in Bacillus Subtilis with Fluorescent Antibiotics. *Proc. Natl. Acad. Sci. U. S. A.* **2006**, *103* (29), 11033–11038. https://doi.org/10.1073/pnas.0600829103.

(19) Heintzmann, R.; Huser, T. Super-Resolution Structured Illumination Microscopy. *Chem. Rev.* **2017**, *117* (23), 13890–13908. https://doi.org/10.1021/acs.chemrev.7b00218.

(20) Roy, R.; Hohng, S.; Ha, T. A Practical Guide to Single-Molecule FRET. *Nat. Methods* **2008**, *5* (6), 507–516. https://doi.org/10.1038/nmeth.1208.

(21) Margineanu, A.; Chan, J. J.; Kelly, D. J.; Warren, S. C.; Flatters, D.; Kumar, S.; Katan, M.; Dunsby, C. W.; French, P. M. W. Screening for Protein-Protein Interactions Using Förster Resonance Energy Transfer (FRET) and Fluorescence Lifetime Imaging Microscopy (FLIM). *Sci. Rep.* **2016**, *6* (February). https://doi.org/10.1038/srep28186.

(22) Ranjit, S.; Malacrida, L.; Jameson, D. M.; Gratton, E. Fit-Free Analysis of Fluorescence

Lifetime Imaging Data Using the Phasor Approach. *Nat. Protoc.* **2018**, *13* (9), 1979–2004. https://doi.org/10.1038/s41596-018-0026-5.

Chapter 3 Supporting Information

Table of Contents

Supplementary data

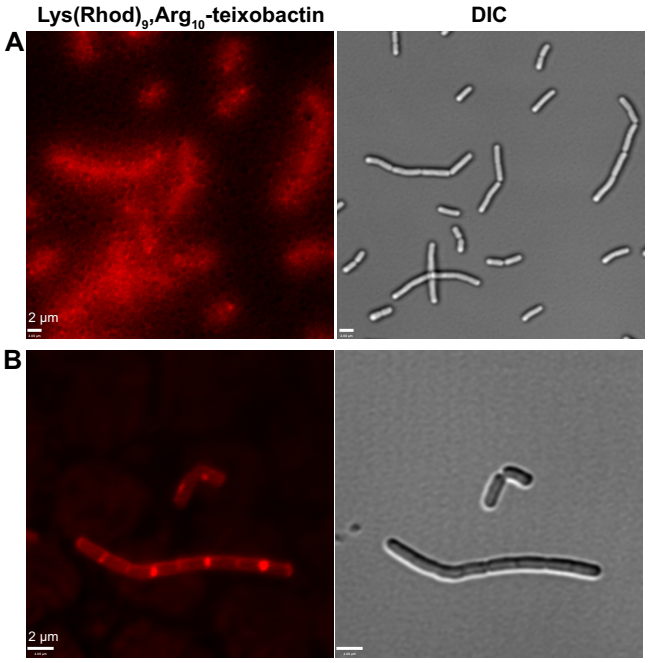

Figure S3.1. *B. subtilis* stained with 4 µg/mL Lys(Rhod)$_9$,Arg$_{10}$-teixobactin in the absence (A) or presence (B) of 0.05% polysorbate 80.

Materials and Methods

General Methods. Amino acids, coupling agents, 2-chlorotrityl chloride resin, DIC, and triisopropylsilane were purchased from Chem-Impex. DMF (amine-free), DIPEA, 2,4,6-collidine, and piperidine were purchased from Alfa-Aesar. DMAP and polysorbate 80 were purchased from Acros Organics. BODIPY FL NHS ester, Cy3 NHS ester, and Cy5 NHS ester were purchased from Lumiprobe. HPLC-grade acetonitrile, and dichloromethane were purchased from Fisher Scientific. TFA and hexafluoroisopropanol were purchased from Oakwood Chemical. Difco Mueller Hinton broth was obtained from Becton, Dickinson and Company.

Reagent-grade solvents, chemicals, amino acids, and resin were used as received, with the exception of dichloromethane, which was dried through an alumina column under argon, and dimethylformamide, which was dried through an alumina column and an amine scavenger resin column under argon. Solid-phase peptide synthesis was carried out manually in a solid phase reaction vessel. Analytical reverse-phase HPLC was performed on an Agilent 1200 instrument equipped with an Aeris PEPTIDE 2.6u XB-C18 column (Phenomonex). Preparative reverse-phase HPLC was performed on a Rainin Dynamax instrument equipped with a ZORBAX SB-C18 column (Agilent). UV detection (214 nm) was used for analytical and preparative HPLC. HPLC grade acetonitrile and 18 MΩ deionized water, each containing 0.1% trifluoroacetic acid, were used for analytical and preparative reverse-phase HPLC. Matrix-assisted laser desorption ionization time-of-flight (MALDI-TOF) mass spectrometry was performed on an AB SCIEX TOF/TOF 5800 system and 2,5-dihydroxybenzoic acid was used as the sample matrix. Electrospray ionization (ESI) mass spectrometry was performed on an LCT ESI LC-TOF instrument in positive mode. All peptides were prepared and used as the trifluoroacetate salts and were assumed to have one trifluoroacetate ion per ammonium group present in each peptide.

Synthesis of Lys_9,Arg_{10}-teixobactin.[1] *Resin loading*. 2-Chlorotrityl chloride resin (300 mg, 1.46 mmol/g) was added to a 10-mL Bio-Rad Poly-Prep chromatography column. The resin was suspended in dry CH_2Cl_2 (10 mL) and allowed to swell for 30 min. The resin was loaded with a solution of Fmoc-Arg(Pbf)-OH (184 mg, 0.28 mmol, 0.78 equiv) and 2,4,6-collidine (300 μL) in dry CH_2Cl_2 (8 mL). The suspension was agitated for 4−12 h until a resin loading of at least 50% was achieved. The solution was drained, and the resin was washed with dry CH_2Cl_2 (3x). A mixture of CH_2Cl_2/MeOH/DIPEA (17:2:1, 5 mL) was added to the resin and agitated for 1 h to cap any unreacted 2-chlorotrityl chloride sites. The solution was drained, and the resin was washed with dry CH_2Cl_2 (3x). The resin was then dried with a flow of nitrogen.

Quantifying resin loading. A small portion of loaded resin was removed from the column and dried under vacuum. 1.0 mg of the dried resin was weighed out and transferred to a scintillation vial containing 3 mL of 20% piperidine/DMF and a small magnetic stirring bar. The reaction mixture was allowed to stir for 10 min and the absorbance at 290 nm was measured. The resin loading was determined to be 0.28 mmol (0.54 mmol/g, 64% loading) using the following formula:

$$\%\ \text{loading} = \frac{\mathrm{A}_{290\ \mathrm{nm}} \times \mathrm{V} \times 10^3}{6089 \times \mathrm{m}_{\mathrm{resin}} \times l} \times 100\%$$

where:

A_{290} nm = Absorbance measured at 290 nm

ε = Molar absorptivity of piperidine adduct (6,089 L mol^{-1} cm^{-1})

m_{resin} = Mass of resin in mg (1.0 mg)

V = Volume of piperidine in DMF in mL (3.0 mL)

l = Cell pathlength in cm (1.0 cm)

Linear peptide synthesis. The loaded resin was suspended in dry DMF and transferred to a solid-phase peptide synthesis reaction vessel for manual peptide synthesis using Fmoc-Lys(Boc)-

OH, Fmoc-D-Thr-OH (free alcohol OH), Fmoc-Ser(*t*-Bu)-OH, Fmoc-Ile-OH, Fmoc-D-*allo*-Ile-OH, Fmoc-D-Gln(Trt)-OH, Fmoc-Ser(*t*-Bu)-OH, Fmoc-Ile-OH, and Boc-*N*-methyl-D-Phe-OH. The linear peptide was synthesized through the following cycles: *i*. Fmoc deprotection with 20% (*v/v*) piperidine in dry DMF (5 mL) for 10 min (2x), *ii*. resin washing with dry DMF (3x), *iii*. coupling of amino acid (0.64 mmol, 4 equiv) with HCTU (267 mg, 0.64 mmol, 4 equiv) in 20% (*v/v*) 2,4,6-collidine in dry DMF (5 mL) for 20 min, and *iv*. resin washing with dry DMF (3x). After the linear synthesis was completed, the resin was then washed with dry CH_2Cl_2 in the solid-phase peptide synthesis reaction vessel (3x).

Esterification.[3] The resin was transferred to a 10-mL Bio-Rad Poly-Prep chromatography column and washed with dry CH_2Cl_2 (3x). In a test tube, Fmoc-Ile-OH (640 mg, 1.8 mmol, 10 equiv) and diisopropylcarbodiimide (281 μL, 1.8 mmol, 10 equiv) were dissolved in dry CH_2Cl_2 (5 mL). The resulting solution was filtered through 0.20-μm nylon filter, and then 4-dimethylaminopyridine (22 mg, 0.18 mmol, 1 equiv) was added to the filtrate. The resulting solution was transferred to the resin and was gently agitated for 1 h. The solution was drained and the resin was washed with dry CH_2Cl_2 (3x) and DMF (3x).

Fmoc deprotection and peptide cleavage. The Fmoc protecting group on Ile_{11} was removed by treatment with 20% piperidine in dry DMF (5 mL) for 10 min (2x). The solution was drained and the resin was washed with dry DMF (3x) and then with dry CH_2Cl_2 (3x). To cleave the peptide, the resin was treated with 20% hexafluoroisopropanol (HFIP) in dry CH_2Cl_2 (6 mL) with agitation for 1 h. The filtrate was collected in a round-bottom flask. The HFIP treatment was repeated, and the filtrate was added to the round-bottom flask. The resin was washed with an additional aliquot of 20% HFIP (6 mL) and then washed with dry CH_2Cl_2 (3x). The combined filtrates and methylene

chloride washes were concentrated under reduced pressure to afford a clear oil. The oil was placed under vacuum (≤ 0.1 mmHg) to remove any residual solvents.

Cyclization. The oil was dissolved in 125 mL of dry DMF. HBTU (412 mg, 1.1 mmol, 6 equiv) and HOBt (147 mg, 1.1 mmol, 6 equiv) were added to the solution. The reaction mixture was stirred under nitrogen for 30 min. DIPEA (170 μL, 1.1 mmol, 6 equiv) was added over ca. 10 s to the solution, and the reaction mixture was stirred for 12 h. The mixture was concentrated under reduced pressure to afford the cyclized peptide as a pink solid. The solid was placed under vacuum (≤ 0.1 mmHg) to remove any residual solvents.

Global deprotection, ether precipitation, and purification. The crude protected peptide was dissolved in a mixture of trifluoroacetic acid (TFA)/triisopropylsilane/H_2O (90:5:5, 10 mL), and the solution was stirred under nitrogen for 1 h. The deprotection mixture was then evenly aliquoted between two 40-mL portions of ice-cold diethyl ether in 50-mL conical tubes. The 50-mL conical tubes were centrifuged (400 x G) for 15 min to precipitate the crude peptide. The diethyl ether supernatant was discarded and the precipitated pellets were dried under a stream of nitrogen. The pellets were dissolved in 40% (*v/v*) CH_3CN in water (8 mL) and centrifuged at 3300 rpm (1380 x G) for 5 min, and the solution was filtered through 0.20-μm nylon filter. The peptide was purified by reverse-phase HPLC with H_2O/CH_3CN (gradient elution of 20–40% CH_3CN with 0.1% TFA over 120 min). Fractions were analyzed by analytical HPLC and MALDI mass spectrometry. The pure fractions were combined and lyophilized to give 14 mg (6% yield based on resin loading) of Lys_9,Arg_{10}-teixobactin trifluoroacetate (TFA) salt as white powder.

Synthesis of Lys_{10}-teixobactin.[1] This peptide was synthesized using identical procedures described above. After purification and lyophilization, 14.5 mg of Lys_{10}-teixobactin (6.4% yield based on resin loading) as a TFA salt were obtained.

Synthesis of Lys(BDY FL)$_9$,Arg$_{10}$-teixobactin. 5 mg of BODIPY FL NHS ester was dissolved in 100 µL of dry DMSO to create a 50 mg/mL stock solution, which was wrapped in black felt to protect it from light and stored in a desiccated container in a −20 °C freezer for subsequent reactions. Lys$_9$,Arg$_{10}$-teixobactin (5.66 mg of the peptide, 3.44 µmol, 1.0 equiv) was weighed out in a tared Eppendorf tube using an analytical balance. The peptide was dissolved in 65 µL of dry DMF and 3 µL of DIPEA (17.2 µmol, 5.0 equiv) was slowly added to the solution. The solution was vortexed to ensure homogeneity. To this solution, 32 µL of 50 mg/mL BODIPY FL NHS ester (4.13 µmol, 1.2 equiv) was added and the solution was mixed by pipetting. The Eppendorf was covered with felt and placed on a rocker. The reaction progress was monitored by ESI-MS and analytical HPLC (using 214 and 488 nm as wavelengths) and the reaction was completed within 1 h [Note: reactions with either Cy3 NHS ester or Cy5 NHS ester were complete within 10 min of reaction with Lys$_{10}$-teixobactin.] The reaction mixture was diluted with 3 mL of 40% (*v/v*) CH_3CN in water and was purified by reverse-phase HPLC with H_2O/CH_3CN (gradient elution of 20–50% CH_3CN with 0.1% TFA over 60 min) equipped with a 9 mm C18 preparative column. The C18 column was heated to 50 °C in a Sterlite plastic bin water bath equipped with a Kitchen Gizmo Sous Vide immersion circulator to maintain the solubility of the peptide during purification. Lys(BDY FL)$_{10}$-teixobactin, Lys(Cy3)$_{10}$-teixobactin, and Lys(Cy5)$_{10}$-teixobactin were prepared using the same procedure, except Lys$_{10}$-teixobactin was used instead of Lys$_9$,Arg$_{10}$-teixobactin. The yields of each purified fluorescent peptide are reported in Table S3.1.

Table S3.1. Yield of purified fluorescent teixobactin analogues.

Fluorescent Analogue	Yield (mg)	Percent yield
Lys(BDY FL)$_9$,Arg$_{10}$-teixobactin	3.0	51%
Lys(BDY FL)$_{10}$-teixobactin	3.3	48%
Lys(Cy3)$_{10}$-teixobactin	3.7	55%
Lys(Cy5)$_{10}$-teixobactin	3.8	53%

Preparation of DMSO Stock Solutions. A 1 mg/mL DMSO stock solution of each fluorescent teixobactin analogue was prepared gravimetrically by dissolving 1.0 mg of the lyophilized peptide in 1 mL of sterile DMSO in an autoclaved Eppendorf tube. The 1 mg/mL DMSO stock solutions were wrapped in black felt and stored in a −20 °C freezer for subsequent experiments.

NOTE: Solutions of fluorescent teixobactin analogues were protected from excessive exposure to light in MIC assays and other experiments by use of an unlit biosafety cabinet, black felt, and minimizing exposure to room lights.

MIC Assays.[22] *Bacillus subtilis* (ATCC 6051), *Staphylococcus epidermidis* (ATCC 14990) and *Escherichia coli* (ATCC 10798) were cultured from glycerol stocks in Mueller-Hinton broth overnight in a shaking incubator at 37 °C. An aliquot of the 1 mg/mL antibiotic stock solution was diluted with culture media to make a 64 μg/mL solution. A 200-μL aliquot of the 64 μg/mL solution was transferred to a 96-well plate. Two-fold serial dilutions were made with media across a 96-well plate to achieve a final volume of 100 μL in each well. These solutions had the following concentrations: 64, 32, 16, 8, 4, 2, 1, 0.5, 0.25, 0.125, and 0.0625 μg/mL. The overnight cultures of each bacterium were diluted with Mueller-Hinton broth to an OD_{600} of 0.075 as measured for 200 μL in a 96-well plate. The diluted mixture was further diluted to 1 x 10^6 CFU/mL with Mueller-Hinton broth (dilution of 50x for *B. subtilis*, 10x for *S. epidermidis*, and 50x for *E. coli*).[22] A 100-μL aliquot of the 1 x 10^6 CFU/mL bacterial solution was added to each well in 96-well plates, resulting in final bacteria concentrations of 5 x 10^5 CFU/mL in each well. As 100 μL of bacteria were added to each well, the teixobactin analogues were also diluted to the following concentrations: 32, 16, 8, 4, 2, 1, 0.5, 0.25, 0.125, 0.0625, and 0.03125 μg/mL. The plate was covered with a lid and incubated at 37 °C for 16 h. The optical

density of each well was recorded at 750 nm, instead of 600 nm, to avoid absorbance by the fluorophore and was measured using a 96-well UV/Vis plate reader (MultiSkan GO, Thermo Scientific). The MIC values were taken as the lowest concentration that had no bacteria growth. Each MIC assay was run in triplicate in three independent runs to ensure reproducibility. MIC assays were performed in test media containing with and without 0.002% polysorbate 80.

Fluorescence Microscopy Studies. *Culturing bacteria for imaging.* Bacteria were allowed to grow overnight (ca. 16 h) in Mueller-Hinton broth in a shaking incubator at 37 °C. The following morning, the cultures were diluted 1:100 in Mueller-Hinton broth and were allowed to grow exponentially in a shaking incubator at 37 °C. Once an OD_{600} of ca. 0.3 was achieved, 500 µL of bacteria was transferred to a sterile Eppendorf tube and the bacteria were centrifuged at 4000 rpm (1300 x G) for 5 min.

Preparation of 2% agarose beds for imaging bacteria. A 2% stock solution of agarose was prepared by adding 1 g of agarose into 50 mL of sodium phosphate buffer (pH 7.4), autoclaving, and allowing the solution to cool until it completely solidified. While the diluted bacteria were growing in the shaking incubator, fresh 2% agarose beds were prepared to immobilize bacteria for fluorescence microscopy studies as follow: On a laboratory bench equipped with an alcohol burner [to help maintain sterility], microscope slides were gently warmed on a hot plate. While the slides were gently warming, the solidified 2% agarose solution was heated in a microwave oven until it became a homogenous liquid. Once the microscope slides were warm to the touch, a 75-µL aliquot of the molten 2% agarose solution was applied to each microscope slide, and a No. 1.5 coverslip was immediately applied gently to the drop of agarose. The assembly was allowed to set for at least 45 minutes before use.

Preparation of fluorescent teixobactin solutions for fluorescence microscopy studies. While the bacteria were being centrifuged, a 1 μg/mL solution of the fluorescent teixobactin was freshly prepared and then used immediately to stain the bacteria. The 1 μg/mL solution was prepared by diluting 2 μL of the 1 mg/mL DMSO stock solution with 1.998 mL of sterile sodium phosphate buffer containing either 0% or 0.05% polysorbate 80. The fluorescent antibiotic solutions were subsequently vortexed for 30 seconds and then used immediately to stain the bacteria.

Staining bacteria for fluorescence microscopy studies. After centrifuging the bacteria (see above), the supernatant was removed, the pellet was resuspended in 500 μL of 1 μg/mL of the probe solution, and the bacteria were incubated in a shaking incubator at 37 °C for 10 min. The bacteria were centrifuged at 4000 rpm (1300 x G) for 5 min, and the supernatant was removed. The pellet was resuspended in 500 μL of sterile sodium phosphate buffer (pH 7.4) containing either 0% or 0.05% polysorbate 80, the suspension was centrifuged at 4000 rpm (1300 x G) for 5 min, and the supernatant was removed. This washing process was repeated two additional times. After the last wash, the cells were resuspended in 200−500 μL of sterile sodium phosphate buffer containing 0.05% polysorbate 80. [The volume of phosphate buffer was selected based on the size of the pellet remaining after the washing steps.] On a sterile bench equipped with an alcohol burner, the coverslip of each agarose bed was removed, and a 5-μL aliquot of the stained bacteria was applied to the coverslip. The coverslip was then sandwiched on top of the agarose bed.

Imaging the bacteria using the Keyence BZ-X810 fluorescence microscope. B. subtilis stained with 1 μg/mL of Lys(BDY FL)$_{10}$-teixobactin were immediately imaged on a Keyence BZ-X810 fluorescence microscope using the eGFP filter cube. The exposure was set to 1/10 s.

Images were collected with a 60x oil immersion objective lens with optical zoom using the high-resolution camera sensitivity and oblique illumination settings. Micrographs acquired from the Keyence microscope were left unadjusted without any modifications to the contrast or brightness of the images.

SIM imaging using the Zeiss Elyra 7. The stained bacteria were immediately imaged on a Zeiss Elyra 7. Images were collected with a 63x oil immersion objective lens, with additional optical zoom used as needed to provide detailed images. Fluorescence micrographs of bacteria treated with either Lys(BDY FL)$_9$,Arg$_{10}$-teixobactin or Lys(BDY FL)$_{10}$-teixobactin were recorded with excitation at 488 nm and emission between 490–544 nm. Fluorescence micrographs of bacteria treated with Lys(Cy3)$_{10}$-teixobactin were recorded with excitation at 561 nm and emission between 568–639 nm. Fluorescence micrographs of bacteria treated with Lys(Cy5)$_{10}$-teixobactin were recorded with excitation at 640 nm and emission between 640–700 nm. The image brightness of the fluorescence channels were adjusted linearly using Volocity 6.3 (Quorum Technologies), and a medium filter in the Volocity software was used to reduce noise in all channels.

FLIM-FRET studies. Exponentially growing *B. subtilis* was treated with either 1 μg/mL of Lys(Cy3)$_{10}$-teixobactin, 1 μg/mL of Lys(Cy5)$_{10}$-teixobactin, 1 μg/mL of Lys(Cy3)$_{10}$-teixobactin and 1 μg/mL of Lys(Cy5)$_{10}$-teixobactin, or sodium phosphate buffer (pH 7.4) containing 0.05% polysorbate 80 as a vehicle control. The cells were treated with the probe solutions for 10 min in a shaking incubator at 37 °C. The cells were washed three times using sodium phosphate buffer containing 0.05% polysorbate 80 and applied to coverslips on agarose beds. FLIM-FRET measurements were carried out by Dr. Alexander Vallmitjana Lees at the Laboratory for Fluorescence Dynamics at UC Irvine. For the FRET sample containing both probes, Lys(Cy3)$_{10}$-teixobactin was excited using 490 nm excitation and Cy5 emission (FRET) was detected at 680

nm. For Lys(Cy3)$_{10}$-teixobactin alone, excitation was set at 490 nm and emission was set at 575 nm. For Lys(Cy5)$_{10}$-teixobactin alone, excitation was set at 645 nm and emission was set at 680 nm.

NRK-52E microscopy. 5,000 NRK-52E (ATCC CRL-1571) cells were plated onto an Ibidi 8-well chamber slide with a polymer coverslip in DMEM media containing 5% FBS and phenol red. The cells were incubated at 37 °C in a 5% CO_2 atmosphere for 24 h. After 24 h, the media from each well in the Ibidi slide were removed and 5 μg/mL of Lys(BDY FL)$_{10}$-teixobactin and Lys(Cy3)$_{10}$-teixobactin were prepared by diluting 5 μL of the 1 mg/mL DMSO stock solution with 995 μL of DMEM without serum. The probe solutions were added to the appropriate wells and the cells were incubated at 37 °C in a 5% CO_2 atmosphere for 24 h. After 24 h, the probe solutions were removed and the cells were rinsed 3 × sterile PBS. The cells were fixed with sterile 4% formalin in PBS for 30 min at r.t. and the cells were rinsed 3 × sterile PBS. The cells were counterstained with 1 μg/mL of DAPI in PBS for 5 min at r.t. and the cells were rinsed 3 × sterile PBS. The cells were imaged on a Keyence BZ-X810 fluorescence microscope using the eGFP filter cube for Lys(BDY FL)$_{10}$-teixobactin, the TRITC/Cy3 filter cube for Lys(Cy3)$_{10}$-teixobactin, and the DAPI filter cube for DAPI. The exposure was set to 1/100, 1/150, and 1/100 s for Lys(BDY FL)$_{10}$-teixobactin, Lys(Cy3)$_{10}$-teixobactin, and DAPI, respectively. Images were collected with a 60x oil immersion objective lens with optical zoom using the high-resolution camera sensitivity and oblique illumination settings. Micrographs acquired from the Keyence microscope were left unadjusted.

Characterization data

Lys_9,Arg_{10}-teixobactin

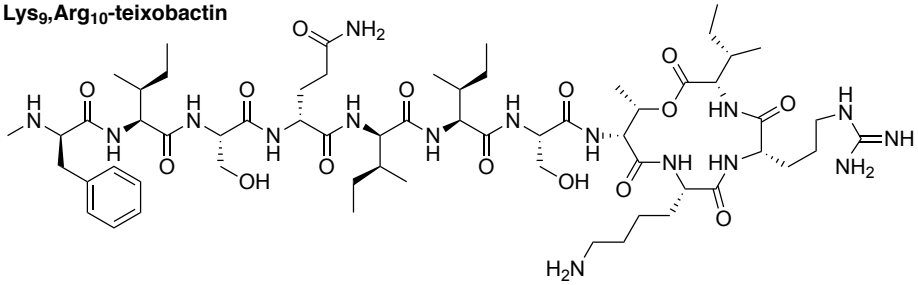

Chemical Formula: $C_{61}H_{104}N_{16}O_{15}$
Exact Mass: 1300.79

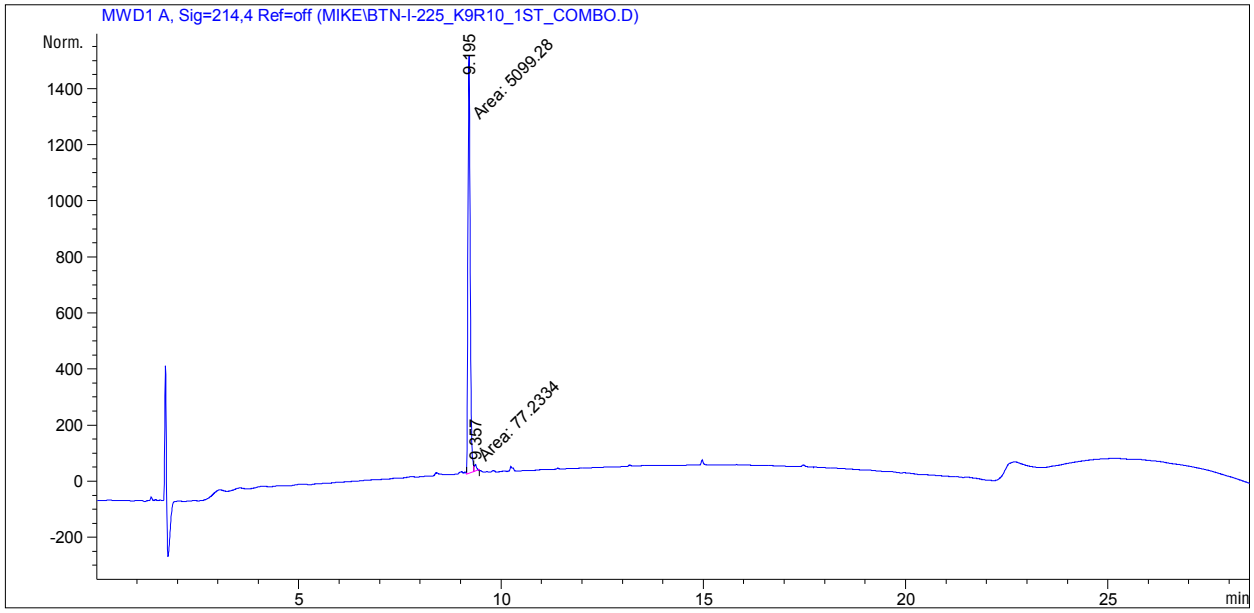

Peak #	RetTime [min]	Type	Width [min]	Area [mAU*s]	Height [mAU]	Area %
1	9.195	MF	0.0632	5099.28418	1345.13147	98.5080
2	9.357	FM	0.0634	77.23338	20.30481	1.4920

Calculated mass for Lys_9,Arg_{10}-teixobactin: $[M+H]^+$ = 1301.79

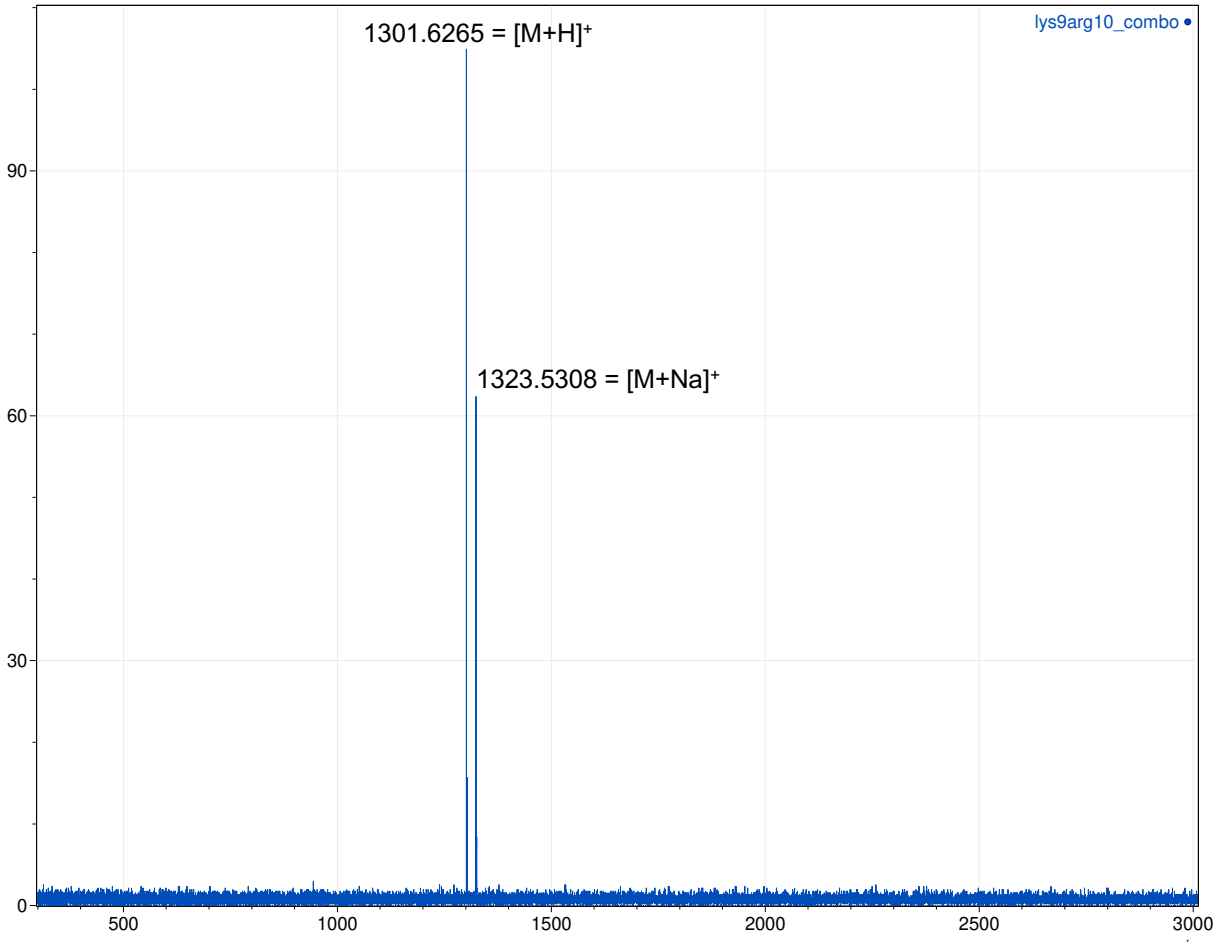

Calculated mass for Lys_9,Arg_{10}-teixobactin: $[M+H]^+$ = 1301.79

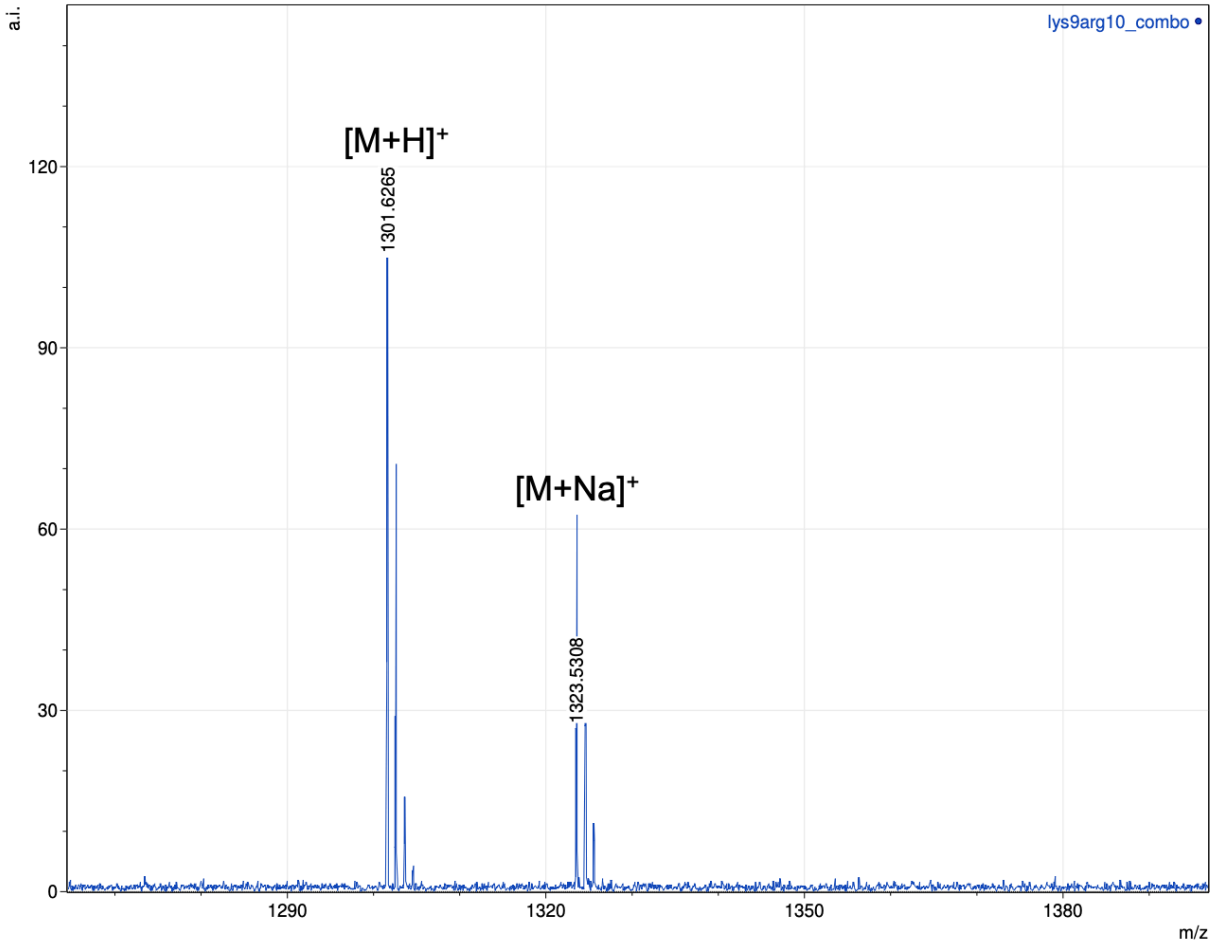

Lys(BDY FL)$_9$,Arg$_{10}$-teixobactin

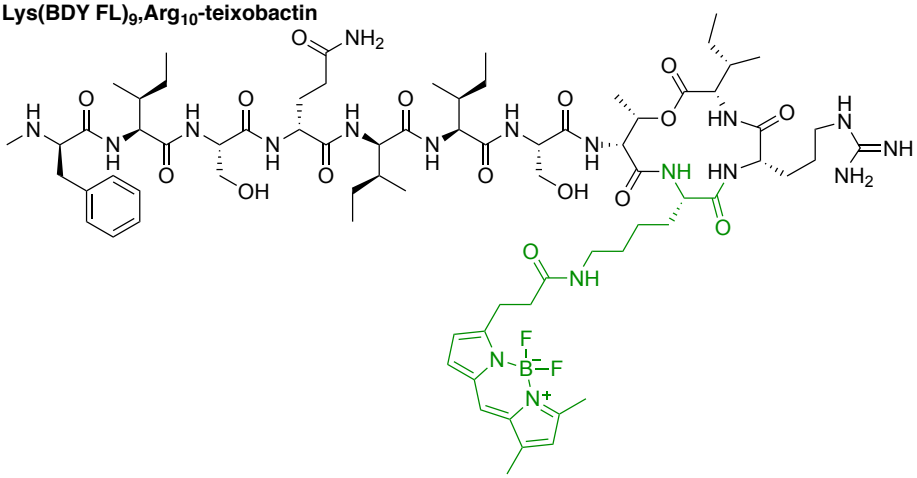

Chemical Formula: $C_{75}H_{117}BF_2N_{18}O_{16}$
Exact Mass: 1574.90

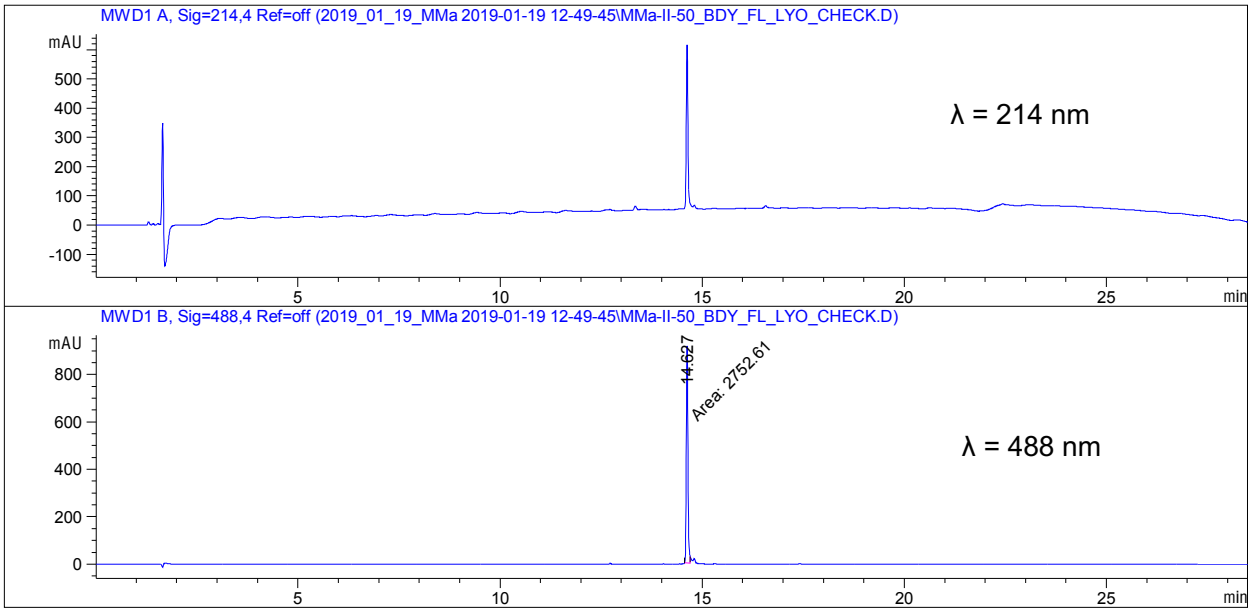

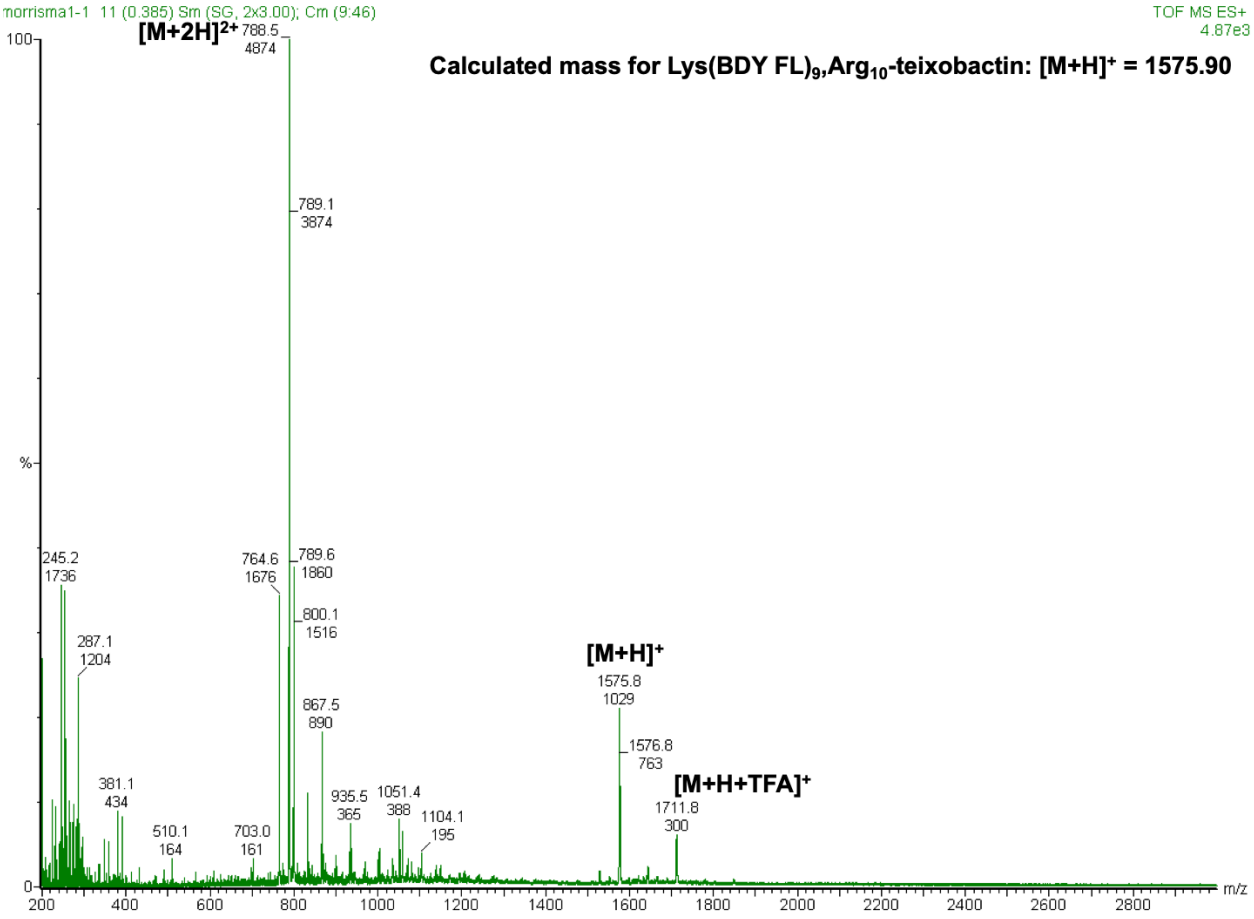
morrisma1-1 11 (0.385) Sm (SG, 2x3.00); Cm (9:46)
TOF MS ES+
4.87e3
Calculated mass for Lys(BDY FL)9,Arg10-teixobactin: [M+H]+ = 1575.90
[M+2H]2+
788.5
4874
789.1
3874
245.2
1736
764.6
1676
789.6
1860
800.1
1516
287.1
1204
[M+H]+
1575.8
1029
867.5
890
1576.8
763
[M+H+TFA]+
1711.8
300
381.1
434
935.5
365
1051.4
388
1104.1
195
510.1
164
703.0
161
100
%
0
200
400
600
800
1000
1200
1400
1600
1800
2000
2200
2400
2600
2800
m/z

Lys$_{10}$-teixobactin

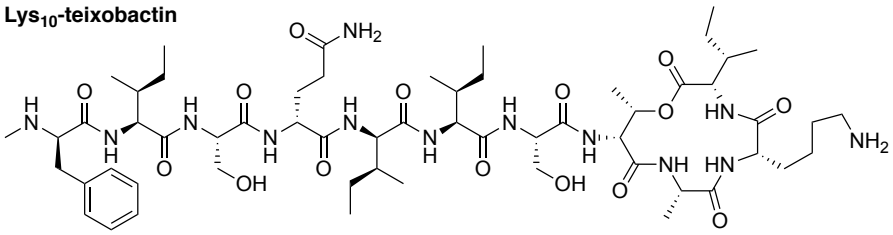

Chemical Formula: $C_{58}H_{97}N_{13}O_{15}$
Exact Mass: 1215.72

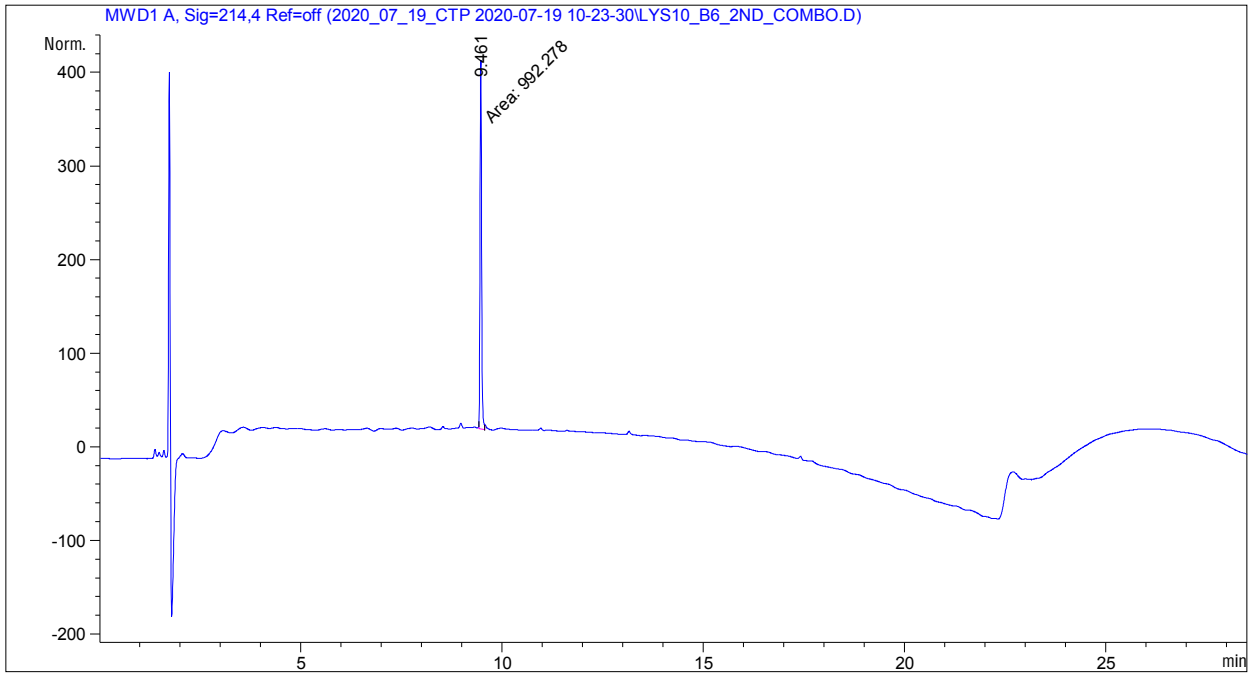

Signal 1: MWD1 A, Sig=214,4 Ref=off

Peak #	RetTime [min]	Type	Width [min]	Area [mAU*s]	Height [mAU]	Area %
1	9.461	MM	0.0462	992.27832	358.02289	100.0000
Totals :				992.27832	358.02289	

Calculated mass for Lys_{10}-teixobactin: $[M+H]^+$ = 1216.73

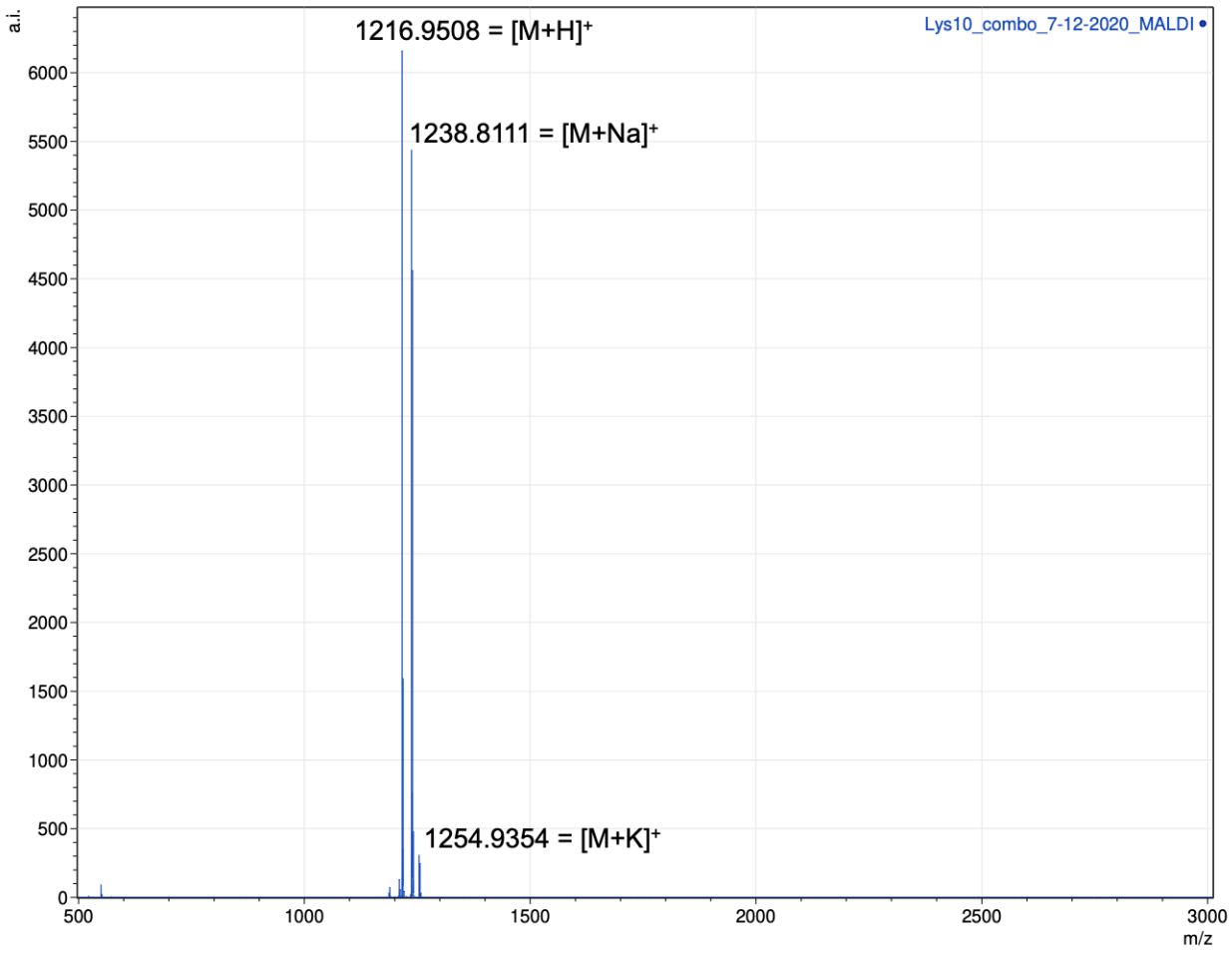

Calculated mass for Lys_{10}-teixobactin: $[M+H]^+$ = 1216.73

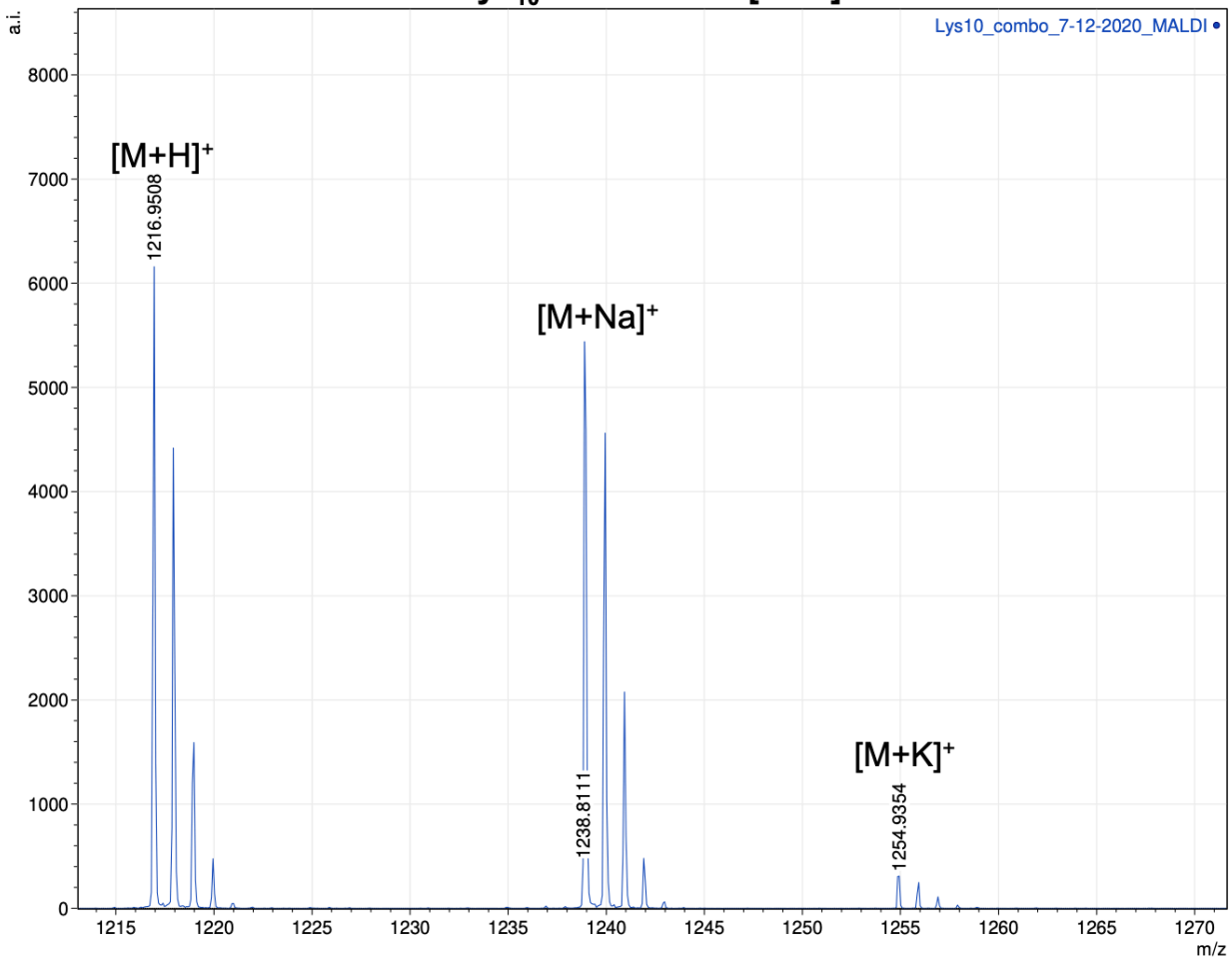

Lys(BDY FL)$_{10}$-teixobactin

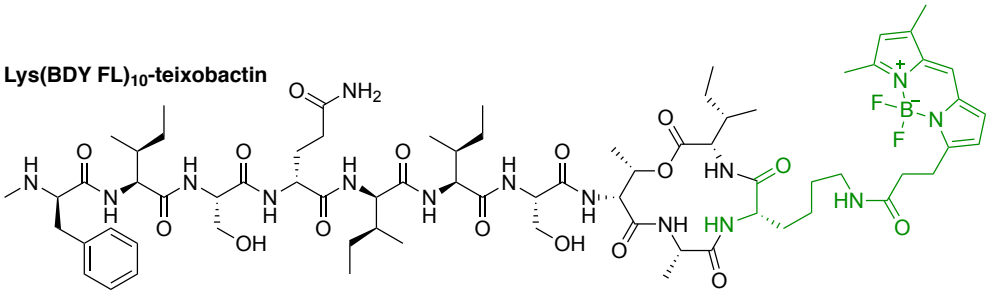

Chemical Formula: $C_{72}H_{110}BF_2N_{15}O_{16}$
Exact Mass: 1489.83

Data File C:\Chem32\...20_06_15_gg3 2020-06-15 10-25-40\BTN-I-10_LYS(BDY_FL)10_LYO_CHECK.D
Sample Name: BTN-I-10_LYS(BDY_FL)10_LYO_CHECK

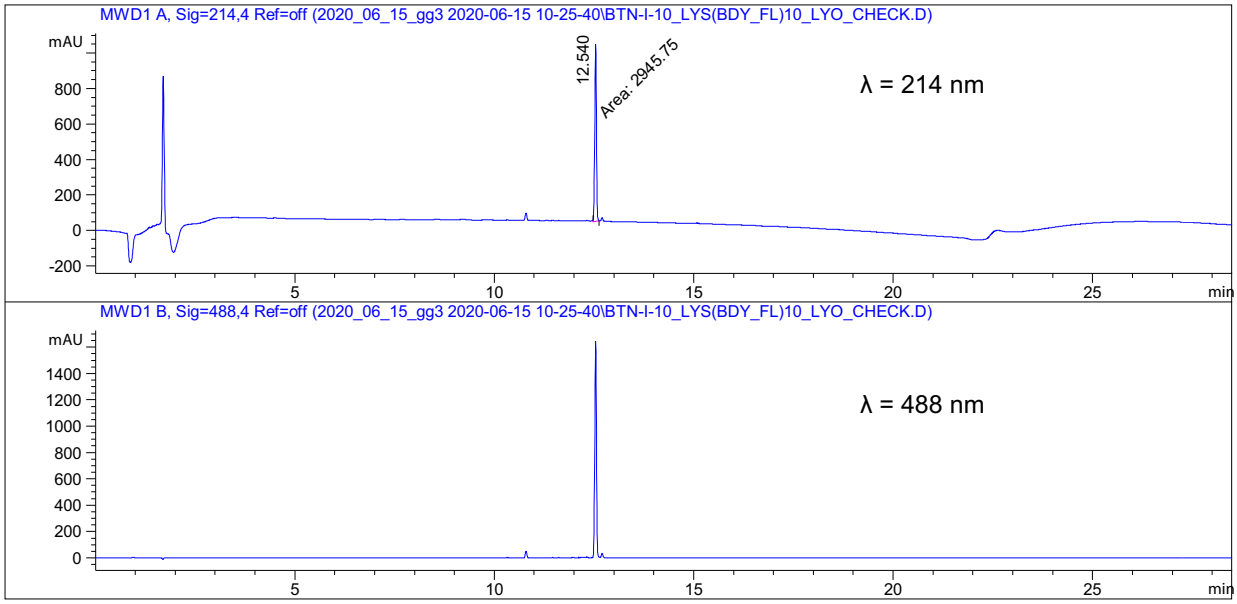


```
=====================================================================
                      Area Percent Report
=====================================================================

Sorted By             :      Signal
Multiplier            :      1.0000
Dilution              :      1.0000
Do not use Multiplier & Dilution Factor with ISTDs


Signal 1: MWD1 A, Sig=214,4 Ref=off

Peak RetTime Type  Width     Area      Height     Area
  #   [min]        [min]   [mAU*s]     [mAU]       %
----|-------|----|-------|----------|----------|--------|
   1  12.540 MM    0.0489 2945.74780 1004.38367 100.0000
```

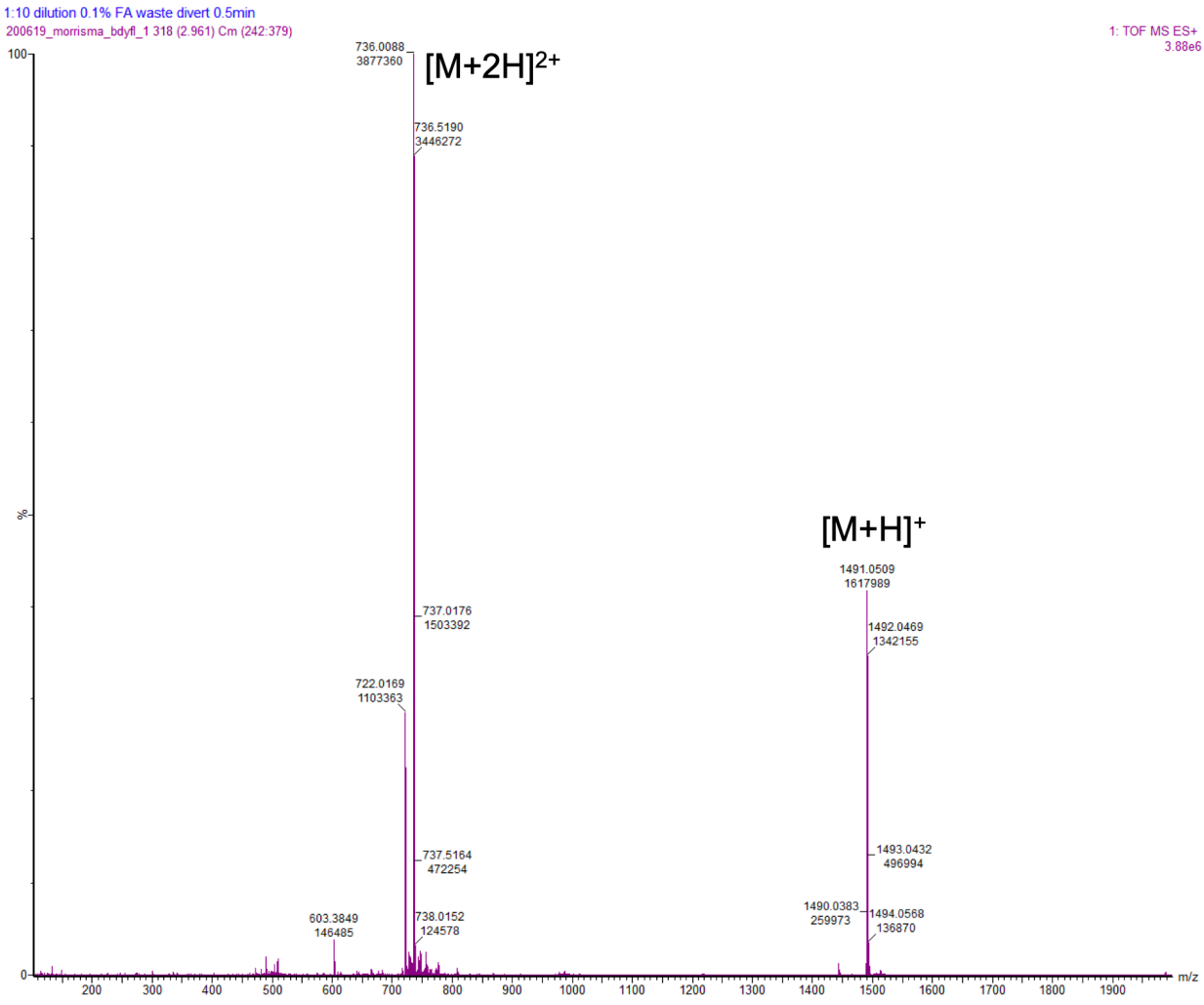
1:10 dilution 0.1% FA waste divert 0.5min
200619_morrisma_bdyfl_1 318 (2.961) Cm (242:379)
1: TOF MS ES+
3.88e6
100
%
0
736.0088
3877360
[M+2H]2+
736.5190
3446272
737.0176
1503392
722.0169
1103363
737.5164
472254
603.3849
146485
738.0152
124578
[M+H]+
1491.0509
1617989
1492.0469
1342155
1493.0432
496994
1490.0383
259973
1494.0568
136870
200
300
400
500
600
700
800
900
1000
1100
1200
1300
1400
1500
1600
1700
1800
1900
m/z

Lys(Cy3)$_{10}$-teixobactin

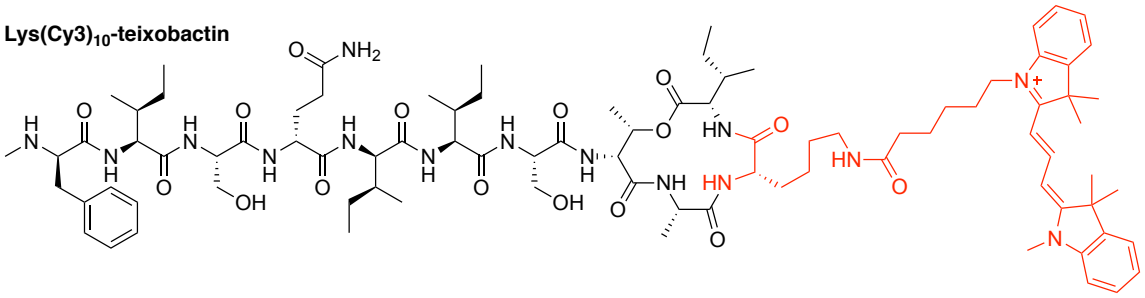

Chemical Formula: $C_{88}H_{132}N_{15}O_{16}^{+}$
Exact Mass: 1655.00

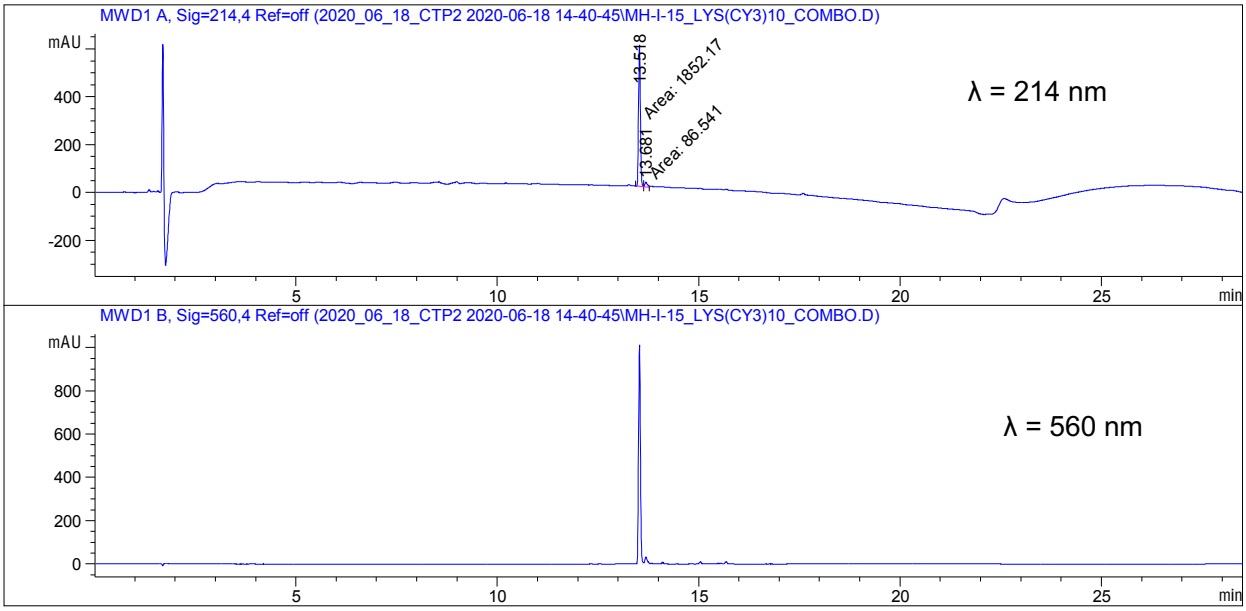

Signal 1: MWD1 A, Sig=214,4 Ref=off

Peak #	RetTime [min]	Type	Width [min]	Area [mAU*s]	Height [mAU]	Area %
1	13.518	MF	0.0520	1852.17371	593.26880	95.5362
2	13.681	FM	0.0761	86.54102	18.95244	4.4638

Calculated mass for $Lys(Cy3)_{10}$-teixobactin: $[M+H]^+$ = 1655.00

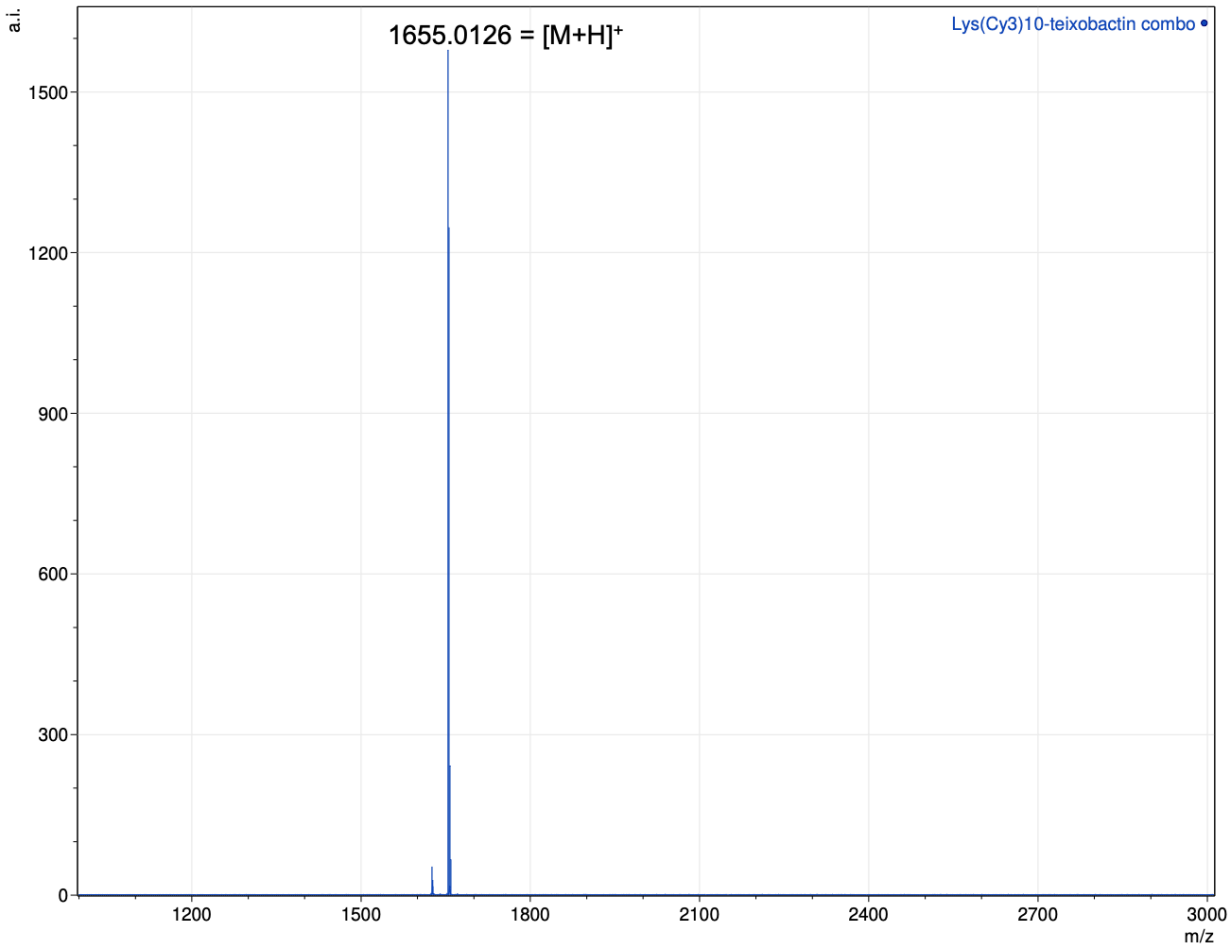

Calculated mass for Lys(Cy3)$_{10}$-teixobactin: $[M+H]^+$ = 1655.00

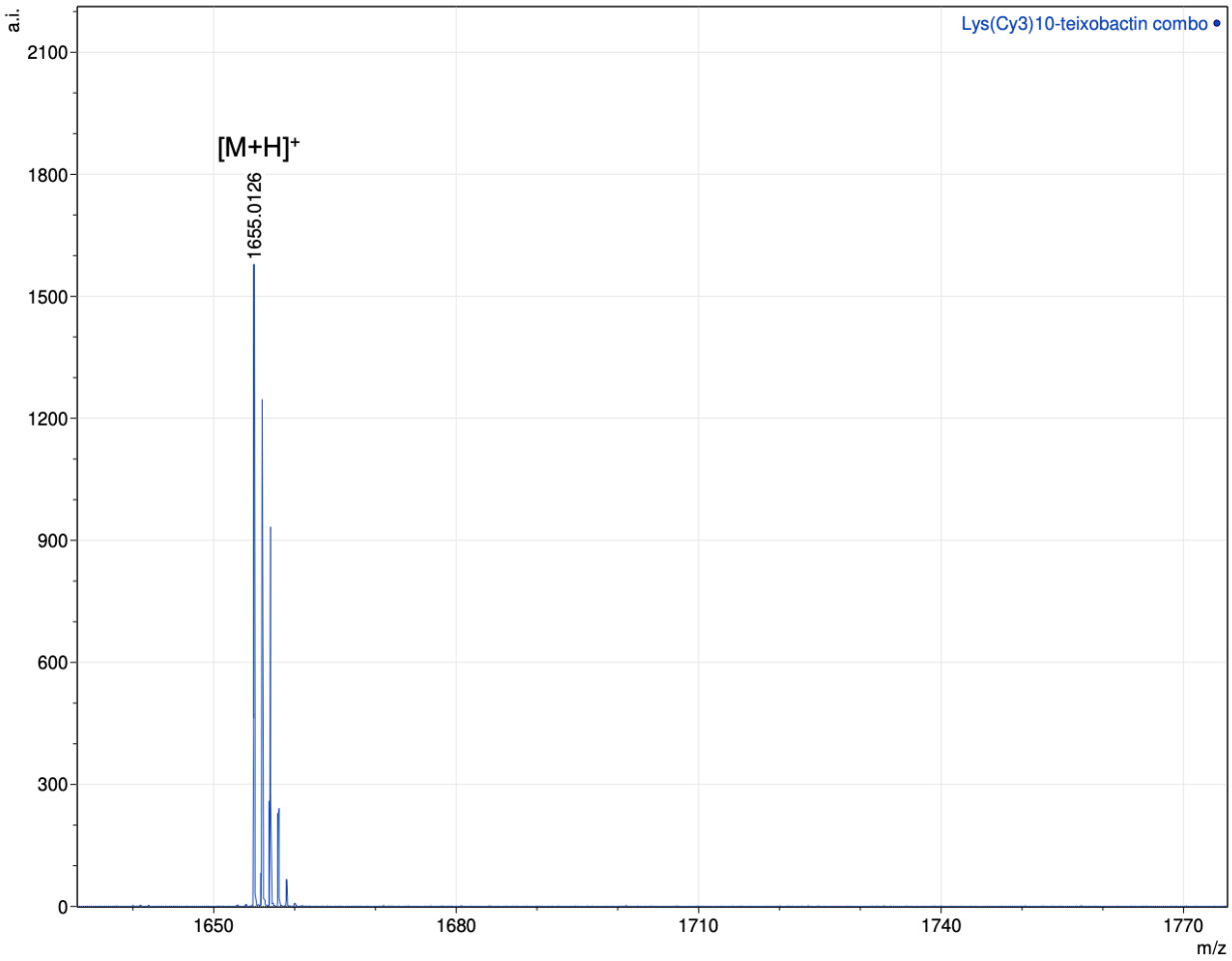

Lys(Cy5)$_{10}$-teixobactin

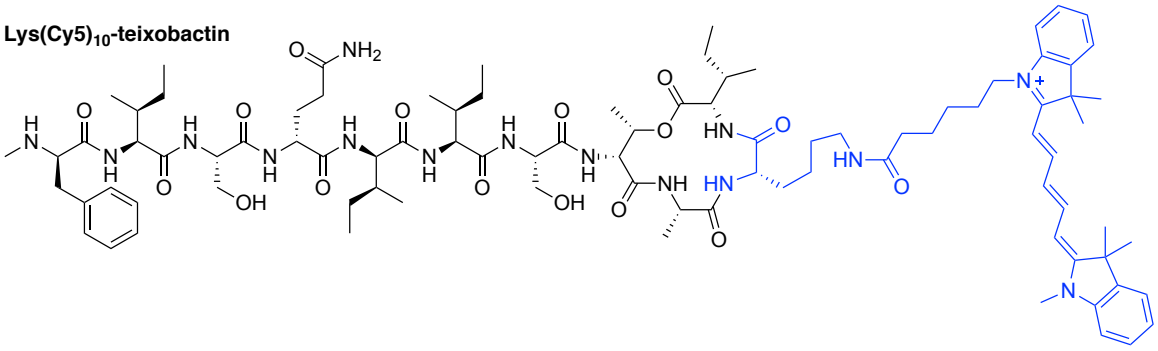

Chemical Formula: $C_{90}H_{134}N_{15}O_{16}^{+}$
Exact Mass: 1681.01

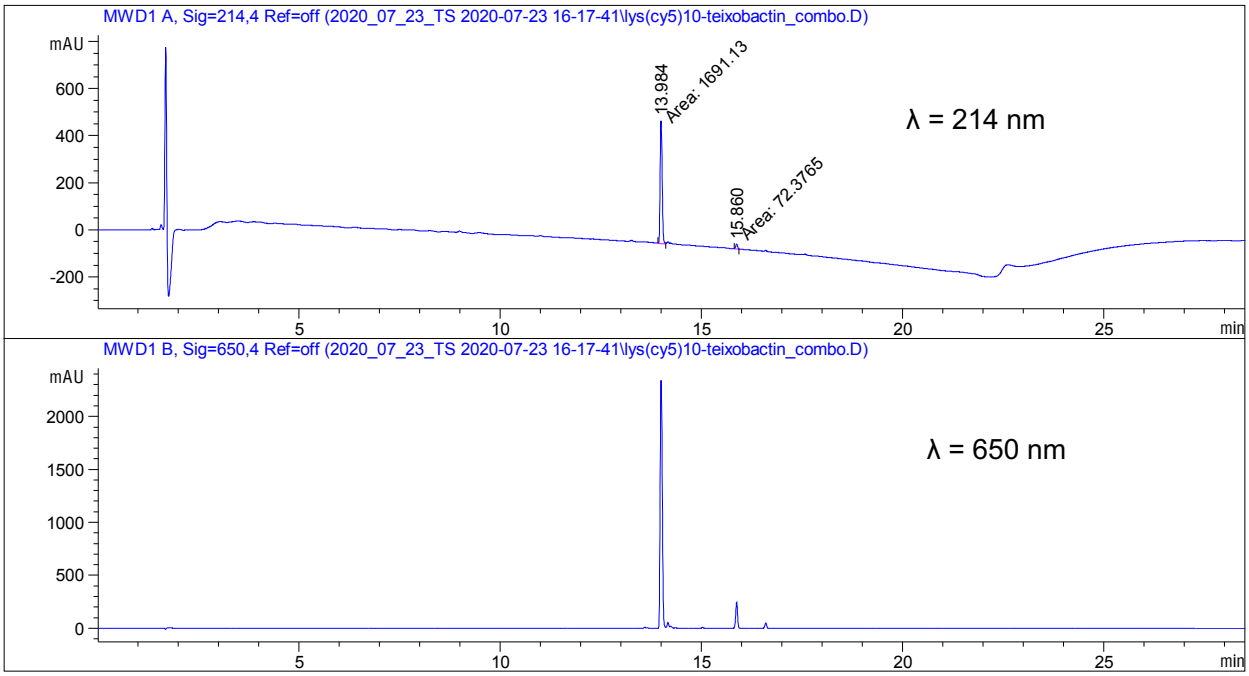

Signal 1: MWD1 A, Sig=214,4 Ref=off

Peak #	RetTime [min]	Type	Width [min]	Area [mAU*s]	Height [mAU]	Area %
1	13.984	MM	0.0536	1691.12512	526.08240	95.8959
2	15.860	MM	0.0540	72.37655	22.33026	4.1041
Totals :				1763.50167	548.41266	

Calculated mass for Lys(Cy5)$_{10}$-teixobactin: $[M+H]^+$ = 1681.01

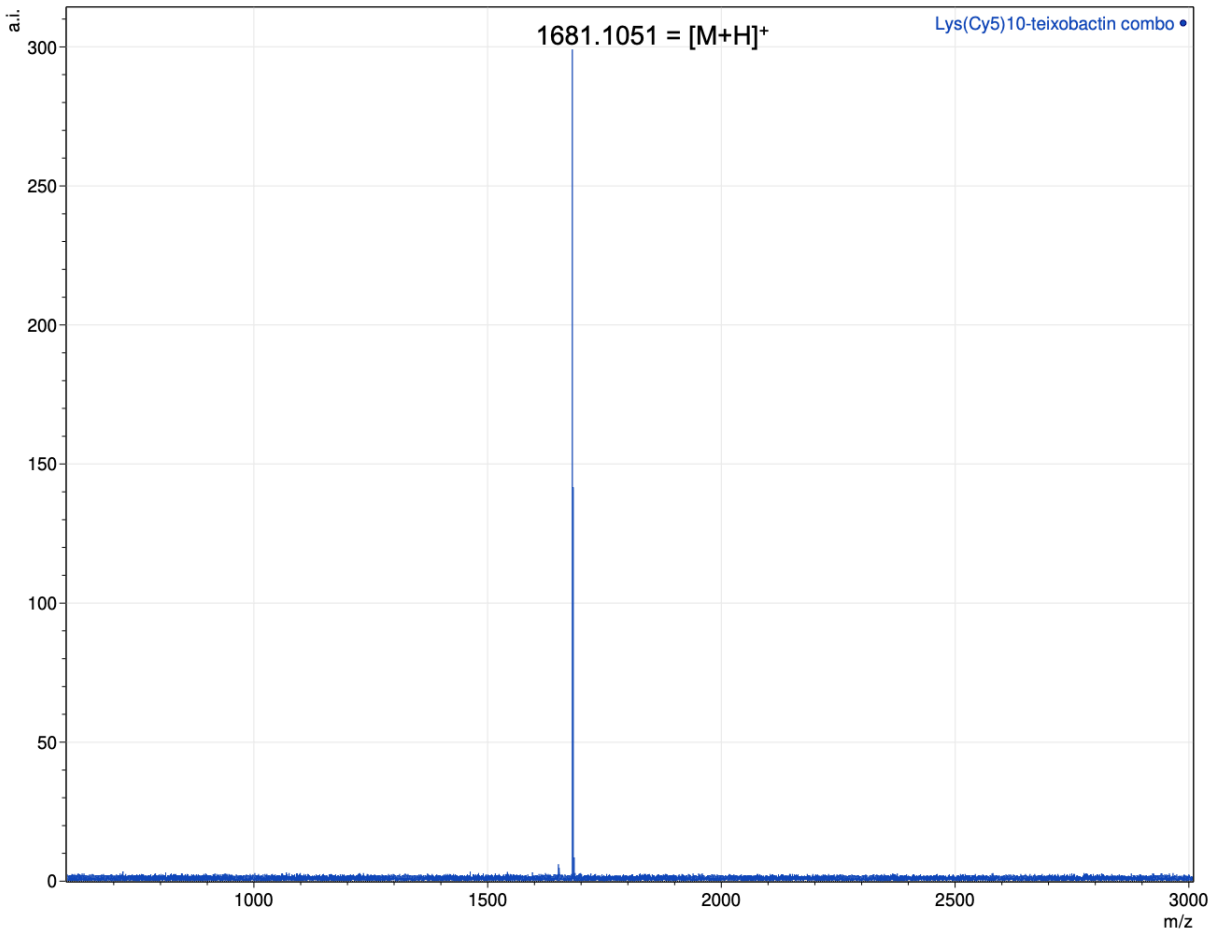

Calculated mass for Lys(Cy5)$_{10}$-teixobactin: [M+H]$^+$ = 1681.01

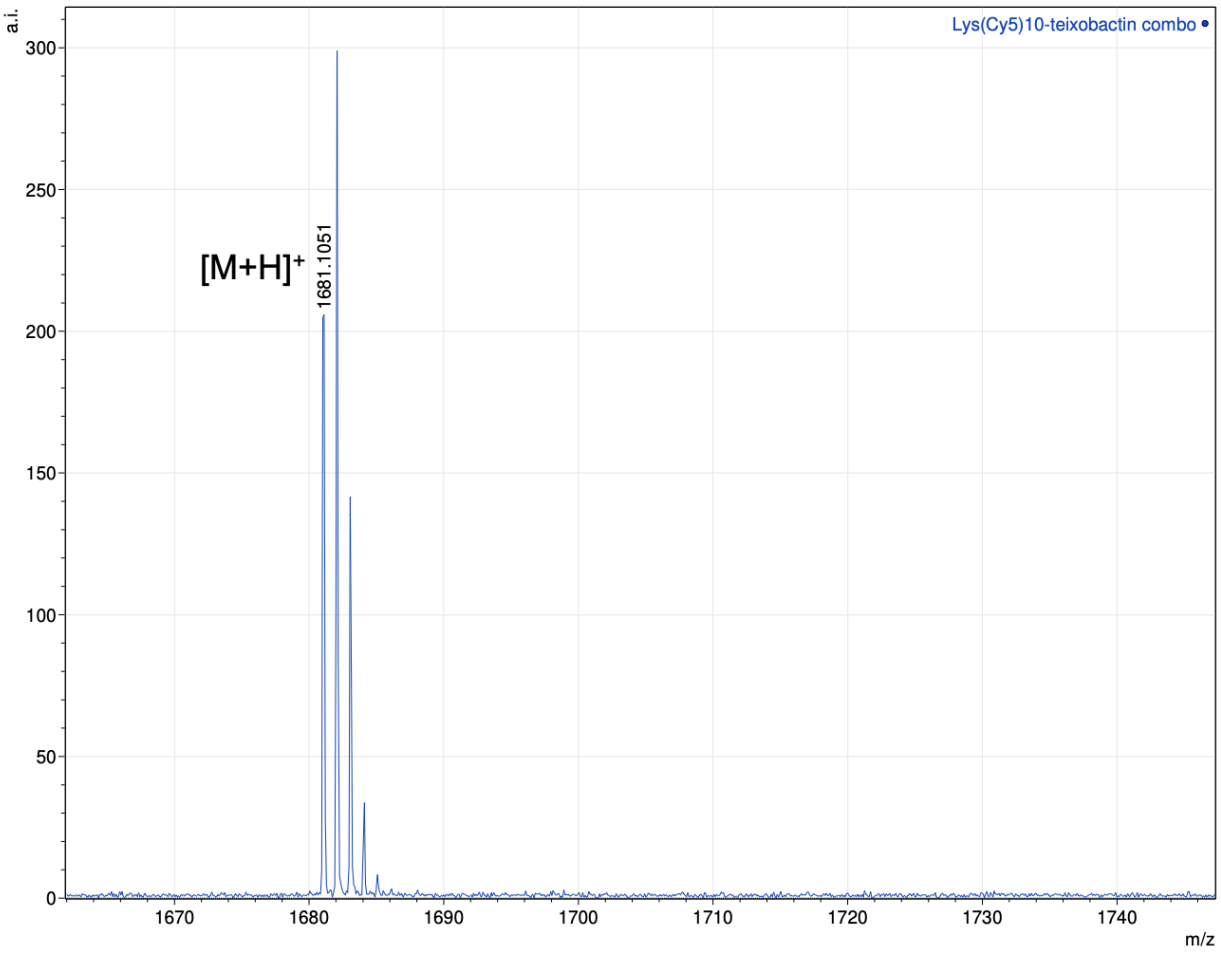

References and notes for Chapter 3 Supporting Information

(1) Yang, H., Chen, K. H., and Nowick, J. S. Elucidation of the Teixobactin Pharmacophore. *ACS Chem. Biol.* **2016**, *11*, 1823−1826.

Chapter 4

Probing the cellular localization of a toxic peptide derived from A$\beta_{15\text{-}36}$

Introduction

In previous chapters, I described syntheses and applications of fluorescent teixobactin analogues to study the mode of action of teixobactin. In this chapter, I transition to describing the synthesis and application of a peptide derived from Aβ, with the goal of understanding how amyloid peptides interact with human neuroblastoma cells.

A hallmark of Alzheimer's disease (AD) is the deposition of senile amyloid plaques resulting from the aggregation of the β-amyloid peptide Aβ.[1-3] During the last two decades, a multitude of studies have shown that Aβ oligomers, but not fibrils, are responsible for the synaptotoxicity and neurodegeneration associated with AD.[4-12] Despite these recent advances that linked neurodegeneration with Aβ oligomers, the mechanism by which Aβ oligomers mediate neurodegeneration is still unclear, where activation of apoptosis, binding to cell-surface receptors, formation of pores in the cellular membrane, or disrupting the structural integrity of the cellular membrane are thought to play a role.[11] Thus, elucidating how soluble Aβ oligomers are neurotoxic is critical for understanding AD pathogenesis, and will advance the development of rationally designed therapeutics to prevent and treat AD.

Peptide mimics derived from amyloidogenic peptides and proteins are useful tools for studying the structural and biological behaviors of amyloidogenic oligomers. By integrating amyloidogenic sequences into a β-hairpin scaffold, it can promote the assembly of well-defined oligomers that can be characterized using spectroscopic methods, including NMR spectroscopy

and X-ray crystallography. In fact, the Nowick lab has pioneered the use of amyloid β-sheet mimics (ABSMs), that contain relevant sequences derived from amyloidogenic peptides and proteins, such as A*β*,[13-17] β_2-microglobulin,[18] and α-synuclein,[19] in a β-hairpin, macrocyclic scaffold in an effort to characterize the structural and biological properties of amyloidogenic oligomers. These ABSMs afforded stable oligomers, which permitted the use of X-ray crystallography to obtain oligomeric structures at atomic-resolution,[13-19] providing insight on how the full-length peptides and proteins may assemble and mediate their toxicity.

One A*β* ABSM of particular interest that our group developed is peptide **1**, which contains key amyloidogenic regions from the central and *C*-terminal regions of the A*β* peptide that have been shown to be important for A*β* oligomerization.[13-17,20] Specifically, peptide **1** incorporates residues 15–21 and 30–36 on the top and bottom strands, respectively, in the ABSM scaffold (Figure 4.1). To enhance β-strand conformation, a δ-linked ornithine ($^{\delta}$Orn) turn unit was utilized to replace the 22–29 loop and to link residues Gln_{15} and Val_{36} in the ABSM. Furthermore, the Phe_{19} residue was replaced with *p*-iodo-phenylalanine (Phe^{I}) in order to utilize single anomalous dispersion (SAD) phasing for X-ray crystallographic analysis. Lastly, a single *N*-methyl-glycine was installed in the bottom strand of the ABSM in order to reduce edge-to-edge hydrogen bonding, thereby preventing the aggregation of an infinite network of β-sheets in solution.

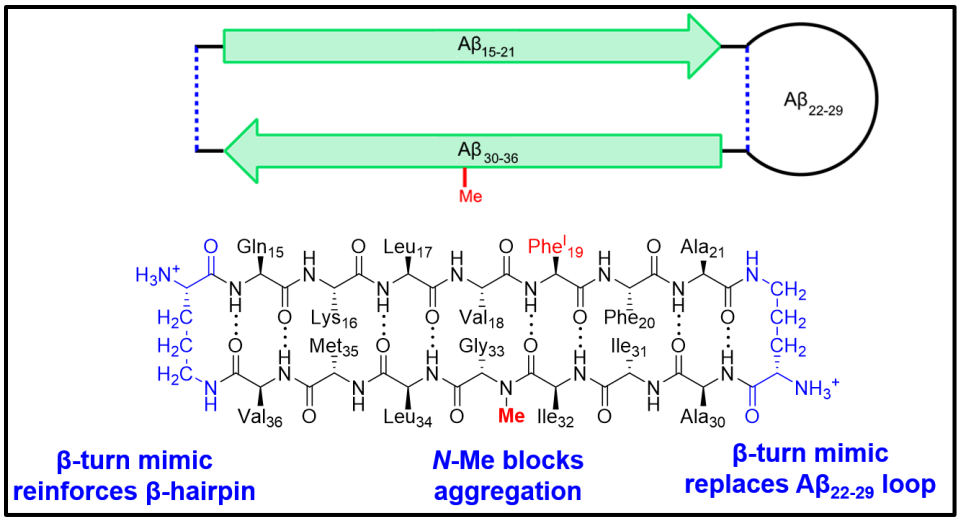

Figure 4.1. Schematic (top) and chemical (bottom) structure of peptide **1**, which is derived from $A\beta_{15\text{-}36}$.

Besides utilizing ABSMs to obtain structural information of A*β* oligomers, our lab has also studied the biological activities of A*β* ABSMs, which could elucidate the molecular mechanisms by which the full length A*β* oligomers elicit neurotoxicity. For example, peptide **1** ($QK_{15\text{-}36}$) was determined to be toxic to human neuroblastoma SH-SY5Y cells at concentrations as low as 25 μM using the lactate dehydrogenase (LDH) release assay (**Figure S4.1**). Thus, it is plausible that peptide **1** may recapitulate similar molecular mechanisms by which the full length A*β* peptide kills neuronal cells.

In my project, I sought to understand how peptide **1** interacts with SH-SY5Y cells in an effort to illuminate the molecular mechanisms behind its toxicity. To do so, I incorporated a fluorescent tag into peptide **1**, hereinafter called peptide **1*** (Figure 4.2, coumarin-$QK_{15\text{-}36}$), and utilized confocal laser scanning microscopy (CLSM) to determine if peptide **1*** exhibits specific localization in SH-SY5Y cells. This is the first time the Nowick lab utilized CLSM to visualize cellular interactions of a toxic ABSM in order to determine a connection between cellular toxicity and localization. Elucidating the localization of peptide **1*** could provide clues into how it is mediating its toxicity and may further expand our understanding of A*β* neurotoxicity.

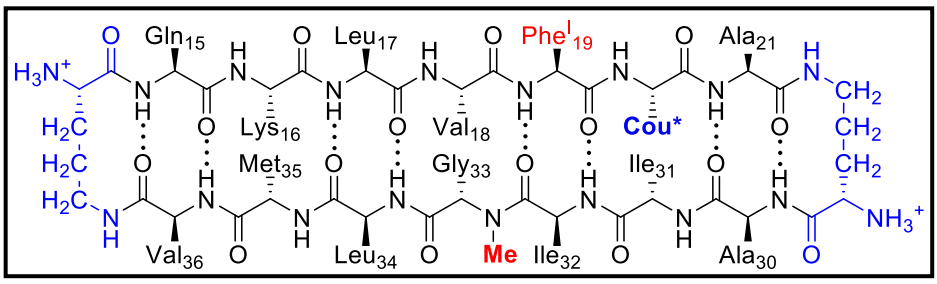

Figure 4.2. Structure of peptide **1*** (coumarin-QK$_{15\text{-}36}$), which contains the Phe20Cou point mutation.

Results and discussion

*Incorporation of fluorescent L-(7-hydroxycoumarin-4-yl) ethyl glycine amino acid in peptide 1**

The L-(7-hydroxycoumarin-4-yl) ethyl glycine (7-HC) amino acid (shown as **2** in Scheme 4.1) is a useful fluorophore that has been utilized to probe the cellular localization, function, and conformation of peptides and proteins.[21,22] Attractive features of the 7-HC amino acid include its high fluorescence quantum yield of 0.63 (in pH 7.4, 100 mM sodium phosphate buffer), relatively large Stoke's shift (**Figure S4.2**), sensitivity to pH, and its non-perturbing small size compared to traditional fluorophores, including GFP, fluorescein, rhodamine, amongst others.[20] Furthermore, Koopmans et al. developed a six-step synthetic route to an orthogonally-protected building block of the 7-HC amino acid that is suitable for solid phase peptide synthesis (SPPS) incorporation, Fmoc-L-7-HC(MOM)-OH (shown as **7** in Scheme 4.1),[22] which possesses the base-labile Fmoc protecting group on the α-amine and an acid-labile methoxymethyl (MOM) ether protecting group on the 7-hydroxy phenol. Following the six-step procedure from Koopmans et al. (Scheme 4.1),[22] the Fmoc-L-7-HC(MOM)-OH amino acid building block **7** was synthesized on a 10 g scale, starting from commercially available Cbz-L-Glu-OBn (shown as **1** in Scheme 4.1) and **7** was obtained in 8% overall yield.

Scheme 4.1. Synthesis of Fmoc-L-7-HC(MOM)-OH (**7**), starting from commercially available *N*-Cbz-L-Glu-*O*Bn **1**. Synthetic route was developed by Koopmans et al.[22]

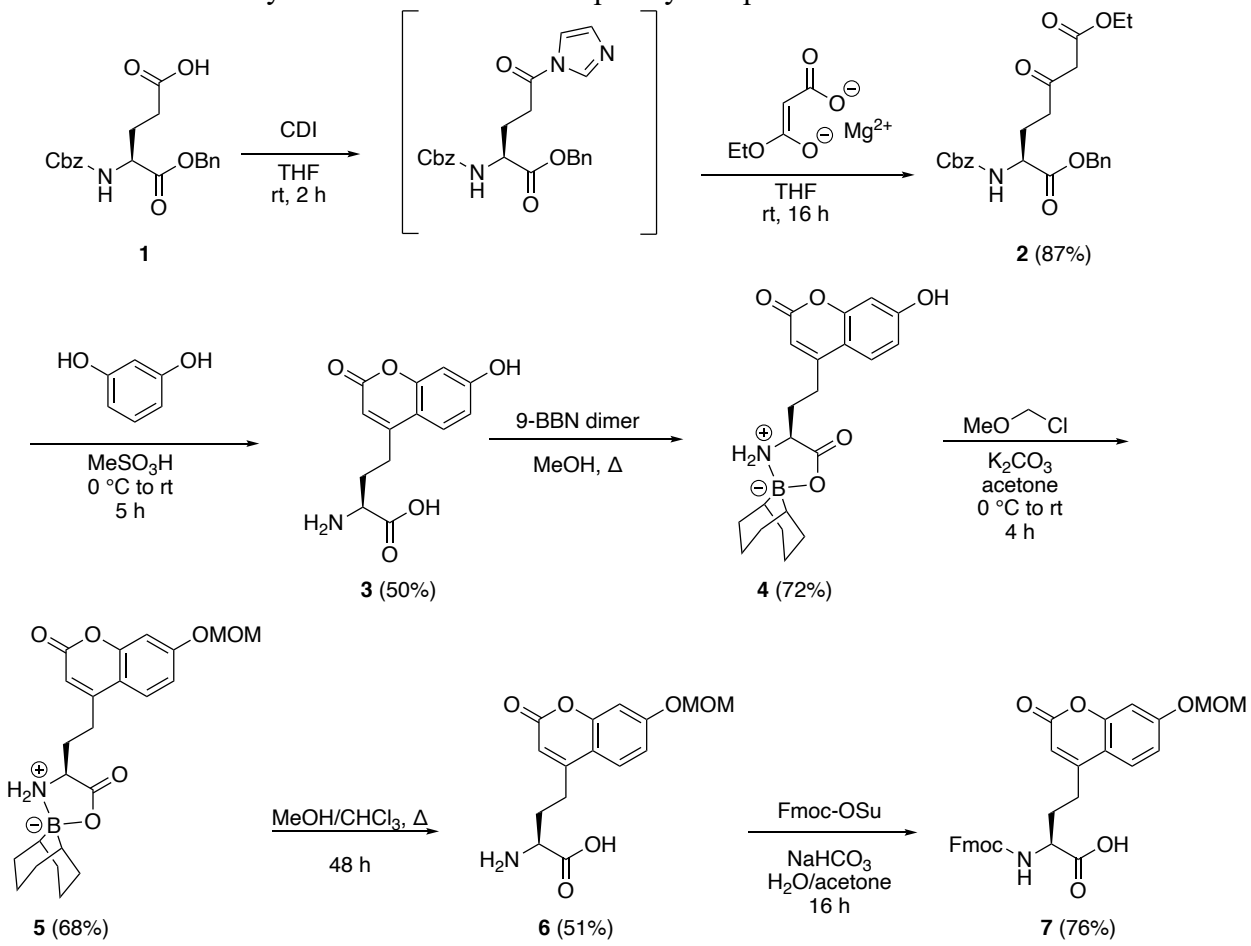

Following the Koopmans et al. protocol, the carboxylic acid side chain of **1** was activated using carbonyldiimidazole (CDI), followed by condensation with ethyl magnesium malonate to form the β-keto-ester **2**. A Pechmann condensation on **2** was executed using excess resorcinol in neat methanesulfonic acid to form the amino acid **3**. The 9-BBN protecting group was subsequently installed at the α-amine and α-carboxylic acid of **3** to form **4**, which permitted the protection of the phenol group using chloromethyl methyl ether to provide the MOM-protected intermediate **5**. Lastly, the 9-BBN moiety was removed using a MeOH/$CHCl_3$ reflux to make **6**, and the α-amine was equipped with the Fmoc protecting group using Fmoc-Osu to form **7**.

The Fmoc-L-7-HC(MOM)-OH amino acid was incorporated into peptide **1*** using standard Fmoc-based SPPS conditions (see Scheme S4.1). Since Phe is the closest resembling amino acid to 7-HC in peptide **1**, the Phe_{20} residue was substituted with 7-HC in peptide **1*** (Figure 4.2). It was hypothesized that the Phe20Cou point mutation was unlikely to perturb the biological activity of the peptide **1*** due to the structural similarity between the Phe and 7-HC amino acids.

Toxicity of peptide 1*

To ensure that the Phe20Cou point mutation in peptide **1*** did not abolish its toxicity to SH-SY5Y cells, an LDH release assay was performed on the peptide (Figure 4.3). As shown by the LDH data, peptide **1*** retained the same levels of relative toxicity as peptide **1** at the same concentrations. Thus, the Phe20Cou point mutation did not significantly perturb the biological activity of peptide **1***, thereby making the peptide suitable for localization experiments using confocal laser scanning microscopy (CLSM).

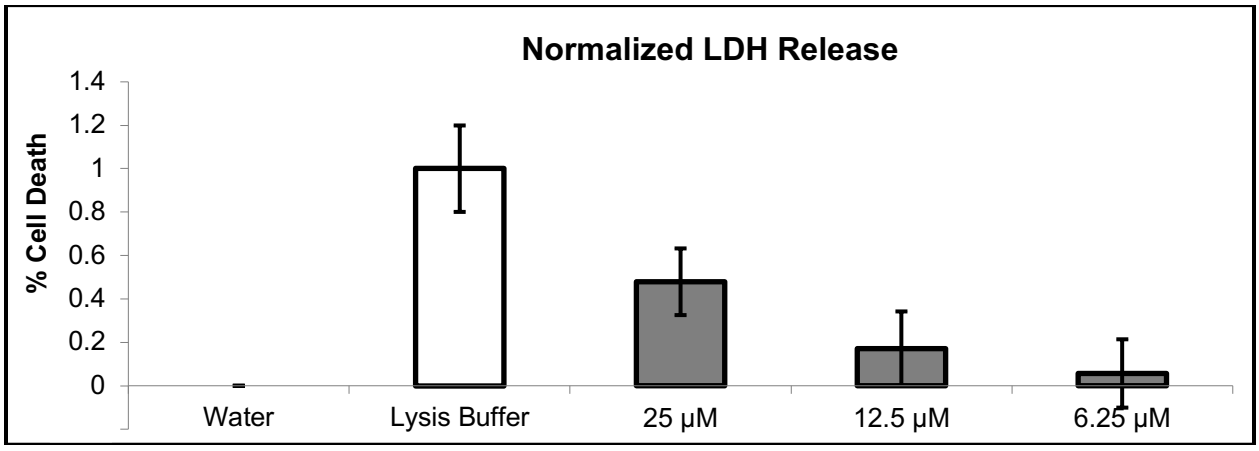

Figure 4.3. LDH release assay of peptide **1*** using SH-SY5Y cells.

Localization studies of peptide 1* on live SH-SY5Y cells

In the first localization experiment, SH-SY5Y cells were treated with 50 μM of peptide **1*** for 2h at 37 °C, and the cells were imaged live, without fixing, using CLSM. Uniform localization to SH-SY5Y cells was observed (Figure 4.4A) and many cells exhibited morphologies consistent with cell death, exhibiting rounded and blebbing membranes. This is the first time the Nowick lab

obtained visual evidence of ABSM peptides directly localizing to SH-SY5Y cells. However, the localization of peptide **1*** to either the cytosol or to the cellular membrane could not be differentiated because the cells were imaged live, where Z-stack imaging analysis could not be used to reliably analyze the peptide's localization. To address this issue, fixation of the cells as well as counterstaining with a membrane-specific fluorophore was required to determine the localization of peptide **1***.

Furthermore, it was important to determine if the observed localization in Figure 4.4A is solely driven by the presence of the 7-HC amino acid in peptide **1*** instead of the entire peptide itself. To answer this question, SH-SY5Y cells were treated with 50 μM of free 7-HC amino acid for 2 h at 37 °C, and the cells were imaged live (no fixation) using CLSM. Upon excitation at 405 nm, no fluorescent emission was detected (Figure 4.4B), which demonstrated that the fluroescent peptide was responsible for interacting with SH-SY5Y cells, and not due to the presence of the 7-HC amino acid. In addition, it is important to note that the cells treated with only the 7-HC amino acid exhibited healthy cellular morphology (Figure 4.4B) whereas the cells treated with peptide 1* were clearly exhibiting morphological signs of cell death (Figure 4.4A).

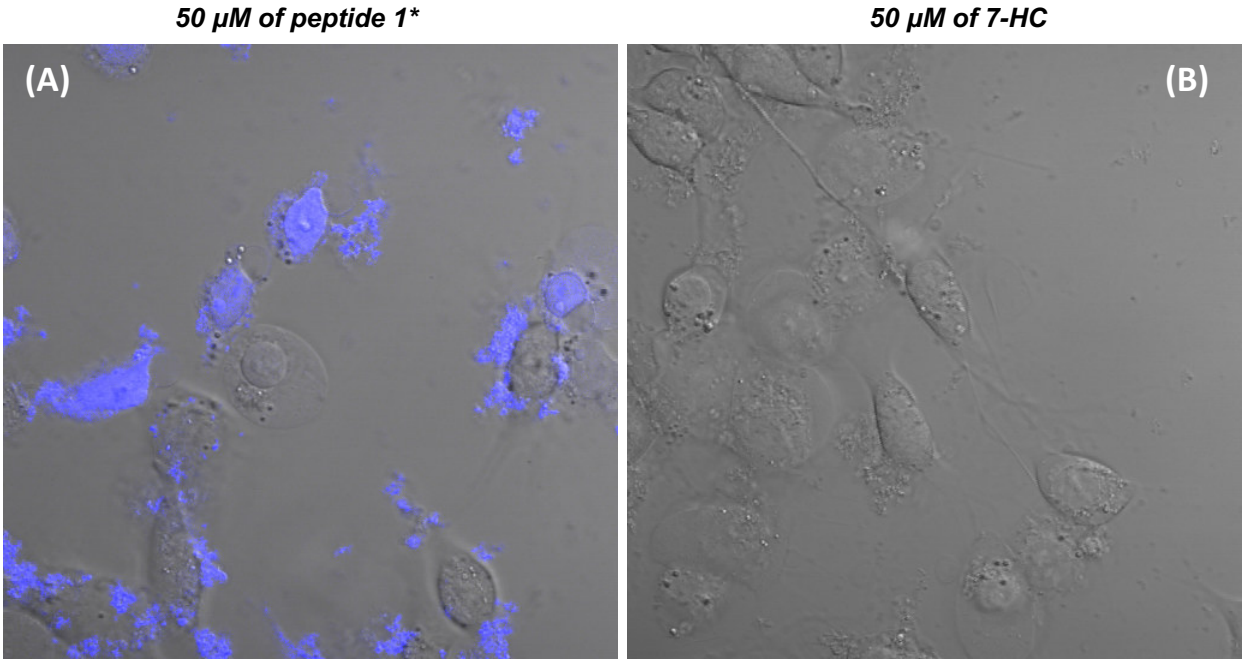

Figure 4.4. **(A)** Micrograph of live SH-SY5Y cells treated with 50 μM peptide **1*** for 2 h. **(B)** Micrograph of live SH-SY5Y cells treated with 50 μM 7-HC amino acid for 2 h. The DIC and 405 nm excitation images were merged using ZEN image analysis software.

Localization studies of peptide 1* in SH-SY5Y cells followed by fixation

In an effort to delineate between cytosol versus cellular membrane localization, another localization experiment was performed. SH-SY5Y cells were treated with 50 μM peptide **1*** for 2 h at 37 °C, followed by fixation with 4% *p*-formaldehyde, and then counterstained with 5 μg/mL of the membrane-specific wheat germ agglutinin (WGA) Alexa Fluor® 488 dye. Uniform localization of peptide **1*** was only observed in the cytosol of SH-SY5Y cells, but not in the cellular membrane (Figure 4.5A), a discrepancy that will need to be investigated. Notably, the membranes of the SH-SY5Y cells appeared to be compromised, as reflected by WGA-stained membrane debris in the extracellular space. This may indicate that peptide 1* perturbs membrane homeostasis in SH-SY5Y cells. In order to confirm the internalization of peptide **1*** in SH-SY5Y cells, a Z-stacking analysis was executed and demonstrated that the peptide primarily localized in the cytosol (Figure S4.6). It is interesting to note that other studies have shown that fluorescent,

oligomeric assemblies of Aβ also internalize into mammalian cells,[23,24] thereby demonstrating that peptide **1*** may be a reliable model of toxic Aβ species. However, it is uncertain how peptide **1*** was internalized into SH-SY5Y cells, with possibilities including self-penetration through the lipid bilayer or endocytosis. Mechanistic experiments, such as endocytosis inhibition, need to be conducted in order to clarify the uptake mechanism of peptide **1***, which could further elucidate how the peptide is mediating toxicity.

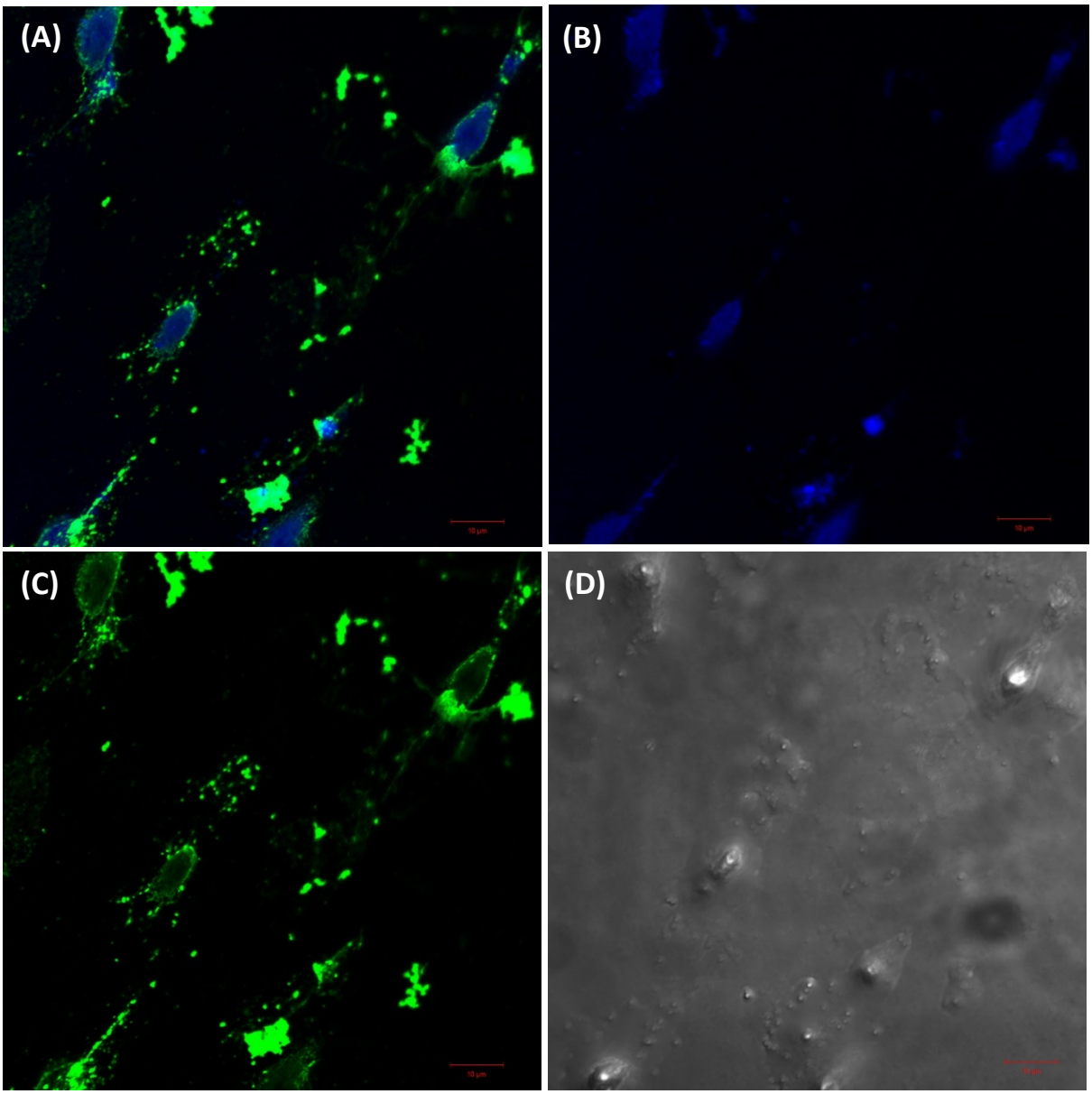

Figure 4.5. Micrograph of fixed SH-SY5Y cells treated with 50 μM peptide **1*** for 2 h and counterstained with 5 μg/mL WGA Alexa Fluor® 488. Expanded images are included in the SI in **Figure S5**. Scale bar: 10 μm. **(A)** Merged 405 and 488 nm excitation images. **(B)** 405 nm excitation only. **(C)** 488 nm excitation only. **(D)** DIC image with no excitation.

The internalization of peptide **1*** in SH-SY5Y cells provides clues into its mechanism of toxicity. Because no localization to the cellular membrane was observed (Figure 4.5A), this suggested that the peptide **1*** did not disrupt cellular membrane integrity (*e.g.*, by generating pores of channels in the membrane), which is one of several proposed hypotheses on how Aβ results in

neurotoxicity.[11,25] Instead of degrading cellular membrane integrity, peptide **1*** most likely disturbed intracellular homeostasis, possibly by initiating apoptosis through a non-membrane activation mechanism, which is another proposed pathway by which Aβ is suspected to cause neurotoxicity.[11,26,27] In order to support this possibility, the caspase-3 activation assay can be utilized to determine if peptide **1*** causes cell death through an apoptotic mechanism.

Conclusions and future directions

In this study, I have reported a fluorescently-tagged ABSM peptide derived from A$\beta_{15\text{-}36}$ that is cytotoxic and is internalized into the cytosol of SH-SY5Y cells. Peptide **1*** exhibited two localization patterns depending on whether the cells were fixed or not. Peptide **1*** appeared to interact with the membranes in the absence of a fixative, whereas the peptide appeared to be internalized in SH-SY5Y cells after fixation. The discrepancy in localization of peptide **1*** needs further investigation to understand how it interacts with SH-SY5Y cells. Thus, the preliminary results described in this report provide a starting ground for understanding how toxic ABSM peptides interact with cells.

Although peptide **1*** has been shown to internalize into SH-SY5Y, further experiments, such as crosslinking the peptide with its targets, need to be done to clarify its toxic behavior. For instance, determining the cellular uptake mechanism of peptide **1*** is important as it can help clarify ways to prevent toxic Aβ species from entering cells. In order to probe the internalization of peptide **1***, SH-SY5Y cells can be treated with an endocytosis inhibitor, such as methyl-β-cyclodextrin, which inhibits both caveolae- and clathrin-dependent endocytosis. The LDH release assay and CLSM can be used to determine cell viability as well as the internalization of peptide **1*** in SH-SY5Y cells. Furthermore, the manner in which peptide **1*** causes cell death needs to be addressed. Because apoptosis is a suggested mechanism for Aβ-induced toxicity, the caspase-3

assay, can be used to establish if peptide **1*** is involved in apoptotic initiation. Lastly, the Nowick lab has developed a number of ABSM peptides, some of which are derived from β_2-microglobulin[18] and α-synuclein,[19] that are toxic to SH-SY5Y cells. The incorporation of a fluorophore, such as the 7-HC amino acid, into these toxic peptides for localization studies would possibly illuminate toxicity mechanisms for these peptides.

References

(1) Annaert, W.; De Strooper, B. A Cell Biological Perspective on Alzheimer's Disease. *Annu. Rev. Cell Dev. Biol*. **2002**, *18*, 25–51.

(2) Hutton, M.; Perez-Tur, J.; Hardy, J. *Essays Biochem*. **1998,** *33*, 117–131.

(3) Taylor, J. P.; Hardy, J.; Fischbeck, K. H. The Amyloid Hypothesis of Alzheimer's Disease: Progress and Problems on the Road to Therapeutics. *Science* **2002**, *296*, 1991–1995.

(4) Kayed, R.; Head, E.; Thompson, J. L.; McIntire, T. M.; Milton, S. C.; Cotman, C. W.; Glabe, C. G. Common Structure of Soluble Amyloid Oligomers Implies Common Mechanism of Pathogenesis. *Science* **2003**, *300*, 486−489.

(5) Haass, C.; Selkoe, D. J. Soluble Protein Oligomers in Neurodegeneration: Lessons from the Alzheimer's Amyloid Beta-Peptide. *Nat. Rev. Mol. Cell Biol*. **2007**, *8*, 101−112.

(6) Walsh, D. M.; Selkoe, D. J. *J.* A Beta Oligomers - A Decade Of Discovery. *Neurochem.* **2007**, *101*, 1172−1184.

(7) Selkoe, D. J. Soluble Oligomers Of The Amyloid Beta-Protein Impair Synaptic Plasticity And Behavior. *Behav. Brain Res*. **2008**, *192*, 106−113.

(8) Glabe, C. G. Structural Classification Of Toxic Amyloid Oligomers. *J. Biol. Chem*. **2008**, *283*, 29639−29643.

(9) Kayed, R.; Canto, I.; Breydo, L.; Rasool, S.; Lukacsovich, T.; Wu, J.; Albay, R., III; Pensalfini, P.; Yeung, S.; Head, E.; Marsh, J. L.; Glabe, C. Conformation Dependent Monoclonal Antibodies Distinguish Different Replicating Strains Or Conformers Of Prefibrillar Aβ Oligomers. *Mol. Neurodegener*. **2010**, *5*, 1−10.

(10) Fändrich, M. Oligomeric Intermediates In Amyloid Formation: Structure Determination And Mechanisms Of Toxicity. *J. Mol. Biol*. **2012**, *421*, 427−440.

(11) Benilova, I.; Karran, E.; De Stooper, B. The Toxic Aβ Oligomer And Alzheimer's Disease: An Emperor In Need Of Clothes. *Nat. Neurosci*. **2012**, *15*, 349−357.

(12) Nussbaum, J. M.; Schilling, S.; Cynis, H.; Silva, A.; Swanson, E.; Wangsanut, T.; Tayler, K.; Wiltgen, B.; Hatami, A.; Rönicke, R.; Reymann, K.; Hutter-Paier, B.; Alexandru, A.; Jagla, W.; Graubner, S.; Glabe, C. G.; Demuth, H.-U.; Bloom, G. S. Prion-Like Behavior and Tau-dependent Cytotoxicity of Pyroglutamylated β-Amyloid. *Nature* **2012**, *485*, 651−655.

(13) Cheng, P. N.; Liu, C.; Zhao, M.; Eisenberg, D.; Nowick, J. S. Amyloid β-Sheet Mimics that Antagonize Amyloid Aggregation and Reduce Amyloid Toxicity. *Nat. Chem*. **2012**, *4*, 927–933.

(14) Pham, J. D.; Chim, N.; Goulding, C. W.; Nowick, J. S. Structures of Oligomers of a Peptide from β-Amyloid. *J. Am. Chem. Soc*. **2013**, *135*, 12460–12467.

(15) Spencer, R.; Li, H.; Nowick, J. S. X-ray Crystallographic Structures of Trimers and Higher-Order Oligomeric Assemblies of a Peptide Derived from Aβ17–36. *J. Am. Chem. Soc*. **2014**, *136*, 5595–5598.

(16) Pham, J. D.; Spencer, R. K.; Chen, K. H.; Nowick, J. S. A Fibril-like Assembly of Oligomers of a Peptide Derived from β-Amyloid. *J. Am. Chem. Soc*. **2014**, *136*, 12682–12690.

(17) Kreutzer, A. G.; Hamza, I. L.; Spencer, R. K.; Nowick, J. S. X-ray Crystallographic Structures of a Trimer, Dodecamer, and Annular Pore Formed by an Aβ17-36 β-Hairpin. *J. Am. Chem. Soc*. **2016**, *138*, 4634–4642.

(18) Spencer, R. K.; Kreutzer, A. G.; Salveson, P. J.; Li, H.; Nowick, J. S. X-ray Crystallographic Structures of Oligomers of Peptides Derived from β2-Microglobulin. *J. Am. Chem. Soc*. **2015**, *137*, 6304–6311.

(19) Salveson, P. J.; Spencer, R. K.; Nowick, J. S. X-Ray Crystallographic Structure Of Oligomers Formed By A Toxic B-Hairpin Derived From A-Synuclein: Trimers And Higher-Order Oligomers. *J. Am. Chem. Soc*. **2016**, *138*, 4458–4467.

(20) Hoyer, W.; Grönwall, C.; Jonsson, A.; Ståhl, S.; Härd, T. *Proc. Natl. Acad. Sci. U. S. A.* **2008**, *105*, 5099–5104.

(21) Wang, J.; Xie, J.; Schultz, P. G. A Genetically Encoded Fluorescent Amino Acid. *J. Am. Chem. Soc*. **2006**, *128*, 8738–8739.

(22) Koopmans, T.; van Haren, M.; Quarles van Ufford, L.; Beekman, J. M.; Martin, N. I. A Concise Preparation Of The Fluorescent Amino Acid L-(7-Hydroxycoumarin-4-yl) Ethylglycine And Extension Of Its Utility In Solid Phase Peptide Synthesis. *Bioorg. Med. Chem.* **2013**, *21*, 553–559.

(23) Chafekar, S. M.; Baas, F.; Scheper W. Oligomer-Specific Abeta Toxicity In Cell Models Is Mediated By Selective Uptake. *Biochim Biophys Acta*. **2008**, *1782*, 523–531.

(24) Jungbauer, L. M.; Yu, C.; Laxton, K. J.; LaDu, M. J. Preparation Of Fluorescently-Labeled Amyloid-Beta Peptide Assemblies: The Effect Of Fluorophore Conjugation On Structure And Function. *J Mol Recognit*. **2009**, *22*, 403–413.

(25) Lashuel, H.A.; Hartley, D.; Petre, B.M.; Walz, T.; Lansbury, P. T. Jr. Amyloid Pores From Pathogenic Mutations. *Nature* **2002**, *418*, 219.

(26) Loo, D.T.; Copani, A.; Pike, C. J.; Whittemore, E. R.; Walencewicz, A. J.; Cotman, C. W. Apoptosis Is Induced By Beta-Amyloid In Cultured Central Nervous System Neurons. *Proc. Natl. Acad. Sci. U. S. A.* **1993**, *90*, 7951–7955.

(27) Nakagawa, T.; Zhu, H.; Morishima, N.; Li, E.; Xu, J.; Yankner, B. A.; Yuan, J. Caspase-12 Mediates Endoplasmic-Reticulum-Specific Apoptosis And Cytotoxicity By Amyloid-Beta. *Nature* **2000**, *403*, 98–103.

Chapter 4 Supporting Information

Table of Contents

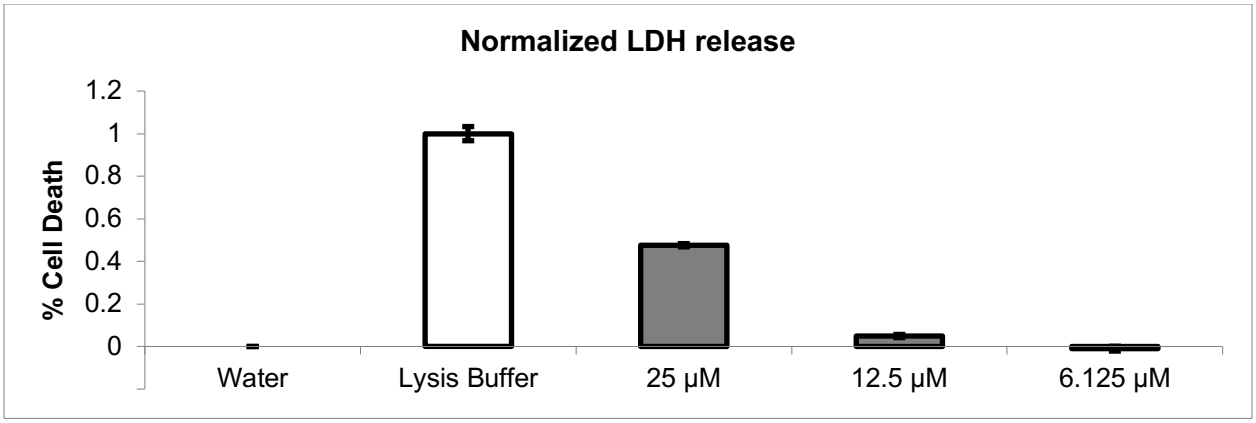

Figure S4.1. LDH release assay of peptide **1** with SH-SY5Y cells. Data courtesy of Dr. Adam Kreutzer.

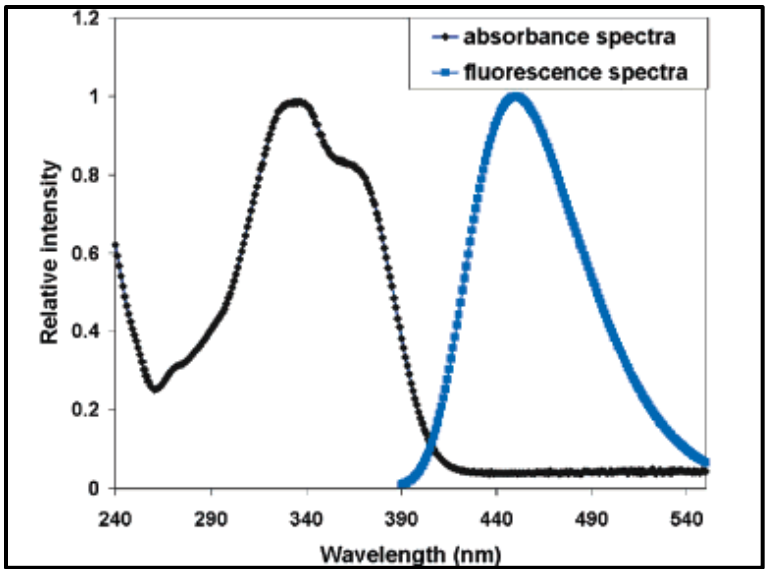

Figure S4.2. Excitation and emission spectra of the 7-HC amino acid in pH 7.4, 100 mM sodium phosphate buffer. The phenolate form of the amino acid has an extinction coefficient of 17,000 cm^{-1} M^{-1} and a quantum yield of 0.63. Image and data were obtained from Wang et al.[1]

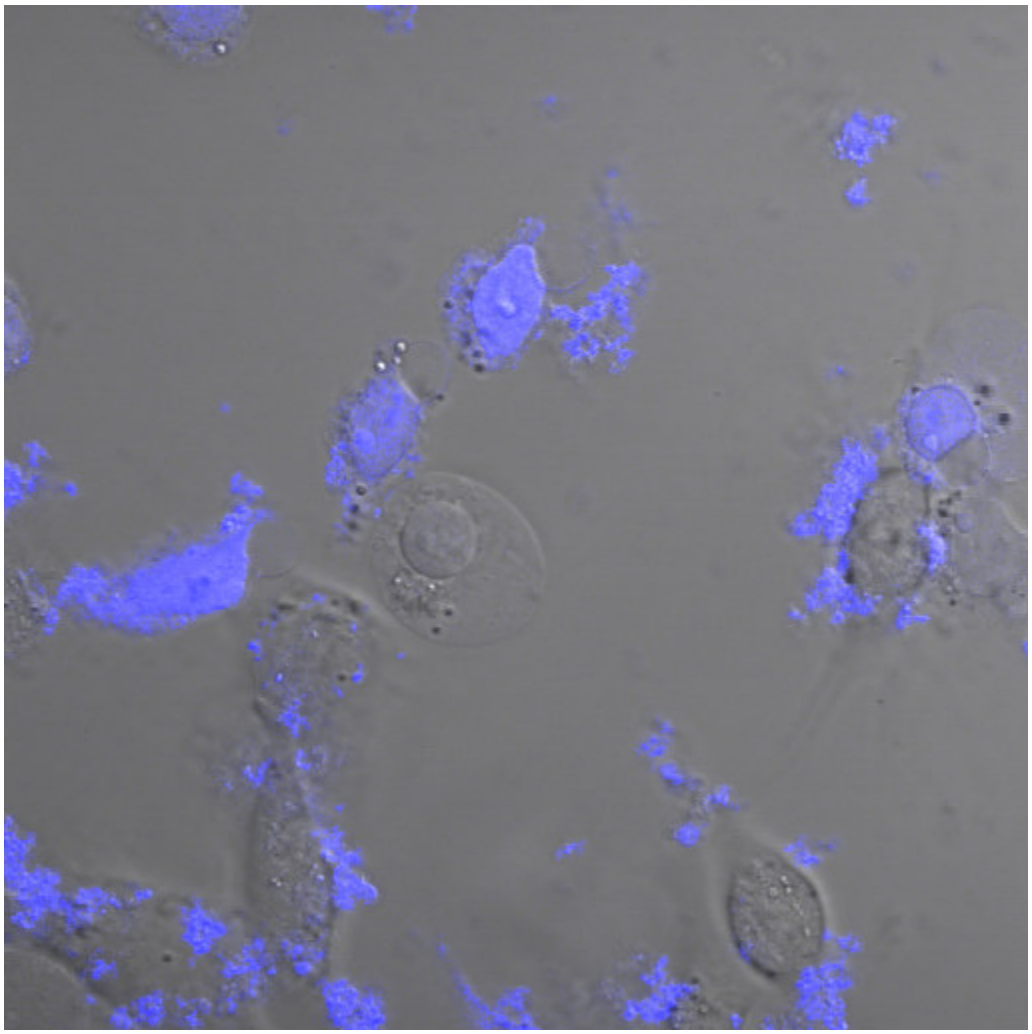

Figure S4.3. Micrograph of live SH-SY5Y cells treated with 50 μM peptide **1*** for 2 h. The cells were imaged live using the Zeiss LSM700 confocal laser scanning microscope. The DIC and 405 nm excitation images were merged using ZEN image analysis software.

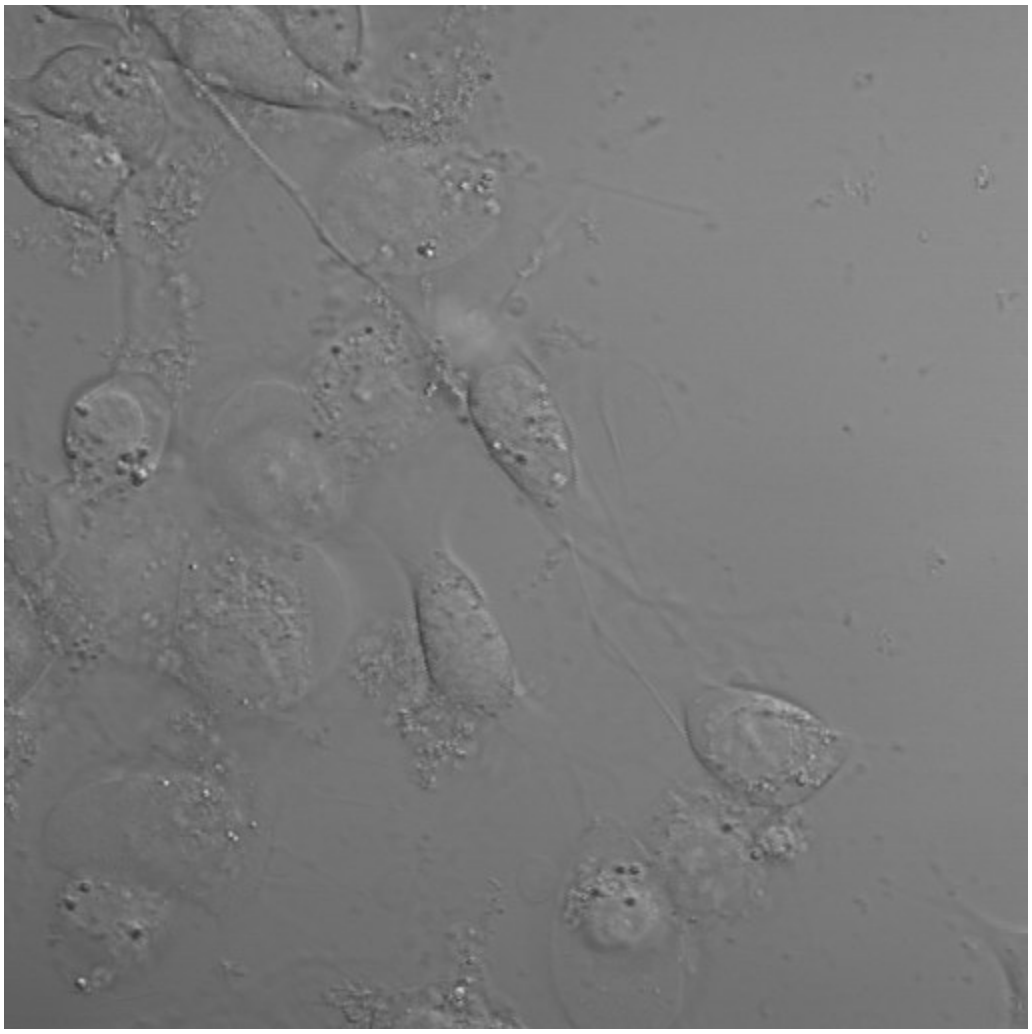

Figure S4.4. Micrograph of live SH-SY5Y cells treated with 50 μM 7-HC amino acid for 2 h. The cells were imaged live using the Zeiss LSM700 confocal laser scanning microscope. The DIC and 405 nm excitation images were merged using ZEN image analysis software.

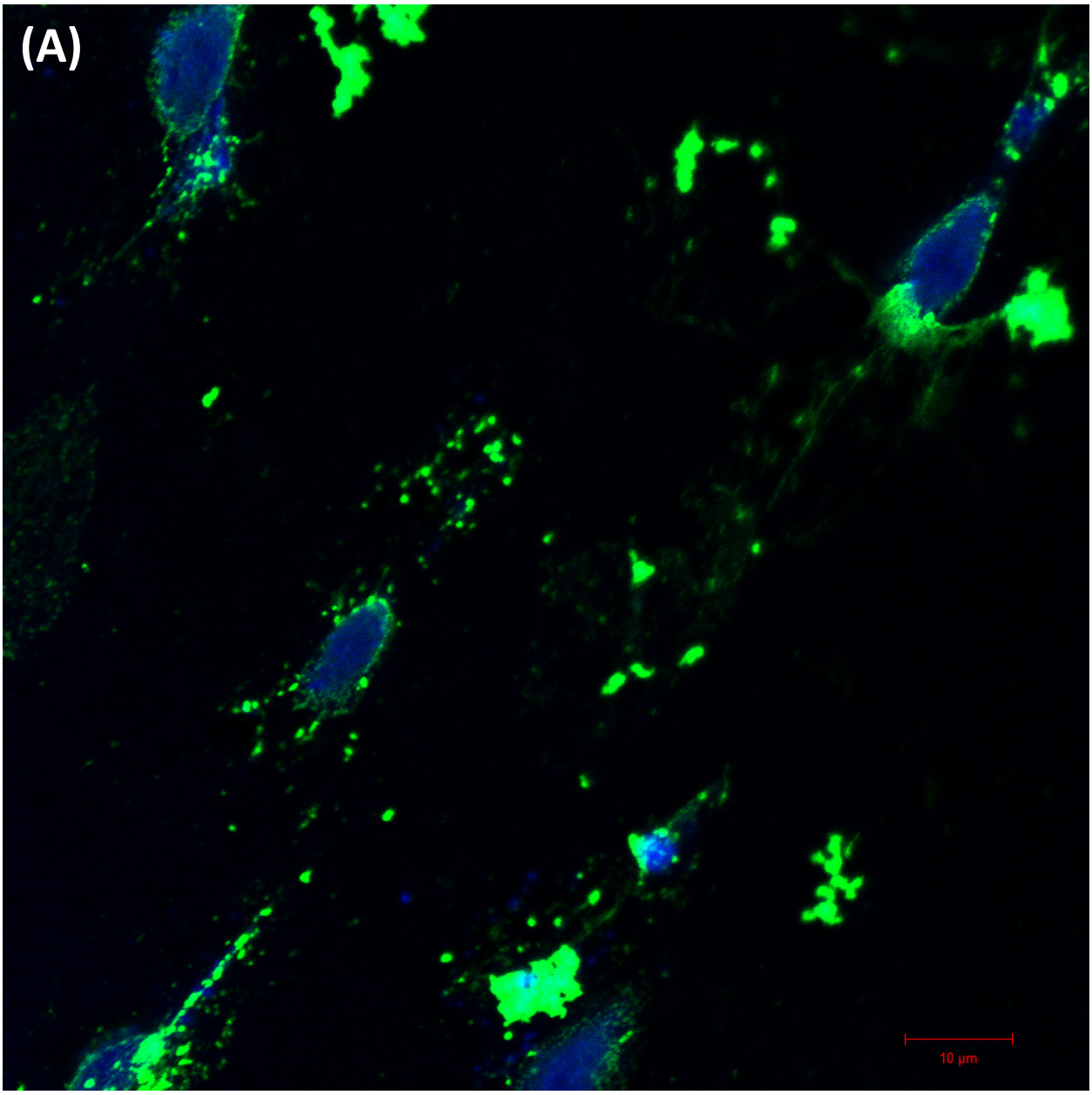

Figure S4.5A. Micrograph of fixed SH-SY5Y cells treated with 50 µM peptide **1*** for 2 h and counterstained with 5 µg/mL WGA Alexa Fluor® 488. The fixed cells were imaged using the Zeiss LSM700 confocal laser scanning microscope, with excitation at 405 and 488 nm. Scale bar: 10 µm. **(A)** Merged 405 and 488 nm excitation images.

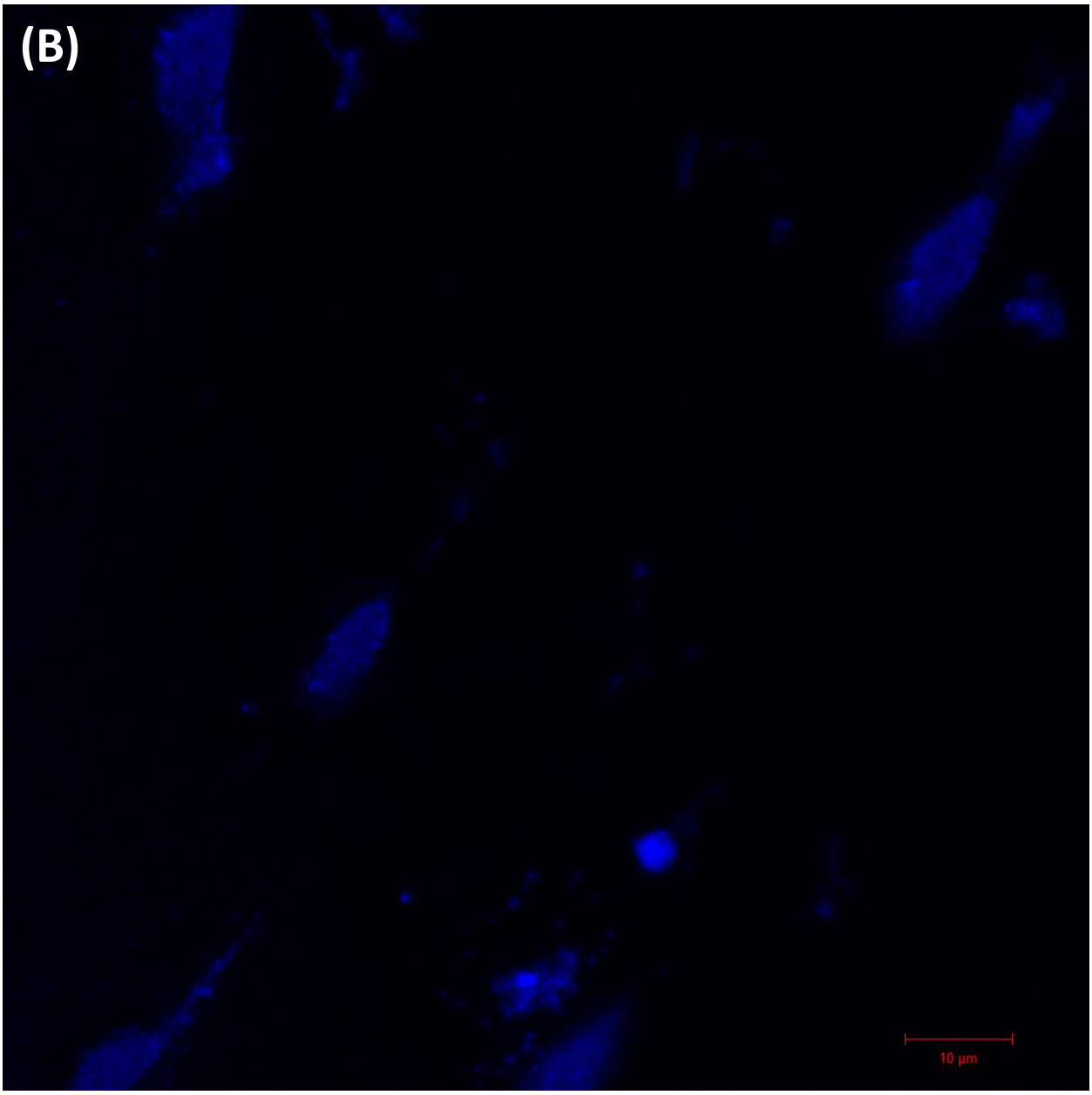

Figure S4.5B. Micrograph of fixed SH-SY5Y cells treated with 50 µM peptide **1*** for 2 h and counterstained with 5 µg/mL WGA Alexa Fluor® 488. The fixed cells were imaged using the Zeiss LSM700 confocal laser scanning microscope. Scale bar: 10 µm. **(B)** 405 nm excitation only.

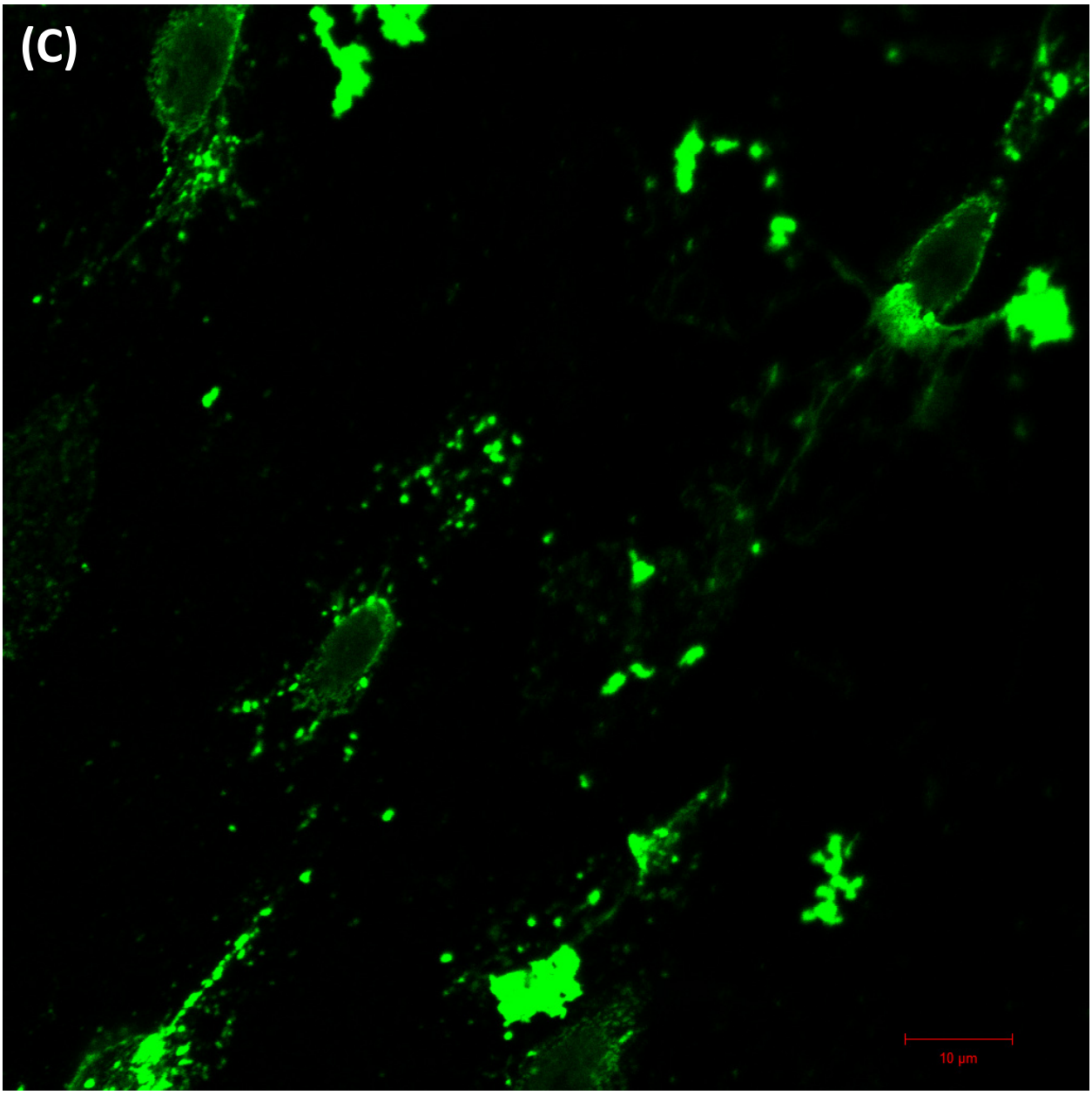

Figure S4.5C. Micrograph of fixed SH-SY5Y cells treated with 50 µM peptide **1*** for 2 h and counterstained with 5 µg/mL WGA Alexa Fluor® 488. The fixed cells were imaged using the Zeiss LSM700 confocal laser scanning microscope. Scale bar: 10 µm. **(C)** 488 nm excitation only.

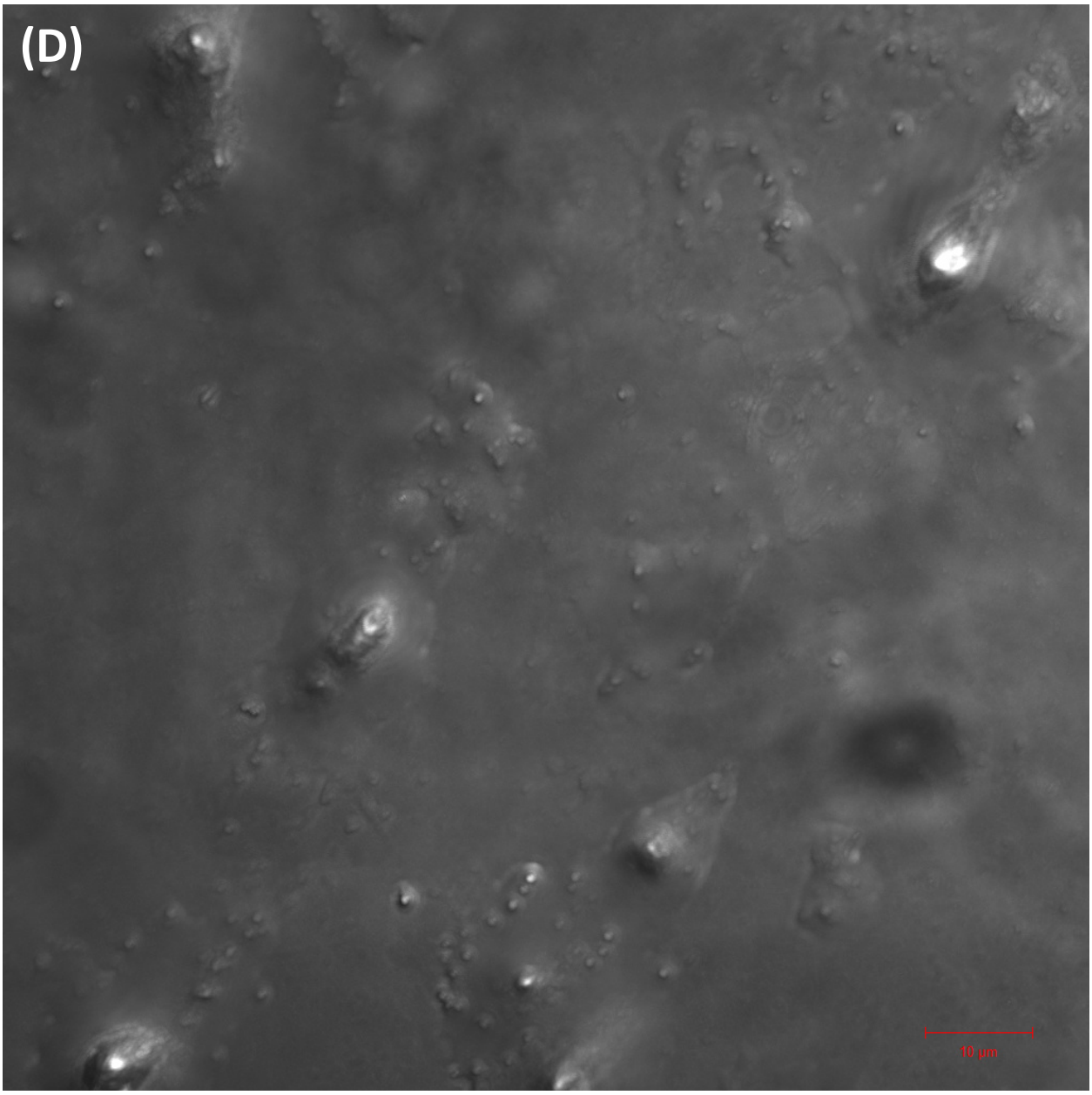

Figure S4.5A. Micrograph of fixed SH-SY5Y cells treated with 50 µM peptide **1*** for 2 h and counterstained with 5 µg/mL WGA Alexa Fluor® 488. The fixed cells were imaged using the Zeiss LSM700 confocal laser scanning microscope. Scale bar: 10 µm. **(D)** DIC image with no excitation.

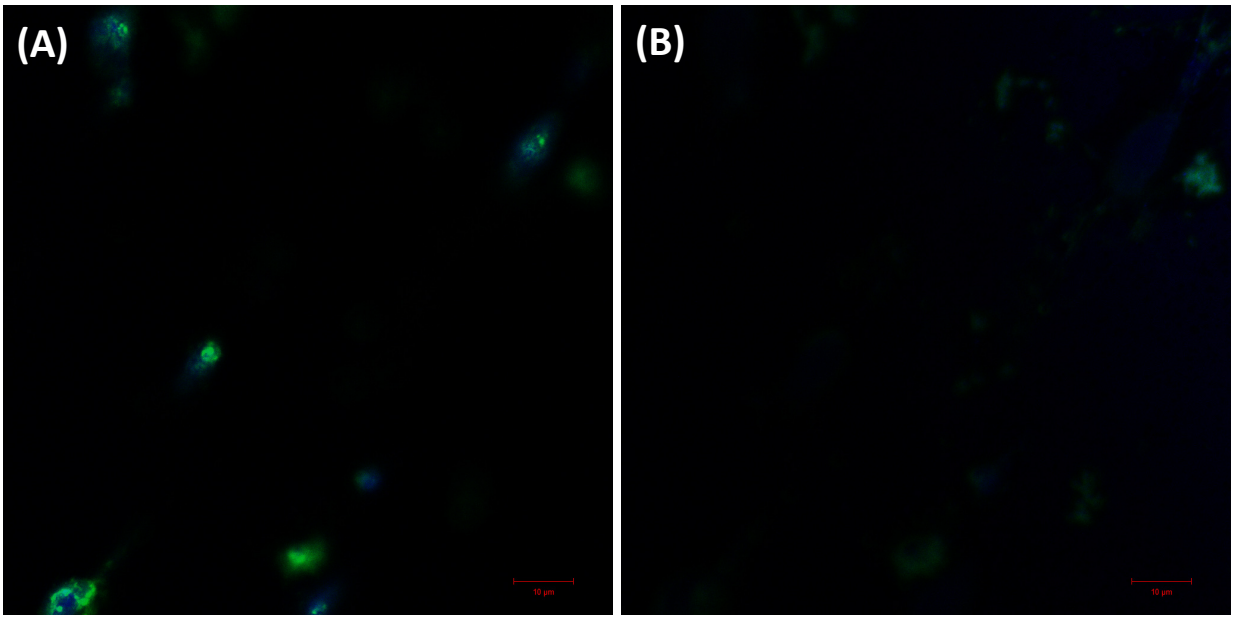

Figure S4.6. The Z-stacking analysis of Figure S5 using a displacement range from 0 to 4 µm. Scale bar: 10 µm **(A)** Lowest level Z-stack image showing the lowest depth of SH-SY5Y cells (0 µm). **(B)** Highest level Z-stack image showing the highest depth of SH-SY5Y cells (4 µm).

Scheme S4.1. Synthesis of peptide **1***.

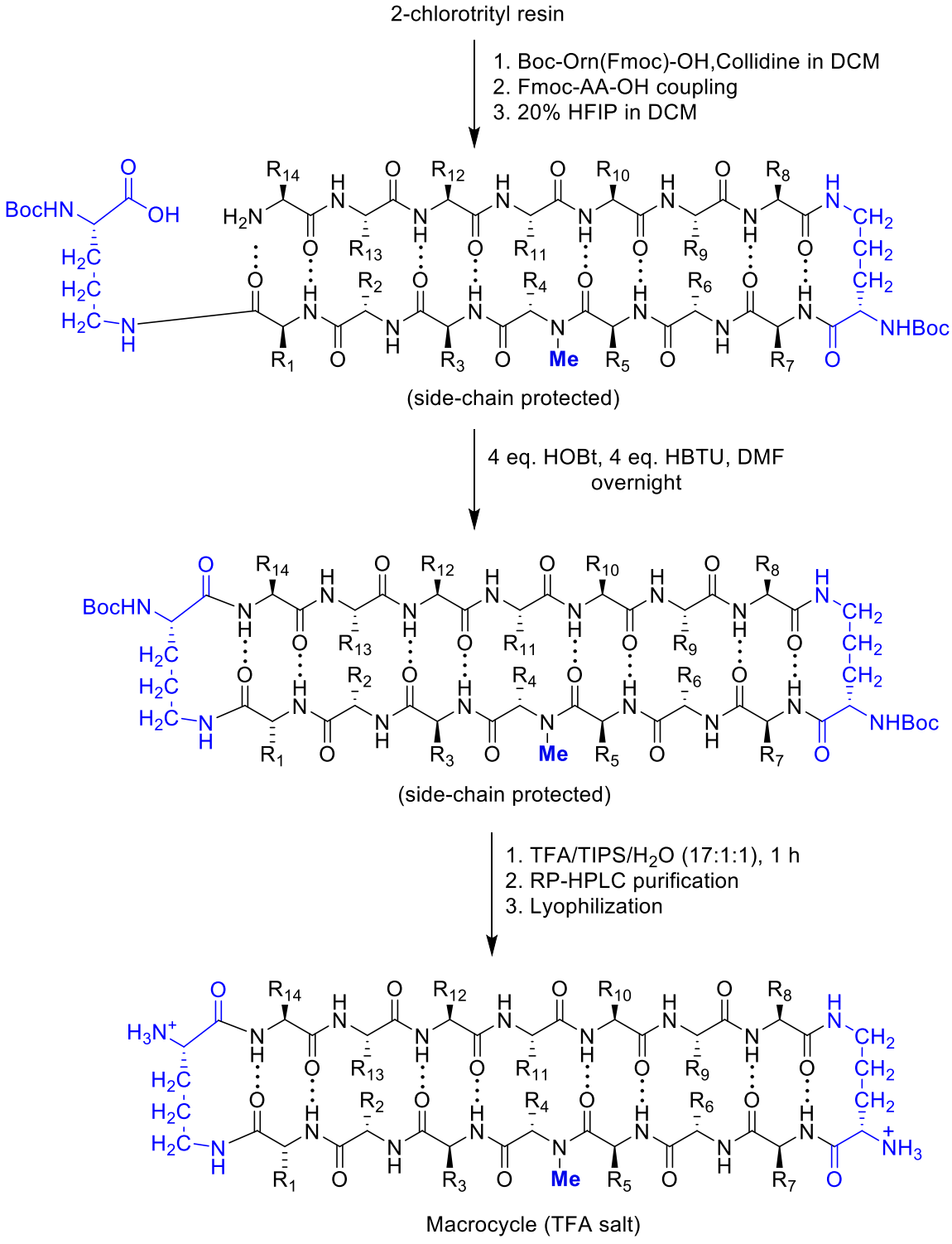

Materials and Methods:

All solvents, chemicals, and resins were used as received, except for dichloromethane (DCM), *N,N*-dimethyformamide (DMF), and diethyl ether, which were dried by passage through an alumina column under argon. Solid phase peptide synthesis was performed on either a PS3 Synthesizer (Protein Technologies, Inc.) or a Liberty One Microwave Peptide Synthesizer (CEM). Reverse phase analytical HPLC was performed on the Agilent A1200 HPLC instrument. Semi-preparative HPLC was performed on a Beckman Gold Series 126/166P instrument.

Synthesis of 7-hydroxycoumarin amino acid for solid phase peptide synthesis incorporation:

The (*S*)-2-(((9*H*-Fluoren-9-yl)methoxy)carbonylamino)-4-(7-(methoxymethoxy)-2-oxo-2*H*-chromen-4-yl)butanoic acid (i.e., Fmoc-L-7-HC(MOM)-OH) amino acid was synthesized according to a published six-step route by Koopmans et al.[2] The obtained overall yield was 8% over six steps on a 10 g scale. The Fmoc-L-7-HC(MOM)-OH was incorporated into peptide **1*** by using solid phase peptide synthesis, as described below.

General procedure for the synthesis of peptide macrocycles:

Loading resin:

2-Chlorotrityl chloride resin (300 mg, 1.2 g/mmol maximum loading) was added to a Bio-Rad Poly-Prep® column, and was allowed to swell for 30 minutes in DCM. After draining the DCM, a solution of Boc-Orn(Fmoc)-OH (0.5 eq., 80 mg, 0.18 mmol) with 0.3 mL of 2,4,6-collidine in DCM was added to the resin. The suspension was agitated overnight. The loading solution was then drained and a solution of DCM/MeOH/DIPEA (17:2:1) was added to the resin. The suspension was agitated for 1 h in order to cap unreacted sites in the resin. The solution was drained and the resin was washed with DCM and then dried using N_2 gas. Resin loading was verified by Fmoc-deprotecting 1 mg of loaded resin using 3 mL of a 20% piperdine in DMF

solution and performing a UV analysis of the Fmoc-deprotection product. Normally 0.30 – 0.40 mmol/g of Boc-Orn(Fmoc)-OH was loaded (60-70% loading).

Solid phase peptide synthesis:

The loaded resin was transferred into a sold-phase peptide synthesizer reaction vessel and was submitted to automated cycles of Fmoc-deprotection and amino acid coupling using Fmoc-protected amino acids. All peptides were synthesized from the *C*-terminus to *N*-terminus. Each coupling step consisted of the following: **(1)** Fmoc-deprotection with 20% piperdine in DMF for 10 minutes; **(2)** resin washing with 3 mL of DMF (3x); **(3)** amino acid coupling using 4 eq. of both the Fmoc-AA-OH amino acid and HCTU in 20% 2,4,6-collidine in DMF for 20 mins. After amino acid coupling was complete, a final Fmoc-deprotection was performed to cleave the terminal Fmoc, and the resin was transferred to a Bio-Rad Poly-Prep® chromatography column.

Cleavage of the linear protected peptide from resin:

In order to cleave the peptide from the resin without deprotecting any side-chain protecting groups, 10 mL of 20% hexafluoroisopropanol (HFIP) in DCM was added to the resin and was agitated for 1 h. The cleaved-peptide solution was filtered into a 250-mL round bottom flask. An additional 10 mL of the 20% HFIP solution was passed through the resin, and collected into the round bottom flask. The combined filtrates were concentrated *in-vacuo* to afford a white solid, and this solid was further dried under high-vacuum overnight.

Peptide cyclization:

The crude, linear, protected peptide was dissolved in 125 mL of anhydrous DMF, and 4 eq. of both HOBt and HBTU were added to the solution. After 30 min of stirring under N_2, 1 mL of *N*-methylmorpholine was added, and the reaction mixture was stirred for 24 h at room temperature. The solvent was removed *in-vacuo* to afford a yellow/orange solid of the cyclized,

crude peptide. This solid was further dried under high-vacuum overnight to remove any residual DMF.

Global deprotection:

The crude, protected macrocycle was dissolved in a 10 mL solution of TFA/TIPS/H_2O (17:1:1) and stirred for 1 h. The solvent was concentrated *in-vacuo* to afford the crude deprotected peptide as a yellow/orange oil.

Reverse phase semi-preparative HPLC purification:

The deprotected peptide was dissolved in 9 mL of 20% acetonitrile in water, and the solution was centrifuged at 3,300 RPM for 5 min. The supernatant was collected and then filtered with a 0.2 μm syringe filter. The peptide was purified by RP-HPLC with a gradient of 20%-50% acetonitrile in water (each containing 0.1% TFA) over 40 mins. The pure fractions were combined and lyophilized to afford purified macrocycles as yellow or white solids.

X-ray crystallography:

Crystal screening and optimization:

The Crystal Screen, Index, and PEG/ION screening kits (Hampton Research, Inc.) were used to screen each peptide for crystal growth. Screening conditions were performed using the three-drop, hanging drop vapor diffusion method in 96 well plates. Each well contained 100 μL of a screening condition and each hanging drop was composed of three different *v/v* ratios of the macrocycle (in filtered 18 mΩ water) and the screening condition, providing 864 separate conditions (3 *v/v* ratios x 3 plates x 96 well plates). The screening trays were set up using the Mosquito pipetting robot. Conditions that afforded crystal growth were further optimized in 4 x 6 matrix Hampton VDX 24-well plate. In these optimizations, the hanging drops were prepared on

glass slides by combing 1 μL of macrocycle solution (in filtered 18 mΩ water) with 1 μL of well solution at ratios of 1:1, 2:1, and 1:2.

Cell assays:

Tissue culture:

The human neuroblastoma cell line SH-SY5Y was generously provided by Dr. Kim Green (Dept. of Biological Sciences, UC Irvine). The cell cultures were kept in a 1:1 mixture of Dulbecco's Modified Eagle's Medium and Ham's F12 (DMEM/F12) medium supplemented with 10% fetal bovine serum (FBS), 100 U/mL penicillin, and 100 μg/mL streptomycin at pH 7.4 (all items were obtained from Thermo Fisher Scientific). The cells were incubated in a humidified 5% CO_2 atmosphere at 37 °C. All experiments were conducted using 60-70% confluent cultures in a biosafety cabinet.

LDH release assay:

SH-SY5Y cells were plated in 96-well plates (either 10,000 or 15,000 cells per well) in 100 μL of 1:1 mixture DMEM/F12 medium supplemented with 10% FBS, 100 U/mL penicillin and 100 μg/mL streptomycin at pH 7.4 and incubated in a humidified 5% CO_2 atmosphere at 37 °C for 24 h. Before treating the cells with a peptide, the media were removed, and was replaced with 90 μL serum-free DMEM/F12 media. The cells were incubated an additional 24 h in a humidified 5% CO_2 atmosphere at 37 °C.

4.0 mM stock solutions of peptides 1, 2, and 3 were prepared in filtered 18 mΩ deionized water. The stock solutions were subsequently serial-diluted with filtered 18 mΩ water to the concentrations required to achieve the desired concentrations in each well (using 10 μL of peptide), bringing the total volume of each well in the 96-well plate to 100 μL. The cells were incubated in replicates of five in the presence of each peptide for 24 h in a humidified 5% CO_2 atmosphere at

37 °C. LDH cytotoxicity (Thermo Fisher Scientific) assays were performed on the same plate of cells, where 50 µL of the media was transferred to a new 96-well plate and analyzed for LDH release, following the manufacturer's instruction. The absorbance of each well was measured at 490 and 680 nm (A_{490} and A_{680}). Data were analyzed by calculating the differential absorbance for each well (A_{490} - A_{680}) and comparing those values to those of the lysis buffer controls and the untreated controls:

$$\%\ \text{LDH release} = \frac{(A_{490} - A_{680})_{peptide} - (A_{490} - A_{680})_{untreated}}{(A_{490} - A_{680})_{lysis} - (A_{490} - A_{680})_{untreated}} \times 100$$

LDH assay data analysis:

LDH results were processed according to Koreniewski and Callewaert's method.[3] Statistical significance was calculated using an unpaired two-tailed T-Test using a P value of 0.01 as the limit for statistical significance.

Localization studies of peptide 1* using live SH-SY5Y cells:

Approximately 15,000 cells were plated onto a culture slide dish with 1.0 mL of 1:1 mixture DMEM/F12 medium supplemented with 10% FBS, 100 U/mL penicillin and 100 µg/mL streptomycin at pH 7.4 and incubated in a humidified 5% CO_2 atmosphere at 37 °C for 24 h. Before treating the cells, the media was removed, and the cells were incubated with 1.0 mL of serum-free DMEM/F12 media. The cells were treated with 50 µM of peptide **1*** for 2 h in a humidified 5% CO_2 atmosphere at 37 °C, then were washed with phenol-red-free, serum-free DMEM/F12 media (3 x 1.0 mL). The cells were imaged live using the Zeiss LSM700 confocal laser scanning microscope. Excitation was provided with diode 405 laser at 405 nm, and the emitted light was detected between 410 and 590 nm. Image data were processed using ZEN image analysis software.

Localization studies of peptide 1* using fixed SH-SY5Y cells:

Approximately 15,000 cells were plated onto a culture slide dish with 1.0 mL of 1:1 mixture DMEM/F12 medium supplemented with 10% FBS, 100 U/mL penicillin and 100 μg/mL streptomycin at pH 7.4 and incubated in a humidified 5% CO_2 atmosphere at 37 °C for 24 h. Before treating the cells, the media was removed, and the cells were incubated with 1.0 mL of serum-free DMEM/F12 media. The cells were treated with 50 μM of peptide **1*** for 2 h in a humidified 5% CO_2 atmosphere at 37 °C, then were washed with phenol-red-free, serum-free DMEM/F12 media (3 x 1.0 mL). The cells were fixed using 1.0 mL of 4% paraformaldehyde (in buffered PBS) for 30 min at room temperature, and then washed with Hank's balanced salt solution without phenol-red (3 x 1.0 mL). The cells were counterstained with 1.0 mL of 5.0 μg/mL WGA, Alexa Fluor® 488 conjugate (purchased from Thermo-Fisher) and were incubated for 10 min at room temperature. The cells were washed with Hank's balanced salt solution without phenol-red (3 x 1.0 mL). One drop of ProLong® Diamond Antifade mountant (purchased from Thermo-Fisher) was added to the specimen and the coverslip was mounted onto a microscope slide and was allowed to cure for 24 h in the dark at room temperature. The fixed cells were imaged using the Zeiss LSM700 confocal laser scanning microscope. Excitation was provided with diode 405 and 488 lasers at 405 nm and at 488 nm respectively, and the emitted light was detected between 410 and 590 nm. Image data were processed using ZEN image analysis software.

References:

1) Wang, J.; Xie, J.; Schultz, P. G. *J. Am. Chem. Soc*. **2006**, *128*, 8738–8739.
2) Koopmans, T.; van Haren, M.; Quarles van Ufford, L.; Beekman, J. M.; Martin, N. I. *Bioorg. Med. Chem*. **2013**, *21*, 553–559.
3) Korzeniewski, C.; Callewaert, D. M. *J. Immunol. Methods* **1983**, *64*, 313–320.

HPLC and ESI-MS of peptide 1*

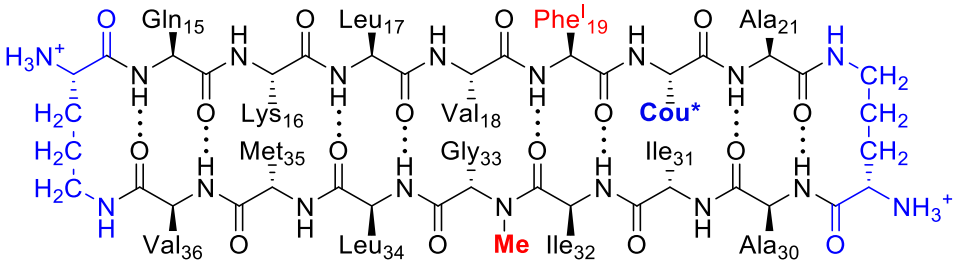

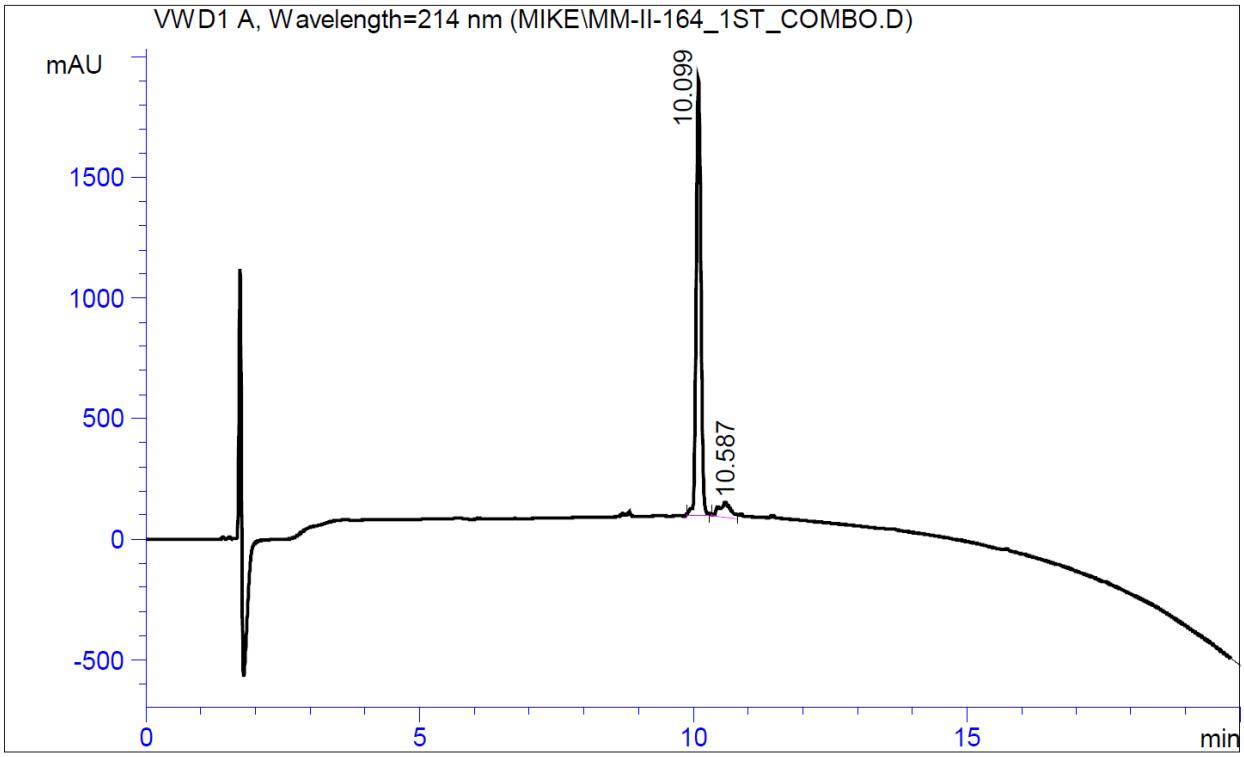

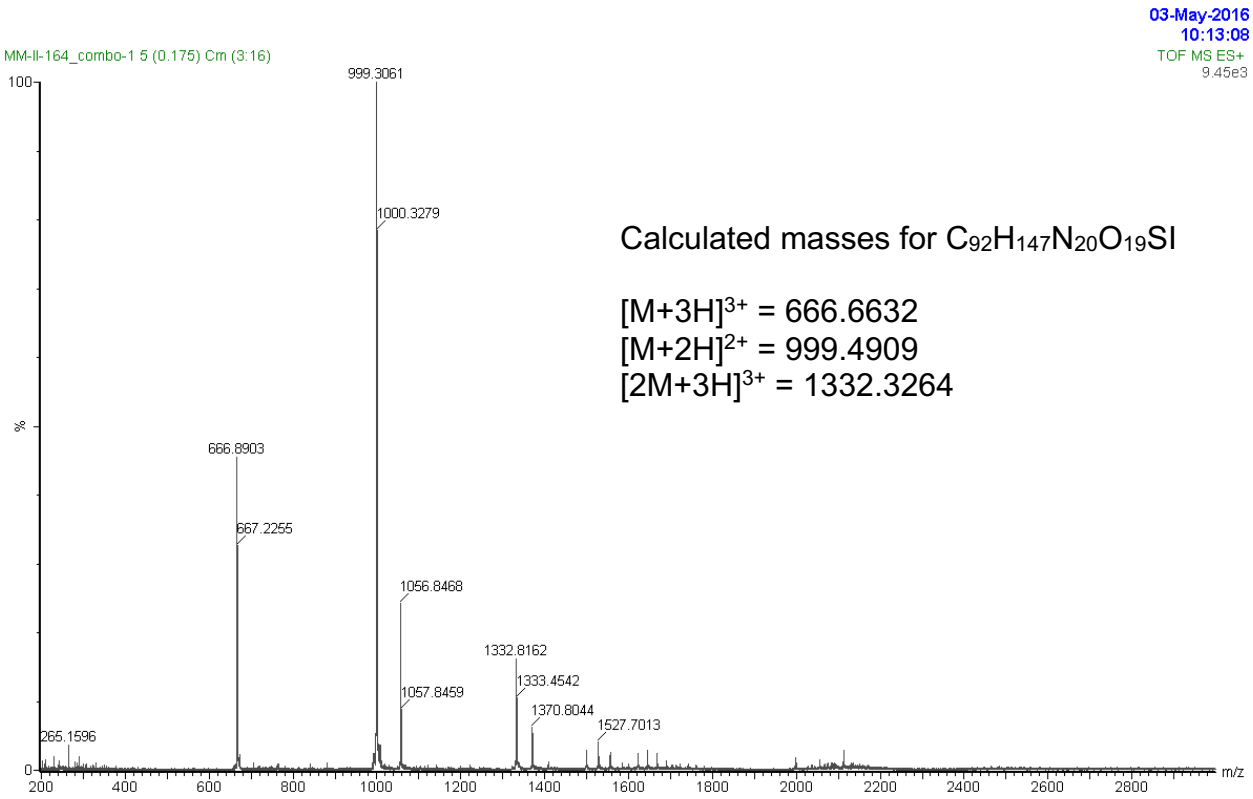

Calculated masses for $C_{92}H_{147}N_{20}O_{19}SI$

$[M+3H]^{3+}$ = 666.6632
$[M+2H]^{2+}$ = 999.4909
$[2M+3H]^{3+}$ = 1332.3264

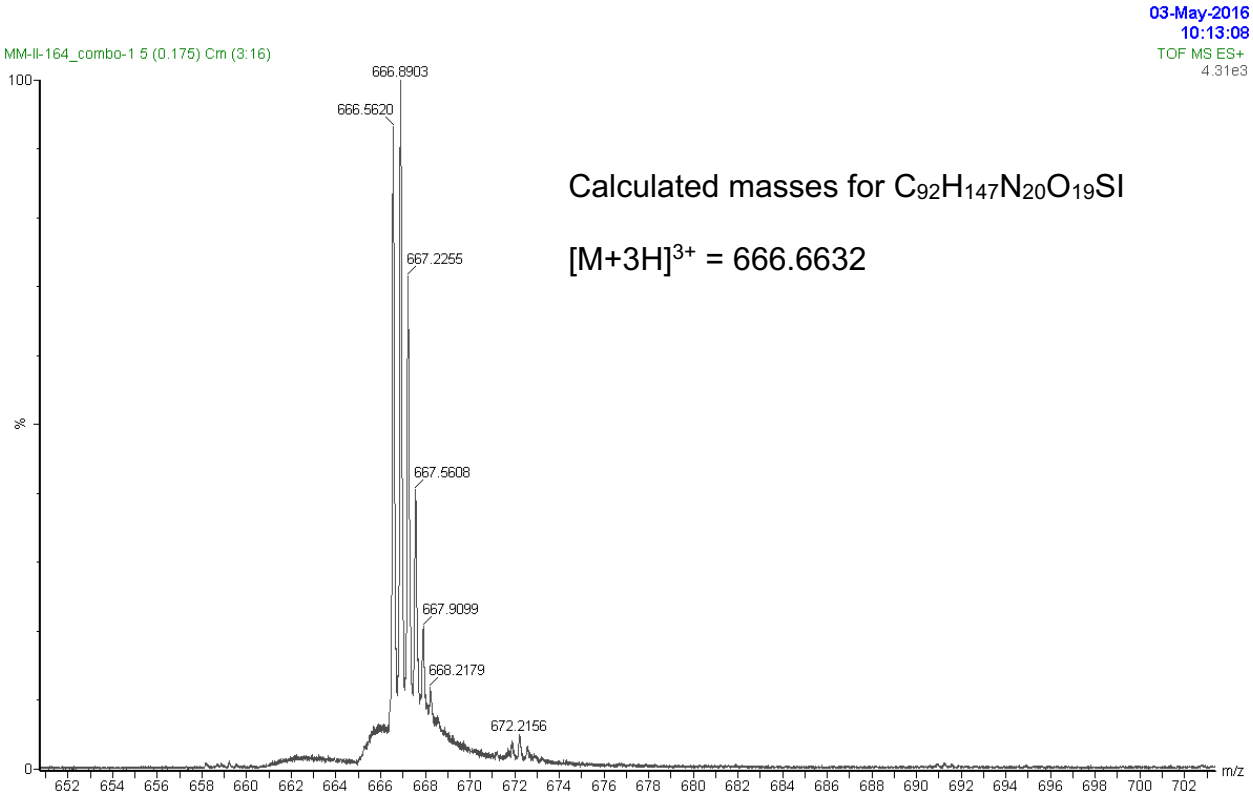

Calculated masses for $C_{92}H_{147}N_{20}O_{19}SI$

$[M+3H]^{3+}$ = 666.6632

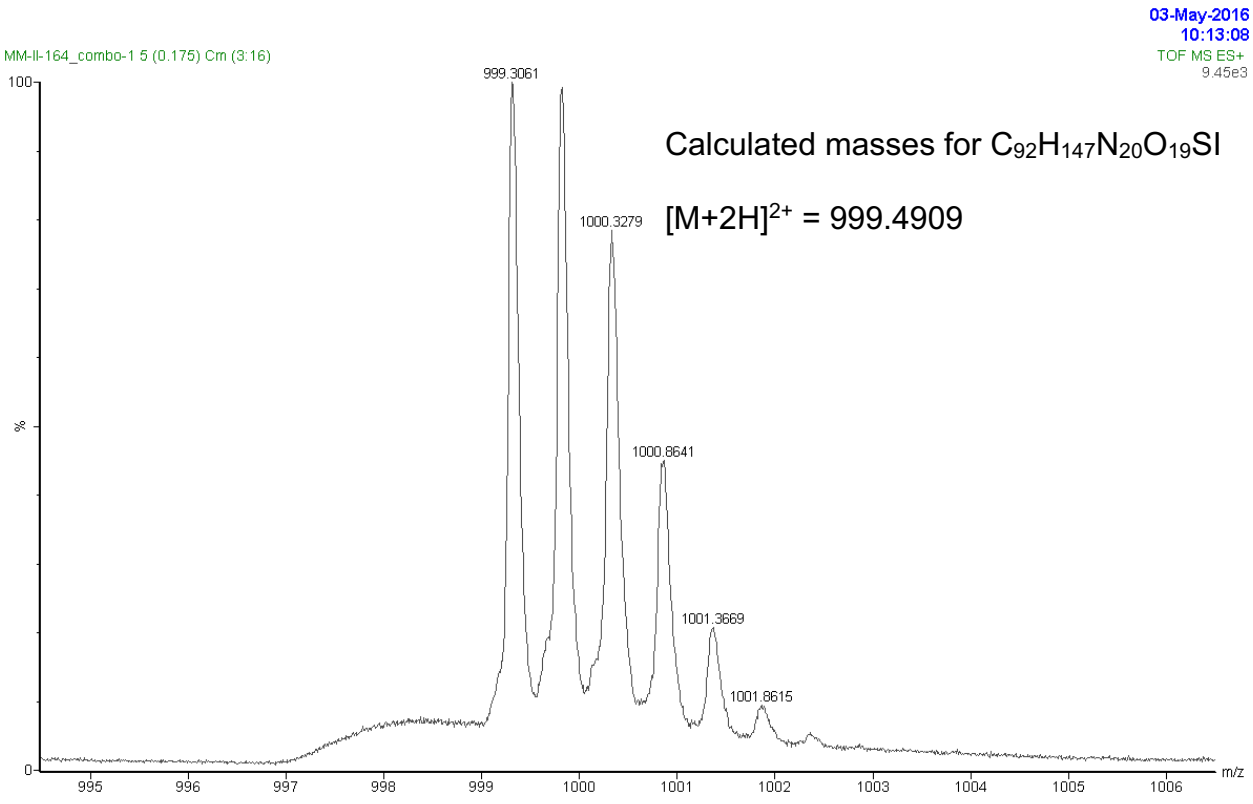

Calculated masses for $C_{92}H_{147}N_{20}O_{19}SI$

$[M+2H]^{2+}$ = 999.4909

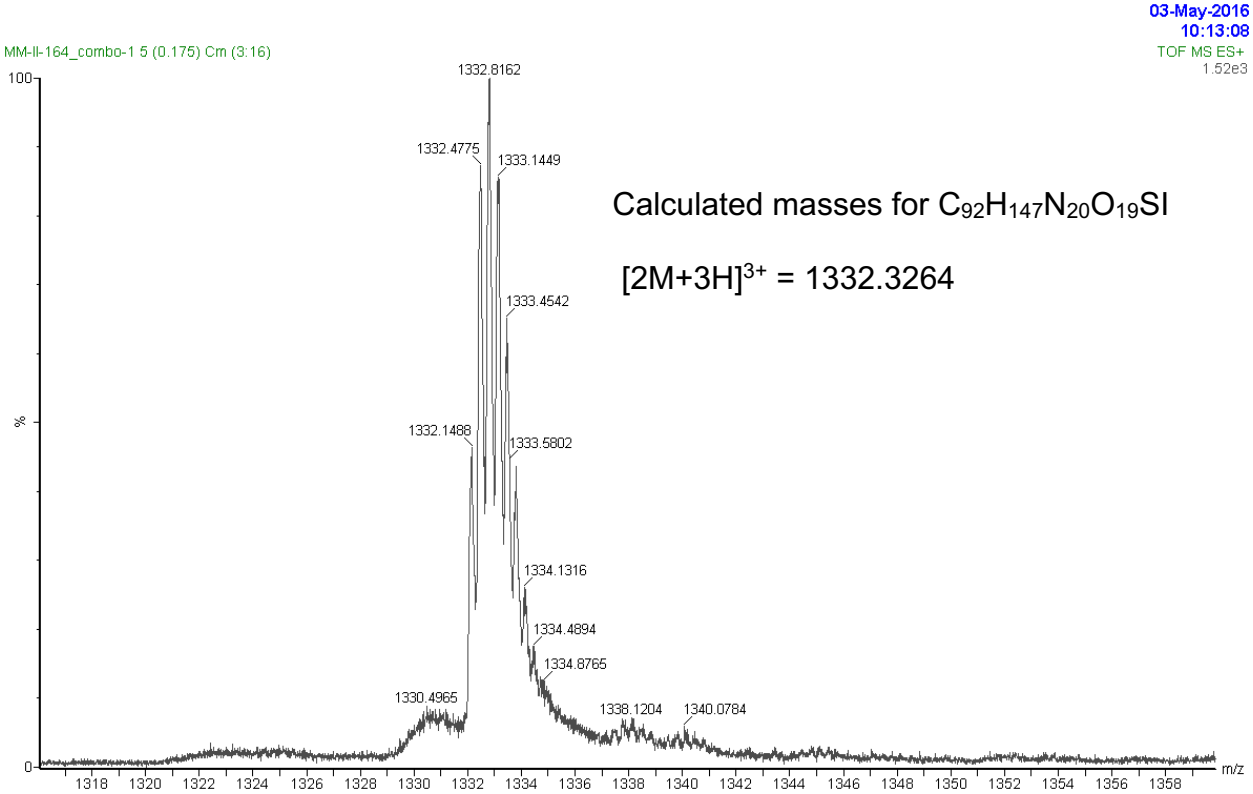

Calculated masses for $C_{92}H_{147}N_{20}O_{19}SI$

$[2M+3H]^{3+}$ = 1332.3264

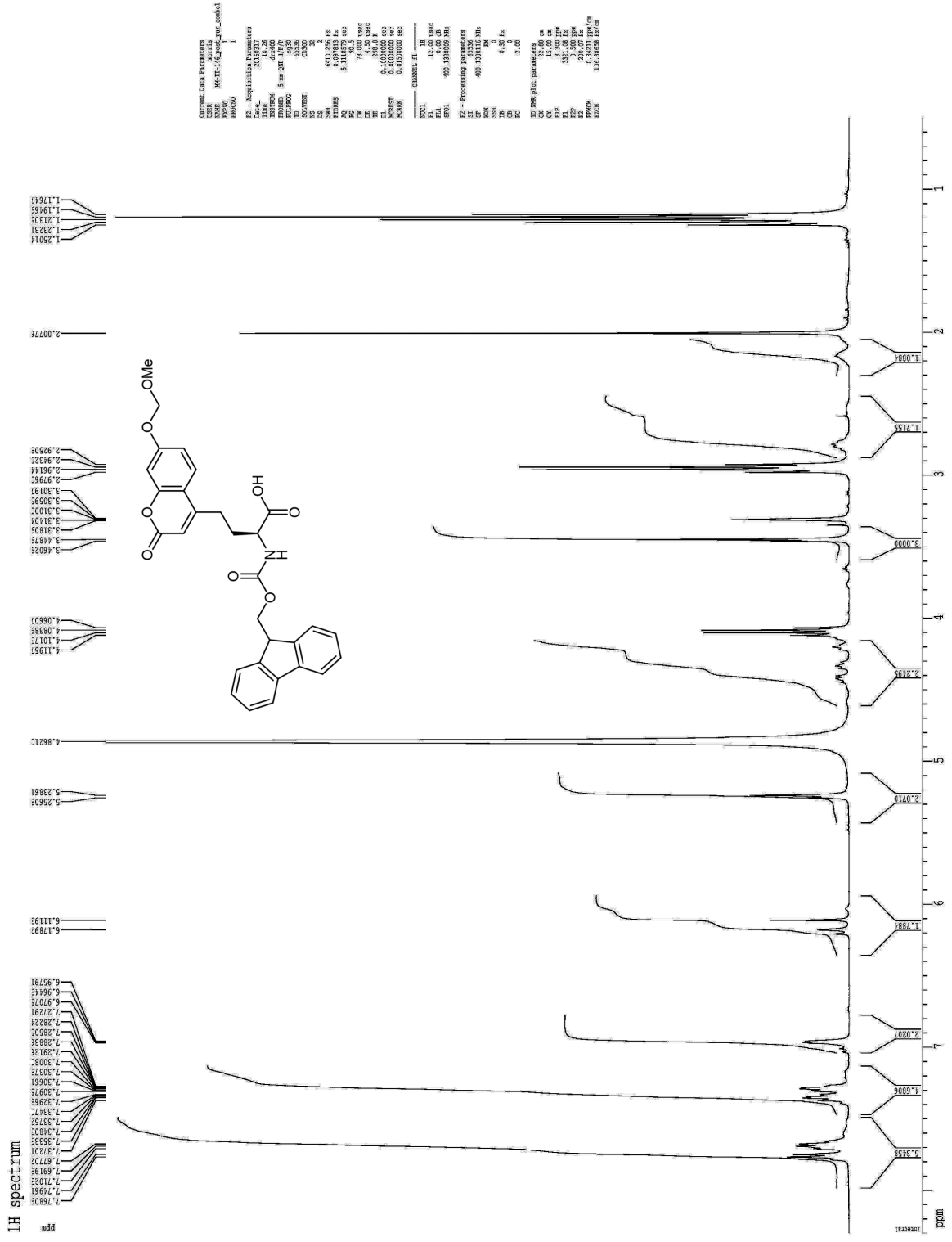

^{1}H NMR of Fmoc-L-7-HC(MOM)-OH (compound **7** in **Scheme 1**). ^{1}H NMR (400 MHz, CD_3OD) δ 7.80–7.73 (m, 2H), 7.72–7.62 (m, 2H), 7.41–7.24 (m, 4H), .99–6.93 (m, 2H), 6.11 (s, 1H), 5.27–5.21 (m, 2H), 4.67–4.16 (m, 4H), 3.45 (s, 3H), 2.84–2.68 (m, 2H), 2.60–2.45 (m, 1H), 2.24–2.10 (m, 1H).

Chapter 5

Teaching and Chemical Education Research

Introduction

Modes of instruction and teaching have not changed significantly since the inception of higher education over 900 years ago in Western Europe, where traditional lecturing has been the enduring and prevalent choice for teaching.[1] However, many academics have questioned the effectiveness of traditional lectures as a mode of learning, stating that students should construct their own understanding of information instead of passively learning it.[2,3] Learning theorists proposed that active learning, where students actively engage in the learning process, is more effective in improving student learning compared to traditional lectures,[4] especially for enhancing student success and retention in undergraduate science, technology, engineering, and mathematics (STEM) courses.[5]

Inclusive and effective teaching techniques are imperative to improve and retain the pool of talent in STEM. A multitude of national, longitudinal studies have shown that there is a leaky pipeline of underrepresented minorities in STEM, where women,[6] people of color,[7] and LGBT[8] students and scientists are more likely to leave STEM programs compared to non-STEM programs. This is worrisome because this reduces the talent pool in STEM and has the detrimental net effect of decreasing our society's scientific productivity, competition, and output. I believe everyone belongs in STEM if they choose to pursue a science career, and the best way to fix the leaky pipeline is to improve STEM instruction, promote representation, and reduce hostile learning and working environments. In this chapter, I will only focus on improving learning in STEM.

In a recent seminal study, Freeman et al. metaanalyzed 225 studies and demonstrated that active learning improves student success in undergraduate STEM courses.[5] The authors

determined that there is a decrease in student failure rate when active learning was used instead of traditional lecturing in every STEM discipline. This finding is significant since the data demonstrated that the number of students doing work of passing quality increases whenever active learning is used, thus providing significant gains for students who typically score in the lower grade range in STEM courses.[5] As such, this metaanalysis from Freeman et al. has a clear conclusion: active learning is a proven teaching method that increases student performance in undergraduate STEM courses. Therefore, if scientists are committed to evidence-based practices, then it is essential for them to use active learning in their classrooms.

In the remaining sections of this chapter, I provide reflections of my teaching experiences as instructor of record for two chemistry courses at UC Irvine. In both courses, I had the privilege to participate as a co-author on two chemical education studies, where I learned about study design and data analysis in the context of chemical education. One of these manuscripts was recently accepted in *J. Chem. Educ.*[9] and the other study[10] is under revision in the same journal. I will also include reflections of my experiences carrying out these research projects.

Teaching Chemistry 51LB as an instructor: reflection and chemical education research

During the summer session of 2019, I was afforded my very first opportunity to teach a chemistry course as an instructor of record. To prepare for this teaching opportunity, I was a fellow in the Pedagogical Fellowship (PF) Program and a trainee in the Summer Teaching Apprenticeship Program (STAP). These programs are designed to equip graduate students from all fields with theoretical and practical skills in pedagogy in order to prepare them for careers in higher education.

As a PF, I was required to take four classes (the 390 series) that is organized and taught by the Division of Teaching Excellence and Innovation (DTEI) at UC Irvine. These courses introduced topics in pedagogy; evidence-based teaching practices; active learning; teaching as

research; assessment and course design; instructional technology; universal design; diversity, inclusion and equity; experiential learning; preparing for the job market; among many other topics. The PF program also provided me with opportunities to get shadowed while I taught a discussion, lecture, or lab course by another PF or by Dr. Daniel Mann. These learning and teaching opportunities were valuable experiences because I learned how to engage students in the learning process while becoming a more confident instructor.

Another highlight of the PF program was designing and executing the TA Professional Development Program (TAPDP) for the Chemistry and Pharmaceutical Sciences departments, which I did in collaboration with Dr. Kate McKnelly in 2018 and Will Howitz in 2019. TAPDP is a two day course to train first year graduate students in TA roles and responsibilities, educational technology, lesson planning, office hours, leading a class, active learning techniques, diversity and inclusion, teaching observation and feedback, and practice in giving a mini-lesson. Organizing TAPDP was a valuable experience because I was able to apply the pedagogical concepts that I learned in the 390 course series, such as backwards design, lesson planning, active learning, and course logistics. TAPDP was also my very first opportunity to teach and lead workshop that lasted longer than one hour, which required careful organization and preparation.

During the 2018–2019 academic year, I participated in the STAP program, where I got to shadow Prof. Renée Link teach the Chemistry 51L lab lecture courses, which focuses on topics and concepts taught in sophomore organic chemistry labs. As an STAP trainee, I learned a lot from Prof. Link about active learning, engaging students during lab lecture, instructional technology, and course logistics. The most helpful component from the STAP program was being able to guest lecture for Prof. Link, where I learned how to engage students with various techniques during lab lecture. For example, I used iClicker questions and guided inquiry during the lab lecture to help

students learn important concepts in the organic chemistry lab course. Taken together, being a STAP trainee and learning from Prof. Link equipped me with the practical skills to carry out an engaging and effective lecture that utilizes active learning tools.

In the summer of 2019, I taught Chemistry 51LB, the introductory organic chemistry lab that undergraduates take in the Chemistry 51L series, with an enrollment of 115 students. As the instructor, I was responsible for managing five TAs, providing a biweekly lab lecture, organizing course logistics, and managing student issues. The PF and STAP programs prepared me well for this instructor position and I felt confident teaching the course material even though it was my first time being an instructor of record. As instructor, I experimented with replacing iClickers with a GoogleForm quiz, thinking that it would be more accessible and less cost prohibitive compared to iClickers. However, I learned from my midquarter student feedback form that my students actually preferred using iClickers simply because they are more convenient than filling out a GoogleForm quiz. Taking my student feedback into consideration, I decided to replace the GoogleForm system with iClicker questions to accommodate my students' preferences. This was a tricky decision to make since I had to ensure that students' grades from the GoogleForm quizzes carried over appropriately in the Canvas gradebook when I switched over to the iClicker system. Another important aspect I learned from teaching this course was managing student academic misconduct and accommodating students with specific issues.

While I was teaching Chemistry 51LB, I carried out a research project in collaboration with Prof. Link and Dr. Zachary Thammavongsy, where we implemented and evaluated a new active learning tool that Dr. Thammavongsy created, titled "^{1}H NMR Spectrum," in my course and in Chemistry 51A (taught by Prof. Link in the same summer session).[9] ^{1}H NMR spectroscopy is a challenging topic for many students, so we thought that the incorporation of ^{1}H NMR spectroscopy

game during the lab lecture would be an effective active learning tool for students to improve their understanding of ^{1}H NMR spectroscopy. ^{1}H NMR Spectrum is the first example of a team-based tabletop game focused on elucidating the structures of organic small molecules using ^{1}H NMR spectra. The tabletop game was designed as a collaborative and competitive group activity to encourage multiple rounds of play to help students reinforce their ^{1}H NMR spectra interpretation skills. While playing in either team-based or free-for-all mode, students analyzed the provided chemical shifts, splitting patterns, integrations, and molecular formula within a designated time limit to correctly deduce the structure associated with the ^{1}H NMR spectrum.

In this research project, I learned how to design research surveys from Prof. Link. We designed pre- and post-surveys that students took before and after playing the game in order to evaluate students' attitudes toward the game and their comfort over solving ^{1}H NMR problems. Learning how to design research surveys was a useful experience, where I learned about crafting proper survey questions and using the Likert scale. When we finished collecting survey data from students, we determined that the students in the two courses felt more comfortable solving ^{1}H NMR spectroscopy questions, found the game to be an appealing study aid, and were able to complete multiple rounds of play to strengthen their skills in interpreting ^{1}H NMR spectra. As such, we concluded that the ^{1}H NMR Spectrum tabletop game might serve as an engaging and competitive group learning tool to supplement teaching on ^{1}H NMR spectroscopy.[9]

Teaching Chemistry 101W as an instructor: reflection and chemical education research

In winter 2020, I was offered the opportunity to teach Chemistry 101W, the upper-division "Writing for Chemists" course, as the instructor of record. Chemistry 101W was designed by Prof. Stephen Mang and Dr. Kate McKnelly to help chemistry majors develop and improve their scientific writing and communication skills. When I began teaching Chemistry 101W, I felt more

confident going into the course for two reasons: (1) it was my second instructor of record experience; and (2) there was a small course enrollment (13 students). This was a unique teaching opportunity due to the small enrollment size, which allowed me to develop stronger mentor-mentee relationships with my students and provide high quality feedback on students' assignments. Teaching this course was also a valuable opportunity for learning how to manage course logistics and handling student accommodations. Having students complete midquarter feedback was also helpful, where I learned that my students needed more time to complete their assignments. Thereafter, I accordingly extended due dates for course assignments, which my students appreciated and emphasized this in their final course evaluations.

While I was an instructor for Chemistry 101W, I participated in a research project designed and led by Prof. Mang and Dr. McKnelly. Chemistry 101W is unique because it is the first example of an upper-division chemistry writing course organized completely around specifications grading. As such, we were interested in determining how specifications grading impacted students' writing habits and attitudes. Specifications grading is a modern method to assess student achievement of student learning objectives (SLOs).[11] In a specifications grading system, the instructor creates criteria based on SLOs that students must meet to obtain a particular grade. The specifications grading rubrics are designed to be more transparent and less subjective than a traditional points-based rubric. Another benefit of specifications system is that grading should be faster and more consistent between instructors, allowing more instructor feedback and student revision opportunities.[12]

In this research project, we wanted to determine if the specifications grading system we used impacted our students' habits and attitudes towards writing. To do this, Prof. Mang and Dr. McKnelly designed pre- and post-surveys that asked students about their writing habits and

attitudes. The surveys were deployed in fall 2019 (when the course was taught by Dr. McKnelly) and winter 2020 (when I taught the course). After both courses were completed, students self-reported increased propensities to pre-write and edit, and several students mentioned that they appreciated the transparency of the specifications rubrics and the control the specifications system gave them over their grades. These survey results are significant because it demonstrated that the specifications grading system made students more likely to organize and revise their writing, which may not have happened if the course used a traditional rubric system.

Conclusion

The PF, STAP, teaching, and research experiences provided me with a variety of skills that have improved my ability and confidence as an instructor. Before these experiences, I had a completely different vision of what "effective" teaching looked like, and this vision consisted of traditional, disengaging lectures. I now know that active learning and student participation in the learning process is essential for an inclusive learning environment that enables all students to succeed in STEM courses. I am excited to use the pedagogical skills I learned at UC Irvine for future teaching opportunities and eager to learn more about evidence-based teaching as I gain more instructor experience.

References

(1) de Ridder-Symoens, H.; Rüegg, W. *A History of the University in Europe: Volume 2, Universities in Early Modern Europe (1500-1800)*; A History of the University in Europe; Cambridge University Press, 2003.

(2) Vygotsky, L. S.; Cole, M.; John-Steiner, V.; Scribner, S.; Souberman, E. *Mind in Society: Development of Higher Psychological Processes*; Harvard University Press, 1978.

(3) Piaget, J. *Language and Thought of the Child: Selected Works*; Jean Piaget: selected works; Taylor & Francis, 2005.

(4) Meyers, C.; Jones, T. B. *Promoting Active Learning. Strategies for the College Classroom.*; ERIC, 1993.

(5) Freeman, S.; Eddy, S. L.; McDonough, M.; Smith, M. K.; Okoroafor, N.; Jordt, H.; Wenderoth, M. P. Active Learning Increases Student Performance in Science, Engineering, and Mathematics. *Proc. Natl. Acad. Sci. U. S. A.* **2014**, *111* (23), 8410–8415. https://doi.org/10.1073/pnas.1319030111.

(6) Blickenstaff, J. C. Women and Science Careers: Leaky Pipeline or Gender Filter? *Gend. Educ.* **2005**, *17* (4), 369–386. https://doi.org/10.1080/09540250500145072.

(7) Holdren, J. P.; Lander, E. Engage to Excel: Producing One Million Additional College Graduates with Degrees in Science, Technology, Engineering, and Mathematics. *PCAST STEM Undergrad. Work. Gr.* **2012**, 130.

(8) Hughes, B. E. Coming out in STEM: Factors Affecting Retention of Sexual Minority STEM Students. *Sci. Adv.* **2018**, *4* (6), 1–6. https://doi.org/10.1126/SCIADV.AAU2554.

(9) Thammavongsy, Z; Morris, Michael A.; Link, R. D. ^{1}H NMR Spectrum: A Team-Based Tabletop Game for Molecular Structure Elucidation. Just accepted manuscript at *J. Chem.*

Educ. **2020**.

(10) McKnelly, Kate J.; Morris, Michael A.; Mang, S. A. Redesigning a "Writing for Chemists" Course Using Specifications Grading. Under revision at *J. Chem. Educ.* **2020**.

(11) Nilson, L. B.; Stanny, C. J. *Specifications Grading: Restoring Rigor, Motivating Students, and Saving Faculty Time*; Stylus Publishing, 2015.

(12) Schepmann, H. G.; Hughes, L. A. Chemical Research Writing: A Preparatory Course for Student Capstone Research. *J. Chem. Educ.* **2006**, *83* (7), 1024–1028. https://doi.org/10.1021/ed083p1024.